

# Non-Lytic Egress of Mycobacterium Tuberculosis from Human Macrophages

Dr Meera Mehta

Division of Infection and Immunity

University College London

Supervisor: Professor Mahdad Noursadeghi

This thesis is submitted for the degree of Doctor of Philosophy

2020

## **DECLARATION**

I, Meera Mehta confirm that the work presented in this thesis is my own. Where information has been derived from other sources, I confirm that this has been indicated in the thesis.

Signed:

Date:

## ABSTRACT

Macrophages are the target cell for *Mycobacterium tuberculosis* (Mtb) infection; a major reservoir for productive infection, as well as crucial effector cells for the control of Mtb. However, the majority of bacteria in the caseous necrotic centre of the TB granuloma are extracellular. Extracellular bacteria may arise from host cell necrosis and release of infecting bacteria, but mycobacteria have also been shown to exit from amoeba using a non-lytic strategy and other pathogens have also developed versatile strategies to exit from their host cell, providing an alternative mechanism to escape intracellular restriction. In this thesis I have developed a high throughput flow cytometric assay to quantify intracellular and extracellular bacteria in an *in vitro* model of human monocyte derived macrophages infected with fluorescent Mtb. I show that extracellular Mtb accumulate in parallel to intracellular bacteria, and make a significant contribution to the overall bacillary burden. These extracellular bacteria do not arise as a result of cellular necrosis in this low multiplicity of infection model. I use computational modelling to predict that a non-lytic process is necessary to explain the observed data. I demonstrate experimentally, for the first time that extracellular Mtb arise by non-lytic egress from human macrophages. I show that this process is related to virulence, since the attenuated *Mycobacterium Bovis* Bacillus Calmette-Guérin does not display this behaviour.

## IMPACT STATEMENT

In this thesis I have developed a novel high-throughput method for quantitating Mtb bacilli based on flow cytometric assessment of fluorescent bacteria. This method correlates well with the current gold standard for bacterial enumeration-colony forming units (CFU). If adopted within the industry, this new methodology will be beneficial for all those undertaking *in vitro* research quantifying mycobacteria, negating the need for laborious CFU measurements, and achieving experimental results within 24 hours rather than the three weeks it takes for mycobacteria to grow on solid agar.

The work presented in the thesis suggests, for the first time, that Mtb is able to escape macrophages via lytic and non-lytic strategies. Importantly, there seems to be a rapid flux of Mtb between the intracellular and extracellular compartments, so the development of strategies for immune control of Mtb infection, as well as antibacterial agents should target both compartments to achieve maximum protection.

My data pave the way to dissecting the molecular mechanism that underpins non-lytic egress. This will allow researchers to find potential new therapeutic targets to contain bacteria within macrophages, and potentially slow the spread of infection. If this were done in combination with host directed therapies to improve macrophage killing of Mtb, greater sterilization of infection might be achieved.

## **ACKNOWLEDGMENTS**

First and foremost, I need to thank my supervisor, Professor Mahdad Noursadeghi. His passion for his work has been a source of inspiration to 'just keep going' during various scientific and personal challenges over the last few years. Himself, Benny Chain, and their wonderful families welcomed me into the lab family that is Innate to Adaptive and I'm very thankful to have been part of such a supportive and stimulating environment.

Thank you to all the members of the Noursadeghi and Chain Lab for valuable critique, discussion and support. In particular, Katharine Best with whom I had the pleasure of collaborating with for the mathematical modelling presented in this thesis. Also the various members of 'Team TB' who all contributed to this work- Jennifer Roe, Gabriele Pollara, Rachel Byng-Maddick and Elspeth Potton. A special thanks to Gabriele, whose enthusiasm for discussing experiments and hypotheses has also been crucial to the work presented herein. Finally, thank you to David Stirling, for all his help with all things related to IT, and being so patient with me through various imaging struggles.

Next I must thank my amazing parents whose belief in me over the years, encouragement, and generosity of time has got me where I am today. I have always been inspired by how hard they work and their resilience, and these two qualities enabled me to complete this work, even when it seemed impossible.

And finally, my husband, Niraj. I am so grateful for his unconditional support of all my endeavours. I dedicate this work to our wonderful children (who both arrived at various points during this thesis!), Kian and Anisa. I hope that from us they

learn the value of perseverance and hard work.

## **CONTRIBUTION OF OTHERS**

I must acknowledge the significant contribution of Katharine Best and Benny Chain, with whom I collaborated to build the mathematical model presented in the thesis. They taught me the principles of modelling and were very patient with me as I learnt the use of computational models to describe biological systems. Katharine and I then subsequently worked together to define the parameters of the model. She performed the analysis to calculate the rate of each parameter and ran the algorithms to fit the data. I directed the questions and generated hypothesis to ask of the model.

Elsbeth Potton and Rachel Byng-Maddick performed the experiments that contributed to Figures 3.1A, 3.3B, and 3.1D. I re-analyzed their data after refining the equation to quantify bacteria by integrated mCherry fluorescence. Rachel Byng-Maddick and Jennifer Roe also contributed 1 experimental replicate each for Figures 3.5 and 3.8. The rest of the experimental work is my own.

## ABBREVIATIONS

ABS	Human AB Serum
AM	Alveolar Macrophage
AMP	Anti Microbial Peptide
BAL	Broncho Alveolar Lavage
BCG	Mycobacterium Bovis Bacillus Calmette-Guérin
BMDM	Bone Marrow Derived Macrophages
CD	Cluster of Differentiation
CFP	Culture Filtrate Protein
CNS	Cerebral Nervous System
CR	Complement Receptor
CT	Computed Tomography
DAPI	4',6-diamidino-2-phenylindole
DC	Dendritic Cells
DC-SIGN	Dendritic Cell ICAM-3-Grabbing Nonintergrin
DMSO	Dimethyl Sulfoxide
DNA	Deoxyribonucleic Acid
DRAM	DNA Damage Regulated Autophagy Modulator
Eis	Enhanced intracellular survival protein
EM	Electron Microscopy
ERK	Extracellular Signal-Regulated Kinase
ESAT	Early Secretory Antigenic Target
ESX	ESAT-6 Secretion System
FcR	Fc Receptors
FRET	Fluorescence Resonance Energy Transfer
cGAMP	cyclic Guanosine Monophosphate–Adenosine Monophosphate
cGAS	cyclic GAMP Synthase
GM-CSF	Granulocyte Macrophage Colony Stimulating Factor
GTP	Guanosine Triphosphate
HIV	Human Immunodeficiency Virus
HKMtb	Heat Killed Mtb
ICAM	Intercellular Adhesion Molecule
IFN	Interferon
IGRA	Interferon Gamma Release Assay

IL	Interleukin
infCoM	Infected Conditioned Media
iNOS	inducible Nitric Oxide Synthase
IRF	Interferon Response Factor
JNK	c-Jun N-terminal kinase
LAM	Lipoarabinomannan
LPS	Lipopolysaccharide
LTBI	Latent Tuberculosis Infection
MAPK	Mitogen-Activated Protein Kinase
M-CSF	Macrophage Colony Stimulating Factor
MDM	Monocyte Derived Macrophage
MHC	Major Histocompatibility Class
MMP	Matrix Metallo Proteinase
Mm	Mycobacterium Marinum
MOI	Multiplicity of Infection
MR	Mannose Receptor
MSMD	Mendelian Susceptibility to Mycobacterial Disease
Mtb	Mycobacterium Tuberculosis
NADPH	Nicotinamide adenine dinucleotide phosphate
NFκB	Nuclear Factor kappa-light-chain-enhancer of Activated B cells
NK	Natural Killer
NLR	Nod Like Receptors
NLRP	Nucleotide-binding oligomerization domain, Leucine rich Repeat and Pyrin domain containing
NO	Nitric Oxide
OADC	Oleic Albumin Dextrose Catalase
OD	Optical Density
ODE	Ordinary Differential Equation
PAMP	Pathogen-Associated Molecular Pattern
PBMC	Peripheral Blood Mononuclear Cells
PBS	Phosphate Buffered Saline
PDIM	Phthiocerol Dimycocerosate
PET	Positron Emission Tomography
PFA	Paraformaldehyde
PGE	Prostaglandin E

PIM	Phosphatidylinositol Mannosides
PRR	Pattern Recognition Receptors
RD	Region of Difference
RLR	Rig Like Receptors
RNA	Ribonucleic Acid
RNI	Reactive Nitrogen Intermediates
RNS	Reactive Nitrogen Species
ROS	Reactive Oxygen Species
SPR	Surfactant Protein Receptors
SR	Scavenger Receptors
STAT	Signal Transducer And Activator Of Transcription
STING	Stimulator of Interferon Genes
TACO	Tryptophan-aspartate-containing coat
TB	Tuberculosis
TGF	Transforming Growth Factor
Th	T helper
TLR	Toll Like Receptors
TNF	Tumour Necrosis Factor
TST	Tuberculin Skin Test

## LIST OF FIGURES

Figure 1.1 Spectrum of Mtb infection and outcomes..	29
Figure 1.2 The inflammatory seesaw of tuberculosis..	39
Figure 1.3 Mechanisms by which Mtb subverts macrophage defences.	51
Figure 1.4 Pathogenic lifecycle of Mtb.	54
Figure 1.5 Intracellular pathogen lytic and non-lytic strategies to exit the host cell.	59
Figure 3.1 High throughput flow cytometric assay for quantitation of fluorescent Mtb.	79
Figure 3.2 Imagestream Analysis of H37Rv mCherry population.	80
Figure 3.3 Detection of intracellular and extracellular Mtb.	82
Figure 3.4 Experimental model to measure extracellular Mtb during MDM infection.	83
Figure 3.5 Extracellular Mtb accumulation following co-culture with macrophages.	84
Figure 3.6 Bacterial accumulation is not simply due to exponential growth.	86
Figure 3.7 Model of Mtb-macrophage interactions	88
Figure 3.8 Measurement of cell death using nuclear counts.	92
Figure 3.9 Cell count analysis in central fields of view.	94
Figure 3.10 Distribution of nuclear area in 3 separate experiments	95
Figure 3.11 Live Dead Staining to identify and enumerate necrotic cells.	97
Figure 3.12 Calculating the macrophage death rate.	99
Figure 3.13 Determining the extracellular growth rate of Mtb.	101
Figure 3.14 Model parameterisation.	104
Figure 3.15 Running the model with a higher death rate	106
Figure 3.16 Incorporating non-lytic egress into the mathematical model	109
Figure 3.17 Model tries to predict $r_I$ , $\beta$ and $\eta$	110
Figure 4.1 Experimental model to look for non-lytic egress of Mtb.	119
Figure 4.2 Evidence for non-lytic egress of Mtb.	120
Figure 4.3 Flow cytometry plots showing rapid extracellular Mtb accumulation	121
Figure 4.4 Mtb egress from macrophages without causing host cell lysis	123
Figure 4.5 Extracellular bacteria at 60mins do not arise from adherent Mtb	126
Figure 4.6 Non-lytic egress is morphologically distinct from cellular necrosis	128
Figure 4.7 Mtb released by non-lytic egress are viable	130
Figure 4.8 Incorporating non-lytic egress into the mathematical model.	133
Figure 4.9 Estimating the rate of uptake of Mtb in silico	134
Figure 5.1 Non-lytic egress is not dependent on MOI.	144
Figure 5.2 Non-lytic egress is not dependent on the aggregation status of Mtb	147
Figure 5.3 Non-lytic egress is associated with virulence.	149

Figure 5.4 Non-lytic egress occurs with heat killed bacteria.....	151
Figure 5.5 Blocking non-lytic egress using Cytochalasin D. ....	155
Figure 5.6 Effect of Nocodazole on $\alpha$ -tubulin.. ....	158
Figure 5.7 Blocking non-lytic egress using Nocodazole. ....	159
Figure 5.8 GM-CSF MDM display the same phenotype as M-CSF MDM.....	161
Figure 5.9 Rate of non-lytic egress is not affected by IFN $\gamma$ priming of MDM. ....	163
Figure 6.1 A model of non-lytic egress contributing to disease pathogenesis.....	173

## LIST OF TABLES

Table 1.1 Microheterogeneity and functions of tissue macrophages .....	18
Table 1.2 Macrophage pro- and anti-inflammatory cytokines .....	23

# TABLE OF CONTENTS

DECLARATION .....	2
ABSTRACT .....	3
IMPACT STATEMENT.....	4
ACKNOWLEDGMENTS .....	5
CONTRIBUTION OF OTHERS.....	7
ABBREVIATIONS.....	8
LIST OF FIGURES .....	11
LIST OF TABLES .....	13
TABLE OF CONTENTS.....	14
1 INTRODUCTION .....	17
1.1 Macrophages.....	17
1.1.1 The Origin and Function of Macrophages.....	17
1.1.2 Macrophage Activation and Polarization.....	19
1.1.3 Pathogen Recognition .....	20
1.1.4 Cytokine Production .....	21
1.1.5 Antimicrobial Actions .....	24
1.2 Tuberculosis.....	27
1.2.1 Epidemiology and Clinical Course of Tuberculosis .....	27
1.2.2 Mycobacterium Tuberculosis .....	30
1.2.3 Overview of the Immune Response to Mtb .....	31
1.3 Macrophages and Mycobacterium Tuberculosis .....	40
1.3.1 Macrophage Restriction of Mtb .....	40
1.3.2 Mtb Subversion of Macrophage Defences .....	43
1.3.3 Macrophage Cell Death and Tuberculosis .....	47
1.4 Extracellular Mycobacterium Tuberculosis.....	52
1.4.1 Presence of Extracellular Mtb in Granulomas.....	52
1.4.2 Extracellular Mtb in Disease Pathogenesis.....	53
1.4.3 Strategies by Which Mycobacteria Become Extracellular .....	55
1.4.4 Exit Strategies of Other Organisms.....	57
1.5 Summary.....	60
1.6 Aim .....	61
1.7 Hypothesis.....	61
1.8 Experimental objectives.....	61
2 MATERIALS AND METHODS .....	62
2.1 Isolation and Culture of Human MDM .....	62

2.2	Mycobacteria .....	62
2.2.1	Strains .....	62
2.2.2	Disaggregation of Mtb.....	63
2.2.3	Heat killing.....	63
2.3	Anti-Mtb Antibody Staining.....	64
2.4	Cell Culture.....	64
2.4.1	Macrophage infection .....	64
2.4.2	Macrophage Conditioned Media .....	65
2.4.3	Chemical inhibitors .....	65
2.5	Bacterial Enumeration .....	66
2.5.1	Flow cytometry .....	66
2.5.2	Colony Forming Units .....	66
2.6	Imaging Techniques .....	67
2.6.1	Imagestream Analysis .....	67
2.6.2	Cell microscopy .....	67
2.6.3	Confocal Microscopy .....	68
2.6.4	Live cell imaging.....	69
2.7	Data for Modelling .....	69
2.8	Mathematical Modelling.....	70
2.9	Parameter Estimation .....	72
3	EXTRACELLULAR MTB ACCUMULATION.....	73
3.1	Introduction.....	73
3.2	Objectives.....	76
3.3	Results .....	77
3.3.1	A high throughput flow cytometric assay to quantify Mtb.....	77
3.3.2	Detection and quantitation of extracellular and intracellular Mtb .....	81
3.3.3	Extracellular bacteria accumulate following culture with MDM .....	83
3.3.4	Extracellular bacteria do not accumulate by extracellular replication.....	85
3.3.5	A mathematical model to describe Mtb accumulation .....	87
3.3.6	Determining the rate of cell death .....	90
3.3.7	Necrotic cell death does not explain extracellular bacillary load.....	98
3.3.8	Extracellular bacteria are predicted to arise from non-lytic egress .....	107
3.4	Discussion .....	111
4	MTB EXITS MACROPHAGES BY NON-LYTIC EGRESS .....	116
4.1	Introduction.....	116
4.2	Objectives.....	118
4.3	Results .....	119

4.3.1	Evidence for rapid Mtb escape from macrophages .....	119
4.3.2	Rapid extracellular accumulation not due to cell death .....	122
4.3.3	Rapid extracellular accumulation not residual adherent bacteria .....	124
4.3.4	Visualisation of non-lytic Mtb egress.....	127
4.3.5	Bacteria remain viable after non lytic egress.....	129
4.3.6	Incorporating non-lytic egress into the mathematical model.....	131
4.3.7	Equivalent intracellular and extracellular rate of growth .....	135
4.4	Discussion .....	136
5	MECHANISM OF NON- LYTIC EGRESS OF MTB.....	140
5.1	Introduction.....	140
5.2	Objectives.....	142
5.3	Results .....	143
5.3.1	Non-lytic egress is not dependent on the MOI .....	143
5.3.2	Non-lytic egress is not dependent on the aggregation status of Mtb ....	145
5.3.3	Non-lytic egress of Mtb is associated with virulence .....	148
5.3.4	Non-lytic egress occurs with heat killed bacteria.....	150
5.3.5	Non-lytic egress is not governed by the actin cytoskeleton .....	152
5.3.6	Non-lytic egress is not governed by the microtubule network.....	156
5.3.7	Non-Lytic Egress of Mtb occurs in alternatively differentiated MDMs ...	160
5.3.8	IFN $\gamma$ does not affect the rate of non-lytic egress .....	162
5.4	Discussion .....	164
6	GENERAL DISCUSSION .....	168
6.1	Overall Conclusion .....	168
6.2	Implications .....	168
6.3	Limitations .....	169
6.4	A Model of Non Lytic Egress in Disease Pathogenesis.....	171
7	FUTURE WORK.....	174
8	REFERENCES .....	177

# 1 INTRODUCTION

## 1.1 Macrophages

---

### 1.1.1 The Origin and Function of Macrophages

Macrophages are present in all tissues (Gordon and Plüddemann, 2017). During organogenesis, macrophages derived from embryonic yolk sac and fetal liver precursors are seeded throughout tissues. Under steady state conditions resident macrophages are largely maintained through local proliferation. Inflammatory responses to trauma or infection however, result in the rapid recruitment of monocytes to the respective tissue macrophage compartment (Yona et al., 2013). Monocytes are derived from myeloid progenitor cells in the bone marrow and released into the bloodstream. Monocytes migrate from the blood into tissue and differentiate into macrophages (Yona et al., 2013). Here, they may adopt different functional characteristics according to in their tissue microenvironment (Haldar and Murphy, 2014), summarised in **Table 1.1**.

Macrophages are avidly phagocytic. This function underpins their ability to participate in host defence by intracellular killing of microbial pathogens and antigen presentation to T lymphocytes, but this function is also important for clearance of apoptotic cells and for recycling of nutrients by digesting waste products from tissues (Gordon et al., 2014). Macrophages are hence essential not only for immunity, but also for tissue homeostasis (Davies et al., 2013).

Tissue	Macrophage Type	Function
<b>Lung</b>	Alveolar macrophage	Immune surveillance of inhaled particles and pathogens, clearance of surfactant
	Interstitial macrophages	Regulation of DC maturation and activation
<b>Liver</b>	Kupffer cells	Clearance of microorganisms, cell debris and aged erythrocytes from blood.
	Motile liver macrophages	Immune surveillance
<b>Gut</b>	Intestinal macrophages	Regulation of immune responses to microbiome
<b>Spleen</b>	Marginal zone macrophages	Immune surveillance of circulation
	Metallophilic macrophages	Immune surveillance
	Red pulp macrophages	Erythrocyte clearance, iron metabolism
	White pulp macrophages	Clearance of apoptotic cells
<b>Heart</b>	Atrioventricular node macrophages	Regulate cardiomyocyte electrical activity
	Myocardial macrophages	Response to myocardial ischaemia, repair and tissue remodelling
<b>CNS</b>	Microglia	Promotion of neuronal survival, immune surveillance, removal of dead neurons, synaptic remodelling
	Perivascular macrophages	Immune surveillance
	Meningeal macrophages	Immune surveillance
<b>Skin</b>	Dermal macrophages	Immune surveillance
	Langerhans cells	Activation of T cells
<b>Adipose Tissue</b>	Adipose associated macrophages	Insulin sensitivity and adaptive thermogenesis
<b>Bone</b>	Osteoclasts	Bone remodelling
	Bone marrow macrophages	Support erythropoiesis
<b>Serosa</b>	Pleural macrophages	Immune surveillance
	Peritoneal macrophages	Immune surveillance

Table 1.1 **Microheterogeneity and functions of tissue macrophages**

Adapted from Davies L. Tissue-resident macrophages. *Nature Immunology* (2013); Gordon S.

Tissue macrophages: heterogeneity and functions. *BMC Biology* (2017)

### 1.1.2 Macrophage Activation and Polarization

In an effort to classify some aspects of macrophage functional heterogeneity, two subsets called M1 and M2 have been widely used to represent the two major opposing activities of macrophages (Martinez and Gordon, 2014). M1 macrophages, experimentally modelled by priming cells with bacterial lipopolysaccharide (LPS) or the cytokine Interferon (IFN)- $\gamma$ , were described as pro-inflammatory. The M1 phenotype was characterized by expression of high production of reactive nitrogen and oxygen intermediates, promotion of a CD4<sup>+</sup> T helper cell (Th)1 response, high levels of pro-inflammatory cytokines, and strong microbicidal and tumoricidal activity. M2 macrophages, experimentally modelled by priming cells with the cytokines interleukin (IL)-4 or IL-13 were described as anti-inflammatory, and involved in tissue repair and remodelling, (Martinez and Gordon, 2014). This paradigm has now been superseded since their existence *in vivo* as pure polarized subsets came under question (Lawrence and Natoli, 2011). Activated macrophage phenotypes have in fact been found to be labile and exhibit temporal re-adaptations (Stout et al., 2005; Stout and Suttles, 2004). They are now understood to be functionally dynamic, long-lived cells which are capable of switching their function between activation states appropriate to their microenvironment (Wynn et al., 2013; Xue et al., 2014). Though the data are incomplete, the plasticity of macrophages is thought to be determined by extracellular mediators (e.g. the local cytokine and cellular milieu (Martinez and Gordon, 2014), hypoxia, lactate production (Murray, 2017)) and mediated by transcriptional regulation which reprograms the function of the cell (Lawrence and Natoli, 2011).

Recently the discovery of the mixed origin of macrophages from yolk sac and fetal liver precursors, as well as postnatally from bone marrow derived cells (Marakalala et al., 2018), has seen a further shift in the understanding of macrophage subpopulations, since the origin of their development has also been shown to influence their function. For example, macrophage sub populations within the same tissue, but with differing cellular ontogeny, have different bactericidal capacity. In a mouse model of *Mycobacterium Tuberculosis* (Mtb) infection (Huang et al., 2018), alveolar macrophages (fetal origin) are pre-programmed to be more permissive for Mtb and facilitate growth, whereas interstitial macrophages (monocyte derived) are able to restrict growth. In the zebrafish model of *Mycobacterium marinum* (Mm) infection resident macrophages are restrictive but recruited monocytes/macrophages are permissive to bacterial growth. Regardless of these opposing findings in different models, the data highlight the importance of cellular ontogeny on the functioning of the cell.

### **1.1.3 Pathogen Recognition**

Macrophages recognize microorganisms via a limited number of germline-encoded pattern-recognition receptors (PRRs) such as Toll Like Receptors (TLRs), Nod Like Receptors (NLRs) and Rig Like Receptors (RLRs) (Medzhitov and Janeway, 2000). They are present on the cell surface or in distinct intracellular compartments. PRRs identify pathogen-associated molecular patterns (PAMPs), which are highly conserved molecular motifs shared by many microbial pathogens (Akira et al., 2006).

TLR engagement by PAMPs leads to activation of archetypal downstream

pathways including the nuclear factor kappa-light-chain-enhancer of activated B cells (NFκB) pathway, the mitogen-activated protein kinase (MAPK) cascades, or interferon response factor 3 (IRF3) signalling (Takeuchi and Akira, 2010). NFκB pathway activation results in NFκB transcription factor translocation to the nucleus to induce innate inflammatory gene expression (Takeuchi and Akira, 2010) for cytokine and chemokine production. Activation of the MAPK cascade also leads to transcription factor activity (Dong et al., 2002). Activation of some NLRs results in the formation of a structure called the inflammasome; this large multiprotein intracellular complex detects pathogenic microorganisms and sterile stressors, and activates the highly pro-inflammatory cytokines IL-1β and IL-18. Inflammasomes also induce a form of cell death termed pyroptosis, discussed in greater detail in **section 1.1.5** (Guo et al., 2015).

#### **1.1.4 Cytokine Production**

A major component of cellular innate immune responses arising from activation of PRRs is the transcriptional upregulation and secretion of low molecular weight proteins called cytokines and chemokines, which mediate intercellular signals. A range of pro and anti-inflammatory cytokines have been described (**Table 1.2**). Pro-inflammatory cytokines further potentiate the microbicidal capacities of macrophages, induce increased vascular permeability and recruitment of inflammatory cells. Aside from local effects, these mediators also produce systemic effects such as fever and the production of acute inflammatory response proteins (Arango Duque and Descoteaux, 2014). The inflammatory response is beneficial for the host when pro-inflammatory cytokines are produced in appropriate amounts, but toxic when produced in an unregulated fashion. For

example, excessive production of the cytokines IL-1 $\beta$  and tumour necrosis factor (TNF) $\alpha$  triggers an acute generalized inflammatory response seen in septic shock and multi-organ failure (Arango Duque and Descoteaux, 2014). Anti-inflammatory cytokines control the pro-inflammatory cytokine response.

Chemokines derive their name from their functional role in chemotaxis. In acute inflammation they drive leucocyte recruitment to inflammatory foci (Griffith et al., 2014).

Once T cells are recruited to sites of inflammation, macrophages and dendritic cells can instruct the adaptive immune response by degrading the intracellular organism and presenting pathogen-derived major histocompatibility complex (MHC) class II-bound peptides to T cells (Davis et al., 1998). Polarised T cell responses then feedback to macrophages to modulate their effector functions.

<b>Pro-inflammatory</b>	<b>Role</b>
<b>TNF<math>\alpha</math></b>	Key cytokine in host defence, induces bacterial killing in macrophages, induces apoptosis, co-ordination of the acute phase response
<b>IFN<math>\gamma</math></b>	Key cytokine in host defence, promotes antigen presentation, induces autophagy and bacterial killing in macrophages, recruits CD4+ T cells
<b>IL-6</b>	Co-ordination of the acute phase response, stimulates production of neutrophils and monocyte recruitment
<b>IL-1<math>\beta</math></b>	Triggers PGE <sub>2</sub> synthesis & negatively regulates type I IFNs. Recruitment of neutrophils and induction of cytokines/ chemokines
<b>IL-12</b>	With IL-18 induces differentiation of T cells into Th1 cells that produce pro-inflammatory cytokines, DC maturation & migration
<b>IL-18</b>	With IL-12 induces production of IFN $\gamma$ and other cytokines, chemokines and transcription factors. Includes polarisation of Th1 cells
<b>Anti-inflammatory</b>	<b>Role</b>
<b>IL-10</b>	Downregulates IL-12 /TNF- $\alpha$ . Blocks phagosome maturation, inhibits antigen presentation, reduces IFN $\gamma$ activity and inhibits T cell responses, blocks trafficking of DC
<b>IFN<math>\beta</math></b>	Inhibits macrophage functions, suppresses IL-1, IL12 and TNF- $\alpha$ , induces IL-10, blocks macrophage activation by Th1 cells
<b>IL-23</b>	Polarisation of Th17 cells
<b>TGF<math>\beta</math></b>	Inhibits ROS and RNI in macrophages, suppresses proliferation of T cells, induces polarization of regulatory T cells and Th17 cells

Table 1.2 **Macrophage pro- and anti-inflammatory cytokines**

Douge G and Descoteaux D. Macrophage cytokines: involvement in immunity and infectious diseases. *Frontiers in Immunology* (2015)

### 1.1.5 Antimicrobial Actions

Through PRRs and phagocytic receptors, pathogens are internalized by phagocytosis. These pathogens are contained in vacuolar structures known as a phagosome, which undergoes maturation to form the phagolysosome. This is a destructive cytoplasmic body on account of its low pH, which also serves as a medium for hydrolytic enzyme activity (Yates et al., 2005). Phagosomal maturation is governed by a network of small Rab guanosine triphosphate (GTP)ases (Gutierrez, 2013)

Macrophages failing to clear pathogens by phagolysosomal fusion can induce autophagy- a highly conserved degradative process involving membrane-bound vesicles that sequester cytoplasmic organelles and intracellular pathogens into an autophagosome (Lamb et al., 2013). The activation of autophagy induces co-localization of the phagosome with autophagosomes and delivers antimicrobial proteins to autolysosomal compartments (autophagolysosomes), achieving enhanced bactericidal activity. Autophagy is also responsible for the turnover of macromolecules and organelles through lysosomal degradation (Germic et al., 2019), as well as participating in the processing of antigens for MHC class II antigen presentation (Dengjel et al., 2005; Paludan et al., 2005; Schmid et al., 2007).

Another critical host defence response to intracellular infection is for the host cell to die by programmed cell death (apoptosis) pre-emptively before the pathogen can replicate and kill the cell en route to further infection. This is a well-established host response to virus infection (Barber, 2001; Clem and Miller, 1993), but has also been frequently reported following bacterial infection,

resulting in reduced pathogen viability (Behar et al., 2011; Molloy et al., 1994; Nogueira et al., 2009; Oddo et al., 1998).

Apoptosis is morphologically characterized by cell shrinking, fragmentation of the nucleus, formation of membrane blebs, and apoptotic bodies (Srinivasan et al., 2014). Two pathways for apoptosis exist- the 'extrinsic' pathway driven by Fas ligand and caspase 8 (Itoh et al., 1991; Nagata and Tanaka, 2017), and the 'intrinsic pathway' governed by B cell lymphoma (BCL)-2 (Patterson et al., 2000) and caspase 9 (Nagata and Tanaka, 2017; Patterson et al., 2000). In their landmark article on apoptosis, Kerr et al found that although large numbers of cells die by this process, no inflammation or tissue destruction is observed (Kerr et al., 1972). They found that almost all of the dead cells were inside histiocytes, indicating that apoptotic cells are quickly engulfed by phagocytes, subsequently termed 'efferocytosis'. Therefore apoptosis and efferocytosis are thought to be immunologically silent and provoke less inflammation than other forms of cellular death, such as necrosis (Szondy et al., 2017).

Two of the most important antimicrobial systems of phagocytic cells are the Nicotinamide adenine dinucleotide phosphate (NADPH) phagocyte oxidase and inducible nitric oxide synthase (iNOS) pathways, which are responsible for the generation of superoxide and nitric oxide (NO) radicals, respectively (Fang, 2004). Although these systems both depend on NADPH and molecular oxygen, and sometimes function together, the NADPH phagocyte oxidase and iNOS are separate enzyme complexes with independent regulation (Fang, 2004). Superoxide and other oxygen intermediates are collectively known as reactive oxygen species (ROS), whereas NO and its derivatives are collectively known as

reactive nitrogen species (RNS).

ROS and RNS are directly toxic to intracellular pathogens. The main mechanism of ROS-dependent antibacterial activity is DNA damage (Imlay and Linn, 1988). RNS inhibit respiration as well as interfering with DNA replication. Both ROS and RNS can target microbial thiols, metal centres, protein tyrosines, and lipids (Nathan and Shiloh, 2000). The role of iNOS in pathogen clearance in murine macrophages is well-established, but evidence for this pathway in human macrophages is less clear (Nathan, 2002).

Inflammasome assembly activates caspase-1 and subsequently pyroptosis, a form of cell death that is important to clearing infection by removing the replicative niche for some intracellular pathogens (Bergsbaken et al., 2009; Man et al., 2017). Inflammasome assembly also promotes secretion of the highly pro-inflammatory cytokines IL-1 $\beta$  and IL-18 (Guo et al., 2015; Ting et al., 2008), both of which have been shown to have a protective function in various bacterial, viral and fungal infections (Sahoo et al., 2011). IL-18 is thought to exert its protective effects via the induction of IFN $\gamma$  which potentiates the microbicidal activity of macrophages (Sahoo et al., 2011). IL-1 $\beta$  has an important role in the recruitment of other immune cells including neutrophils, as well as negatively regulating Type 1 IFNs, which have a detrimental role in several bacterial infections (Boxx and Cheng, 2016).

Another layer of macrophage defence occurs via antimicrobial peptides (AMPs). These have direct antimicrobial activity, as well as functioning as chemoattractants (Niyonsaba et al., 2004) and DC activators (Biragyn et al., 2002). The two main AMP families are defensins and cathelicidins. Most AMP

peptides act by damaging microbial membranes (Zasloff, 2002). This is suggested to be achieved by electrostatic interactions with the polar head groups of membrane lipids (Hoover et al., 2000) or through the creation of membrane pores (Ganz, 2003). AMPs exhibit a wide range of microbial targets including bacteria, fungi and parasites (Giacometti et al., 1999; Shin et al., 2000; Zanetti, 2004) Specifically, the antimicrobial peptide, cathelicidin, has been shown to have broad-spectrum activity against Gram-positive and Gram-negative microorganisms (Bals et al., 1998), as well as mycobacteria (covered in greater detail in **section 1.3.1**)

## **1.2 Tuberculosis**

---

### **1.2.1 Epidemiology and Clinical Course of Tuberculosis**

Tuberculosis (TB) is a communicable infectious disease, transmitted by cough aerosols containing Mtb bacilli. Although global tuberculosis incidence has slowly declined at a rate of 3% per year (World Health Organization, 2017), its impact remains considerable; it is the seventh leading cause of death worldwide. In 2019 there were approximately 10 million new cases and 1.4 million deaths from TB disease (World Health Organization, 2020). However, the status of TB as the leading cause from a single infectious agent may now be superseded; the global pandemic of COVID-19 (caused by the infectious agent Severe Acute Respiratory Syndrome-Coronavirus-2, SARS-CoV-2) caused 2.5million deaths worldwide in 2020 alone (World Health Organization, 2021).

Exposure to Mtb results in a spectrum of clinical outcomes including primary progressive disease and latent Mtb infection (LTBI) (Möller et al., 2010; Pai et al., 2016). LTBI is defined as immunological memory (as evidenced by positive

Interferon Gamma Release Assay (IGRA) or Tuberculin Skin Test (TST)) to Mtb antigens but no clinical symptoms of active tuberculosis disease. It has long been thought that in individuals with latent disease, the bacilli were not cleared but instead persisted in a dormant state from which they would reactivate at later stages (Tufariello et al., 2003). In fact, recent epidemiological analyses have suggested that between 1% and 11% of people with TB immunoreactivity continue to harbour viable bacteria capable of causing disease (Behr et al., 2019). In the remainder the bacilli are likely cleared or exist in a non-pathogenic state. As a result, a small proportion of individuals (~5-10% lifetime risk) progress to develop active disease, typically within the first two years after exposure (Behr et al., 2018).

Results of studies in non-human primates and humans have recently highlighted the spectrum of biological states encompassed by the term 'LTBI'. Necropsy of cynomolgus macaques with latent disease has demonstrated a striking range of active lesions with bacterial replication, to sterile granulomas and infected lymph nodes, all in individual animals (Lin et al., 2014). Positron emission tomography (PET) combined with computed tomography (PET/CT) imaging in 35 adults with 'LTBI' and asymptomatic HIV-1 infection revealed a spectrum of abnormal lesions in the lungs of 25 individuals, 10 of which had imaging indicative of active disease, with a high chance of disease progression. These data illustrate the complex phenotypes encompassed by the term 'LTBI'. (Möller et al., 2018, 2010; Pai et al., 2016).

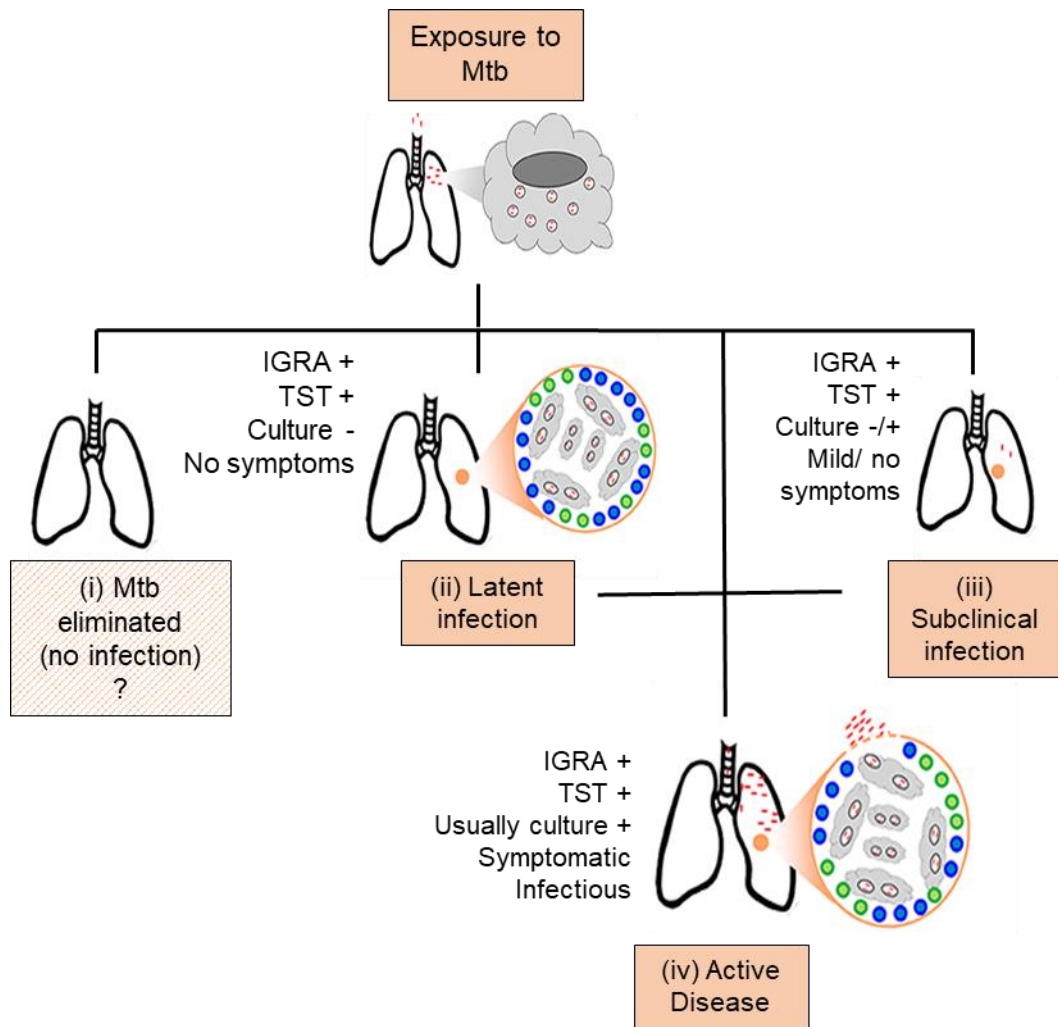


Figure 1.1 **Spectrum of Mtb infection and outcomes.** The bacteria enter the respiratory system of the host via inhaled droplets and are engulfed by macrophages. There are four potential outcomes after bacterial inhalation: (i) Mtb is immediately eliminated by the pulmonary immune system, though it remains unclear if this actually occurs (ii) the bacteria are contained in granulomas by recruited adaptive immune cells and infection does not progress to active TB. Although this containment can last for a lifetime, in some patients reactivation or reinfection with another mycobacterial strain can occur, resulting in active TB (iii) subclinical infection characterized by intermittent symptoms and periodic infectiousness, or (iv) infection develops into active TB.

Adapted from Pai M. Tuberculosis. Nature Reviews Disease Primers (2016); Moller M. Past, present and future directions in human genetic susceptibility to tuberculosis. FEMS Immunol Med Microbiol. (2010); Moller M. Genetic Resistance to Mycobacterium Tuberculosis infection and disease. Front. Immunol (2018)

In most cases, the reason for reactivation from 'latent' to active disease remains poorly understood. Some risk factors related to a failure of immune control measures have been well described, the most striking of which is co-infection with HIV that increases risk of active TB by ~20 fold (World Health Organization, 2011). Diabetes is associated with an approximate three-times increase (Jeon and Murray, 2008). Immunosuppressive drugs such as corticosteroids (Jick et al., 2006), and TNF $\alpha$  antagonists for the treatment of rheumatological disorders are also associated with additive risk (Zhang et al., 2017).

Active TB disease is accompanied by active bacterial replication and high bacillary load. TB is characterised by pulmonary consolidation in the well aerated lung apices, and if untreated, the chronic inflammatory response results in destruction of lung tissue with consequent cavitation (Elkington, 2013). Extra-pulmonary involvement of virtually any organ can occur likely due to haematogenous spread; tuberculous meningitis and disseminated disease are particularly severe manifestations of infection.

### **1.2.2 Mycobacterium Tuberculosis**

Mtb is an aerobic, non-motile, acid-fast bacteria that appears rod shaped, 1-10 $\mu$ m in length and 0.2-0.6 $\mu$ m in diameter (Pfyffer and Palicova, 2011). These bacteria have a highly unique and complex cell wall structure composed of proteins, lipids and long-chain mycolic acids that are covalently linked to peptidoglycan via an arabinogalactan network (Brennan, 2003; Hoffmann et al., 2008). The thick, hydrophobic cell wall structure provides Mtb with an efficient permeability barrier to harmful compounds, resistance to degradation from lysosomal enzymes, and contributes to the high intrinsic resistance of Mtb to many drugs (Brennan, 2003).

Loss of various mycobacterial cell wall components is associated with decreased virulence, suggesting the pathogen's cell wall is crucial to ensuring its survival (Dubnau et al., 2000; Glickman et al., 2000; Rao et al., 2005).

### **1.2.3 Overview of the Immune Response to Mtb**

#### *1.2.3.1 Early Events Following Mtb Infection*

After inhalation, Mtb rapidly reaches the lung's alveolar space where it is preferentially taken up by alveolar macrophages (Armstrong and Hart, 1975; Cohen et al., 2018). Mtb has also been shown to be ingested by, and replicate within, epithelial Type II pneumocytes *ex vivo* (Bermudez and Goodman, 1996; Harriff et al., 2014; McDonough and Kress, 1995). DCs are also able to phagocytose Mtb, and play an important role in the early host response to infection due to their antigen presenting capacity in activating T cells (Banchereau and Steinman, 1998).

The entry of Mtb into macrophages may occur via a variety of different receptors (Ernst, 1998) including complement receptors (CR1, CR3, CR4) (Malik et al., 2000; Schlesinger et al., 1990), mannose receptors (MR) (Kang et al., 2005; Schlesinger et al., 1994), the dendritic cell-specific intercellular adhesion molecule (ICAM)-3-grabbing nonintergrin (DC-SIGN) (Lugo-Villarino et al., 2018), surfactant protein receptors (SPR) (Downing et al., 1995), scavenger receptors (SR) (Zimmerli et al., 1996) and Fc receptors (FcR) (Caron and Hall, 1998). The precise receptor involved in phagocytic entry into the cell may have an impact on the fate of Mtb once inside the macrophage (Pieters, 2008). For example, FcR ligation is accompanied by the activation of the respiratory burst, and production of arachidonic acid metabolites and cytokines, such as TNF $\alpha$  (Caron and Hall,

1998; Gresham et al., 1988; Hmama et al., 2015). However, binding of opsonized bacteria to the CR does not trigger a respiratory burst or even inflammatory signals (Caron and Hall, 1998; Gresham et al., 1988; Schäfer et al., 2009). Engagement of the MR during the phagocytic process is a key step in limiting phagolysosomal fusion that would ultimately lead to Mtb degradation (Kang et al., 2005).

On entry into a host macrophage, Mtb initially resides in an endocytic vacuole called the phagosome (Queval et al., 2017). If phagosomal maturation occurs, these bacteria can encounter a hostile environment that includes acidic pH in the phagolysosome, ROS, lysosomal enzymes, and toxic peptides. RNIs produced by activated mouse macrophages are major elements in antimycobacterial activity (Nathan, 2002; Nathan and Hibbs, 1991), and mice with mutations in the gene encoding iNOS are more susceptible to TB (MacMicking et al., 1997). The presence of RNIs in human macrophages and their potential role in disease has been the subject of some controversy.

Mtb has co evolved with its host to persist within macrophages for years without being completely cleared by the host immune system (Höner zu Bentrup and Russell, 2001). Inside the hostile environment of the macrophage, Mtb is able to co-ordinate its global gene expression patterns in a way that suits its intracellular survival (Rohde et al., 2012). The strategies by which Mtb subverts macrophage defences will be covered in greater detail in **section 1.3.2**.

#### *1.2.3.2 The granuloma as a host protective and pathogenic structure*

Phagocytosis of Mtb by AMs and DCs initiates a cascade of events involving the production of cytokines and chemokines, which stimulate the activation of

phagocyte anti-microbial activities and recruitment of CD4<sup>+</sup> and CD8<sup>+</sup> T cells, natural killer cells and neutrophils to the site of infection. The accumulation of mononuclear leukocytes around foci of infected cells leads to the formation of a macrophage-rich cell mass known as the granuloma. Over time, the granuloma takes on a more organized form, exhibiting the following structure: a central acellular necrotic core, termed the caseum, surrounded by a diverse population of macrophages including epithelioid cell, multinucleated giant cell (Helming and Gordon, 2007) and foamy cell (Russell et al., 2009) phenotypes. This is circumscribed by a lymphocytic cuff of CD4<sup>+</sup> and CD8<sup>+</sup> T cells and B cells, and may have a peripheral fibrotic edge (Ramakrishnan, 2012; Russell et al., 2009).

Granulomas have long been thought of as protective structures, containing bacteria and preventing their dissemination. Indeed, there is an association between hypersusceptibility to Mtb infection, and poorly formed granulomas. Disorganised granuloma occur in immunocompromised individuals with deficiencies of TNF $\alpha$  (Clay et al., 2008; Flynn et al., 1995), IFN $\gamma$  (Cooper et al., 1993), IL-12 (Cooper et al., 1997), and in those with advanced HIV disease (Diedrich et al., 2016; Nusbaum et al., 2016). Further evidence for the granuloma as a host protective structure is inferred from the fact that there is rapid bacterial growth in the initial period following infection, which plateaus after the onset of adaptive immunity and mature granuloma formation (Desvignes and Ernst, 2009; Moguees et al., 2001; Russell et al., 2010a; Saunders et al., 2002). However, evidence from zebrafish models suggest that granulomas may actually contribute to early Mtb proliferation and dissemination.

Zebrafish models of Mtb infection have shed light on the early events in disease

pathogenesis following infection of macrophages. Infection of zebrafish is with *Mm* rather than *Mtb*, but this species is the closest non tuberculous relative of the *Mtb* complex, and a natural fish pathogen. In addition, zebrafish larvae are optically transparent, allowing researchers to directly observe the process of active infection in real time (Davis et al., 2002).

In zebrafish larvae, following phagocytosis by macrophages, *Mm* harbouring the Region of Difference (RD)-1 locus (encoding several virulence factors) drives the recruitment of monocyte/ macrophages to the site of infection (Volkman et al., 2004). Recruited monocytes are more permissive to *Mtb* replication (Cambier et al., 2017) and also engulf infected dying cells, facilitating the spread of infection to new cells (Davis and Ramakrishnan, 2009). The primary granuloma then seeds secondary granulomas through the migration of infected cells (Davis and Ramakrishnan, 2009). Mycobacterial virulence protein 6 kDa early secretory antigenic target (ESAT-6) induces the secretion of host matrix metalloproteinase-9 (MMP-9) by epithelial cells which also drives the recruitment of new macrophages into the granuloma (Volkman et al., 2004). Reprogramming of the adhesion pathways that are dependent on epithelial cadherin result in disordered granuloma formation (Cronan et al., 2016) normally associated with bacterial clearance, further supporting a role for the granuloma in contributing to disease pathogenesis (Cronan et al., 2016).

Recent studies using both macaques (Capuano et al., 2003; Lin et al., 2014, 2006) and rabbits with TB (Via et al., 2012), as well as surgically resected tissue from humans (Marakalala et al., 2016) suggest that several types of granuloma with different characteristics co-exist in active TB disease. These granuloma are

localized microenvironments that have differing trajectories (Cadena et al., 2017; Lin et al., 2014, 2009). For example, macaques with clinically active disease have both sterile granulomas and regions of severe pathology with very different profiles of bacterial killing. These findings shift the view of host control from a systemic response to a localized response within individual granulomas (Cadena et al., 2017). The mechanisms that establish diverging granuloma fates are unclear, but involve complex interactions between tissue inflammation, balanced host immune responses (**section 1.2.3.4**) and bacterial factors (Cadena et al., 2017).

#### *1.2.3.3 Induction of T Cell Responses*

Induction of T cell responses immunity to Mtb is thought to be slow (Reiley et al., 2008; Wolf et al., 2008), perhaps due to Mtb's ability to actively modulate antigen presentation (Gercken et al., 1994; Hmama et al., 2015; Noss et al., 2001). In mouse models, Mtb grows progressively in the lungs for ~20 days prior to the arrival of antigen specific T cells, which coincides with a plateau in bacterial replication (Wolf et al., 2008). When Th1 CD4<sup>+</sup> T cells are presented with antigens in the context of MHC Class II, they produce pro-inflammatory cytokines such as IFN $\gamma$ , TNF $\alpha$  and IL-12, which help to restrict mycobacterial growth (Cooper, 2009). In contrast Th2 CD4<sup>+</sup> T cells induce an alternative immune response including production of IL-4 and IL-10. These, together with regulatory T cells may dampen the host response and reduce the bactericidal capacity of macrophages (Cardona and Cardona, 2019; Fiorentino et al., 1991; Mosser and Edwards, 2008; O'Leary et al., 2011).

That CD4<sup>+</sup> T cells are critical mediators of anti-tuberculous immunity has been

shown in mice antibody depleted of CD4 T cells, and those deficient in the CD4 molecule (Caruso et al., 1999; Moguees et al., 2001; Scanga et al., 2000). Mtb infection following depletion of CD4<sup>+</sup> T cells in cynomolgus macaques results in severe exacerbation of primary TB with increased extrapulmonary spread and mycobacterial burden (Lin et al., 2012). The relevance of these studies to the human condition is demonstrated by the observation that HIV-mediated loss of CD4<sup>+</sup> T cell renders patients susceptible to tuberculosis (Geldmacher et al., 2010). The protection afforded to the host by CD4<sup>+</sup> T cells is presumed to be mediated primarily by IFN $\gamma$ .

IFN $\gamma$  is a potent activator of macrophage function, and genetic defects of the IL-12 and IFN $\gamma$  signalling axis cause Mendelian susceptibility to mycobacterial diseases (MSMD), in which patients present with severe infections caused by both weakly virulent mycobacteria and Mtb (Al-Muhsen and Casanova, 2008). Individuals with mutations in the IFN $\gamma$  receptor and its key downstream signalling molecule Signal Transducer And Activator Of Transcription (STAT) 1 are extremely susceptible to mycobacterial infections (Dorman and Holland, 1998; Jouanguy et al., 1999).

However, whether CD4<sup>+</sup> T cells and its effector cytokines are sufficient for protection is unclear, and the means by which they mediate this protection are still not defined (Sakai et al., 2014). The fact that most individuals exposed to TB, including those with active disease, develop a TB-specific Th1 response as evidenced by positive IFN $\gamma$  release assays (IGRAs) and tuberculin skin tests (TSTs) demonstrates that although a Th1 response is necessary for protection against TB, it is not sufficient for protection.

Mtb-specific CD8<sup>+</sup> T cells are also being increasingly recognized for their role in anti-tuberculous immunity. They recognize Mtb-infected macrophages (Kamath et al., 2004; Lazarevic and Flynn, 2002) and are present in granulomas (Gideon et al., 2015; Lin et al., 2009, 2006). Cytotoxic activity of CD8<sup>+</sup> T cells includes direct killing of Mtb via the AMPs perforin and granulysin, as well as inducing apoptosis of infected cells via the Fas-FasL pathway (S. Stenger et al., 1998; Stenger et al., 1997). Further *in vivo* evidence for the importance of CD8<sup>+</sup> T cells comes from the non-human primate model, where rhesus macaques depleted of CD8<sup>+</sup> T cells and challenged with high dose Mtb are no longer partially protected by Mycobacterium Bovis bacillus Calmette-Guérin (BCG) vaccination (Chen et al., 2009)

#### *1.2.3.4 The Importance of a Balanced Immune Response*

The exact immune components that constitute protection following Mtb infection have remained elusive. However, experimental studies have recently suggested that it is the presence of a dynamic balance between a pro- and anti-inflammatory response that is necessary for achieving proper granuloma formation and control of Mtb (Cadena et al., 2016; Flynn et al., 2011; Lerner et al., 2015; Lin et al., 2006; Marakalala et al., 2016; Marino et al., 2015). Skewing towards a robust pro-inflammatory response may lead to enhanced killing of Mtb, but is also responsible for much of the pathophysiology seen in TB disease, including necrosis, liquefaction, cavity formation and destruction of the lung parenchyma (Cadena et al., 2017). It is essential that the infected host controls this inflammatory reaction with an opposing anti-inflammatory response. Anti-inflammatory cytokines such as IL-10 and TGF- $\beta$ , and cells such as regulatory T cells likely play roles in this counterbalance.

The need for a balanced immune response is further exemplified by investigations into the role of TNF $\alpha$  in the zebrafish Mm model, in which it is demonstrated that either too little or too much production of TNF $\alpha$  can drive disease, whereas the “just-right” amount of TNF $\alpha$  is protective (Roca and Ramakrishnan, 2013; Tobin et al., 2012) – a so-called “Goldilocks effect”. The downstream effects of either low or high TNF $\alpha$  result in macrophage necrosis and uncontrolled extracellular replication of bacteria (Roca and Ramakrishnan, 2013), and the potential relevance of this phenotype to human TB has been confirmed via genetic studies of homologues of implicated factors (Tobin et al., 2012). TNF $\alpha$  dysregulation in this zebrafish model is caused by lipid mediators such as leukotrienes and eicosanoids (Tobin et al., 2012). In the mouse model, a balance of pro-inflammatory IL-1 and anti-inflammatory Type 1 IFN responses controls the outcome of TB disease and is also functionally linked to eicosanoids (Mayer-Barber et al., 2014).

Overall, these investigations have begun to describe a system in which the early granuloma may facilitate replication and dissemination of infection. The ensuing cell mediated response driven by T cells and IFN $\gamma$  is protective, but only in the context of a cytokine milieu which allows macrophages to appropriately regulate the burden of inflammation caused by this response, while also ensuring it can sterilize the pathogen. Aberrant or absent immunoregulation, within the same patient, and perhaps even within a single granuloma, is then suggested to lead to active TB disease characterized by bacterial growth and immunopathology (**Figure 1.2 The inflammatory seesaw of tuberculosis**. Infection by Mtb can result in different disease states depending on the host response. When a pro-inflammatory response predominates, excessive granuloma formation and

necrosis occur. At the other extreme, when the anti-inflammatory response predominates, granulomas are poorly formed, macrophages are less likely to be activated, and bacterial replication is not well controlled, also resulting in active TB. When pro- and anti-inflammatory forces are optimally balanced, granulomas are well structured and controlled with activated macrophages capable of restricting bacterial proliferation, resulting in latent infection or bacterial clearance.

Adapted from Scanga C. Mycobacterial Infections and the Inflammatory Seesaw. *Cell Host and Microbe* 2010; Cadena A. Heterogeneity in Tuberculosis. *Nature Reviews Immunology* 2017

**Figure 1.3 Mechanisms by which Mtb subverts macrophage defences**

1. The type of receptor that mediates phagocytosis can prevent activation of the macrophage.
2. Mtb blocks phagolysosomal fusion.
3. Mtb can block autophagy.
4. Mtb can translocate from the phagosome into the cytosol where it can further replicate, as well as stimulating the release of Type 1 IFNs that promote its survival.
5. Mtb can modify signalling via PRRs that would otherwise lead to macrophage activation and killing, for example, via NFκB
6. Mtb can inhibit antigen presentation to impair recognition by T cells.
7. Mtb can block apoptosis that would result in bacterial killing.

Figure 1.2)

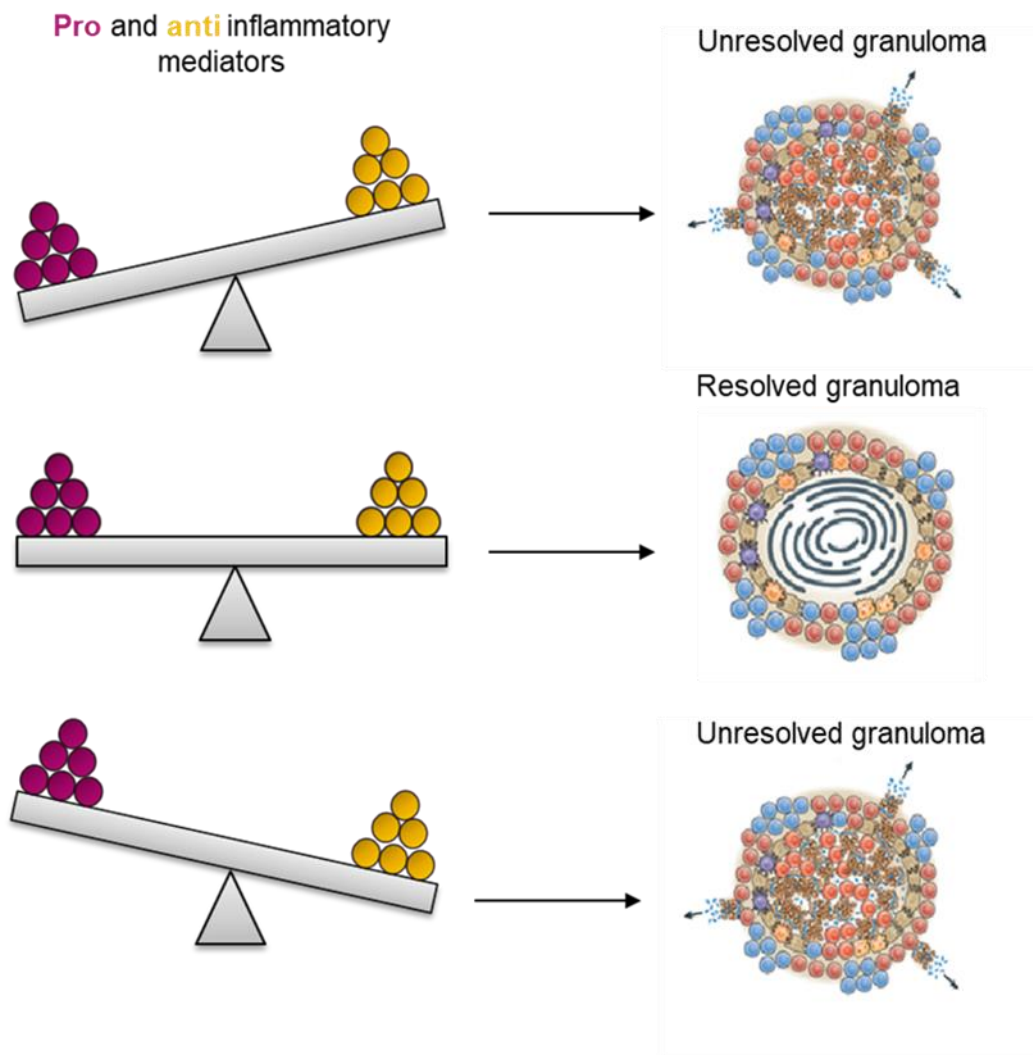


Figure 1.4 **The inflammatory seesaw of tuberculosis.** Infection by Mtb can result in different disease states depending on the host response. When a pro-inflammatory response predominates, excessive granuloma formation and necrosis occur. At the other extreme, when the anti-inflammatory response predominates, granulomas are poorly formed, macrophages are less likely to be activated, and bacterial replication is not well controlled, also resulting in active TB. When pro- and anti-inflammatory forces are optimally balanced, granulomas are well structured and controlled with activated macrophages capable of restricting bacterial proliferation, resulting in latent infection or bacterial clearance.

Adapted from Scanga C. Mycobacterial Infections and the Inflammatory Seesaw. *Cell Host and Microbe* 2010; Cadena A. Heterogeneity in Tuberculosis. *Nature Reviews Immunology* 2017

### **1.3 Macrophages and Mycobacterium Tuberculosis**

---

As has been described in the preceding sections, TB is a complex disease with a spectrum of disease states. Most humans who are exposed do not become diseased, but exposure to the pathogen does result in the development of T cell memory to Mtb antigens. This suggests some degree of immune mediated microbial control in the majority of people. The alveolar macrophage response in Mtb infection is critical because it is the target cell for early infection (Cohen et al., 2018), and a major reservoir for productive infection (Cohen et al., 2018). Despite this, macrophages are also primary effector cells against intracellular Mtb; they have been shown to display some bactericidal activity, drive both the pro and anti-inflammatory response, and instruct T cell mediated immunity.

#### **1.3.1 Macrophage Restriction of Mtb**

Macrophages are key to achieving restriction of Mtb growth- models associated with a reduction in macrophage numbers (Clay et al., 2007), increased macrophage death (Clay et al., 2008; Roca and Ramakrishnan, 2013) or delayed macrophage recruitment (Davis and Ramakrishnan, 2009) are all associated with greater mycobacterial growth. Further, genetic deficiencies of interleukin IL-12 and IFN $\gamma$  dependent pathways that function to enhance antimicrobial pathways in macrophages, cause substantially increased susceptibility to mycobacterial infection (Casanova and Abel, 2002; Cooper et al., 1997, 1993; Dorman et al., 2004).

IFN $\gamma$  is reported as the archetypal cytokine that modulates macrophage function and enhances microbial killing. Murine macrophage studies clearly show that

IFN $\gamma$  induces Mtb killing via the generation of RNIs (Denis, 1991; Flynn, 1993). RNIs are critical to antimycobacterial activity in mice (Nathan, 2002; Nathan and Hibbs, 1991). Though they play a less established role in humans, the alveolar macrophages of a majority of TB-infected patients have also been shown to exhibit iNOS activity (Nicholson et al., 1996), so RNIs are likely to be involved, to some degree, in human macrophage restriction of Mtb.

Aside from the generation of RNIs, the other mechanisms by which IFN $\gamma$  elicits Mtb restriction in human macrophages remains controversial (Douvas et al., 1985; Rook et al., 1986; Warwick-Davies et al., 1994). One landmark study showed that IFN $\gamma$  can enhance autophagy, phagosomal maturation, the production of antimicrobial peptides such as cathelicidin, to restrict Mtb growth via a vitamin D–dependent pathway (Fabri et al., 2011). In the presence of specific culture conditions for human macrophages, such as physiological O $_2$  levels and GM-CSF, IFN $\gamma$  has also been shown to mediate antimycobacterial activity (Vogt and Nathan, 2011).

Vitamin D has long been thought important in the defence against Mtb. Vitamin D has no direct antimicrobial activity but its active metabolite 1,25(OH) $_2$ D $_3$  is able to control Mtb proliferation in human monocytes and macrophages (Crowle and Ross, 1989; Rook et al., 1986). It is possible that the antimycobacterial effect is due to the AMP cathelicidin, since 1,25(OH) $_2$ D $_3$  induces the colocalization of mycobacterial phagosomes with autophagosomes in a LL-37 (the active metabolite of cathelicidin) dependent manner (Yuk et al., 2009). Addition of exogenous LL-37 to macrophages can significantly reduce the intracellular survival of Mtb (Martineau et al., 2007; Sonawane et al., 2011). Furthermore,

activation of TLRs by Mtb triggers a Vitamin D dependent pathway, the induction of cathelicidin and direct killing activity (Liu et al., 2006; Thoma-Uszynski et al., 2001). Consistent with these observations, siRNA against cathelicidin has been shown to inhibit antimicrobial activity and enhance intracellular growth of the bacilli (Liu et al., 2007).

Another macrophage function that has come to the fore with regard to anti-mycobacterial activity in recent years is autophagy. Although Mtb displays some countermeasures against autophagy (**section 1.3.2.2**), this mode of killing has been shown to reduce Mtb survival in human macrophages, mouse models and macrophage cell lines (Fabri et al., 2011; Ponpuak et al., 2010; Watson et al., 2012). Activation of autophagy results in the delivery of Mtb to autolysosomes, which are much more robust antimicrobial compartments than conventional phagosomes (Ponpuak et al., 2010). Autophagy also triggers the generation of neo-antimicrobial peptides, to enhance mycobacterial killing (Alonso et al., 2007; Ponpuak et al., 2010). Autophagy by macrophages can be activated by IFN $\gamma$  (Fabri et al., 2011; Klug-Micu et al., 2013; MacMicking et al., 2003), 1,25(OH) $_2$ D $_3$  (Fabri et al., 2011), Vitamin D receptor and TLR signalling (Shin et al., 2010b), Mtb- specific T cells (Petruccioli et al., 2012), and extracellular vesicles released by neutrophils (Alvarez-Jiménez et al., 2018). (Bonilla et al., 2013). Recognition of extracellular Mtb deoxyribonucleic acid (DNA) by the Stimulator of interferon genes (STING) cytosolic pathway has also been shown to induce the ubiquitin mediated autophagy pathway (Watson et al., 2012).

In keeping with these *in vitro* observations, autophagy protects *in vivo* against bacillary burden, inflammation, lung pathology, and death from Mtb in mice with

autophagy defective myeloid cells (Castillo et al, 2012). Zebrafish embryos deficient in the autophagy inducer DNA damage regulated autophagy modulator (DRAM1) also show increased mycobacterial load (van der Vaart et al., 2014).

### **1.3.2 Mtb Subversion of Macrophage Defences**

Through pro-longed coevolution with its host, Mtb has developed its own mechanisms to subvert macrophage defences and persist within the cell. A summary of these mechanisms is provided in **Figure 1.3 Mechanisms by which Mtb subverts macrophage defences**

1. The type of receptor that mediates phagocytosis can prevent activation of the macrophage.
2. Mtb blocks phagolysosomal fusion.
3. Mtb can block autophagy.
4. Mtb can translocate from the phagosome into the cytosol where it can further replicate, as well as stimulating the release of Type 1 IFNs that promote its survival.
5. Mtb can modify signalling via PRRs that would otherwise lead to macrophage activation and killing, for example, via NF $\kappa$ B.
6. Mtb can inhibit antigen presentation to impair recognition by T cells.
7. Mtb can block apoptosis that would result in bacterial killing.

**Figure 1.4 Pathogenic lifecycle of Mtb.** Mtb infection initiates when fine aerosol particles containing the bacteria coughed up by an individual with active disease are deposited in the lungs. The bacteria recruit macrophages to the surface of the lung, which become infected, and serve to transport the bacteria across the lung epithelium to deeper tissues. As adaptive immunity develops, the granuloma can restrict bacterial growth. However, under many circumstances, the infected granuloma macrophages can undergo necrosis, forming a necrotic core that

supports bacterial growth and transmission to the next host. Figure 1.3.

#### *1.3.2.1 Phagolysosomal Fusion*

Following phagocytosis, Mtb is contained in the early endosome/ phagosome, characterized by the presence of Rab5. The departure of Rab5 and acquisition of Rab7 is the key event in transforming the phagosome into a degradative, lysosomal compartment (Via et al., 1997). Mtb arrests the maturation of phagosome at this critical point in its pathway, i.e. the acquisition of Rab 7 (Rink et al., 2005). Mtb also recruits to its phagosome Rab22a (Roberts et al., 2006). Rab22a controls the terminal stages of endosomal recycling and, upon recycling of the necessary reusable components, its change in activation status sends a signal to the trafficking machinery, allowing Rab5 to Rab7 conversion to proceed. The recruitment to, and maintenance of, Rab22a on Mtb phagosomes blocks Rab conversion, thus prohibiting acquisition of Rab7 and blocking subsequent acidification and proteolytic competency of a phagosome (Roberts et al., 2006). Recruitment of Rab20 (Schnettger et al., 2017) and sortilin (Vázquez et al., 2016) to Mtb phagosomes can enhance lysosomal delivery but Mtb is able to evade Rab20 acquisition through its ESAT-6 Secretion System (ESX-1) (Schnettger et al., 2017). Tryptophan-aspartate-containing coat protein (TACO), a host protein normally released from phagosomes prior to fusion with lysosomes, is actively retained by Mtb to prevent phagolysosomal maturation (Jayachandran et al., 2007).

A bacterial factor shown to govern phagosomal arrest is the secreted protein tyrosine phosphatase (PtpA) (Bach et al., 2008; Wong et al., 2011), which binds to, and blocks, subunit H of the macrophage vacuolar-H(+)-ATPase (V-ATPase)

machinery. This multisubunit protein complex in the phagosome membrane is reported to drive luminal acidification (Wong et al., 2011).

Mtb is able to survive inside the phagosome not only by enhancing phagosomal arrest, but also by acquiring nutrients such as iron-loaded transferrin, from early endosomal organelles (Clemens and Horwitz, 1996).

#### *1.3.2.2 Autophagy*

A few reports have also recently revealed that Mtb has evolved immune evasion strategies to counteract the effects of autophagy, thus improving its intracellular survival. Several mycobacterial factors have been implicated including Enhanced intracellular survival (Eis) protein inhibition of ROS generation via the c-Jun N-terminal kinase (JNK) signalling pathway in murine macrophages (Kim et al., 2012; Shin et al., 2010a), the ESX-1 secretion system (Cardenal-Muñoz et al., 2017; Romagnoli et al., 2012) that simultaneously induces autophagy and represses autophagic flux (Cardenal-Muñoz et al., 2017), Mtb proteins PE\_PGRS47 (Saini et al., 2016) and Mannosylated Lipoarabinomannan (ManLAM) (Shui et al., 2011) via as yet undetermined pathways.

Autophagy may also be limited by the manipulation of host factors, for example upregulation of the expression of host anti-autophagic factor Bfl-1/A1 (Kathania et al., 2011) and Coronin 1a (Seto et al., 2012). A genome-wide analysis identified additional host genes involved in autophagy inhibition during Mtb infection (Kumar et al., 2010), though their role remains ill-defined.

#### *1.3.2.3 Phagosomal Egress*

In addition to residing within non-acidified phagosomal compartments, Mtb has

been visualized outside of phagosomal compartments, within the cytoplasm of macrophages. This phenomenon, referred to a 'phagosomal egress' was initially demonstrated by electron microscopy (EM) of infected J774 mouse myeloid cell line, and seemed to be an event related to virulence- BCG was nearly always surrounded by a distinct vacuolar membrane, whereas Mtb H37Rv was only seen in in membrane enclosed vacuoles approximately half of the time, and H37Ra, an avirulent laboratory strain of Mtb displayed an intermediate phenotype (McDonough et al., 1993). These results were subsequently contradicted by Xu et al in primary mouse BMDMs, citing differences in the technical preparation of samples (Xu et al., 1994).

The idea of phagosomal egress of Mtb therefore remained a subject of debate until recently when more definitive evidence was provided in a study by Stamm and colleagues. This demonstrated phagosomal egress of Mm by both EM and confocal microscopy (Stamm et al., 2003). Mm was found free in the cytosol, being propelled by actin tails (Stamm et al., 2003). Second, a study by van der Wel and colleagues in 2007 used sophisticated cryo-electron microscopy to demonstrate the cytosolic presence of Mtb at later stages of infection (van der Wel et al., 2007). Simeone et al subsequently demonstrated cytosolic access of Mtb using a fluorescence resonance energy transfer (FRET) based method (Simeone et al., 2012). In this study, and others (Hagedorn et al., 2009; Houben et al., 2012; Simeone et al., 2015; Stamm et al., 2003; van der Wel et al., 2007), phagosomal egress was dependent on the ESX-1 secretion system and its effector proteins including ESAT-6. BCG does not display such behaviour, owing to the deletion of the RD1 gene set, which contains the ESX-1 secretion system.

These *in vitro* data demonstrating phagosomal egress have been corroborated *in vivo* using an experimental mouse model, where phagosomal membrane disruption occurs as early as 3 hours post infection, and peaks after 2-3 days (Simeone et al., 2015).

Cytoplasmic localization favours more effective suppression of autophagy in the host macrophage (Jamwal et al., 2016). Cytosolic translocation of Mtb also triggers signalling via the mammalian cytosolic DNA sensor cyclic guanosine monophosphate–adenosine monophosphate (cGAMP) synthase cGAS in an ESX-1-dependent manner (Collins et al., 2015; Majlessi and Brosch, 2015; Wassermann et al., 2015). cGAS catalyses the production of cGAMP, which triggers type I IFN (such as IFN- $\beta$ ) production through the stimulator of IFN genes (STING) (Manzanillo et al., 2012; Sun et al., 2013). IFN- $\beta$  promotes bacterial expansion (Manca et al., 2005, 2001; Manzanillo et al., 2012; Mayer-Barber et al., 2011; Stanley et al., 2007), perhaps by suppressing protective IFN $\gamma$  and IL-1 $\beta$  responses (Novikov et al., 2011; Teles et al., 2013)

#### 1.3.2.4 Cell Signalling

Following engagement of Mtb PAMPs by TLRs, the adaptor protein MyD88 and subsequent MAPK signalling are crucial to achieving phagolysosome fusion. However, Mtb LAM can block the activation of MAPK (Knutson et al., 1998). Phthiocerol dimycocerosate (PDIM), another cell wall lipid masks underlying PAMPs to prevent TLR signalling in zebrafish infected with Mm (Cambier et al., 2014) . A related cell wall glycolipid phosphatidylinositol mannosides (PIM), and secreted protein ESAT-6 (or a peptide derived from it) have also been shown to dampen TLR signalling by inhibition of MyD88, preventing NF $\kappa$ B translocation

(Doz et al., 2009; Pathak et al., 2007) and activation of macrophages.

#### 1.3.2.5 Antigen Presentation

Several studies have demonstrated that Mtb infected macrophages express less antigen on their surface, and are deficient in their ability to signal CD4<sup>+</sup> T helper cells and stimulate T cell proliferation (Gercken et al., 1994; Hmama et al., 1998; Noss et al., 2001). Mtb also impairs DC-mediated antigen presentation and the migration of DCs to the draining lymph nodes, thereby affecting the kinetics of adaptive immunity (Wolf et al., 2007). Thus, Mtb can actively modulate antigen presentation to avoid early immune recognition by T cells (Harding and Boom, 2010)

### 1.3.3 Macrophage Cell Death and Tuberculosis

It is apparent that macrophage cell death occurs in TB, as dead or dying macrophages are observed *in vivo* within granulomata (Ramakrishnan, 2012). The mechanisms of macrophage death in TB has been the subject of extensive research, but is inconsistent across different infection models.

Several lines of evidence suggest that macrophage apoptosis in response to mycobacterial infection represents an innate defence, analogous to the established role for apoptosis of virus-infected cells (Barber, 2001). BCG and the attenuated strain Mtb H37Ra are strong apoptosis inducers (Chen et al., 2006; Keane et al., 1997; Molloy et al., 1994; Oddo et al., 1998; Riendeau and Kornfeld, 2003) resulting in the reduced viability of these strains. Furthermore, Mtb infection has been shown to be contained via efferocytosis of apoptotic cells (Martin et al., 2012).

In order to escape macrophage restriction by programmed cell death, a significant body of evidence indicates that Mtb is anti-apoptotic in macrophages, diverting the cell to death by necrosis, and that this process is associated with virulence (Behar et al., 2010; Chen et al., 2008, 2006, 2006; Divangahi et al., 2009; Velmurugan et al., 2007). For example, virulent Mtb H37Rv rather than H37Ra prevents formation of the apoptotic envelope resulting in necrosis rather than apoptosis of the host cell (Gan et al., 2008). H37Rv, but not H37Ra can also cause significant mitochondrial inner membrane damage leading to necrosis (Chen et al., 2006). Macrophage necrosis is more consistently reported at high multiplicity of infection, with 10-25 bacteria representing a burst size threshold (Repasy et al., 2013; Welin et al., 2011). Some Mtb anti-apoptotic genes identified include SecA2 (Hinchey et al., 2007), PtpA (Bach et al., 2008) and nuoG (Velmurugan et al., 2007).

However, the evidence for necrosis induced by virulent Mtb is conflicting. Particularly, when macrophages internalize low numbers of Mtb (<10), the frequency of cell death is similar to that of bystander cells (Mahamed et al., 2017). In addition, some reports show Mtb (Keane et al., 1997; Oddo et al., 1998) , and its virulence factor ESAT-6 (Aguilo et al., 2013; Butler et al., 2012; Martin et al., 2012), have also been shown to induce apoptosis. One study even suggests apoptosis propagates Mtb infection as infected apoptotic cells are engulfed by bystander macrophages (Aguilo et al., 2013).

While the data on the mode of death induced by Mtb is somewhat conflicting, studies do mostly support the prevailing view that apoptosis is a host defence mechanism and reduces bacterial viability, whereas virulent Mtb (in association

with a high bacterial burden) induces necrotic cell death (Behar et al., 2010). Importantly, the association between active TB and necrotic phenotypes in granulomata (Ramakrishnan, 2012) suggests that necrosis may be a particularly host-detrimental process. This cell death modality may confer more benefit to the bacteria, as two recent studies tracking human macrophages by live cell imaging also demonstrated acceleration in bacterial growth within cells undergoing necrosis (Lerner et al., 2017; Mahamed et al., 2017). The dying cells are engulfed by uninfected cells, leading to a macrophage killing cascade, thereby facilitating the survival and spread of Mtb (Mahamed et al., 2017).

Mtb is not an obligate intracellular pathogen, and can survive outside of macrophages (Eum et al., 2010). Importantly in the context of this thesis, uncontrolled intracellular replication in necrotic cells followed by cell lysis may be particularly beneficial for the bacteria because bacteria are released for extracellular propagation. In both the zebrafish and human macrophage *in vitro* model (Clay et al., 2008, 2007; Mahamed et al., 2017), the extracellular environment is extremely growth permissive for Mtb. Specifically in zebrafish, macrophage death and deficiency results in Mtb growing extracellularly with a cording morphology typical of unfettered growth (Clay et al., 2008, 2007).

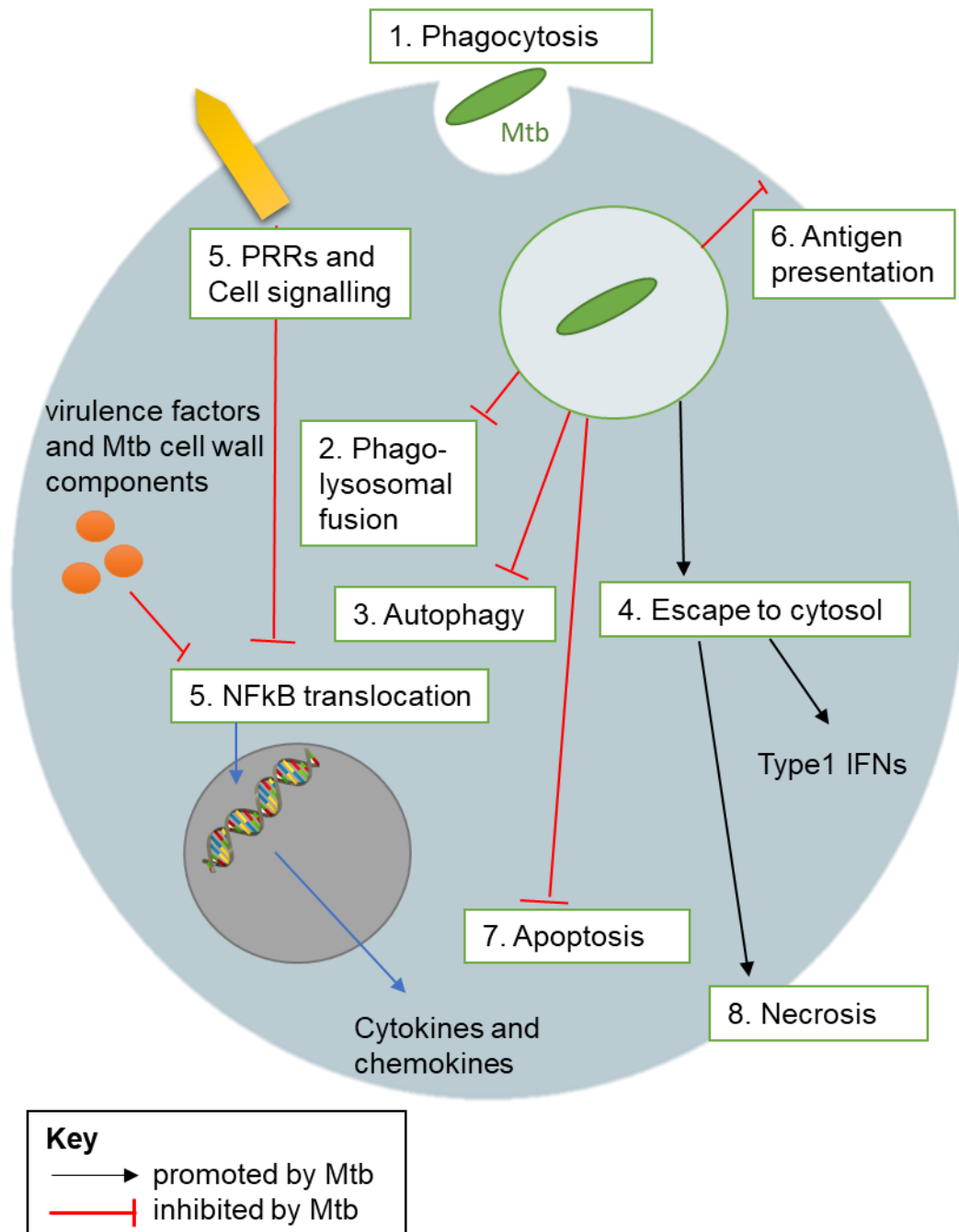


Figure 1.7 **Mechanisms by which Mtb subverts macrophage defences** 1. The type of receptor that mediates phagocytosis can prevent activation of the macrophage. 2. Mtb blocks phagolysosomal fusion. 3. Mtb can block autophagy. 4. Mtb can translocate from the phagosome into the cytosol where it can further replicate, as well as stimulating the release of Type 1 IFNs that promote its survival. 5. Mtb can modify signalling via PRRs that would otherwise lead to macrophage activation and killing, for example, via NFkB 6. Mtb can inhibit antigen presentation to impair recognition by T cells. 7. Mtb can block apoptosis that would result in bacterial killing.

Figure 1.8 **Pathogenic lifecycle of Mtb**. Mtb infection initiates when fine aerosol particles containing the bacteria coughed up by an individual with active disease are deposited in the lungs. The bacteria recruit macrophages to the surface of the lung, which become infected, and serve to transport the bacteria across the lung epithelium to deeper tissues. As adaptive immunity develops, the granuloma can restrict bacterial growth. However, under many circumstances, the infected granuloma macrophages can undergo necrosis, forming a necrotic core that supports bacterial growth and transmission to the next host. Figure 1.9 **Mechanisms by which Mtb subverts macrophage defences** 1. The type of receptor that mediates phagocytosis can prevent activation of the macrophage. 2. Mtb blocks phagolysosomal fusion. 3. Mtb can block autophagy. 4. Mtb can translocate from the phagosome into the cytosol where

## **1.4 Extracellular Mycobacterium Tuberculosis**

---

### **1.4.1 Presence of Extracellular Mtb in Granulomas**

Several significant bodies of work have demonstrated the presence of extracellular bacteria in tuberculous lesions (Lenaerts et al., 2015). Seminal work by Canetti et al conducted in the pre chemotherapy era comprehensively detailed lesion morphology, bacterial number and location from specimens obtained at autopsy of patients with active tuberculosis (Canetti, 1955). Numerous extracellular bacteria were found in necrotic centre of granulomas. More recently, improved immunostaining techniques have successfully demonstrated intracellular as well as free mycobacteria in the biopsies of patients with active tuberculosis (Ulrichs et al., 2005). In a study of six patients with incurable TB disease undergoing surgery histologic examination of lung lesions revealed acid-fast bacilli mainly at the surface of cavities (Kaplan et al., 2003). More recently, a study analyzing the localization of Mtb bacilli in various samples from patients with active TB, found 60% of bacteria located extracellularly in sputum and BAL. Strikingly, 80% of bacteria were located extracellularly in the cavity caseum (Eum et al., 2010).

In rabbits, liquefaction of the caseous necrotic centre of granulomas is associated with extracellular bacterial growth (Dannenbergh and Lurie, 2006); similarly in guinea pigs infected with Mtb, the majority of bacilli in an advanced disease state are found to be extracellular in necrotic lesions (Hoff et al., 2011).

### 1.4.2 Extracellular Mtb in Disease Pathogenesis

An obligate step in all infectious diseases is transmission to new hosts. Mtb can enhance its own transmission by becoming extracellular (Ramakrishnan, 2012). Extracellular bacilli residing within the caseum of necrotic foci (Eum et al., 2010), or the luminal surface of cavities (Kaplan et al., 2003) constitute the reservoir from which large bacterial numbers emerge following connection to patent airways, which facilitates efficient expectoration of the bacteria (Ernst, 2012; Grosset, 2003; Ramakrishnan, 2012) (**Figure 1.4 Pathogenic lifecycle of Mtb.** Mtb infection initiates when fine aerosol particles containing the bacteria coughed up by an individual with active disease are deposited in the lungs. The bacteria recruit macrophages to the surface of the lung, which become infected, and serve to transport the bacteria across the lung epithelium to deeper tissues. As adaptive immunity develops, the granuloma can restrict bacterial growth. However, under many circumstances, the infected granuloma macrophages can undergo necrosis, forming a necrotic core that supports bacterial growth and transmission to the next host.

Taken from Cambier et al. Host Evasion and Exploitation Schemes of Mycobacterium Tuberculosis. Cell (2014)

Figure 1.5 **Intracellular pathogen lytic and non-lytic strategies to exit the host cell.**Figure 1.4).

The exit of intracellular organisms is also a crucial stage of pathogenesis since cellular exit is thought to facilitate spread of infection to neighbouring cells (Behar

et al., 2010; Roca and Ramakrishnan, 2013). Dissemination of infection *can* occur without the transfer of bacteria into the extracellular space. For example, direct cell to cell transfer of Mm in amoeba (Stamm et al., 2003) and zebrafish macrophages (Cambier et al., 2017) has been demonstrated. Mtb has also been demonstrated to move directly between human fibroblasts (Byrd et al., 1998) and an epithelial cell line (Castro-Garza et al., 2002). Nevertheless, as for other organisms which have established an intracellular habitat, escaping out of host cells is an efficient and necessary route to dissemination (Hybiske and Stephens, 2007; Weddle and Agaisse, 2018). Crucially, in amoeba infected with Mm, becoming extracellular by non-lytic ejection (covered in detail in **section 1.4.3**) is directly correlated with spreading infection (Hagedorn et al., 2009).

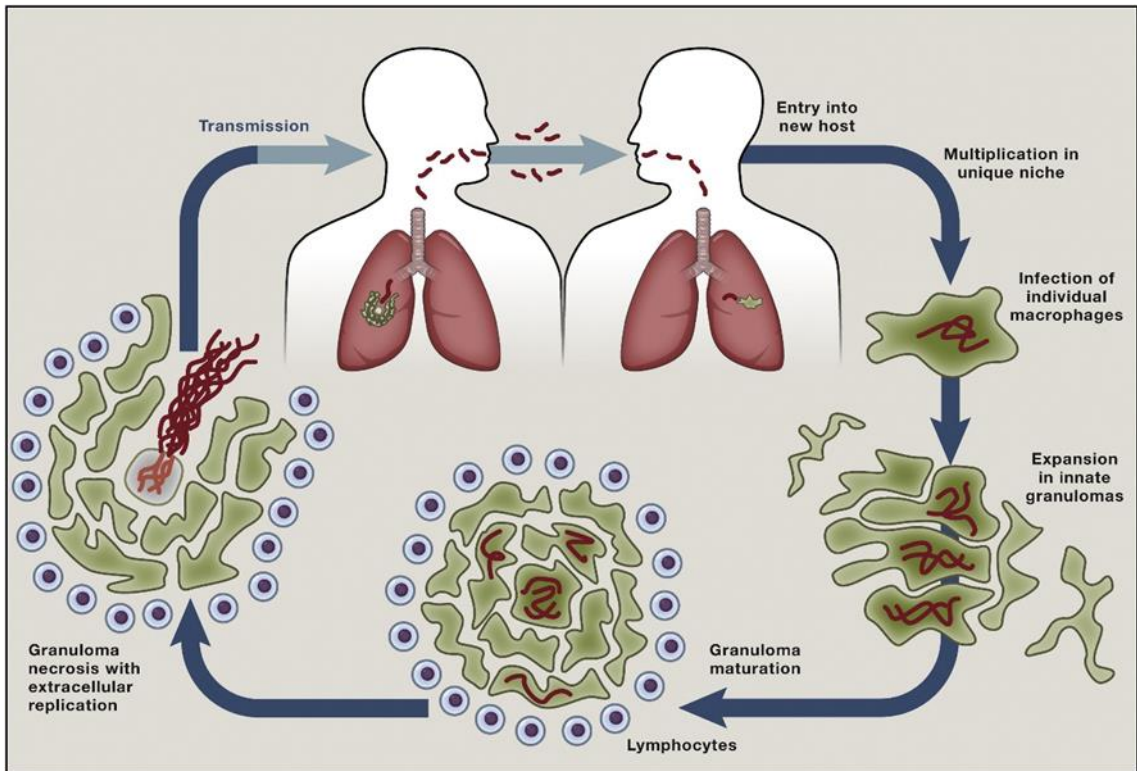


Figure 1.10 **Pathogenic lifecycle of Mtb.** Mtb infection initiates when fine aerosol particles containing the bacteria coughed up by an individual with active disease are deposited in the lungs. The bacteria recruit macrophages to the surface of the lung, which become infected, and serve to transport the bacteria across the lung epithelium to deeper tissues. As adaptive immunity develops, the granuloma can restrict bacterial growth. However, under many circumstances, the infected granuloma macrophages can undergo necrosis, forming a necrotic core that supports bacterial growth and transmission to the next host.

Taken from Cambier et al. Host Evasion and Exploitation Schemes of Mycobacterium Tuberculosis. Cell (2014)

### 1.4.3 Strategies by Which Mycobacteria Become Extracellular

The prevailing view is that extracellular Mtb are thought to arise from cellular necrosis leading to release of mycobacteria, as discussed in **section 1.3.3** Necrosis, rather than apoptosis, allows Mtb to establish a new replicative niche (the extracellular milieu) through the release of intracellular contents following cell lysis.

However, necrosis may not be the only means by which Mtb can escape the hostile intracellular environment of human macrophages. Several organisms have developed versatile strategies for escape (covered in **section 1.4.3**). In fact, although both Mtb and Mm can induce cellular necrosis (as well as pyroptosis), both mycobacteria can also escape out of the host cell in a non-lytic manner. The seminal studies demonstrating the non-lytic exit of mycobacteria were conducted in the social amoeba *Dictyostelium*.

*Dictyostelium* is an alternative macrophage infection model. It is a genetically tractable host for pathogenic mycobacteria (Stamm et al., 2003). Amoeba naturally feed on different soil bacteria and have developed efficient phagocytosis and defence mechanisms. While not a natural host of Mtb, amoeba do interact with other environmental mycobacteria. Since the basic mechanisms of host pathogen interactions are conserved (Stamm et al., 2003), this model is emerging as a useful tool to study the relationship between Mtb and phagocytes.

In amoeba, bacteria are visualized to protrude through a bulging plasma membrane and exit directly into another cell, or into the extracellular space (Hagedorn et al., 2009; Stamm et al., 2003). The host cell is left intact thereafter. Exit of mycobacteria is dependent on vacuolar escape into the cytosol, and

subsequent escape via the plasma membrane via a structure termed the 'ejectosome', dense in F actin, coronin and myosin (Hagedorn et al., 2009). Non-lytic egress is dependent on both host factors (the small GTPase RacH in amoeba) and bacterial factors (ESAT-6) (Hagedorn et al., 2009). Although Mm (but not Mtb) have been observed to harbour actin tails when free in the cytoplasm (Stamm et al., 2003), during egress through the ejectosome the bacteria are not accompanied by actin tails, therefore the forces governing the propulsion of Mm are not yet fully understood. More recent data suggests a role for the autophagic machinery in this process (Gerstenmaier et al., 2015).

Therefore, it is plausible, though never previously described, that both lytic and non-lytic strategies contribute to Mtb becoming extracellular following infection of human macrophages.

#### 1.4.4 Exit Strategies of Other Organisms

One of the first reports of different modes by which intracellular organisms may exit cells was demonstrated with *Chlamydia*, characterized by 2 distinct and independent processes (i) cellular lysis and (ii) a packaged release named extrusion. The latter leaves the host cell intact after release of *Chlamydia*, and involves pinching of the bacterial inclusion, protrusion out of the cell within a cell membrane compartment, and ultimately detachment from the cell. Similarly, *Listeria* and *Shigella* can trigger lytic cell death in the form of pyroptosis, by activation of the Nucleotide-binding oligomerization domain, Leucine rich Repeat and Pyrin domain containing (NLRP)1B inflammasome (Neiman-Zenevich et al., 2017), but also use actin based motility to propel themselves out of the host cell in a non-lytic manner and directly into neighbouring cells (Hybiske and Stephens, 2008). *O. tsutsugamushi* buds out of cells by migrating to the periphery of the cell and slowly extruding from the cell into filamentous structures that protrude from the cell surface (Schaechter et al., 1957). Buds consist of a membranous structure, the outermost of which is the plasma membrane (Schaechter et al., 1957). Little is known about the molecular mechanisms underpinning budding.

Non-lytic expulsion or 'vomocytosis' of *Cryptococcus* was first reported over a decade ago by two separate groups (Alvarez and Casadevall, 2006; Ma et al., 2006). While cryptococci have been found to replicate within macrophages and subsequently induce host cell necrosis for their release (Tucker and Casadevall, 2002), non-lytic expulsion has also been demonstrated by live cell imaging (Johnston and May, 2010; Ma et al., 2006). The molecular mechanisms underpinning the latter process have remained relatively elusive. Non-lytic

expulsion is dependent on live cryptococci since it does not occur with dead organisms (Johnston and May, 2010). Contrary to other organisms that escape leaving the host cell intact, cryptococcal expulsion was in fact found to be inhibited by actin polymerization (Johnston and May, 2010). Recently, in a significant step forward to understanding of the molecular mechanisms underpinning non-lytic expulsion, the atypical MAP/ERK (Extracellular Signal-Regulated Kinase) has been identified as a critical regulator of this process (Gilbert et al., 2017).

Since non-lytic expulsion has been observed for a diverse range of pathogens (Friedrich et al., 2012; Hybiske and Stephens, 2008; Smith and May, 2013) and in phagocytic cells from mammals (Nicola et al., 2011) , birds (Johnston et al., 2016) , fish (Bojarczuk et al., 2016), and amoeba (Hagedorn et al., 2009), it may well be an evolutionary conserved process (Gilbert et al., 2017)

A figure summarizing the diverse repertoire of cytolytic and non-lytic processes by which intracellular organisms exit their host cell is shown in **Figure 1.5 Intracellular pathogen lytic and non-lytic strategies to exit the host cell.**

Adapted from Hybiske K and Stevens R. Exit strategies of intracellular organisms. Nature Reviews Microbiology (2008)

Figure 3.1 **High throughput flow cytometric assay for quantitation of fluorescent Mtb.** **A** Growth curves for Wild Type H37RV and H37Rv mCherry. Bacterial cultures were subpassaged to a starting OD of 0.05, and measured daily thereafter **B** representative flow cytometry plots of H37Rv mCherry and gating strategy to isolate bacterial population from debris and beads (which are fluorescent in all channels) **C** calculation of integrated mCherry Mtb fluorescence

used to enumerate bacteria **D** bacteria were plated and counted by CFU/ml. In parallel, bacteria were analysed by flow cytometry and enumerated by integrated (Int.) mCherry Mtb fluorescence. Figure 1.5.

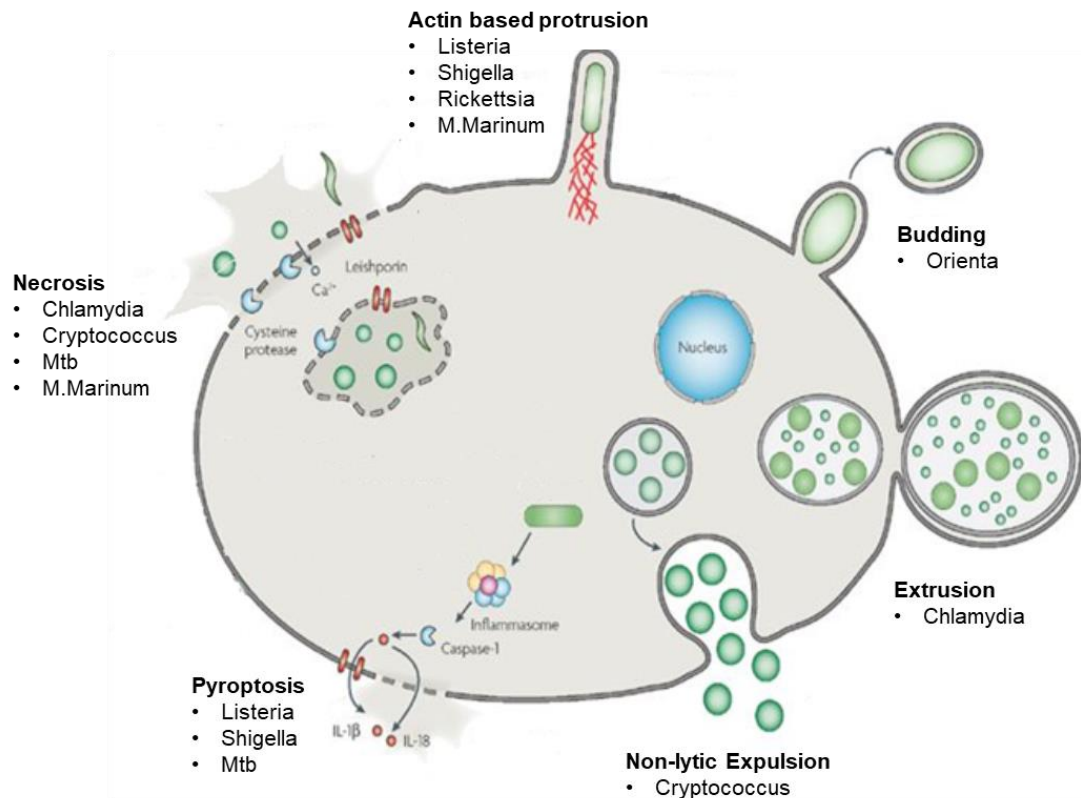


Figure 1.13 **Intracellular pathogen lytic and non-lytic strategies to exit the host cell.**

Adapted from Hybiske K and Stevens R. Exit strategies of intracellular organisms. Nature Reviews Microbiology (2008)

Figure 1.14 **High throughput flow cytometric assay for quantitation of fluorescent Mtb. A** Growth curves for Wild Type H37RV and H37Rv mCherry. Bacterial cultures were subpassaged to a starting OD of 0.05, and measured daily thereafter **B** representative flow cytometry plots of H37Rv mCherry and gating strategy to isolate bacterial population from debris and beads (which are fluorescent in all channels) **C** calculation of integrated mCherry Mtb fluorescence used to enumerate bacteria **D** bacteria were plated and counted by CFU/ml. In parallel, bacteria were analysed by flow cytometry and enumerated by integrated (Int.) mCherry Mtb fluorescence. Figure 1.15 **Intracellular pathogen lytic and non-lytic strategies to exit the host cell.**

Adapted from Hybiske K and Stevens R. Exit strategies of intracellular organisms. Nature Reviews Microbiology (2008)

## 1.5 Summary

---

Macrophages are crucial effector cells for the control of Mtb infection. Although they serve as the preferred niche for Mtb, they also help to alert the immune system to the presence of Mtb, and, in certain circumstances, can eliminate or control it directly. As with most studies on the host–pathogen interactions that occur between the residing infecting agent and its niche cell, the focus of research has been concentrated on the pathogenic manipulation of macrophage entry and intracellular subversion of macrophage defences. The exit of Mtb from human macrophages has been relatively overlooked. Further, because studies examining mycobacterial control in various *in vitro* and *in vivo* models have not sought to quantify extracellular Mtb, the relative proportion of bacteria that reside extracellularly remains to be determined.

How Mtb accumulates in the extracellular space is also a matter of debate. Certainly, there is a contribution from necrotic cell death and host cell lysis. However, at low bacterial burden early in the course of infection this may not be the primary means of exit from macrophages. Other pathogens have developed versatile strategies to exit from their host cell and there is increasing evidence that microbial exit is an organized and directed process mediated by both bacterial and cellular factors. Mtb may also display this behaviour, though never previously described to escape in a non-lytic manner from human macrophages.

## 1.6 Aim

---

I aim to contribute to our understanding of the mechanisms by which Mtb evades intracellular restriction by macrophages.

## 1.7 Hypothesis

---

I hypothesise that Mtb escape from human macrophages by non-lytic egress prior to any cellular lysis, and that the resulting extracellular bacteria grow more rapidly than intracellular bacteria, consistent with a model in which non-lytic egress contributes to evasion of macrophage defence in early infection and onward transmission of infection.

## 1.8 Experimental objectives

---

1. Confirm the presence of extracellular Mtb is an *in vitro* model of human macrophage infection, and determine if these bacteria accumulate as a result of necrotic cell death (Chapter 1)
2. To investigate if Mtb is able to escape human macrophages by non-lytic egress (Chapters 1 and 2)
3. To develop a mathematical model to determine the intracellular growth rate of Mtb (which cannot be experimentally measured) and thereby understand the niche in which the bacteria prefers to replicate (Chapter 2)
4. To investigate the mechanism by which non-lytic egress of Mtb occurs (Chapter 3)

## **2 MATERIALS AND METHODS**

### **2.1 Isolation and Culture of Human MDM**

---

Human MDM were prepared from healthy individual donors. Briefly, peripheral blood mononuclear cells (PBMC) from heparinized whole blood were separated either using Leucosep Centrifuge Tubes or obtained by density gradient centrifugation with Ficoll-Paque™ PLUS (GE Healthcare Biosciences) at 800 x g for 20 minutes according to the manufacturer's instructions. After repeated washing, PBMC were resuspended at  $1 \times 10^7$  cells/ml in RPMI 1640 with L-glutamine (GIBCO, Invitrogen) containing 5% heat inactivated (56°C for 45 minutes) pooled type AB human serum (ABS) (Sigma Aldrich) and seeded onto tissue culture plates (TPP). After one hour at 37°C, non-adherent cells were removed by sequential washes and adherent cells were incubated in RPMI 1640 with L-glutamine containing 10% autologous serum (AS) and 20ng/ml M-CSF (R&D Systems) for three days at 37°C. On day 3, any remaining non-adherent cells and the media was refreshed with RPMI 1640 with L-glutamine (GIBCO, Invitrogen) supplemented with 5% ABS (Sigma Aldrich). On day 6 cells were considered fully differentiated and maintained in culture for up to 10 days, refreshing the media every 3 days.

### **2.2 Mycobacteria**

---

#### **2.2.1 Strains**

Mtb H37Rv strain constitutively expressing a fluorescent reporter (mCherry) (courtesy of Tanya Parish, Queen Mary University of London, United Kingdom) was cultured in Middlebrook 7H9 medium (BD Bioscience) supplemented with

10% oleic acid- albumin-dextrose-catalase supplement (OADC) (BD Bioscience) enrichment medium, 0.2% glycerol, 0.05% Tween 20, and 40mcg/ml hygromycin (Invitrogen) and agitated on a rotating platform at 100 rpm at 37°C. Growth curves of H37Rv mCherry were compared to wild type H37Rv, grown in log phase liquid culture and measured by optical density (OD<sub>600</sub>).

Mycobacterium Bovis BCG harbouring phsp60-dsRed (courtesy of Maximiliano Gutierrez, Crick Institute) was similarly cultured in Middlebrook 7H9 medium (BD Bioscience) supplemented with 10% OADC enrichment medium, 0.2% glycerol and 0.05% Tween 20 and agitated on a rotating platform at 100 rpm at 37°C.

### **2.2.2 Disaggregation of Mtb**

Where required, Mtb was disaggregated using the following procedure. H37Rv mCherry growing at log phase was pelleted by centrifugation at 3000g for 10mins. The pellet was then shaken vigorously by hand with ~10 sterile 2mm glass beads for one minute to break up clumps. Aerosols were allowed to settle. Bacteria were then re-suspended in media and any residual clumps allowed to settle over 5 minutes. Bacterial concentration was determined by OD measurement from the top of the bacterial suspension.

### **2.2.3 Heat killing**

1ml of H37Rv Mtb suspension growing at log phase was aliquoted into eppendorfs and placed in a dry heat block pre-warmed to 80°C. Bacteria were heat killed over 30 mins. Prior to, and after, heat killing 1 aliquot was inoculated onto solid agar and liquid 7H9 media supplemented with 10% OADC enrichment medium, 0.2% glycerol and 0.05% Tween 20, 40mcg/ml hygromycin. Bacteria

were only removed from Biosafety Level 3 conditions if both solid and liquid cultures were negative after 8 weeks.

### **2.3 Anti-Mtb Antibody Staining**

---

H37Rv mCherry was grown to log phase. A 10ml culture suspension was centrifuged at 3000g for 20mins to pellet the bacteria and resuspended in 3% normal goat serum to block non-specific binding. 10µl of Mtb culture was diluted in 200µl phosphate buffered saline (PBS) in round bottom tissue culture plates (TPP) and centrifuged again at 3000g for 20mins. PBS was carefully removed and Anti-Mycobacterium tuberculosis antibody (FITC) ab20962 (Abcam) up to a concentration of 1:10 added to H37Rv mCherry for 20mins in the dark at room temperature. Bacteria were subsequently re-pelleted, washed in PBS and re-pelleted again. Bacteria were fixed in 4% PFA overnight and analyzed on the LSR Fortessa (BD) using excitation at 488nm to identify Anti-Mtb FITC and 610nm to identify H37Rv mCherry.

### **2.4 Cell Culture**

---

#### **2.4.1 Macrophage infection**

MDM were prepared as above. Bacterial cultures were used at mid log phase at OD 0.6-1. Cells were infected with H37Rv mCherry or BCG dsRed at multiplicity of infection (MOI) 1 (unless otherwise specified) for four hours at 37°C, resuspended in RPMI supplemented with 5% ABS. After 4 hours, extracellular bacteria were removed and cells washed extensively PBS. For some experiments, the media was replaced for a short time (5seconds), and any remaining extracellular bacteria harvested for bacterial quantitation (post wash

supernatant). RPMI supplemented with 5% ABS was replaced after washing and cells incubated at 37°C. At the relevant time point, extracellular bacteria in the supernatant were collected for quantification by gentle agitation. Cells washed extensively again. Intracellular bacteria were released by cell lysis using distilled water containing 0.05% tween.

#### **2.4.2 Macrophage Conditioned Media**

In order to determine the extracellular growth rate, macrophage conditioned medium (infCoM) was generated by infecting MDM as described for 24 hours at MOI 1. The supernatant was harvested and filter sterilized through spin filters (Costar Spin-X, Corning) (primed with RPMI + 5% ABS to reduce protein binding). infCoM was collected in this way for 3-4 donors, and pooled to reduce donor variability. Both 7H9 with hygromycin 40mcg/ml (supplemented with 10% OADC and 0.2% glycerol) and infCoM with hygromycin were subsequently re-infected with  $5 \times 10^4$  cfu/ml, the same number of bacteria used to infect MDM. Bacteria were enumerated by flow cytometry at inoculation and after 120h to determine extracellular bacillary growth.

#### **2.4.3 Chemical inhibitors**

Where required chemical inhibition of the cytoskeleton was achieved using Cytochalasin D (Sigma) or Nocadazole (Sigma) in Dimethyl Sulfoxide (DMSO, Sigma) at various concentrations.

## 2.5 Bacterial Enumeration

---

### 2.5.1 Flow cytometry

I developed a high throughput assay based on flow cytometric assessment of fluorescent bacteria to quantitate bacterial burden. Extracellular and intracellular bacteria harvested as described above were fixed in a final concentration of 4% paraformaldehyde (PFA) for deactivation. For more details on the gating strategy and calculation for quantification see **Figure 3.1 High throughput flow cytometric assay for quantitation of fluorescent Mtb.** **A** Growth curves for Wild Type H37RV and H37Rv mCherry. Bacterial cultures were subpassaged to a starting OD of 0.05, and measured daily thereafter **B** representative flow cytometry plots of H37Rv mCherry and gating strategy to isolate bacterial population from debris and beads (which are fluorescent in all channels) **C** calculation of integrated mCherry Mtb fluorescence used to enumerate bacteria **D** bacteria were plated and counted by CFU/ml. In parallel, bacteria were analysed by flow cytometry and enumerated by integrated (Int.) mCherry Mtb fluorescence.

**Figure 3.2 Imagestream Analysis of H37Rv mCherry population.** H37Rv mCherry was passed through the Imagestream. 5000 images in the bright field channel and the fluorescence emission channels at 561 nm (mCherry) were recorded. The acquired images were analyzed with IDEAS software (Amnis). A scatter plot of area/ mCherry fluorescence was generated. Image analysis was then performed on the bacteria, overlaying brightfield and fluorescent images to assess for the extent of bacterial clumping. **Figure 3.1** .H37Rv mCherry

fluorescence was measured on the LSR Fortessa (BD) using excitation wavelength 610nm. Results were recorded in BD FACSDiva Software v8.0.1 and analysed using FlowJo (version 7.6). I collected 10 000 events gated on standardised 10µm (nominal diameter) polystyrene fluorescent microsphere counting beads (Flow-Check Fluorospheres, Beckman Coulter). The counting beads were gated on the Fluorescein isothiocyanate (FITC) channel (excitation wavelength 488nm), thus could be excluded from further analysis on the mCherry channel, to ensure only fluorescent mycobacteria were quantified. Singlets beads were identified, and quantified for a more precise number of beads. Bacterial fluorescence and count was standardized to bead fluorescence and count.

### **2.5.2 Colony Forming Units**

In some experiments, intracellular and extracellular H37Rv mCherry were enumerated by CFU/ml. Bacterial suspensions were collected as described and serially diluted and plated onto 7H10 agar supplements with OADC and 40mcg/ml hygromycin in triplicate. Plates were incubated at 37°C, 5% CO<sub>2</sub> for 3 weeks when bacterial colonies were visible for counting.

## **2.6 Imaging Techniques**

---

### **2.6.1 Imagestream Analysis**

Bacterial suspensions were analysed an imaging flow cytometer (Image Stream, Amnis, Seattle, USA) acquiring 5000 images in the bright field channel and the fluorescence emission channels at 561 nm (mCherry). The acquired images were analysed with IDEAS software (Amnis). A scatter plot of area/ mCherry fluorescence was generated. Image analysis was then performed on the bacteria,

overlaying brightfield and fluorescent images to assess for the extent of bacterial clumping.

### **2.6.2 Cell microscopy**

MDM were infected as described, or left uninfected. At the relevant time points, cells were washed to remove extracellular bacteria, and fixed in 4% PFA. For enumeration, cells were washed permeabilised with 0.1% Triton-X, then counterstained with 2µg/ml 4',6-diamidino-2-phenylindole (DAPI, nuclear DNA stain) and 0.5µg/ml HCS Cell Mask™ Cells were imaged using Hermes Wiscan microscope at 10x magnification with 75% coverage of each well. Metamorph automated software was used to count cells per well as defined by DAPI+ nuclei and segmented using the cell mask. Cells were included in the analysis if the nuclear area fell within the 5<sup>th</sup> to 95<sup>th</sup> centiles in order to discount cell debris, incompletely imaged cells at the boundary of each image, and the occasional clump of cells where the number of nuclei could not be accurately discriminated. Enumeration was performed in duplicate or triplicate for each condition at each time point.

In experiments where I sought to determine the number of dying infected cells within a culture, MDM were infected for 4 hours as described. 0.5µl LIVE/ DEAD Fixable Stain (Life Technologies) was spiked into each well and the culture gently agitated. Cultures were left for 20mins at room temperature, then gently washed and fixed in 4% PFA, counterstained with DAPI and cell mask, and imaged using Hermes Wiscan microscope. Metamorph software was used to identify DAPI+ cells (segmented by cell mask), that were infected with Mtb (or uninfected), and positive for live dead stain above a background threshold.

### 2.6.3 Confocal Microscopy

MDM were grown on coverslips in 24 well tissue culture treated plates (TPP). On Day 6, cells were stimulated with nocodazole at the relevant concentration for 1 hour, then washed and fixed in 4% PFA. Cells were washed and permeabilised with 0.1% Triton-X, blocked with 3% normal goat serum then stained with rat monoclonal 1:1000 anti- tubulin YOL1/34 primary antibody (Abcam) for one hour at room temperature. Cells were washed with PBS and stained with anti rat secondary antibody. Coverslips were mounted onto glass slides using Vectashield + DAPI (Vector Laboratories) and allowed to harden overnight. Confocal microscopy was performed on a Zeiss Observer Z1 LSM 700 Confocal Microscope. Single field images of 1024 x 1024 pixels were collected using excitation by 488 nm to visualize DAPI stained nuclei and 555 nm to visualize red fluorescent  $\alpha$  tubulin. Images were taken using Zen 2012 software and reviewed using ImageJ

### 2.6.4 Live cell imaging

Prior to infection, macrophages were differentiated on a glass bottom live-cell dish (WillcoWells GWST-3512) in RPMI with 5% human AB serum. Mtb was disaggregated as described in **section 2.2.2**. Bacterial concentration was determined by OD<sub>600</sub> measurement and macrophages were infected at a multiplicity of infection of 5. After two hours, cells were washed three times to remove unattached bacteria.

48 hours post-infection, dishes were washed three times with media, wrapped in

parafilm and secured in a clamp. This was placed on the pre-warmed stage of a Leica SP5 confocal microscope at 37°C and 5% CO<sub>2</sub>. The dish was allowed 30 minutes for temperature equilibration then imaged in brightfield and red fluorescence with excitation by the 561 laser. 7 z planes 1.88 microns apart were captured per frame at a resolution of 2048 x 2048 pixels, with frames every 120 seconds. The red fluorescence channel is shown as a maximum projection of all in-focus planes.

## **2.7 Data for Modelling**

---

To calculate an extracellular bacterial replication rate from the data from infected conditioned media, we assumed a constant rate of exponential growth and, using the average four-hour normalized fluorescence as an initial condition, found the rate that minimizes the error between the exponential growth model and the average data at 24 and 120 hours.

To experimentally estimate the macrophage death rate, we first noted that cell loss in infected wells was not greater than cell loss in control wells, so we assumed that all macrophages, infected or not, had the same rate of cell death. We calculated the rate of macrophage loss in infected cells (attrition in cell number over time), assuming exponential death.

To experimentally estimate the non-lytic egress rate, we used changes in measured fluorescence across 1 hour. Non-lytic egress is assumed to occur at a constant per-bacteria rate, resulting in exponential decay of intracellular fluorescence and an equivalent increase in extracellular fluorescence. The increase in extracellular fluorescence over one hour provides the calculated egress rate. Where an extracellular measurement at the start of the hour isn't

available for an experiment it is assigned the average value.

## 2.8 Mathematical Modelling

---

We used ordinary differential equation (ODE) models to describe the intracellular and extracellular bacterial fluorescence, incorporating terms describing processes that contribute to the bacterial burden in each compartment. We do not explicitly model macrophages, since the experimental setup is such that macrophages available for infection are not limiting. Instead, we model total intracellular and extracellular bacterial burden only.

A model of intracellular and extracellular bacterial growth only, with no processes allowing for transfer of bacteria between compartments, is given by equations:

$$\frac{dE}{dt} = r_E E$$

Equation 1

$$\frac{dI}{dt} = r_I I$$

where  $E$  is the extracellular bacterial fluorescence with exponential growth rate  $r_E$  and  $I$  is the intracellular bacterial fluorescence with exponential growth rate  $r_I$ .

This system has the explicit solution

$$E(t_2) = E(t_1)e^{r_E(t_2-t_1)} \text{ and } I(t_2) = I(t_1)e^{r_I(t_2-t_1)}.$$

We included macrophage death, contributing to bacterial transfer from the intracellular compartment to the extracellular compartment, and bacterial infection of macrophages, contributing to bacterial transfer from the extracellular to intracellular compartment, giving ODEs:

$$\frac{dE}{dt} = r_E E - \beta E + \delta I$$

**Equation 2**

$$\frac{dI}{dt} = r_I I + \beta E - \delta I$$

In this model, the bacterial infection of macrophages occurs at a per capita rate  $\beta$ . Macrophage death occurs at rate  $\delta$ , and we assumed that all intracellular bacteria from a dying infected macrophage becomes extracellular. We also made the simplifying assumption that intracellular bacteria are distributed equally amongst infected macrophages, and as such the change in bacterial burdens due to the death of macrophages is described simply with a  $\delta I$  term.

We included non-lytic egress at rate  $\eta$ , giving ODEs:

$$\frac{dE}{dt} = r_E E - \beta E + \delta I + \eta I$$

**Equation 3**

$$\frac{dI}{dt} = r_I I + \beta E - \delta I - \eta I$$

$\eta$  has the following solution  $-\frac{1}{t} \ln\left(1 - \frac{E(t) - E(0)}{I(0)}\right)$  (**Equation 4**) which describes the change in the extracellular bacillary load  $E$  normalised to the intracellular bacillary load at time 0  $I(0)$ .

For each of these models, the initial condition (at four hours) for intracellular bacterial burden was taken from the observed data. However, an initial condition was not available for all experiments for extracellular bacterial burden, which should be minimal due to the thorough wash procedure occurring at that time point. Instead, to estimate the initial conditions, we used four-hour extracellular fluorescence measurements from 8 additional experiments and after normalizing by the average inoculum fluorescence.

## **2.9 Parameter Estimation**

---

We solved the systems of ODEs using the `odeint` function of the `integrate` package in SciPy. Parameters were estimated to minimize the sum of squared error (SSE) between the model and observations for both intracellular and extracellular normalized fluorescence, using the `optimize` package in SciPy, using a Nelder-Mead method. Multiple model fits are performed starting from randomly selected initial guesses. The estimated parameter set providing the minimum SSE is presented.

## 3 EXTRACELLULAR MTB ACCUMULATION

### 3.1 Introduction

---

The fact that Mtb can evade intracellular microbicidal pathways, and adapt metabolically to the intracellular environment has allowed it to survive and replicate as a facultative intracellular pathogen (Pieters, 2008; Russell et al., 2010b). Nonetheless, macrophage intracellular restriction of Mtb is necessary for protective host defence, as discussed in **section 1.3.1**

In pathological specimens from the site of TB disease, Mtb is also evident outside cells (Canetti, 1955). This has been attributed to Mtb escape from macrophages as a result of lytic host cell death (Behar et al., 2010), and is likely to be necessary for its onward transmission to new hosts (Ramakrishnan, 2012).

Interestingly however other facultative intracellular pathogens, have been shown to egress from live macrophages (see **section 1.4.4**), and even Mtb has been shown to do this from live amoeba (Hagedorn et al., 2009). This raises the possibility that Mtb can escape from live macrophages, and in so doing, escape intracellular macrophage restriction. Importantly, experimental models to study Mtb restriction by macrophages, have focused exclusively on the intracellular bacillary burden. If substantial cell death or non-lytic egress of Mtb does occur, then present models to study bacillary control in macrophage cultures, may significantly underestimate the total bacillary burden. In this chapter, I sought to test the hypothesis that extracellular bacteria accumulate following intracellular Mtb infection. I then set out to develop a mathematical model to test whether this accumulation is exclusively associated with cell death or occurs via non-lytic egress.

*In vitro* models of macrophages typically involve the differentiation of human peripheral blood monocytes or bone marrow derived macrophages (BMDM) from mouse in growth factors such as macrophage colony stimulating factor (M-CSF), granulocyte macrophage colony stimulating factor (GM-CSF) and cytokines including IL-4/IL-13 and IL-6.

In order to model macrophage responses *in vitro*, we use human monocytes differentiated in the growth factor M-CSF to generate monocyte derived macrophages (MDMs). M-CSF has been shown to be a critical circulating regulator of the mononuclear phagocyte system (Hume et al., 1988) and macrophage development *in vivo* is thought to be driven principally by M-CSF and its cognate receptor- CSF1R (Hume et al., 1988).

GM-CSF differentiated MDM are thought to more closely resemble alveolar macrophages according to their surface antigen expression profile (Akagawa et al., 2006). Patients suffering from a deficiency in GM-CSF do not suffer from macrophage deficiency, but have a functional defect of surfactant clearance and suffer from a condition termed pulmonary alveolar proteinosis (Martinez-Moczygemba and Huston, 2010). This demonstrates the major role of GM-CSF in alveolar macrophage (AM) physiology.

The substantial heterogeneity of tissue macrophage phenotypes suggests it is unlikely that *in vitro* MDMs can precisely model all their highly specialized phenotypes. However, evidence for shared morphological and functional features, as well as a common developmental requirement for M-CSF, suggests M-CSF MDMs are a reasonable reductionist model to study often inaccessible tissue macrophages *in vitro*, with the clear caveat of any *in vitro* study - that the

absence of the tissue microenvironment may influence the function of the cell type under investigation.

## 3.2 Objectives

---

1. To develop and validate a rapid high throughput assay in order to evaluate the intracellular and extracellular Mtb growth in human macrophage cultures.
2. To investigate whether bacterial load derived from intracellular Mtb is restricted to the intracellular compartment and whether extracellular Mtb is exclusively associated with cell death.
3. To use a mathematical model to show whether Mtb egress from human macrophages is wholly explained by host cell death.

### 3.3 Results

---

#### 3.3.1 A high throughput flow cytometric assay to quantify Mtb

Traditional methods of quantifying mycobacterial load in cell cultures or infected tissues depends largely on seeding samples onto Mtb culture media (Middlebrook 7H10 or Lowenstein Jensen) and counting colony-forming units after three to four weeks. These are time consuming and incur a biohazard risk. In addition mycobacterial clumping can undermine accurate quantitation (van Zyl-Smit et al., 2011).

In collaboration with others in our group (Elspeth Potton and Rachel Byng Maddick), I developed a high throughput flow cytometric assay for quantitation of intracellular mycobacterial growth. I utilized a virulent laboratory strain of Mtb, H37Rv, which constitutively expresses a fluorescent reporter protein mCherry fluorophore (H37Rv mCherry). H37Rv mCherry is stable and detectable under hypoxic conditions *in vitro*, (Carroll et al., 2010). Fluorescence does not diminish upon addition of the bacteriostatic agent chloramphenicol, but there is a loss of fluorescent signal with bactericidal agents, suggesting that mCherry could be used as a reporter for mycobacterial death (Carroll et al., 2010).

First, I confirmed that constitutive expression of mCherry by H37Rv did not affect bacterial fitness by comparing the growth curves of H37Rv mCherry to wild type H37Rv, as measured by optical density (**Figure 3.1 High throughput flow cytometric assay for quantitation of fluorescent Mtb. A** Growth curves for Wild Type H37RV and H37Rv mCherry. Bacterial cultures were subpassaged to a starting OD of 0.05, and measured daily thereafter **B** representative flow cytometry plots of H37Rv mCherry and gating strategy to isolate bacterial

population from debris and beads (which are fluorescent in all channels) **C** calculation of integrated mCherry Mtb fluorescence used to enumerate bacteria **D** bacteria were plated and counted by CFU/ml. In parallel, bacteria were analysed by flow cytometry and enumerated by integrated (Int.) mCherry Mtb fluorescence.

**Figure 3.2 Imagestream Analysis of H37Rv mCherry population.** H37Rv mCherry was passed through the Imagestream. 5000 images in the bright field channel and the fluorescence emission channels at 561 nm (mCherry) were recorded. The acquired images were analyzed with IDEAS software (Amnis). A scatter plot of area/ mCherry fluorescence was generated. Image analysis was then performed on the bacteria, overlaying brightfield and fluorescent images to assess for the extent of bacterial clumping. **Figure 3.1A**).

Next, I showed that H37Rv mCherry can be detected by flow cytometry (**Figure 3.1 High throughput flow cytometric assay for quantitation of fluorescent Mtb.** **A** Growth curves for Wild Type H37RV and H37Rv mCherry. Bacterial cultures were subpassaged to a starting OD of 0.05, and measured daily thereafter **B** representative flow cytometry plots of H37Rv mCherry and gating strategy to isolate bacterial population from debris and beads (which are fluorescent in all channels) **C** calculation of integrated mCherry Mtb fluorescence used to enumerate bacteria **D** bacteria were plated and counted by CFU/ml. In parallel, bacteria were analysed by flow cytometry and enumerated by integrated (Int.) mCherry Mtb fluorescence.

Figure 3.2 **Imagestream Analysis of H37Rv mCherry population.** H37Rv mCherry was passed through the Imagestream. 5000 images in the bright field channel and the fluorescence emission channels at 561 nm (mCherry) were recorded. The acquired images were analyzed with IDEAS software (Amnis). A scatter plot of area/ mCherry fluorescence was generated. Image analysis was then performed on the bacteria, overlaying brightfield and fluorescent images to assess for the extent of bacterial clumping. Figure 3.1**B**). In the flow cytometric plots, Mtb displayed a wide range of forward scatter (as a measure of size), co-variant with fluorescence intensity (**Figure 3.1 High throughput flow cytometric assay for quantitation of fluorescent Mtb.** **A** Growth curves for Wild Type H37RV and H37Rv mCherry. Bacterial cultures were subpassaged to a starting OD of 0.05, and measured daily thereafter **B** representative flow cytometry plots of H37Rv mCherry and gating strategy to isolate bacterial population from debris and beads (which are fluorescent in all channels) **C** calculation of integrated mCherry Mtb fluorescence used to enumerate bacteria **D** bacteria were plated and counted by CFU/ml. In parallel, bacteria were analysed by flow cytometry and enumerated by integrated (Int.) mCherry Mtb fluorescence.

Figure 3.2 **Imagestream Analysis of H37Rv mCherry population.** H37Rv mCherry was passed through the Imagestream. 5000 images in the bright field channel and the fluorescence emission channels at 561 nm (mCherry) were recorded. The acquired images were analyzed with IDEAS software (Amnis). A scatter plot of area/ mCherry fluorescence was generated. Image analysis was then performed on the bacteria, overlaying brightfield and fluorescent images to assess for the extent of bacterial clumping. Figure 3.1**B**). I reasoned that this

represented bacterial clumping and tested this hypothesis using Imagestream to visualize flow cytometric events with low forward scatter and fluorescence, compared to events with high forward scatter and high fluorescence. This analysis confirmed that the latter population represented clumps of bacteria (**Figure 3.2 Imagestream Analysis of H37Rv mCherry population.** H37Rv mCherry was passed through the Imagestream. 5000 images in the bright field channel and the fluorescence emission channels at 561 nm (mCherry) were recorded. The acquired images were analyzed with IDEAS software (Amnis). A scatter plot of area/ mCherry fluorescence was generated. Image analysis was then performed on the bacteria, overlaying brightfield and fluorescent images to assess for the extent of bacterial clumping. Bacteria imaged in the top right of the plot display high mCherry fluorescence and high area. The composite image indicates that these are clumps of mycobacteria. Bacteria imaged in the bottom left display low mCherry fluorescence and smaller area. Composite images indicate that these are single bacteria.

Figure 3.2). In order to account for bacterial clumping, I used the product of event counts and mean fluorescence intensity of the bacterial population as a measure of total bacterial load and standardized the quantitation in each sample with fluorescent counting beads (**Figure 3.1 High throughput flow cytometric assay for quantitation of fluorescent Mtb.** **A** Growth curves for Wild Type H37RV and H37Rv mCherry. Bacterial cultures were subpassaged to a starting OD of 0.05, and measured daily thereafter **B** representative flow cytometry plots of H37Rv mCherry and gating strategy to isolate bacterial population from debris

and beads (which are fluorescent in all channels) **C** calculation of integrated mCherry Mtb fluorescence used to enumerate bacteria **D** bacteria were plated and counted by CFU/ml. In parallel, bacteria were analysed by flow cytometry and enumerated by integrated (Int.) mCherry Mtb fluorescence.

Figure 3.2 **Imagestream Analysis of H37Rv mCherry population.** H37Rv mCherry was passed through the Imagestream. 5000 images in the bright field channel and the fluorescence emission channels at 561 nm (mCherry) were recorded. The acquired images were analyzed with IDEAS software (Amnis). A scatter plot of area/ mCherry fluorescence was generated. Image analysis was then performed on the bacteria, overlaying brightfield and fluorescent images to assess for the extent of bacterial clumping. Figure 3.1**C**). This method generated an integrated mCherry Fluorescence with a linear correlation to colony forming unit count/ml (CFU/ml (**Figure 3.1 High throughput flow cytometric assay for quantitation of fluorescent Mtb.** **A** Growth curves for Wild Type H37RV and H37Rv mCherry. Bacterial cultures were subpassaged to a starting OD of 0.05, and measured daily thereafter **B** representative flow cytometry plots of H37Rv mCherry and gating strategy to isolate bacterial population from debris and beads (which are fluorescent in all channels) **C** calculation of integrated mCherry Mtb fluorescence used to enumerate bacteria **D** bacteria were plated and counted by CFU/ml. In parallel, bacteria were analysed by flow cytometry and enumerated by integrated (Int.) mCherry Mtb fluorescence.

Figure 3.2 **Imagestream Analysis of H37Rv mCherry population.** H37Rv

mCherry was passed through the Imagestream. 5000 images in the bright field channel and the fluorescence emission channels at 561 nm (mCherry) were recorded. The acquired images were analyzed with IDEAS software (Amnis). A scatter plot of area/ mCherry fluorescence was generated. Image analysis was then performed on the bacteria, overlaying brightfield and fluorescent images to assess for the extent of bacterial clumping. Figure 3.1D). The relationship remained linear but with lower  $R^2$  correlation coefficient under ~100 bacteria (equivalent to 50 integrated mCherry fluorescence units), which I used to represent the lower limit of sensitivity of the assay.

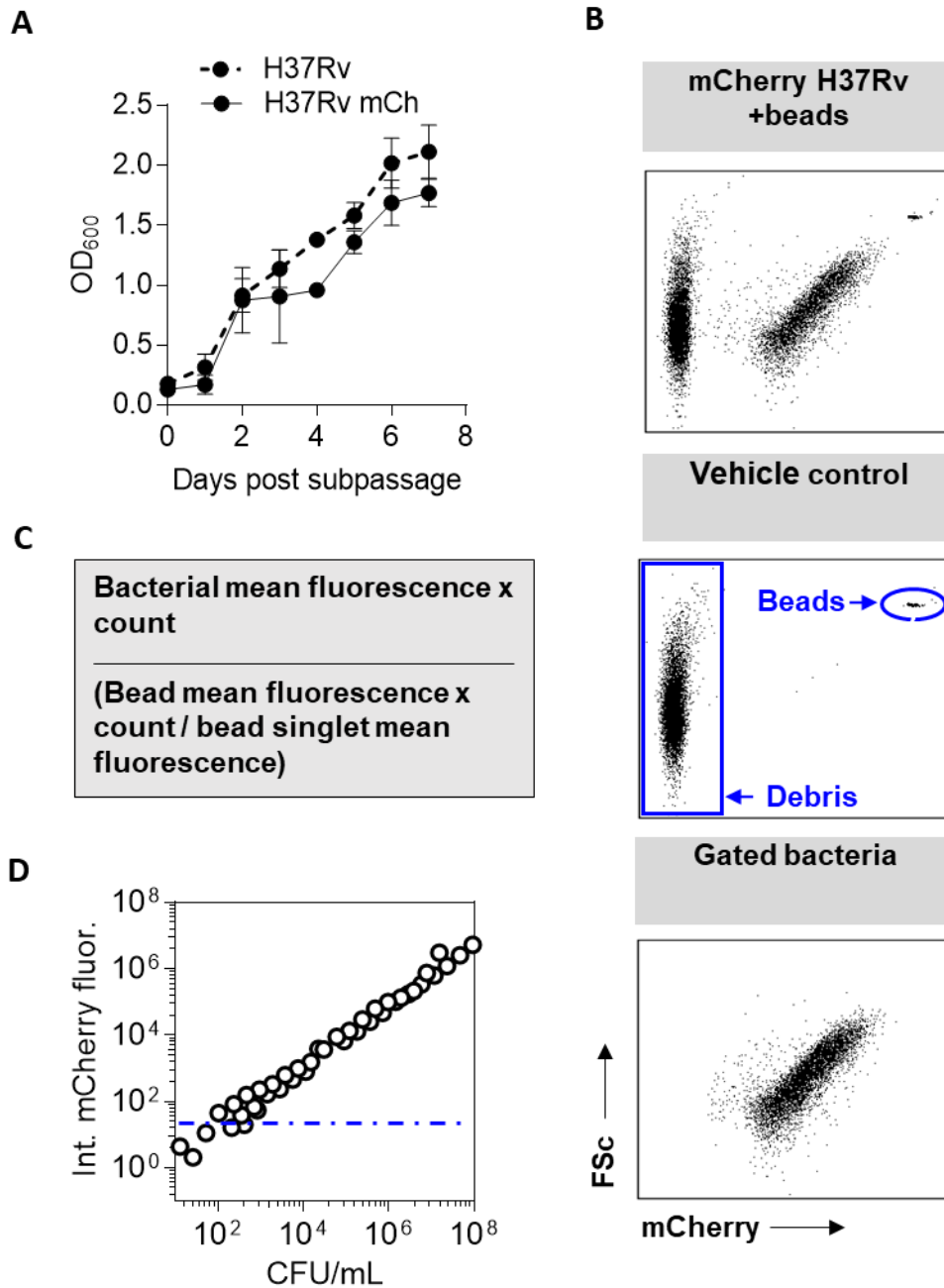


Figure 3.1 **High throughput flow cytometric assay for quantitation of fluorescent Mtb. A** Growth curves for Wild Type H37RV and H37Rv mCherry. Bacterial cultures were subpassaged to a starting OD of 0.05, and measured daily thereafter **B** representative flow cytometry plots of H37Rv mCherry and gating strategy to isolate bacterial population from debris and beads (which are fluorescent in all channels) **C** calculation of integrated mCherry Mtb fluorescence used to enumerate bacteria **D** bacteria were plated and counted by CFU/ml. In parallel, bacteria were analysed by flow cytometry and enumerated by integrated (Int.) mCherry Mtb fluorescence.

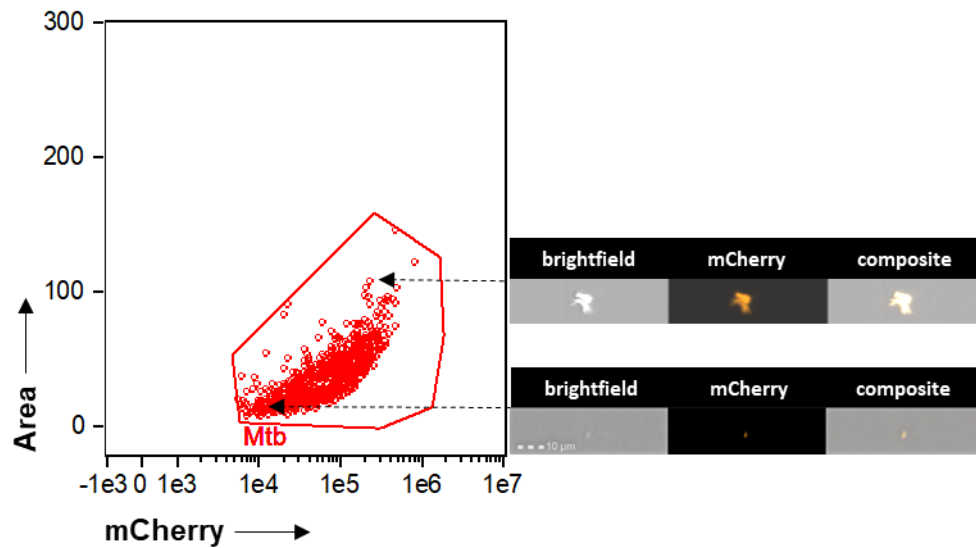
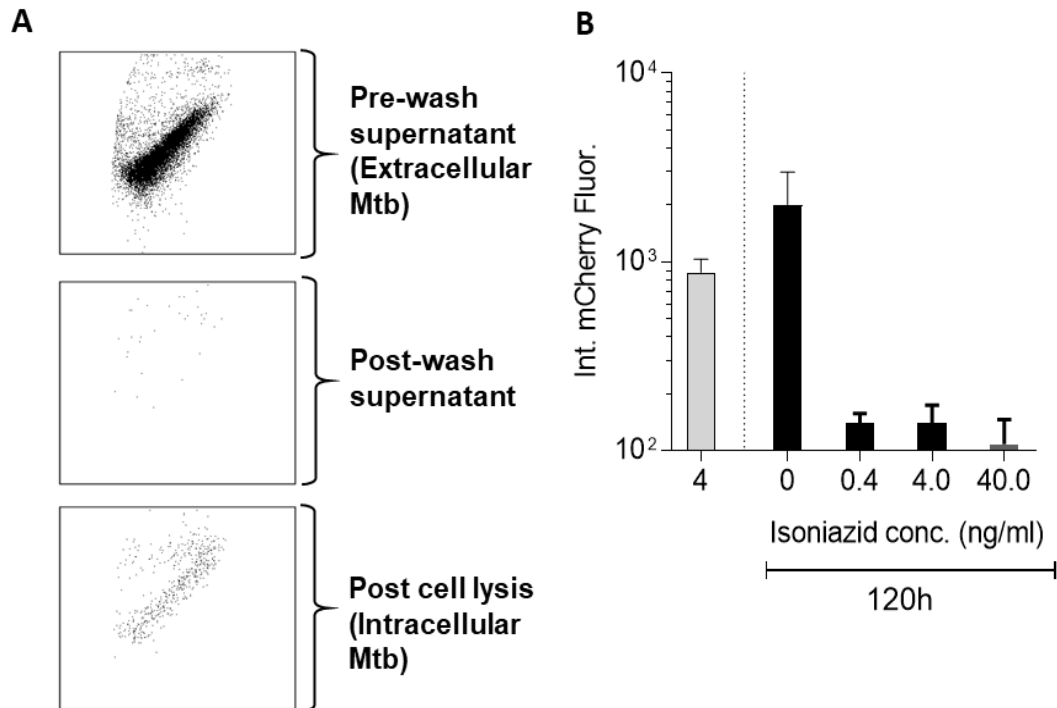


Figure 3.4 **Imagestream Analysis of H37Rv mCherry population.** H37Rv mCherry was passed through the Imagestream. 5000 images in the bright field channel and the fluorescence emission channels at 561 nm (mCherry) were recorded. The acquired images were analyzed with IDEAS software (Amnis). A scatter plot of area/ mCherry fluorescence was generated. Image analysis was then performed on the bacteria, overlaying brightfield and fluorescent images to assess for the extent of bacterial clumping. Bacteria imaged in the top right of the plot display high mCherry fluorescence and high area. The composite image indicates that these are clumps of mycobacteria. Bacteria imaged in the bottom left display low mCherry fluorescence and smaller area. Composite images indicate that these are single bacteria.

### 3.3.2 Detection and quantitation of extracellular and intracellular Mtb

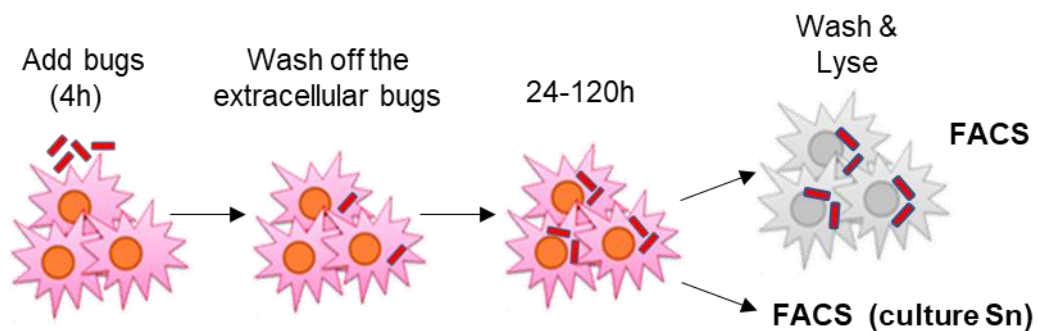
I used flow cytometric quantitation of Mtb to assess intracellular and extracellular bacillary load in MDM cultures inoculated with Mtb at an approximate ratio of one bacteria per cell (MOI = 1). MDM were infected with Mtb for four hours to allow phagocytosis of bacteria. Flow cytometric analysis of the culture supernatants at this time point revealed residual extracellular bacilli (**Figure 3.3A**). Cells were then washed extensively. Sampling the cell culture media after washing revealed very few bacilli (**Figure 3.3A**). Finally, the cells were lysed in water and flow cytometric analysis of the lysates revealed further bacilli (**Figure 3.3A**). Hence, the pre-wash culture supernatant could be used to quantify extracellular bacilli and the post-wash cell lysate to quantify intracellular bacillary load. In order to validate that this assay could be used to quantify Mtb growth and restriction, I investigated the change in intracellular Mtb load between four and 120 hours in MDM culture, with and without the anti-mycobacterial drug, isoniazid. Consistent with the literature on this model (Liu et al., 2016), my data revealed an increase in intracellular Mtb load with time, and a reduction in bacterial load in the presence of isoniazid (Error! Reference source not found.**B**).



**Figure 3.6 Detection of intracellular and extracellular Mtb** **A** hMDM were infected with H37Rv mCherry at MOI 1. After 4 hours the supernatant was removed (extracellular Mtb). hMDM were washed three times with phosphate buffered saline. After the third wash, fresh media was placed on the cells and subsequently removed for analysis (post wash supernatant). hMDM were lysed to release intracellular Mtb **B** hMDM were infected with H37Rv mCherry for 4h and then co-cultured for a further 120h +/- isoniazid. Cells were washed and lysed at each timepoint and intracellular Mtb detected by flow cytometry.

### 3.3.3 Extracellular bacteria accumulate following culture with MDM

In the literature on Mtb-MDM infection, studies have generally focused on mechanisms of intracellular control of Mtb, and therefore exclusively measure the intracellular load of bacteria over time. As well as collecting intracellular bacteria from lysed cells, I collected the culture supernatants at 24 and 120 hours after infection, in order to quantify extracellular bacteria (**Figure 3.4 Experimental**



**model to measure extracellular Mtb during MDM infection.** MDM were infected with H37Rv mCherry for four hours at MOI 1. Cultures were washed three times with PBS to remove all extracellular bacteria. Fresh media (RPMI + 5% ABS) was added for the times specified. At the relevant time point extracellular bacteria in the supernatant were collected. Intracellular bacteria were harvested by washing and lysing cells. Bacteria were fixed in 4% PFA and analysed by flow cytometry

**Figure 3.5 Extracellular Mtb accumulation following co-culture with macrophages** A MDM were infected with H37Rv mCherry for four hours at MOI 1. Cultures were washed three times with PBS to remove all extracellular bacteria. Fresh media was added for the times specified. At the relevant time point extracellular bacteria in the supernatant were collected. Intracellular

bacteria were harvested by washing and lysing cells. Bacteria were fixed in 4% PFA and analysed by flow cytometry. Bacteria quantified by integrated mCherry fluorescence at each time point in each compartment. Mean  $\pm$  SEM 7 separate experiments conducted in duplicate or triplicate. **B** Example flow cytometry plots of H37Rv mCherry population in each compartment at each time point (one representative experiment) (Figure 3.4).

Extracellular Mtb was clearly evident in these experiments by 24 hours after infection, and is quantitatively equivalent to the intracellular bacillary load by 120 hours (**Figure 3.5 Extracellular Mtb accumulation following co-culture**

Figure 3.7 **Experimental model to measure extracellular Mtb during MDM infection.** MDM were infected with H37Rv mCherry for four hours at MOI 1. Cultures were washed three times with PBS to remove all extracellular bacteria. Fresh media (RPMI + 5% ABS) was added for the times specified. At the relevant time point extracellular bacteria in the supernatant were collected. Intracellular bacteria were harvested by washing and lysing cells. Bacteria were fixed in 4% PFA and analysed by flow cytometry

**with macrophages A** MDM were infected with H37Rv mCherry for four hours at MOI 1. Cultures were washed three times with PBS to remove all extracellular bacteria. Fresh media was added for the times specified. At the relevant time point extracellular bacteria in the supernatant were collected. Intracellular bacteria were harvested by washing and lysing cells. Bacteria were fixed in 4% PFA and analysed by flow cytometry. Bacteria quantified by integrated mCherry fluorescence at each time point in each compartment. Mean  $\pm$  SEM 7 separate experiments conducted in duplicate or triplicate. **B** Example flow cytometry plots of H37Rv mCherry population in each compartment at each time point (one representative experiment)

Figure 3.6 **Bacterial accumulation is not simply due to exponential growth**

**A** model of exponential growth in each compartment (lines, intracellular = orange, extracellular = purple) to predict the observed data (squares, **Figure 3.5B**).

Experimental data for bacterial load at four hours post wash is not available. **B**

The extracellular bacillary load in the post wash supernatant is determined from a separate series of experiments where MDM are infected for four hours.

Extracellular bacteria are removed and cultures washed three times with PBS.

Fresh media is replaced for 30 seconds and subsequently fixed in 4% PFA for quantification by flow cytometric analysis. The values are normalised to average

integrated mCherry fluorescence of inocula. Line represents median. **Figure**

**3.5A**)<sup>1</sup>. Consequently, only measuring intracellular Mtb significantly

underestimates the total mycobacterial load. A representative FACS plot of one

experiment is presented in **Figure 3.5 Extracellular Mtb accumulation**

**following co-culture with macrophages A** MDM were infected with H37Rv

mCherry for four hours at MOI 1. Cultures were washed three times with PBS to

remove all extracellular bacteria. Fresh media was added for the times specified.

At the relevant time point extracellular bacteria in the supernatant were collected.

Intracellular bacteria were harvested by washing and lysing cells. Bacteria were

fixed in 4% PFA and analysed by flow cytometry. Bacteria quantified by integrated

mCherry fluorescence at each time point in each compartment. Mean  $\pm$  SEM 7

separate experiments conducted in duplicate or triplicate. **B** Example flow

cytometry plots of H37Rv mCherry population in each compartment at each time

---

<sup>1</sup> Experiments by MM, Jennifer Roe and Rachel Byng Maddick

point (one representative experiment)

Figure 3.6 **Bacterial accumulation is not simply due to exponential growth**

**A** model of exponential growth in each compartment (lines, intracellular = orange, extracellular= purple) to predict the observed data (squares, **Figure 3.5B**).

Experimental data for bacterial load at four hours post wash is not available. **B**

The extracellular bacillary load in the post wash supernatant is determined from

a separate series of experiments where MDM are infected for four hours.

Extracellular bacteria are removed and cultures washed three times with PBS.

Fresh media is replaced for 30 seconds and subsequently fixed in 4% PFA for

quantification by flow cytometric analysis. The values are normalised to average

integrated mCherry fluorescence of inocula. Line represents median. **Figure 3.5B**.

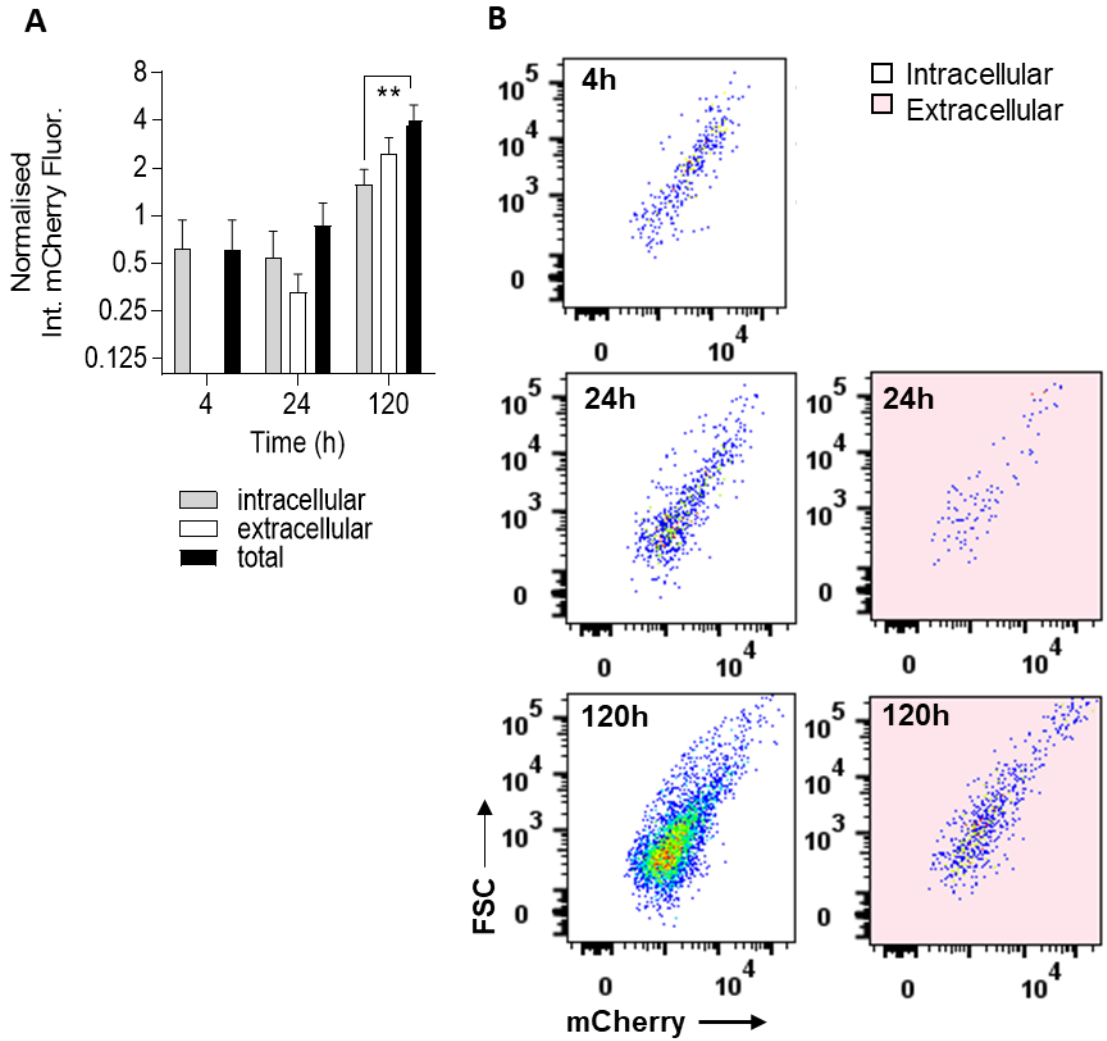


Figure 3.10 **Extracellular Mtb accumulation following co-culture with macrophages** A MDM were infected with H37Rv mCherry for four hours at MOI 1. Cultures were washed three times with PBS to remove all extracellular bacteria. Fresh media was added for the times specified. At the relevant time point extracellular bacteria in the supernatant were collected. Intracellular bacteria were harvested by washing and lysing cells. Bacteria were fixed in 4% PFA and analysed by flow cytometry. Bacteria quantified by integrated mCherry fluorescence at each time point in each compartment. Mean  $\pm$  SEM 7 separate experiments conducted in duplicate or triplicate. B Example flow cytometry plots of H37Rv mCherry population in each compartment at each time point (one representative experiment)

### 3.3.4 Extracellular bacteria do not accumulate by extracellular replication

I next conducted a series of analyses to try to explain the observed extracellular bacillary accumulation. My first hypothesis was that the increase in extracellular bacilli reflect growth of the residual extracellular bacteria after washing the cells at four hours.

In the experiments where I measured extracellular bacillary accumulation over 120 hours, I had not collected post wash supernatant samples at four hours in order to test this hypothesis directly. Instead, I used data from 24 and 120 hours to determine the intracellular and extracellular growth rates of Mtb assuming no other processes were occurring in the system. We used the following equation describing the exponential rate of increase of extracellular ( $E$ ) and intracellular bacterial loads ( $I$ ), (**Equation 1, Materials and Methods**)

$$\frac{dE}{dt} = r_E E$$

$$\frac{dI}{dt} = r_I I$$

This equation gives an exponential growth rate that can be used to derive the doubling time of bacteria. We were able to fit the observed data at 24 and 120 hours using an extracellular bacteria doubling time of 23.7 hours and intracellular bacteria doubling time of 43 hours. Firstly, the large discrepancy between the rates of growth in each compartment was surprising. In addition, we used these exponential growth rates and fitted the data back to the start of the experiment (post wash residual extracellular bacteria). We discovered that if Mtb was actually

growing at these rates, there would need to be an extracellular bacterial load at four hours of 0.17 integrated fluorescence. This was far higher than the 0.004 integrated fluorescence value obtained from a separate series of experiments where I measured the amount of residual extracellular bacteria in the post wash supernatant at four hours (**Figure 3.6 Bacterial accumulation is not simply due to exponential growth** **A** model of exponential growth in each compartment (lines, intracellular = orange, extracellular= purple) to predict the observed data (squares, **Figure 3.5B**). Experimental data for bacterial load at four hours post wash is not available. **B** The extracellular bacillary load in the post wash supernatant is determined from a separate series of experiments where MDM are infected for four hours. Extracellular bacteria are removed and cultures washed three times with PBS. Fresh media is replaced for 30 seconds and subsequently fixed in 4% PFA for quantification by flow cytometric analysis. The values are normalised to average integrated mCherry fluorescence of inocula. Line represents median.

Figure 3.7 **Model of Mtb-macrophage interactions** (1) Bacterial uptake by macrophages (2) Mtb replication within live macrophages (3) Macrophage cell death leading to release of bacteria into extracellular space (4) Extracellular Mtb replication (5) Non-lytic egress of bacteria from live macrophages into the extracellular space **Figure 3.6B**).<sup>2</sup>

This analysis disproved my hypothesis and suggested that the accumulation of

---

<sup>2</sup> Modelling by KB, data from MM

extracellular Mtb was not simply due to the replication of residual extracellular bacilli.

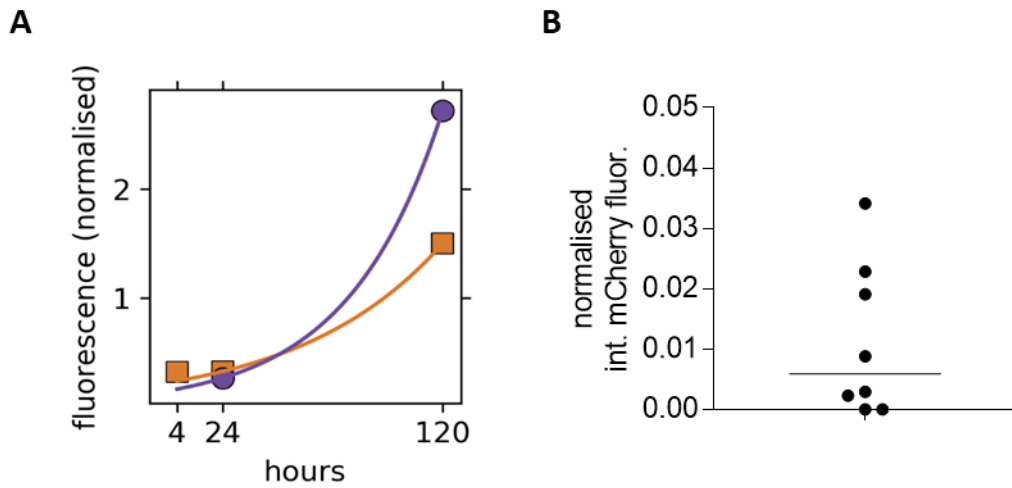


Figure 3.13 **Bacterial accumulation is not simply due to exponential growth** A model of exponential growth in each compartment (lines, intracellular = orange, extracellular= purple) to predict the observed data (squares, **Figure 3.10 Extracellular Mtb accumulation following co-culture with macrophages** A MDM were infected with H37Rv mCherry for four hours at MOI 1. Cultures were washed three times with PBS to remove all extracellular bacteria. Fresh media was added for the times specified. At the relevant time point extracellular bacteria in the supernatant were collected. Intracellular bacteria were harvested by washing and lysing cells. Bacteria were fixed in 4% PFA and analysed by flow cytometry. Bacteria quantified by integrated mCherry fluorescence at each time point in each compartment. Mean  $\pm$  SEM 7

### 3.3.5 A mathematical model to describe Mtb accumulation

Next I sought to test the hypothesis that the extracellular Mtb is derived from intracellular bacilli. The biological processes that govern the movement of bacteria between the extracellular and intracellular compartments are complex. Intracellular bacteria may be transferred to the extracellular compartment after cells die by necrosis, characterized by plasma membrane damage and release of intracellular contents, or by non-lytic egress. In addition, extracellular bacteria can move into the intracellular compartment as they are taken up by macrophages, where they may further replicate.

My research question was whether extracellular bacillary accumulation is exclusively associated with cell death, or whether non-lytic egress might also be predicted to contribute. I was unable to address this question experimentally since each cellular process is inter-dependent. I therefore chose to develop a mathematical model to replicate the behaviour of the system I was modelling, specifically to determine which of these processes had the most impact on extracellular bacillary accumulation.

The first step in the development of a computational model is the formulation of a conceptual model, outlining the pertinent processes that are involved in the system of interest (Brodland, 2015; Ingalls, 2013). The processes leading to accumulation of Mtb in the intracellular and extracellular compartments can be described by the model shown in **Figure 3.7 Model of Mtb-macrophage interactions** (1) Bacterial uptake by macrophages (2) Mtb replication within live macrophages (3) Macrophage cell death leading to release of bacteria into extracellular space (4) Extracellular Mtb replication (5) Non-lytic egress of

bacteria from live macrophages into the extracellular space

**Figure 3.8 Measurement of cell death using nuclear counts** **A** Example microscopy image of DAPI stained MDM nuclei. **B** MDM were infected (or mock infected) with H37Rv mCherry for four hours at MOI 1. Cultures were washed three times with PBS to remove all extracellular bacteria. Fresh media was added for the times specified. At the relevant time point the supernatant was removed and cells washed again three times with PBS. Cells were fixed in 4% PFA for 24 hours. Cells were washed and stained with DAPI nuclear stain for 15 minutes, and subsequently imaged on the Hermes high content microscope. Nuclei were enumerated using Metamorph software. Mean  $\pm$  SEM 7 separate experiments conducted in triplicate. Figure 3.7

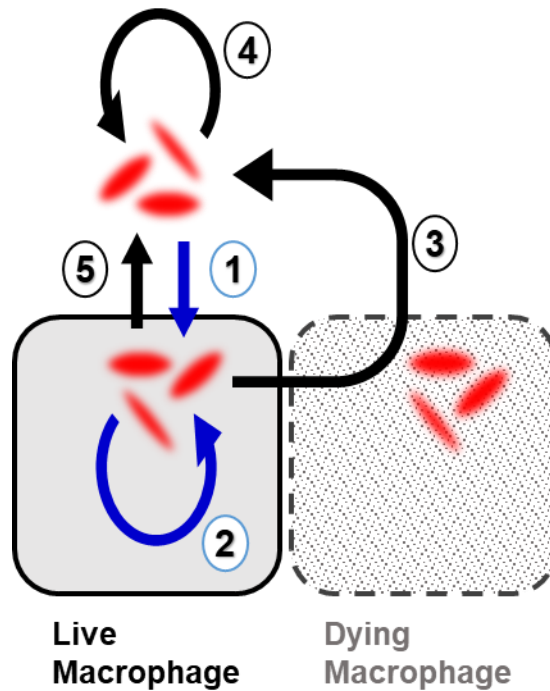


Figure 3.16 **Model of Mtb-macrophage interactions** (1) Bacterial uptake by macrophages (2) Mtb replication within live macrophages (3) Macrophage cell death leading to release of bacteria into extracellular space (4) Extracellular Mtb replication (5) Non-lytic egress of bacteria from live macrophages into the extracellular space

We then used an ordinary differential equation (ODE) approach to mathematical modelling. The majority of quantitative models in cell and molecular biology are formulated in terms of ordinary differential equations because in these systems, as in ours, time is a continuous variable (Ingalls, 2013). The rate of each process becomes a parameter of the ODE model. Some parameters may be experimentally determined *in vitro* (e.g. the rate of cell death and extracellular replication), and where this is not possible, the model can be used to generate values for the unknown parameters *in silico* (e.g. rate of bacterial uptake and intracellular replication) in order to best replicate the behaviour of the system (Fischer, 2008).

As the quote goes by George Fox- 'all models are wrong but some models are useful'. I was aware that the computational model I had developed could not

incorporate every parameter that described the movement of intracellular and extracellular bacteria. However, I did believe this to be a useful exercise by which I might understand the most important contributing factor to extracellular bacillary load.

### 3.3.6 Determining the rate of cell death

Cytolytic cell death has been most consistently reported at high MOI; 10-25 bacteria per cell has been found to represent a 'burst size' threshold (Divangahi et al., 2009; Repasy et al., 2013; Welin et al., 2011). Internalization of less than 10 bacteria per cell does not induce significantly more death than in bystander cells (Mahamed et al., 2017). I hypothesized that at low MOI of infection, which represents events during early infection of macrophages (typically few bacteria required to establish *in vivo* infection), there would be little lytic cell death contributing to extracellular bacillary accumulation.

I wanted to quantify the contribution of necrotic cell death to extracellular bacterial accumulation, since only necrotic cells release their cytoplasmic and nuclear contents, whereas apoptotic cells remain relatively intact until they undergo secondary necrosis. Also, because I was more interested in the rate at which cells die, I addressed this question by counting the number of adherent cells by *in situ* microscopy, as a surrogate for viability, at each time point, using the reduction of adherent macrophage nuclei over time as a measure of rate of cellular necrosis. Other groups employ a range of death markers in order to assess for the cell death pathways induced by Mtb e.g. Terminal deoxynucleotidyl transferase dUTP nick end labelling (TUNEL), caspase or Annexin V staining for apoptotic cell death and propidium iodide (PI) staining to identify necrotic cell death. However, staining for dead or dying cells *in situ* may underestimate cell death by not counting the cells that have detached, and quantifying the products of necrosis in culture supernatants (eg LDH) or mitochondrial function as a measure cell viability are difficult to relate accurately to cell number. Flow

cytometric live dead stains are a useful and widely used tool to assess for cell death, but methods used to detach the cells may confound the results of these stains. In any case, MDMs generated using the adherence method are, by definition, difficult to detach for flow cytometric assessment. Indeed, the number of washes in my experimental protocol to remove extracellular bacteria is dependent on generating strongly adherent MDM when they are alive. Finally, in situ microscopy allowed me to evaluate other parameters in the same experiment and to retain single cell data for alternative analyses.

In parallel to the experiments conducted in **Figure 3.5 Extracellular Mtb accumulation following co-culture with macrophages** **A** MDM were infected with H37Rv mCherry for four hours at MOI 1. Cultures were washed three times with PBS to remove all extracellular bacteria. Fresh media was added for the times specified. At the relevant time point extracellular bacteria in the supernatant were collected. Intracellular bacteria were harvested by washing and lysing cells. Bacteria were fixed in 4% PFA and analysed by flow cytometry. Bacteria quantified by integrated mCherry fluorescence at each time point in each compartment. Mean  $\pm$  SEM 7 separate experiments conducted in duplicate or triplicate. **B** Example flow cytometry plots of H37Rv mCherry population in each compartment at each time point (one representative experiment)

Figure 3.6 **Bacterial accumulation is not simply due to exponential growth** **A** model of exponential growth in each compartment (lines, intracellular = orange, extracellular= purple) to predict the observed data (squares, **Figure 3.5B**). Experimental data for bacterial load at four hours post wash is not available. **B**

The extracellular bacillary load in the post wash supernatant is determined from a separate series of experiments where MDM are infected for four hours. Extracellular bacteria are removed and cultures washed three times with PBS. Fresh media is replaced for 30 seconds and subsequently fixed in 4% PFA for quantification by flow cytometric analysis. The values are normalised to average integrated mCherry fluorescence of inocula. Line represents median. Figure 3.5A, I fixed and stained plates with DAPI (**Figure 3.8 Measurement of cell death using nuclear counts A** Example microscopy image of DAPI stained MDM nuclei. **B** MDM were infected (or mock infected) with H37Rv mCherry for four hours at MOI 1. Cultures were washed three times with PBS to remove all extracellular bacteria. Fresh media was added for the times specified. At the relevant time point the supernatant was removed and cells washed again three times with PBS. Cells were fixed in 4% PFA for 24 hours. Cells were washed and stained with DAPI nuclear stain for 15 minutes, and subsequently imaged on the Hermes high content microscope. Nuclei were enumerated using Metamorph software. Mean  $\pm$  SEM 7 separate experiments conducted in triplicate.

Figure 3.9 **Cell count analysis in central fields of view. A** MDM were infected (or mock infected) with H37Rv mCherry for four hours at MOI 1. Cultures were washed three times with PBS to remove all extracellular bacteria. Fresh media was added for the times specified. At the relevant time point the supernatant was removed and cells washed again three times with PBS. Cells were fixed in 4% PFA, washed and stained with DAPI nuclear stain for 15 minutes, and subsequently imaged on the Hermes high content microscope. Montages of all

fields of view per well per time point were created using Metamorph software. Panels i and ii are representative of 2 separate experiments. White arrows represent areas of physical manipulation of cells **B** Nuclei in the central 12 fields of view were enumerated using Metamorph software. Mean  $\pm$  SEM 7 separate experiments conducted in triplicate. Figure 3.8A) and enumerated the cells using a high content microscope covering 75% of each well. The data were analysed by Metamorph software, where nuclei were defined by both their size and staining intensity over the local background. Cells were included in the analysis if the nuclear area fell within the 5th to 95th centiles in order to discount incompletely imaged cells at the boundary of each image, and low frequency clumps of cells where the nuclei could not be accurately segmented.

Surprisingly I found a significant reduction in cell number in the first 24 hours within my experimental model (**Figure 3.8 Measurement of cell death using nuclear counts** **A** Example microscopy image of DAPI stained MDM nuclei. **B** MDM were infected (or mock infected) with H37Rv mCherry for four hours at MOI 1. Cultures were washed three times with PBS to remove all extracellular bacteria. Fresh media was added for the times specified. At the relevant time point the supernatant was removed and cells washed again three times with PBS. Cells were fixed in 4% PFA for 24 hours. Cells were washed and stained with DAPI nuclear stain for 15 minutes, and subsequently imaged on the Hermes high content microscope. Nuclei were enumerated using Metamorph software. Mean  $\pm$  SEM 7 separate experiments conducted in triplicate.

Figure 3.9 **Cell count analysis in central fields of view.** **A** MDM were infected

(or mock infected) with H37Rv mCherry for four hours at MOI 1. Cultures were washed three times with PBS to remove all extracellular bacteria. Fresh media was added for the times specified. At the relevant time point the supernatant was removed and cells washed again three times with PBS. Cells were fixed in 4% PFA, washed and stained with DAPI nuclear stain for 15 minutes, and subsequently imaged on the Hermes high content microscope. Montages of all fields of view per well per time point were created using Metamorph software. Panels i and ii are representative of 2 separate experiments. White arrows represent areas of physical manipulation of cells **B** Nuclei in the central 12 fields of view were enumerated using Metamorph software. Mean  $\pm$  SEM 7 separate experiments conducted in triplicate. Figure 3.8**B**). This was evident in both Mtb infected and uninfected cultures, and therefore not due to infection with Mtb. The attrition in cell number did not continue for the remainder of the experiment between 24 and 120 hours. I concluded that the reduction in cell numbers counted in this way represented a technical confounding in the model and sought to investigate the possible causes.

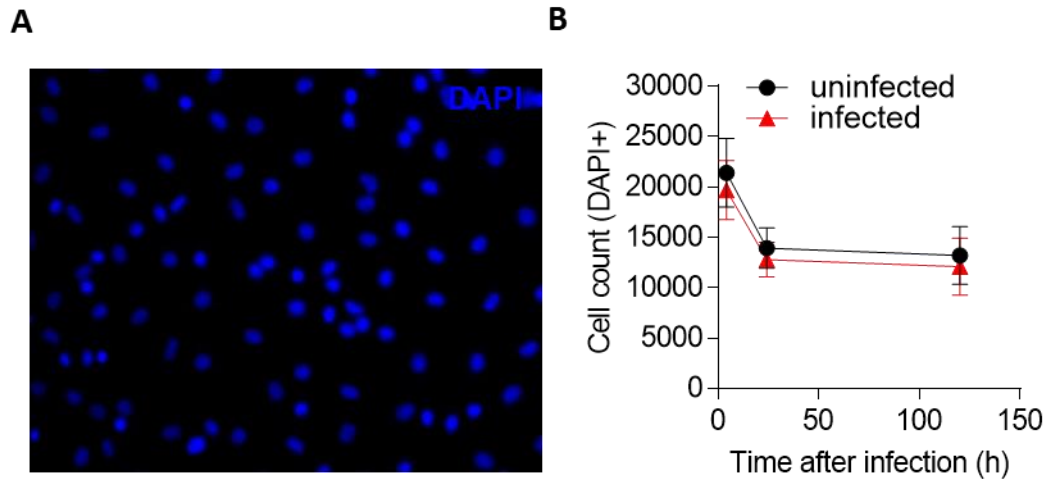


Figure 3.19 **Measurement of cell death using nuclear counts** **A** Example microscopy image of DAPI stained MDM nuclei. **B** MDM were infected (or mock infected) with H37Rv mCherry for four hours at MOI 1. Cultures were washed three times with PBS to remove all extracellular bacteria. Fresh media was added for the times specified. At the relevant time point the supernatant was removed and cells washed again three times with PBS. Cells were fixed in 4% PFA for 24 hours. Cells were washed and stained with DAPI nuclear stain for 15 minutes, and subsequently imaged on the Hermes high content microscope. Nuclei were enumerated using Metamorph software. Mean  $\pm$  SEM 7 separate experiments conducted in triplicate.

First, I tested the hypothesis that the physical manipulation of cell cultures in this time interval may have caused technical confounding. Montages of all the fields of view taken per well, revealed disruption of the cell monolayer in peripheral fields most likely disturbed by the pipette tip during washes at four hours (**Figure 3.9 Cell count analysis in central fields of view. A** MDM were infected (or mock infected) with H37Rv mCherry for four hours at MOI 1. Cultures were washed three times with PBS to remove all extracellular bacteria. Fresh media was added for the times specified. At the relevant time point the supernatant was removed and cells washed again three times with PBS. Cells were fixed in 4% PFA, washed and stained with DAPI nuclear stain for 15 minutes, and subsequently imaged on the Hermes high content microscope. Montages of all fields of view per well per time point were created using Metamorph software. Panels i and ii are representative of 2 separate experiments. White arrows represent areas of physical manipulation of cells **B** Nuclei in the central 12 fields of view were enumerated using Metamorph software. Mean  $\pm$  SEM 7 separate experiments conducted in triplicate.

Figure 3.10 **Distribution of nuclear area in 3 separate experiments** MDM were mock infected with RPMI + 5% human ABS for four hours. Cultures were washed three times with PBS. Fresh media was added for the times specified. At the relevant time point the supernatant was removed and cells washed again three times with PBS. Cells were fixed in 4% PFA, washed and stained with DAPI nuclear stain for 15 minutes, and subsequently imaged on the Hermes high

content microscope. Nuclear area was generated per cell by Metamorph software. Histograms show distribution nuclear area of both measurements at each time point. **Figure 3.9A, panels i and ii**). I therefore focused my analysis of cell numbers (counting DAPI+ nuclei) at each time point to the central 12 fields of view. However, the reduction in cell numbers from four-24 hours were still evident in this analysis (**Figure 3.9 Cell count analysis in central fields of view**. **A** MDM were infected (or mock infected) with H37Rv mCherry for four hours at MOI 1. Cultures were washed three times with PBS to remove all extracellular bacteria. Fresh media was added for the times specified. At the relevant time point the supernatant was removed and cells washed again three times with PBS. Cells were fixed in 4% PFA, washed and stained with DAPI nuclear stain for 15 minutes, and subsequently imaged on the Hermes high content microscope. Montages of all fields of view per well per time point were created using Metamorph software. Panels i and ii are representative of 2 separate experiments. White arrows represent areas of physical manipulation of cells **B** Nuclei in the central 12 fields of view were enumerated using Metamorph software. Mean  $\pm$  SEM 7 separate experiments conducted in triplicate.

**Figure 3.10 Distribution of nuclear area in 3 separate experiments** MDM were mock infected with RPMI + 5% human ABS for four hours. Cultures were washed three times with PBS. Fresh media was added for the times specified. At the relevant time point the supernatant was removed and cells washed again three times with PBS. Cells were fixed in 4% PFA, washed and stained with DAPI

nuclear stain for 15 minutes, and subsequently imaged on the Hermes high content microscope. Nuclear area was generated per cell by Metamorph software. Histograms show distribution nuclear area of both measurements at each time point. Figure 3.9**B**), though not quite as marked.

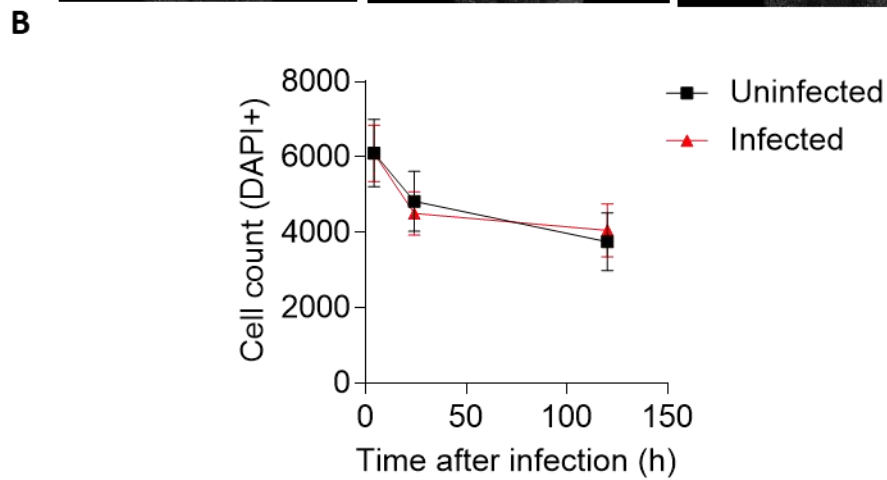
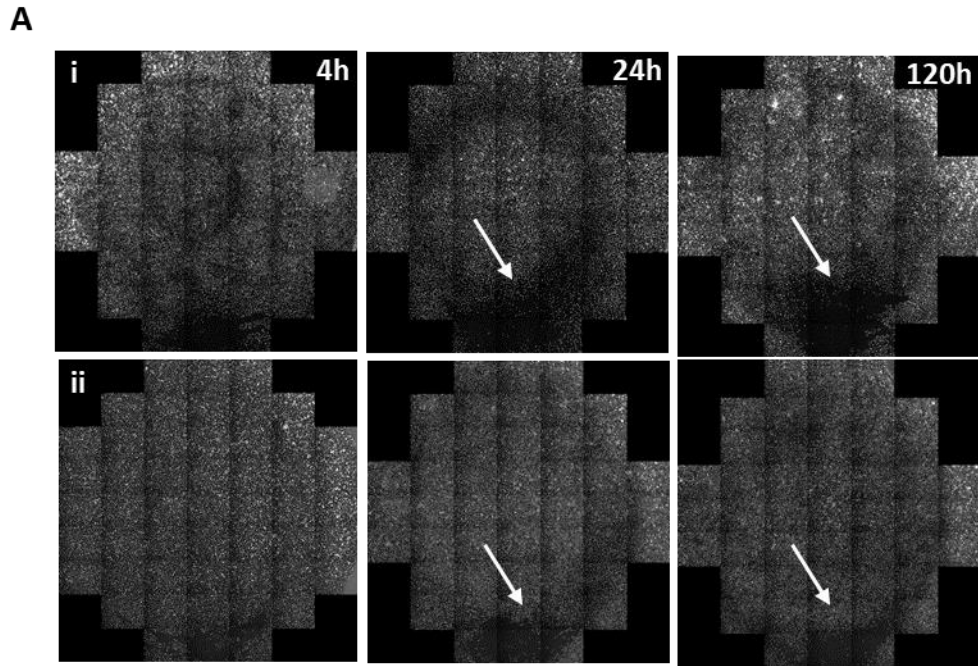
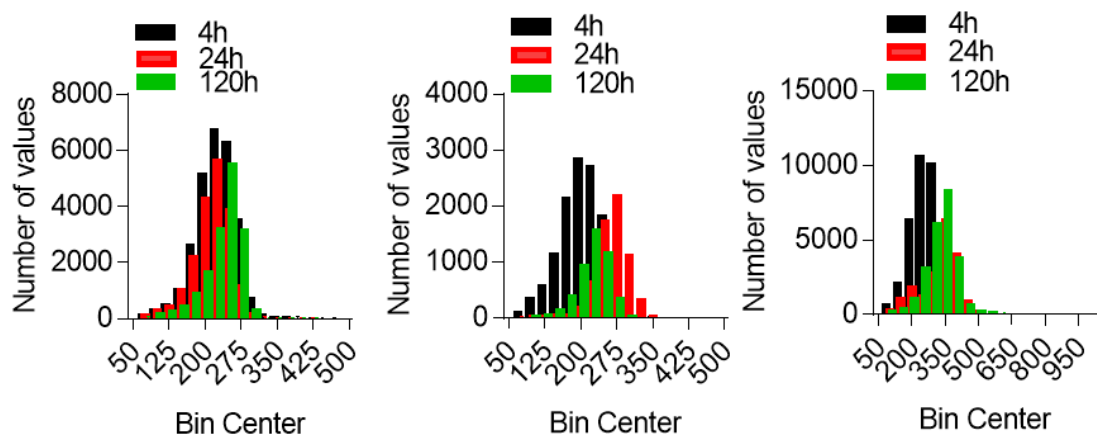


Figure 3.22 **Cell count analysis in central fields of view.** **A** MDM were infected (or mock infected) with H37Rv mCherry for four hours at MOI 1. Cultures were washed three times with PBS to remove all extracellular bacteria. Fresh media was added for the times specified. At the relevant time point the supernatant was removed and cells washed again three times with PBS. Cells were fixed in 4% PFA, washed and stained with DAPI nuclear stain for 15 minutes, and subsequently imaged on the Hermes high content microscope. Montages of all fields of view per well per time point were created using Metamorph software. Panels i and ii are representative of 2 separate experiments. White arrows represent areas of physical manipulation of cells **B** Nuclei in the central 12 fields of view were enumerated using Metamorph software. Mean  $\pm$  SEM 7 separate experiments conducted in triplicate.

Next, I sought to test the hypothesis that the cell numbers at four hours were over-inflated by contaminating lymphocytes or cellular debris in the MDM preparation. These are significantly smaller than MDM. Therefore, such contamination might be expected to generate a bimodal distribution in nuclear area and the loss of small lymphocytes would shift the frequency distribution of nuclear area to the right.

In fact, the nuclear area of the cells was normally distributed (rather than bimodal) at four hours, and I did not observe a consistent shift to the right the nuclear area distribution between four and 24 hour data (**Figure 3.10 Distribution of nuclear area in 3 separate experiments** MDM were mock infected with RPMI + 5%



human ABS for four hours. Cultures were washed three times with PBS. Fresh

**Figure 3.25 Distribution of nuclear area in 3 separate experiments** MDM were mock infected with RPMI + 5% human ABS for four hours. Cultures were washed three times with PBS. Fresh media was added for the times specified. At the relevant time point the supernatant was removed and cells washed again three times with PBS. Cells were fixed in 4% PFA, washed and stained with DAPI nuclear stain for 15 minutes, and subsequently imaged on the Hermes high content microscope. Nuclear area was generated per cell by Metamorph software. Histograms show distribution nuclear area of both measurements at each time point.

media was added for the times specified. At the relevant time point the supernatant was removed and cells washed again three times with PBS. Cells were fixed in 4% PFA, washed and stained with DAPI nuclear stain for 15

minutes, and subsequently imaged on the Hermes high content microscope. Nuclear area was generated per cell by Metamorph software. Histograms show distribution nuclear area of both measurements at each time point.

**Figure 3.11 Live Dead Staining to identify and enumerate necrotic cells** **A** MDM were treated with 30% hydrogen peroxide for 3 hours. Cells were washed and incubated for 20 minutes with live dead stain at room temperature, then fixed in 4% PFA. Nuclei were counterstained for DAPI and imaged using Hermes high content microscope **B** MDM were infected with H37Rv mCherry for four hours. Extracellular bacteria were removed by extensive washing and cells incubated for 20 minutes with live dead stain at room temperature, then fixed in 4% PFA. Nuclei were counterstained for DAPI, and imaged using Hermes high content microscope. White arrow head shows infect dead/ dying cell capable of releasing bacteria into extracellular space. Pink arrowhead shows dying uninfected cell. **C** As in B. Dead/ dying and live cells were enumerated using Metamorph software. Mean  $\pm$  SEM four separate experiments conducted in triplicate.

Figure 3.10).

Finally, I sought to test the hypothesis that the reduction in cells during four-24 hours represented an induction of cell death pathways during this time interval only. This seemed highly unlikely, since a true induction of cell death would be expected to continue past 24 hours.

In order to test this hypothesis, I used an alternative approach staining for dead or dying cells using a proprietary Live-Dead stain that detects the interior and exterior amines of dead cells following plasma membrane damage. Although, the premise of my cell counting assay is that adherent cells are viable, I reasoned that the live-dead stain would identify cell death before they detach. In this event, live-dead staining of cell cultures just after washing at the four hour time point may be expected to reveal a substantial number of cells committed to dying in the interval between four-24 hours.

First, I confirmed that the live-dead stain will stain dying adherent cells by using hydrogen peroxide to induce necrosis. As expected, this leads to a marked reduction in adherent cells. Importantly however all the cells that remained adherent stained positively for cell death (**Figure 3.11 Live Dead Staining to identify and enumerate necrotic cells A** MDM were treated with 30% hydrogen peroxide for 3 hours. Cells were washed and incubated for 20 minutes with live dead stain at room temperature, then fixed in 4% PFA. Nuclei were counterstained for DAPI and imaged using Hermes high content microscope **B** MDM were infected with H37Rv mCherry for four hours. Extracellular bacteria were removed by extensive washing and cells incubated for 20 minutes with live dead stain at room temperature, then fixed in 4% PFA. Nuclei were counterstained for DAPI, and imaged using Hermes high content microscope.

White arrow head shows infect dead/ dying cell capable of releasing bacteria into extracellular space. Pink arrowhead shows dying uninfected cell. **C** As in B. Dead/ dying and live cells were enumerated using Metamorph software. Mean  $\pm$  SEM four separate experiments conducted in triplicate.

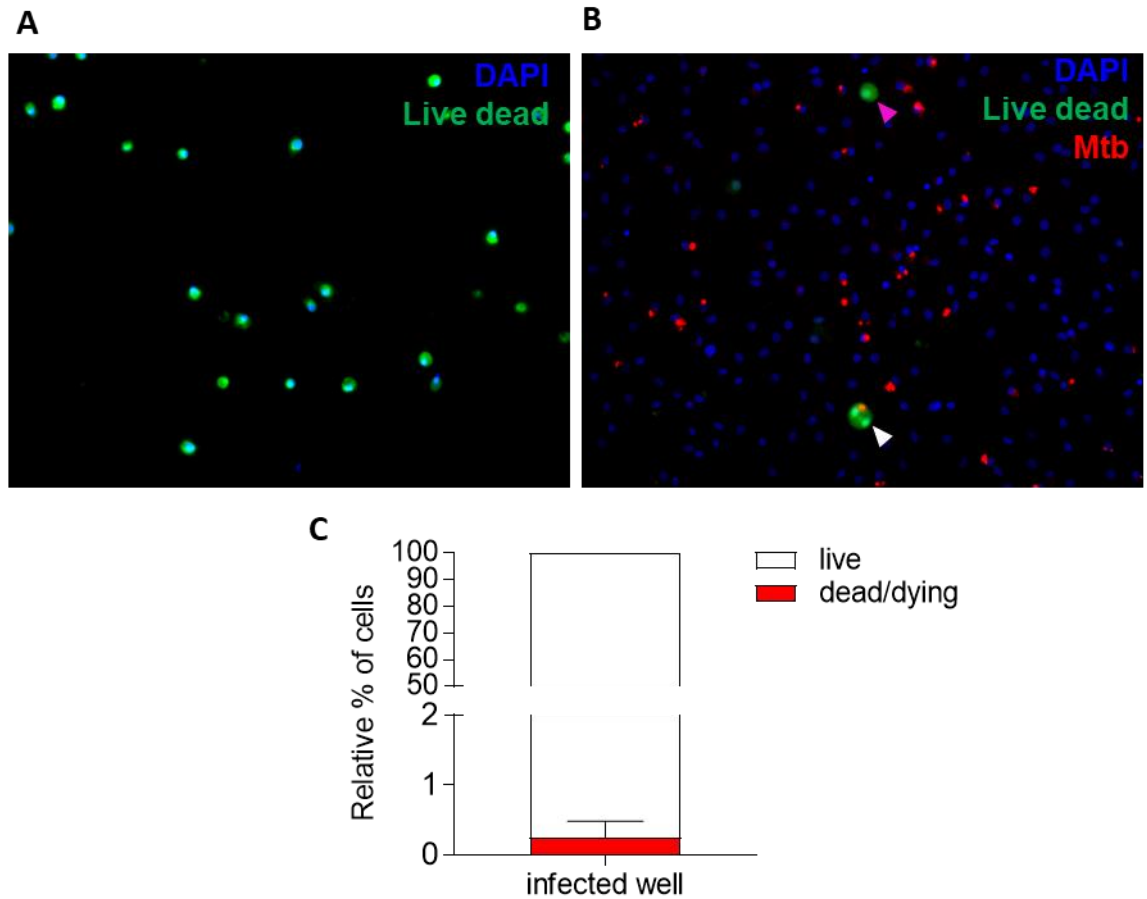
Figure 3.12 **Calculating the macrophage death rate** **A** Mathematically determined death rate ( $\delta$ ) between 24 and 120 hours using data in Figure 3.8 **B** MDM were infected (or mock infected) with H37Rv mCherry for four hours at MOI 1. Cultures were washed three times with PBS to remove all extracellular bacteria. Fresh media (RPMI + 5% human AB serum) was added for the times specified. At the relevant time point the supernatant was removed and cells washed again three times with PBS. Cells were fixed in 4% PFA, washed and stained with DAPI nuclear stain for 15 minutes, and subsequently imaged on the Hermes high content microscope. Nuclei were enumerated using Metamorph software. Nuclear counts in infected wells were normalised to uninfected wells. Mean  $\pm$  SEM 7 separate experiments conducted in triplicate

Figure 3.11**A**). In contrast, the same stain revealed very few dying cells in my Mtb infected experimental model after the washing step at 4 hours (**Figure 3.11 Live Dead Staining to identify and enumerate necrotic cells** **A** MDM were treated with 30% hydrogen peroxide for 3 hours. Cells were washed and incubated for 20 minutes with live dead stain at room temperature, then fixed in 4% PFA. Nuclei were counterstained for DAPI and imaged using Hermes high content microscope **B** MDM were infected with H37Rv mCherry for four hours. Extracellular bacteria were removed by extensive washing and cells incubated for 20 minutes with live dead stain at room temperature, then fixed in 4% PFA. Nuclei were counterstained for DAPI, and imaged using Hermes high content microscope. White arrow head shows infect dead/ dying cell capable of releasing bacteria into extracellular space. Pink arrowhead shows dying uninfected cell. **C** As in B. Dead/ dying and live cells were enumerated using Metamorph software. Mean  $\pm$  SEM four separate experiments conducted in triplicate.

Figure 3.12 **Calculating the macrophage death rate** **A** Mathematically determined death rate ( $\delta$ ) between 24 and 120 hours using data in Figure 3.8 **B** MDM were infected (or mock infected) with H37Rv mCherry for four hours at MOI 1. Cultures were washed three times with PBS to remove all extracellular bacteria. Fresh media (RPMI + 5% human AB serum) was added for the times specified. At the relevant time point the supernatant was removed and cells washed again three times with PBS. Cells were fixed in 4% PFA, washed and stained with DAPI nuclear stain for 15 minutes, and subsequently imaged on the Hermes high content microscope. Nuclei were enumerated using Metamorph software. Nuclear counts in infected wells were normalised to uninfected wells. Mean  $\pm$  SEM 7 separate experiments conducted in triplicate

Figure 3.11**B and C**).

These data suggested that the reduction in adherent cells between four-24 hours may not represent a true rate of cell death.



**Figure 3.28 Live Dead Staining to identify and enumerate necrotic cells** **A** MDM were treated with 30% hydrogen peroxide for 3 hours. Cells were washed and incubated for 20 minutes with live dead stain at room temperature, then fixed in 4% PFA. Nuclei were counterstained for DAPI and imaged using Hermes high content microscope **B** MDM were infected with H37Rv mCherry. Extracellular bacteria were removed by extensive washing and cells incubated for 20 minutes with live dead stain at room temperature, then fixed in 4% PFA. Nuclei were counterstained for DAPI, and imaged using Hermes high content microscope. White arrow head shows infect dead/ dying cell capable of releasing bacteria into extracellular space. Pink arrowhead shows dying uninfected cell. **C** As in B. Dead/ dying and live cells were enumerated using Metamorph software. Mean  $\pm$  SEM four separate experiments conducted in triplicate.

### 3.3.7 Necrotic cell death does not explain extracellular bacillary load

Following all of the analyses conducted in **section 3.3.6**, I was confident that the nuclear count data at four hours were subject to technical confounding as per my original hypothesis, and needed to be excluded. I therefore used the nuclear counts between 24 and 120 hours to determine the true rate of cell death following infection or mock infection with Mtb, and input this into the model.

Macrophage death occurs at rate  $\delta$  (**Figure 3.12 Calculating the macrophage death rate A** Mathematically determined death rate ( $\delta$ ) between 24 and 120 hours using data in Figure 3.8 **B** MDM were infected (or mock infected) with H37Rv mCherry for four hours at MOI 1. Cultures were washed three times with PBS to remove all extracellular bacteria. Fresh media (RPMI + 5% human AB serum) was added for the times specified. At the relevant time point the supernatant was removed and cells washed again three times with PBS. Cells were fixed in 4% PFA, washed and stained with DAPI nuclear stain for 15 minutes, and subsequently imaged on the Hermes high content microscope. Nuclei were enumerated using Metamorph software. Nuclear counts in infected wells were normalised to uninfected wells. Mean  $\pm$  SEM 7 separate experiments conducted in triplicate

Figure 3.13 **Determining the extracellular growth rate of Mtb.** **A** Macrophage conditioned medium (infCoM) was generated by infecting MDM for 24 hours at MOI 1. The supernatant was harvested and filter sterilized through spin filters. infCoM was collected in this way for four donors, and pooled to reduce donor variability. Both 7H9 (supplemented with 10% OADC and 0.2% glycerol) and infCoM were subsequently re-infected with  $5 \times 10^4$  cfu. **B** Bacteria were enumerated by flow cytometry at inoculation, and at 120 hours to determine extracellular bacillary growth. Mean  $\pm$  SEM 7 separate experiments conducted in triplicate **C** Mathematically determined extracellular growth rate in 7H9 and infCoM between 0 and 120 hours. Open circles represent extracellular growth rate in individual experiments. Triangles = Mean extracellular growth rate.

Figure 3.12A), calculated simply by the change in cell number over time, and is assumed to occur at an exponential rate. There is minimal attrition in nuclear count between 24 and 120 hours in both infected and uninfected cells. Since any cell death that does occur is not secondary to Mtb infection (the number of cells in the infected culture is equivalent to the number of cells in the uninfected culture at each time point (**Figure 3.12 Calculating the macrophage death rate A** Mathematically determined death rate ( $\delta$ ) between 24 and 120 hours using data in Figure 3.8 **B** MDM were infected (or mock infected) with H37Rv mCherry for four hours at MOI 1. Cultures were washed three times with PBS to remove all extracellular bacteria. Fresh media (RPMI + 5% human AB serum) was added for the times specified. At the relevant time point the supernatant was removed and cells washed again three times with PBS. Cells were fixed in 4% PFA, washed and stained with DAPI nuclear stain for 15 minutes, and subsequently imaged on the Hermes high content microscope. Nuclei were enumerated using Metamorph software. Nuclear counts in infected wells were normalised to uninfected wells. Mean  $\pm$  SEM 7 separate experiments conducted in triplicate

Figure 3.13 **Determining the extracellular growth rate of Mtb.** A Macrophage conditioned medium (infCoM) was generated by infecting MDM for 24 hours at MOI 1. The supernatant was harvested and filter sterilized through spin filters. infCoM was collected in this way for four donors, and pooled to reduce donor variability. Both 7H9 (supplemented with 10% OADC and 0.2% glycerol) and infCoM were subsequently re-infected with  $5 \times 10^4$  cfu. **B** Bacteria were enumerated by flow cytometry at inoculation, and at 120 hours to determine extracellular bacillary growth. Mean  $\pm$  SEM 7 separate experiments conducted in triplicate **C** Mathematically determined extracellular growth rate in 7H9 and infCoM between 0 and 120 hours. Open circles represent extracellular growth rate in individual experiments. Triangles = Mean extracellular growth rate.

Figure 3.12B), both uninfected and infected cells are therefore presumed to die at the same rate.



These dying infected macrophages (albeit in small numbers) release intracellular Mtb to become extracellular. I hypothesized that necrosis, in combination with extracellular Mtb replication, might account for the observed bacterial loads. I first determined the rate of extracellular Mtb replication *in vitro*.

I obtained the rate of extracellular Mtb replication in macrophage cultures by inoculating Mtb into filter sterilized conditioned media from MDM cultures infected with Mtb for 24 hours (infCoM), pooled from four donors to mitigate against any donor specific confounding effects (**Figure 3.13 Determining the extracellular growth rate of Mtb**). A Macrophage conditioned medium (infCoM) was generating by infecting MDM for 24 hours at MOI 1. The supernatant was harvested and filter sterilized through spin filters. infCoM was collected in this way for four donors, and pooled to reduce donor variability. Both 7H9 (supplemented with 10% OADC and 0.2% glycerol) and infCoM were subsequently re-infected with  $5 \times 10^4$  cfu. **B** Bacteria were enumerated by flow cytometry at inoculation, and at 120 hours to determine extracellular bacillary growth. Mean  $\pm$  SEM 7 separate experiments conducted in triplicate **C** Mathematically determined extracellular growth rate in 7H9 and infCoM between 0 and 120 hours. Open circles represent extracellular growth rate in individual experiments. Triangles = Mean extracellular growth rate.

Figure 3.14 **Model parameterisation**. **A** Mathematical model attempts to find a pair of values for the intracellular replication rate ( $r_I$ ) and rate of Mtb uptake ( $\beta$ ) after the values for extracellular growth rate and cell death rate are fixed. 200000 pairs of values were chosen at random and the SSE calculated for each of these pairs. The SSE describes the smallest deviation from the actual values of the data. The 'best' parameter values achieve a SSE of 5.15 **B** Using the pair of values for  $r_I$  and  $\beta$  with the lowest SSE in combination with the experimentally measured extracellular growth rate and cell death rate, the model (lines) attempts to find the best fit to the observed data (dots)

Figure 3.13A.). I then quantitated bacterial growth in the infCoM by flow cytometry after 120 hours (**Figure 3.13 Determining the extracellular growth rate of Mtb.** A Macrophage conditioned medium (infCoM) was generating by infecting MDM for 24 hours at MOI 1. The supernatant was harvested and filter sterilized through spin filters. infCoM was collected in this way for four donors, and pooled to reduce donor variability. Both 7H9 (supplemented with 10% OADC and 0.2% glycerol) and infCoM were subsequently re-infected with  $5 \times 10^4$  cfu. **B** Bacteria were enumerated by flow cytometry at inoculation, and at 120 hours to determine extracellular bacillary growth. Mean  $\pm$  SEM 7 separate experiments conducted in triplicate **C** Mathematically determined extracellular growth rate in 7H9 and infCoM between 0 and 120 hours. Open circles represent extracellular growth rate in individual experiments. Triangles = Mean extracellular growth rate.

Figure 3.14 **Model parameterisation.** **A** Mathematical model attempts to find a pair of values for the intracellular replication rate ( $r_I$ ) and rate of Mtb uptake ( $\beta$ ) after the values for extracellular growth rate and cell death rate are fixed. 200000 pairs of values were chosen at random and the SSE calculated for each of these pairs. The SSE describes the smallest deviation from the actual values of the data. The 'best' parameter values achieve a SSE of 5.15 **B** Using the pair of values for  $r_I$  and  $\beta$  with the lowest SSE in combination with the experimentally measured extracellular growth rate and cell death rate, the model (lines) attempts to find the best fit to the observed data (dots)

Figure 3.13B). Assuming exponential growth, we used (**Equation 1, Materials and Methods**)

$$\frac{dI}{dt} = r_I I$$

describing the rate of increase of bacteria over time, to give an extracellular Mtb growth rate of as  $0.0219 \text{ h}^{-1}$  (doubling time 31.7 h) (**Figure 3.13 Determining the extracellular growth rate of Mtb**). A Macrophage conditioned medium (infCoM) was generating by infecting MDM for 24 hours at MOI 1. The supernatant was harvested and filter sterilized through spin filters. infCoM was collected in this way for four donors, and pooled to reduce donor variability. Both 7H9 (supplemented with 10% OADC and 0.2% glycerol) and infCoM were subsequently re-infected with  $5 \times 10^4$  cfu. **B** Bacteria were enumerated by flow cytometry at inoculation, and at 120 hours to determine extracellular bacillary growth. Mean  $\pm$  SEM 7 separate experiments conducted in triplicate **C** Mathematically determined extracellular growth rate in 7H9 and infCoM between 0 and 120 hours. Open circles represent extracellular growth rate in individual experiments. Triangles = Mean extracellular growth rate.

Figure 3.14 **Model parameterisation**. **A** Mathematical model attempts to find a pair of values for the intracellular replication rate ( $r_l$ ) and rate of Mtb uptake ( $\beta$ ) after the values for extracellular growth rate and cell death rate are fixed. 200000 pairs of values were chosen at random and the SSE calculated for each of these pairs. The SSE describes the smallest deviation from the actual values of the data. The 'best' parameter values achieve a SSE of 5.15 **B** Using the pair of values for  $r_l$  and  $\beta$  with the lowest SSE in combination with the experimentally measured extracellular growth rate and cell death rate, the model (lines) attempts to find the best fit to the observed data (dots)

Figure 3.13**C**).

Interestingly, Mtb growth in infCoM was equivalent to its growth in 7H9 broth that is conventionally used for its propagation in the laboratory, suggesting that the extracellular milieu is growth permissive.

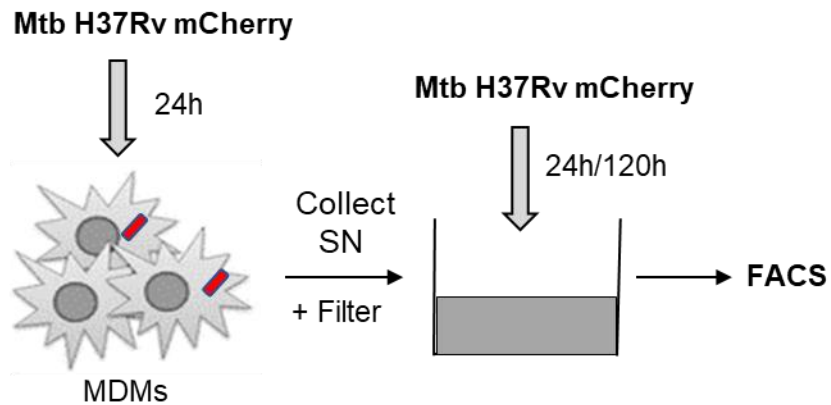
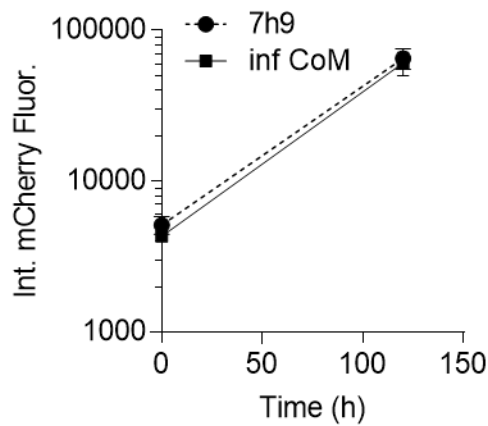
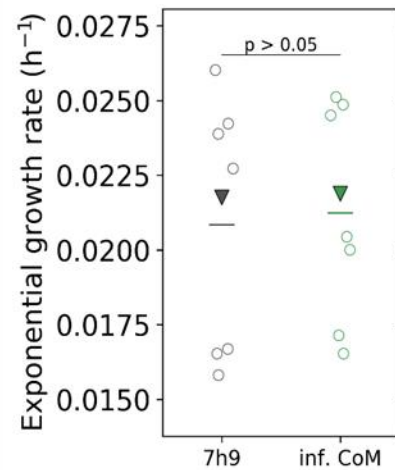
**A****B****C**

Figure 3.34 **Determining the extracellular growth rate of Mtb.** A Macrophage conditioned medium (infCoM) was generated by infecting MDM for 24 hours at MOI 1. The supernatant was harvested and filter sterilized through spin filters. infCoM was collected in this way for four donors, and pooled to reduce donor variability. Both 7H9 (supplemented with 10% OADC and 0.2% glycerol) and infCoM were subsequently re-infected with  $5 \times 10^4$  cfu. **B** Bacteria were enumerated by flow cytometry at inoculation, and at 120 hours to determine extracellular bacillary growth. Mean  $\pm$  SEM 7 separate experiments conducted in triplicate **C** Mathematically determined extracellular growth rate in 7H9 and infCoM between 0 and 120 hours. Open circles represent extracellular growth rate in individual experiments. Triangles = Mean extracellular growth rate.

I next embarked on a series of modelling exercises to address my hypothesis that necrotic cell death in conjunction with extracellular replication of bacteria would account for the extracellular bacillary load. I used the mathematical model depicted in **Figure 3.7 Model of Mtb-macrophage interactions** (1) Bacterial uptake by macrophages (2) Mtb replication within live macrophages (3) Macrophage cell death leading to release of bacteria into extracellular space (4) Extracellular Mtb replication (5) Non-lytic egress of bacteria from live macrophages into the extracellular space

Figure 3.8 **Measurement of cell death using nuclear counts** **A** Example microscopy image of DAPI stained MDM nuclei. **B** MDM were infected (or mock infected) with H37Rv mCherry for four hours at MOI 1. Cultures were washed three times with PBS to remove all extracellular bacteria. Fresh media was added for the times specified. At the relevant time point the supernatant was removed and cells washed again three times with PBS. Cells were fixed in 4% PFA for 24 hours. Cells were washed and stained with DAPI nuclear stain for 15 minutes, and subsequently imaged on the Hermes high content microscope. Nuclei were enumerated using Metamorph software. Mean  $\pm$  SEM 7 separate experiments conducted in triplicate. Figure 3.7.

This mathematical model incorporates rates for bacterial replication ( $r$ ), internalization of extracellular bacteria by macrophages ( $\beta$ ) and macrophage death ( $\delta$ ) resulting in transfer of bacteria from the intracellular (I) to extracellular (E) compartments.

The change in extracellular bacillary load over time is thereby given by the equation (**Equation 2, Materials and Methods**)

$$\frac{dE}{dt} = r_E E - \beta E + \delta I$$

where  $r_E E$  is the rate of extracellular Mtb growth,  $\beta E$  is the rate of Mtb uptake by macrophages and  $\delta I$  is the rate of cell death of infected cells releasing extracellular bacteria. The change in intracellular bacillary load over time is given by the equation (**Equation 2, Materials and Methods**):

$$\frac{dI}{dt} = r_I I + \beta E - \delta I$$

where  $r_I I$  is the rate of intracellular Mtb growth,  $\beta E$  is the rate of Mtb uptake by macrophages and  $\delta I$  is the rate of cell death of infected cells releasing extracellular bacteria.

Having determined the rate of cell death and the rate of extracellular Mtb replication experimentally, I next sought to estimate the remaining model parameters- the intracellular replication rate ( $r_I$ ) and the rate of bacterial uptake ( $\beta$ ) in silico. The aim of the model is to find values for these parameters that give the lowest sum of squared errors of prediction (SSE). The SSE describes the smallest deviation from the actual values of the data (i.e. the closer the SSE is to 0, the better the fit). We used a 'parameter search' method, whereby 200,000 pairs of values for  $r_I$  and  $\beta$  were chosen at random and the SSE calculated for each of these pairs (**Figure 3.14 Model parameterisation. A** Mathematical model attempts to find a pair of values for the intracellular replication rate ( $r_I$ ) and rate of Mtb uptake ( $\beta$ ) after the values for extracellular growth rate and cell death

rate are fixed. 200000 pairs of values were chosen at random and the SSE calculated for each of these pairs. The SSE describes the smallest deviation from the actual values of the data. The 'best' parameter values achieve a SSE of 5.15

**B** Using the pair of values for  $r_l$  and  $\beta$  with the lowest SSE in combination with the experimentally measured extracellular growth rate and cell death rate, the model (lines) attempts to find the best fit to the observed data (dots)

Figure 3.15 **Running the model with a higher death rate** **A** Mathematical model attempts to find a pair of values for the intracellular replication rate ( $r_l$ ) and rate of Mtb uptake ( $\beta$ ) after the values for extracellular growth rate and cell death rate are fixed. The cell death rate is calculated from the rate of change in nuclear count between four and 24 hours, and then 24 to 120hours. 200000 pairs of values for  $r_l$  and  $\beta$  were chosen at random and the SSE calculated for each of these pairs. The SSE describes the smallest deviation from the actual values of the data. The 'best' parameter values achieve a SSE of 5.15 **B** Using the pair of values for  $r_l$  and  $\beta$  with the lowest SSE in combination with the experimentally measured extracellular growth rate and cell death rate, the model (lines) attempts to find the best fit to the observed data (dots)

Figure 3.14**A**). The best SSE that could be achieved was 5.15, which indicates very poor fitting of the model to the observed data. This is further depicted in

**Figure 3.14 Model parameterisation.** **A** Mathematical model attempts to find a pair of values for the intracellular replication rate ( $r_l$ ) and rate of Mtb uptake ( $\beta$ ) after the values for extracellular growth rate and cell death rate are fixed. 200000 pairs of values were chosen at random and the SSE calculated for each of these pairs. The SSE describes the smallest deviation from the actual values of the data. The 'best' parameter values achieve a SSE of 5.15 **B** Using the pair of values for  $r_l$  and  $\beta$  with the lowest SSE in combination with the experimentally measured extracellular growth rate and cell death rate, the model (lines) attempts to find the best fit to the observed data (dots)

Figure 3.15 **Running the model with a higher death rate** **A** Mathematical model attempts to find a pair of values for the intracellular replication rate ( $r_i$ ) and rate of Mtb uptake ( $\beta$ ) after the values for extracellular growth rate and cell death rate are fixed. The cell death rate is calculated from the rate of change in nuclear count between four and 24 hours, and then 24 to 120 hours. 200000 pairs of values for  $r_i$  and  $\beta$  were chosen at random and the SSE calculated for each of these pairs. The SSE describes the smallest deviation from the actual values of the data. The 'best' parameter values achieve a SSE of 5.15 **B** Using the pair of values for  $r_i$  and  $\beta$  with the lowest SSE in combination with the experimentally measured extracellular growth rate and cell death rate, the model (lines) attempts to find the best fit to the observed data (dots)

Figure 3.14**B**, where we use the estimates for the parameter values that give this 'best' SSE, as well as the experimentally determined extracellular growth rate and rate of cell death to run the model, and find poor fitting to the observed data points. Extracellular bacterial accumulation therefore cannot be explained by macrophage death and bacterial replication alone.

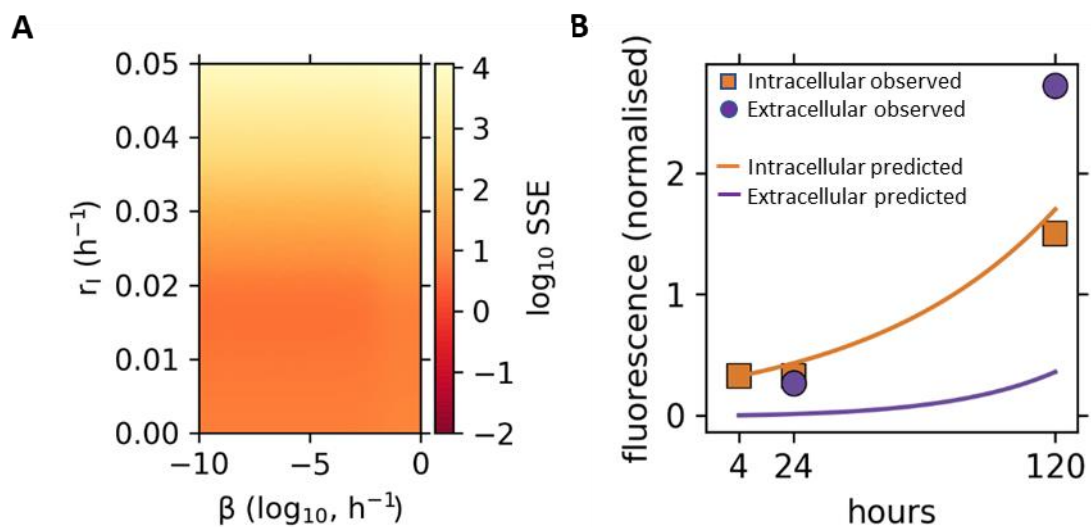


Figure 3.37 **Model parameterisation.** **A** Mathematical model attempts to find a pair of values for the intracellular replication rate ( $r_i$ ) and rate of Mtb uptake ( $\beta$ ) after the values for extracellular growth rate and cell death rate are fixed. 200000 pairs of values were chosen at random and the SSE calculated for each of these pairs. The SSE describes the smallest deviation from the actual values of the data. The 'best' parameter values achieve a SSE of 5.15 **B** Using the pair of values for  $r_i$  and  $\beta$  with the lowest SSE in combination with the experimentally measured extracellular growth rate and cell death rate, the model (lines) attempts to find the best fit to the observed data (dots)

Next I used a different value for cell death to see if I was able to fit the observed data. Although I was confident that the four hour cell count data represented technical confounding in my experiments, I thought it prudent to use a mathematical modelling approach to ask the question- if the sharp attrition in cell number between four and 24 hours was true, followed by a stabilization in the death rate (as implied by the nuclear counts) could *this* level of cell death explain the amount of bacteria accumulating in the extracellular milieu? I used the experimentally determined Mtb extracellular growth rate, and the cell death rate as calculated by the change in cell numbers at four and 24 hours, and then 24 to 120 hours to input into the model. Again, the remaining model parameters were unknown (i.e. the intracellular replication rate ( $r_i$ ), and the rate of Mtb uptake by macrophages ( $\beta$ )). We conducted the same parameter search as described above. The best SSE that we could achieve was 5.6, indicating poor fitting between the model and the observed data, as shown in Figure **3.15 Running the model with a higher death rate**

**A** Mathematical model attempts to find a pair of values for the intracellular replication rate ( $r_i$ ) and rate of Mtb uptake ( $\beta$ ) after the values for extracellular growth rate and cell death rate are fixed. The cell death rate is calculated from the rate of change in nuclear count between four and 24 hours, and then 24 to 120hours. 200000 pairs of values for  $r_i$  and  $\beta$  were chosen at random and the SSE calculated for each of these pairs. The SSE describes the smallest deviation from the actual values of the data. The 'best' parameter values achieve a SSE of 5.15

**B** Using the pair of values for  $r_i$  and  $\beta$  with the lowest SSE in combination with the experimentally measured extracellular growth rate and cell death rate, the model (lines) attempts to find the best fit to the observed data (dots)

Figure 3.16 **Incorporating non-lytic egress into the mathematical model** A set of randomly selected parameter values is used to run an optimization algorithm. The initial parameter values are optimized (up to a maximum of 600 re-iterations) until it converges to the lowest SSE. This process is repeated 50,000 times, and as such generates 50,000 parameter estimates and their associated SSEs. Using the parameter values that give the lowest SSE, this model (incorporating non-lytic egress) is able to describe the observed data well. **Figure 3.15A and B.**

I concluded that even if the cell counts at 4 hours were 'true', and there really was significant cell death between 4 and 24 hours, we were still unable to account for the amount of bacteria measured in the extracellular milieu.

I concluded that cell death (using different death rates) and extracellular bacterial replication were insufficient to account for the observed data, and that an additional parameter describing the movement of bacteria from the intracellular to the extracellular compartment needed to be incorporated into the model.

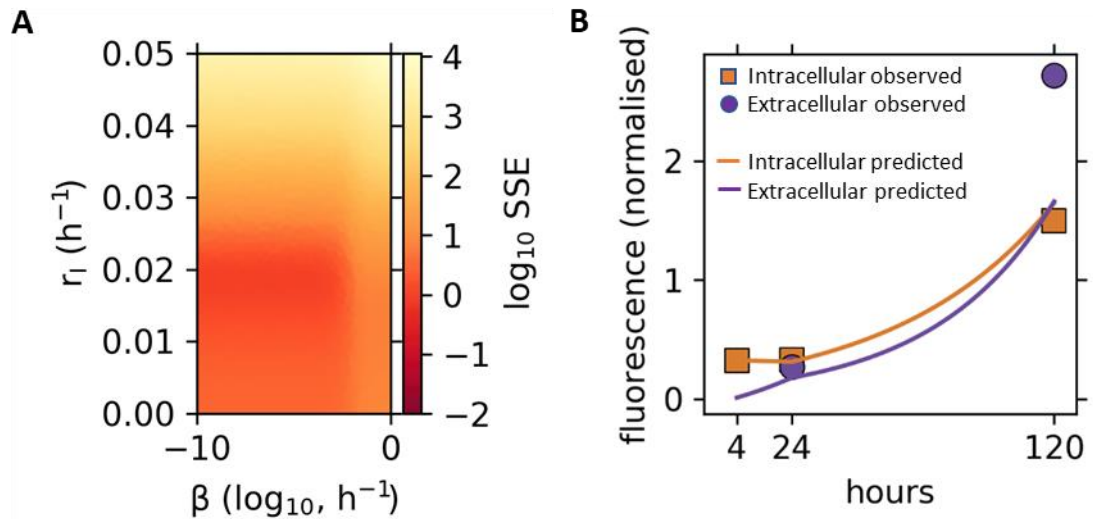


Figure 3.40 **Running the model with a higher death rate** **A** Mathematical model attempts to find a pair of values for the intracellular replication rate ( $r_i$ ) and rate of Mtb uptake ( $\beta$ ) after the values for extracellular growth rate and cell death rate are fixed. The cell death rate is calculated from the rate of change in nuclear count between four and 24 hours, and then 24 to 120hours. 200000 pairs of values for  $r_i$  and  $\beta$  were chosen at random and the SSE calculated for each of these pairs. The SSE describes the smallest deviation from the actual values of the data. The 'best' parameter values achieve a SSE of 5.15 **B** Using the pair of values for  $r_i$  and  $\beta$  with the lowest SSE in combination with the experimentally measured extracellular growth rate and cell death rate, the model (lines) attempts to find the best fit to the observed data (dots)

### 3.3.8 Extracellular bacteria are predicted to arise from non-lytic egress

I introduced an additional term to the mathematical model describing a process

of non-lytic egress allowing bacterial transfer from the intracellular compartment to the extracellular compartment (**Equation 3, Materials and Methods**).

$$\frac{dE}{dt} = r_E E - \beta E + \delta I + \eta I$$

$$\frac{dI}{dt} = r_I I + \beta E - \delta I - \eta I$$

The change in extracellular and intracellular loads is given by the same terms as in **Equation 2**, but here we also incorporate  $\eta I$  describing the movement of bacteria from the intracellular environment to the extracellular milieu.

After fixing the Mtb extracellular replication rate and rate of MDM cell death observed between 24-120 hours, we used the model to estimate values for the intracellular bacterial replication rate ( $r_I$ ), the rate of Mtb uptake ( $\beta$ ), and the non-lytic egress rate ( $\eta$ ).

We used the Nelder-Mead algorithm, implemented using the optimize function of Scipy in Python. This is a standard model fitting approach that uses an optimization algorithm to find estimates of the values of  $r_I$ ,  $\beta$ , and  $\eta$  that minimise the SSE between the model and the observed intra and extracellular fluorescence at 24 and 120 hours.

We take a set of randomly selected parameter values and run the algorithm. The initial parameter values are optimized (up to a maximum of 600 re-iterations) until it converges to the lowest SSE. This process is repeated 50,000 times, and as such generates 50,000 parameter estimates and their associated SSEs. We identified the minimum SSE from these sets of estimates, and then selected the

other sets of estimates that provided an SSE within 1% of this minimum, which we consider to be an equivalently good model fit.

One might imagine an uneven landscape with several valleys, each of which represent an SSE. The Nelder Mead algorithm takes the initial parameter value and tries to find its way down the valley floor. With each run, the algorithm may derive the parameters that lead to a valley floor, but there may be other valley floors that are lower. We therefore run the algorithm 50,000 times to find the 'true' valley floor.

Using the parameter values that give the lowest SSE, we found that a model incorporating non-lytic egress was able to describe the observed data well (**Figure 3.16 Incorporating non-lytic egress into the mathematical model** A set of randomly selected parameter values is used run an optimization algorithm. The initial parameter values are optimized (up to a maximum of 600 re-iterations) until it converges to the lowest SSE. This process is repeated 50,000 times, and as such generates 50,000 parameter estimates and their associated SSEs. Using the parameter values that give the lowest SSE, this model (incorporating non-lytic egress) is able to describe the observed data well

Figure 3.17 **Model tries to predict  $r_{il}$  (rate of intracellular replication),  $\beta$  (rate of Mtb uptake by macrophages) and  $\eta$  (rate of non-lytic egress)** to best fit the observed data. A set of randomly selected parameter values is used run an optimization algorithm. The initial parameter values are optimized (up to a maximum of 600 re-iterations) until it converges to the lowest SSE. This process is repeated 50,000 times, and as such generates 50,000 parameter estimates and their associated SSEs. Figure shows scatter plot of the parameter values that give the minimum SSE, and other sets of values that provide an SSE within 1% of this minimum. A number of values for  $r_{il}$ ,  $\beta$ , and  $\eta$  can be used to describe the data. These parameters are strongly correlated.

Figure 3.16)

However, as can be seen in **Figure 3.17 Model tries to predict  $r_{il}$  (rate of**

**intracellular replication),  $\beta$  (rate of Mtb uptake by macrophages) and  $\eta$  (rate of non-lytic egress)** to best fit the observed data. A set of randomly selected parameter values is used to run an optimization algorithm. The initial parameter values are optimized (up to a maximum of 600 re-iterations) until it converges to the lowest SSE. This process is repeated 50,000 times, and as such generates 50,000 parameter estimates and their associated SSEs. Figure shows scatter plot of the parameter values that give the minimum SSE, and other sets of values that provide an SSE within 1% of this minimum. A number of values for  $r_{il}$ ,  $\beta$ , and  $\eta$  can be used to describe the data. These parameters are strongly correlated.

Figure 4.1 **Experimental model to look for non-lytic egress of Mtb.** MDM were infected with H37Rv mCherry for 4 hours at MOI 1. Cultures were washed three times with PBS to remove all extracellular bacteria. Fresh media was added for 60min. Extracellular bacteria in the supernatant were collected and intracellular bacteria were harvested by washing and lysing cells. Bacteria were fixed in 4% PFA and analysed by flow cytometry. Figure 3.17, the optimization algorithm found a number of combinations of parameter values of  $r_{il}$  and  $\beta$ , and  $r_{il}$  and  $\eta$ , (represented by each dot) that fit the model to the observed data within 1% of the lowest SSE. Therefore we could not definitively derive the rates of any of these parameters. We also found that the values  $\beta$  and  $\eta$  were strongly correlated. From these data I inferred that, perhaps unsurprisingly, more uptake results in more non-lytic egress. The rate of one of these variables needs to be calculated experimentally in order for the model to derive the rate of the other.

I concluded that non-lytic egress of Mtb from human macrophages is likely to be

a crucial strategy by which extracellular bacteria accumulate, since a mathematical model is unable to predict the observed data without incorporating this process. However, using the mathematical model alone, we were unable to definitively estimate the rate at which all of these processes occur<sup>3</sup>.

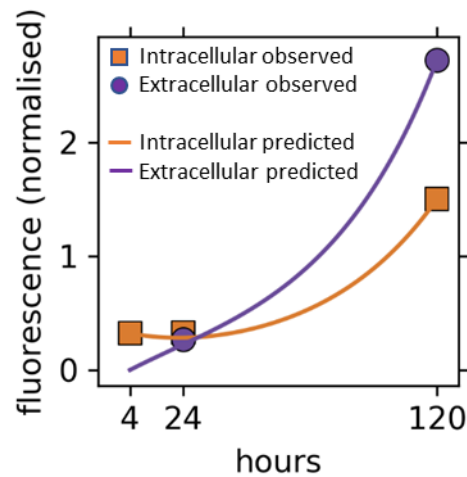


Figure 3.43 **Incorporating non-lytic egress into the mathematical model** A set of randomly selected parameter values is used to run an optimization algorithm. The initial parameter values are optimized (up to a maximum of 600 re-iterations) until it converges to the lowest SSE. This process is repeated 50,000 times, and as such generates 50,000 parameter estimates and their associated SSEs. Using the parameter values that give the lowest SSE, this model (incorporating non-lytic egress) is able to describe the observed data well

<sup>3</sup> Modelling by KB, data from MM

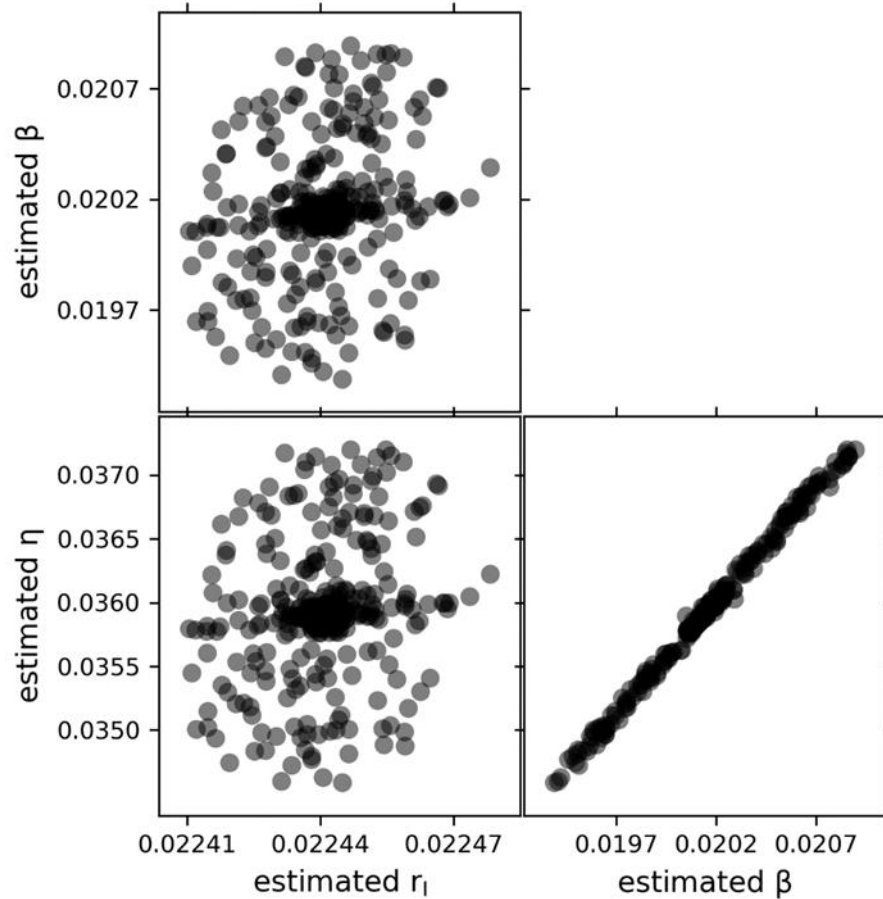


Figure 3.46 **Model tries to predict  $r_1$  (rate of intracellular replication),  $\beta$  (rate of Mtb uptake by macrophages) and  $\eta$  (rate of non-lytic egress) to best fit the observed data.** A set of randomly selected parameter values is used run an optimization algorithm. The initial parameter values are optimized (up to a maximum of 600 re-iterations) until it converges to the lowest SSE. This process is repeated 50,000 times, and as such generates 50,000 parameter estimates and their associated SSEs. Figure shows scatter plot of the parameter values that give the minimum SSE, and other sets of values that provide an SSE within 1% of this minimum. A number of values for  $r_1$ ,  $\beta$ , and  $\eta$  can be used to describe the data. These parameters are strongly correlated.

### 3.4 Discussion

---

I have developed a robust and reliable method for the quantitation of Mtb with a high throughput flow cytometric assay using H37Rv Mtb expressing mCherry. This method correlates with the current gold standard of bacterial counting (CFU/ml) but is less time consuming and more accurate since we are able to account for bacterial clumping. One limitation of our assay is that, although bacterial fluorescence is lost as Mtb dies in the presence of isoniazid, the time it takes to lose fluorescence is not known. Therefore, some non-viable bacteria may retain fluorescence and confound our data.

I used this assay to determine the extracellular as well as intracellular bacillary loads following infection of human MDM with Mtb. As with any in vitro study, one major limitation of this experimental system is the absence of the tissue microenvironment and other cell types that may influence the function of macrophages. Nevertheless, a reductionist approach allowed me to answer questions specifically regarding human MDM-Mtb interactions, and modelled the early host pathogen interaction.

Following intracellular infection of human MDM, I found that Mtb accumulates in the extracellular milieu, at least over the first 5 days of infection. Prevailing measurements exclusively of intracellular bacillary load significantly underestimate the true bacillary burden. It would have been useful to corroborate the flow cytometric quantitation with CFU/ml to determine the proportion of Mtb that is viable. It is likely that the CFU/ml data would closely reflect the integrated fluorescence measurements in each compartment, since integrated fluorescence of Mtb mCherry strongly correlates with CFU/ml. We also know that the bacteria

are actively replicating in the extracellular milieu and therefore must be mostly viable.

Together with Katharine Best, I then developed a mathematical model to determine the contribution of cellular necrosis to extracellular bacillary accumulation.

In order to determine the MDM death rate, I measured the attrition of cell number (by nuclear counting) over time. I considered other established methods of defining dead cells (e.g. PI staining), but I hypothesized that these would underestimate the true death rate. This is because only the remaining cells at each time-point would be available for staining and I would not be accounting for cells that had died and become non-adherent. In the absence of live cell imaging to track single macrophages over time, I felt the strategy I employed was the best way to experimentally address the question.

Surprisingly, the nuclear count data showed a sharp decline in cell count between four and 24 hours which seems to be due to technical confounding based on the following observations:

1. The apparent decline in cell number between four and 24 hours occurs in both infected and uninfected cells (where the culture media is simply changed to fresh, warmed, RPMI + 5% human AB serum)
2. Only a small proportion of infected and uninfected cells stain for necrotic cell death at four hours
3. The cell count stabilizes between 24 hours and 120 hours. If there were a true induction of cell death pathways by hours, this would be expected to

continue over the duration of the experiment

4. Data from the literature supporting minimal death of host cells at low MOI (Repasy et al., 2013; Welin et al., 2011). Mtb infection, even at high MOI, has been shown to cause significant necrosis only at later time points (48 hours or more), (Divangahi et al., 2009; Lerner et al., 2017; Mahamed et al., 2017)
5. Using a modelling approach, we find that simulating the sharp attrition in cell number between four and 24 hours was still unable to fit my observed intracellular and extracellular bacterial loads.

In some experiments, but not consistently, I observed an apparent shift in nuclear area between four and 24 hours (even in the uninfected wells). This was not due to the loss of contaminating lymphocytes or debris since it did not occur in every experiment, even when there was an attrition in cell number. Macrophages have remarkable plasticity in response to environmental cues and are able to acquire a spectrum of activation status, best exemplified by pro-inflammatory (M1) and anti-inflammatory (M2) phenotypes at the two ends of the spectrum (Gordon and Plüddemann, 2017). Characterization of M1 and M2 subsets is usually carried out by quantification of multiple cell surface markers, transcription factors and cytokine profiles. More recently image based machine learning has been used to define macrophage subsets (Rostam et al., 2017), including measurement of nuclear size. M1 and M2 macrophages show remarkable similarity in the distribution of their nuclear areas. Therefore, differential activation states cannot explain the differences in nuclear area seen at four and 24 hours in my *in vitro* model. Between 24 and 120 hours, there is more consistency in the nuclear

distributions. This again suggests to me that the four hour nuclear count in the data set are technically erroneous.

Contrary to the commonly held view that extracellular bacteria arise from intracellular bacteria being released by necrosis, neither death (at various different rates), nor extracellular Mtb replication could account for the observed bacterial load in this compartment. The mathematical modelling identified a novel process by which Mtb may be exiting the human host cell. Our model suggests non-lytic egress is a crucial mechanism by which Mtb accumulates extracellularly, since we are unable to fit the observed data without incorporating it.

I found that the extracellular milieu is permissive to Mtb replication. This is also true in the zebrafish model of Mm infection, where extracellular bacteria display the cording phenotype characteristic of unfettered growth in cases of macrophage deficiency (Clay et al., 2007).

Computational modelling is necessary to gain insights into the complex interactions that occur in biological systems (Brodland, 2015; Ingalls, 2013) such as the dynamic relationship between Mtb and its host cell. As has been shown, it allows researchers to make several in silico simulations to see if different parameter adjustments can mimic the behaviour of the system, and therefore identify which interactions are crucial to its operation. Sometimes the model cannot find definitive estimates for each unknown parameter, because several parameter sets may fit the data (as is the case here). Asking the model to find values for 3 unknown parameters (rate of intracellular replication, rate of Mtb uptake, and rate of non-lytic egress) based on relatively few biological data points presents difficulty. Nevertheless, the modelling exercise does provide useful

predictions (for example, that non-lytic egress is likely to be contributing to extracellular bacillary accumulation), to guide future experiments. Another limitation of the model is that it cannot incorporate every parameter that might affect the behaviour of a biological system. For example, we make the assumption that all bacteria are equally distributed between cells, but this is unlikely to be the case. Since more heavily infected cells are more likely to die, this parameter may also need to be incorporated into the model in the future.

## 4 MTB EXITS MACROPHAGES BY NON-LYTIC EGRESS

### 4.1 Introduction

---

In Chapter 3, I used a mathematical model to show that non-lytic egress is predicted to occur following intracellular infection of human MDM, and is an important strategy by which intracellular bacteria become extracellular, at least early in the course of infection where bacterial burden is low and there is little contribution from necrotic cell death.

In this chapter I first set out to show non-lytic egress occurs experimentally. I next wanted to test the hypothesis that growth of Mtb is restricted within the macrophage, and escaping the host cell into the extracellular milieu is beneficial to Mtb because it is more permissive to bacillary growth. Several lines of evidence suggest that macrophages are able to control Mtb replication to some degree. Data from the mouse model showing restriction of Mtb by macrophages (particularly when primed with IFN $\gamma$ ) is difficult to extrapolate to human hosts because killing is mediated by NO, which human macrophages do not produce to the same extent. That aside, the literature suggests that despite a diverse repertoire of subversion strategies against its defences, the internal environment of the macrophage would still be hostile to Mtb on account of nutrient deprivation, activation by IFN $\gamma$  (Fabri et al., 2011; Klug-Micu et al., 2013) and other mechanisms to counteract Mtb subversion (Robinson and Nau, 2008), detailed in **section 1.3.2**. Data from human in vitro macrophage models (Mahamed et al., 2017; Raffetseder et al., 2014), mouse (Huang et al., 2018) and zebrafish (Clay et al., 2007) show that certain phenotypes of macrophages are restrictive to mycobacteria, while the extracellular environment is growth permissive (Clay et

al., 2008, 2007; Mahamed et al., 2017).

To address my hypothesis, I needed to determine the intracellular growth rate of Mtb. However, our model suggests that Mtb is constantly moving between the intracellular and extracellular compartments, therefore measuring the intracellular growth rate of Mtb *in vitro* in isolation would not be feasible. In Chapter 3, I found that using the model to derive parameters for the non-lytic egress rate, the rate of bacterial uptake and intracellular replication rate was not possible because a number of values provided equivalently good fits to explain bacterial accumulation. I therefore set out to experimentally measure the rate at which non-lytic egress of Mtb occurs, verify that this rate allowed the model to fit the data, and allow the model to derive the intracellular replication rate.

## 4.2 Objectives

---

1. To confirm experimentally that Mtb is able to escape human macrophages by non-lytic egress
2. To experimentally determine the rate at which non-lytic egress occurs and incorporate this rate into the mathematical model describing the movement of Mtb into and out of macrophages
3. To subsequently use this model to derive rates for processes I am unable to measure- i.e. the rate of uptake of Mtb and the intracellular replication rate (and therefore understand the preferred growth niche of Mtb)

## 4.3 Results

---

### 4.3.1 Evidence for rapid Mtb escape from macrophages

In order to determine if Mtb can escape MDM by non-lytic egress, I sought to show movement of bacteria from the intracellular to the extracellular compartment in the absence of extracellular Mtb replication, intracellular bacterial killing, and MDM necrosis. I infected MDM for 4 hours to establish an intracellular infection, and washed off any remaining extracellular bacteria as previously shown (Error! eference source not found.**A**). I then quantified intracellular and extracellular bacteria 1 hour after washing off the extracellular bacteria (**Figure 4.1 Experimental model to look for non-lytic egress of Mtb**. MDM were infected with H37Rv mCherry for 4 hours at MOI 1. Cultures were washed three times with PBS to remove all extracellular bacteria. Fresh media was added for 60min. Extracellular bacteria in the supernatant were collected and intracellular bacteria were harvested by washing and lysing cells. Bacteria were fixed in 4% PFA and analysed by flow cytometry.

Figure 4.2 **Evidence for non-lytic egress of Mtb. A** MDM were infected with H37Rv mCherry for 4 hours at MOI 1. Cultures were washed three times with PBS to remove all extracellular bacteria. Any residual extracellular bacteria in the post wash supernatant (time 0) were collected by adding PBS to the well for a few seconds and gently agitating. Intracellular bacteria at time 0 were harvested by lysing the cells. In a separate well, fresh media was added for 60min. Extracellular bacteria in the supernatant were collected and intracellular bacteria were harvested by washing and lysing cells. Bacteria were fixed in 4% PFA and quantified by flow cytometry to generate integrated mCherry fluorescence (Int. mCherry fluor.) Mean  $\pm$  SEM 14 experiments. \*\*Paired t-test of intracellular bacillary load **B** Total bacillary load at 0 mins and 1 hour thereafter.

Figure 4.1)

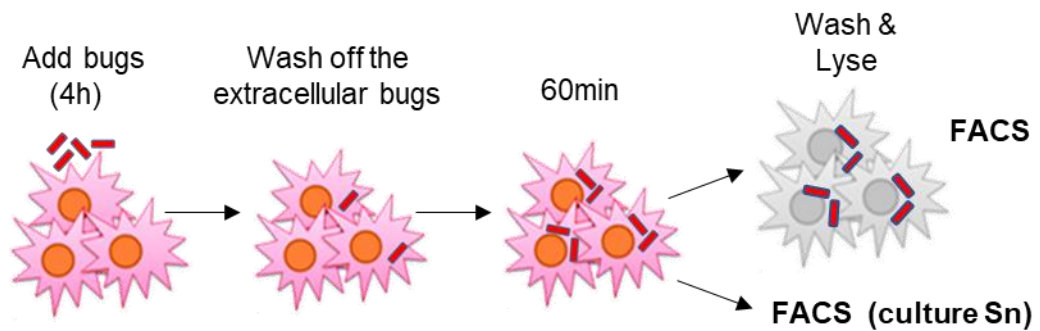


Figure 4.1 **Experimental model to look for non-lytic egress of Mtb.** MDM were infected with H37Rv mCherry for 4 hours at MOI 1. Cultures were washed three times with PBS to remove all extracellular bacteria. Fresh media was added for 60min. Extracellular bacteria in the supernatant were collected and intracellular bacteria were harvested by washing and lysing cells. Bacteria were fixed in 4% PFA and analysed by flow cytometry.

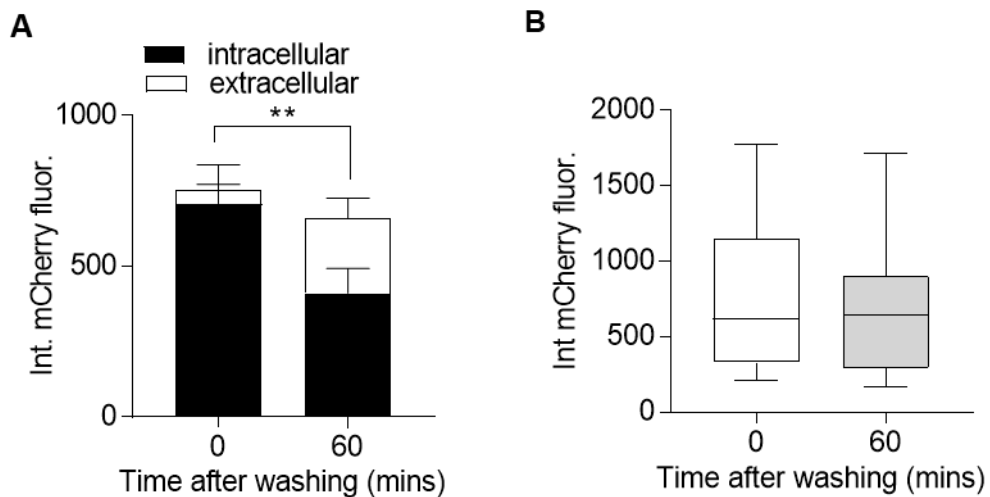
The significant reduction of bacteria in the intracellular compartment did not represent bacterial killing by macrophages, because the total number of bacteria in the intracellular and extracellular compartments over the 60 minute timeframe remained the same (**Figure 4.2 Evidence for non-lytic egress of Mtb. A** MDM were infected with H37Rv mCherry for 4 hours at MOI 1. Cultures were washed three times with PBS to remove all extracellular bacteria. Any residual extracellular bacteria in the post wash supernatant (time 0) were collected by adding PBS to the well for a few seconds and gently agitating. Intracellular bacteria at time 0 were harvested by lysing the cells. In a separate well, fresh media was added for 60min. Extracellular bacteria in the supernatant were collected and intracellular bacteria were harvested by washing and lysing cells.

Bacteria were fixed in 4% PFA and quantified by flow cytometry to generate integrated mCherry fluorescence (Int. mCherry fluor.) Mean  $\pm$  SEM 14 experiments. \*\*Paired t-test of intracellular bacillary load **B** Total bacillary load at 0 mins and 1 hour thereafter.

Figure 4.3 **Flow cytometry plots showing rapid extracellular Mtb accumulation.** MDM were infected with H37Rv mCherry for 4 hours at MOI 1. Cultures were washed three times with PBS to remove all extracellular bacteria. Any residual extracellular bacteria in the post wash supernatant (time 0) were collected by adding PBS to the well for a few seconds and gently agitating. Intracellular bacteria at time 0 were harvested by lysing the cells. In a separate well, fresh media was added for 60min. Extracellular bacteria in the supernatant were collected and intracellular bacteria were harvested by washing and lysing cells. Bacteria were fixed in 4% PFA and analysed by flow cytometry. 1 representative experiment demonstrating the appearance of extracellular bacteria after 60 mins and the simultaneous decrease in intracellular bacillary burden.

Figure 4.2**B**).

Example flow cytometry plots demonstrating the appearance of extracellular bacteria 60min after washing are shown in **Figure 4.3 Flow cytometry plots showing rapid extracellular Mtb accumulation.** MDM were infected with



H37Rv mCherry for 4 hours at MOI 1. Cultures were washed three times with PBS to remove all extracellular bacteria. Any residual extracellular bacteria in the post wash supernatant (time 0) were collected by adding PBS to the well for a

few seconds and gently agitating. Intracellular bacteria at time 0 were harvested by lysing the cells. In a separate well, fresh media was added for 60min. Extracellular bacteria in the supernatant were collected and intracellular bacteria were harvested by washing and lysing cells. Bacteria were fixed in 4% PFA and analysed by flow cytometry. 1 representative experiment demonstrating the appearance of extracellular bacteria after 60 mins and the simultaneous decrease in intracellular bacillary burden.

Figure 4.4 **Mtb egress from macrophages without causing host cell lysis** **A** MDM were infected with H37Rv mCherry for 4 hours at MOI 1. Cultures were washed three times with PBS to remove all extracellular bacteria (Time 0). Fresh media was added for 60min. At both time points, uninfected and infected cell cultures were fixed with 4% PFA. Nuclei were counterstained for DAPI and counted in each condition at each time point **B** MDM were infected with Mtb for 4h. Prior to washing, cells were incubated with Live/Dead stain for necrotic cells for 20min at room temperature. Cells were gently washed to remove the stain and fixed in 4%PFA. Cells were permeabilized and counterstained with DAPI + Cell Mask. White arrow heads = live infected MDM, Red arrowheads= dead/ dying infected MDM. **C** Dead/ dying (red) and live cells (white) were enumerated using high content microscopy.

Figure 4.3.

Figure 4.4 **Evidence for non-lytic egress of Mtb.** **A** MDM were infected with H37Rv mCherry for 4 hours at MOI 1. Cultures were washed three times with PBS to remove all extracellular bacteria. Any residual extracellular bacteria in the post wash supernatant (time 0) were collected by adding PBS to the well for a few seconds and gently agitating. Intracellular bacteria at time 0 were harvested by lysing the cells. In a separate well, fresh media was added for 60min. Extracellular bacteria in the supernatant were collected and intracellular bacteria were harvested by washing and lysing cells. Bacteria were fixed in 4% PFA and quantified by flow cytometry to generate integrated mCherry fluorescence (Int. mCherry fluor.) Mean  $\pm$  SEM 14 experiments. \*\*Paired t-test of intracellular bacillary load **B** Total bacillary load at 0 mins and 1

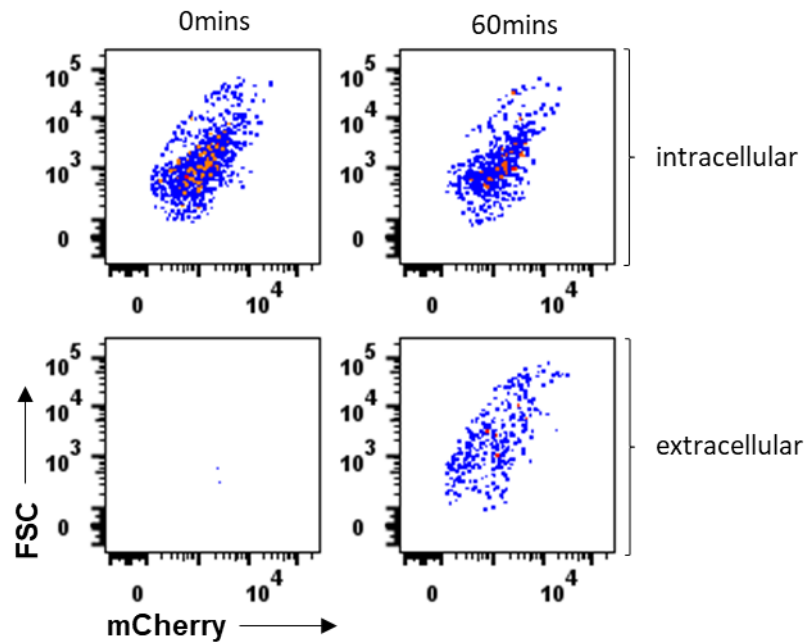


**Figure 4.7 Flow cytometry plots showing rapid extracellular Mtb accumulation.** MDM were infected with H37Rv mCherry for 4 hours at MOI 1. Cultures were washed three times with PBS to remove all extracellular bacteria. Any residual extracellular bacteria in the post wash supernatant (time 0) were collected by adding PBS to the well for a few seconds and gently agitating. Intracellular bacteria at time 0 were harvested by lysing the cells. In a separate well, fresh media was added for 60min. Extracellular bacteria in the supernatant were collected and intracellular bacteria were harvested by washing and lysing cells. Bacteria were fixed in 4% PFA and analysed by flow cytometry. 1 representative experiment demonstrating the appearance of extracellular bacteria after 60 mins and the simultaneous decrease in intracellular bacillary burden.

### 4.3.2 Rapid extracellular accumulation not due to cell death

Extracellular bacteria may accumulate as a result of lytic or non-lytic strategies. Having shown that extracellular bacteria appear within one hour, I sought to test if there was any evidence of cell death at this time point.

I enumerated adherent cells after four hours infection and one hour later. This analysis showed no significant loss of cells (**Figure 4.4 Mtb egress from macrophages without causing host cell lysis** **A** MDM were infected with H37Rv mCherry for 4 hours at MOI 1. Cultures were washed three times with PBS to remove all extracellular bacteria (Time 0). Fresh media was added for 60min. At both time points, uninfected and infected cell cultures were fixed with 4% PFA. Nuclei were counterstained for DAPI and counted in each condition at each time point **B** MDM were infected with Mtb for 4h. Prior to washing, cells were incubated with Live/Dead stain for necrotic cells for 20min at room temperature. Cells were gently washed to remove the stain and fixed in 4%PFA. Cells were permeabilized and counterstained with DAPI + Cell Mask. White arrow heads = live infected MDM, Red arrowheads= dead/ dying infected MDM. **C** Dead/ dying (red) and live cells (white) were enumerated using high content microscopy.

Figure 4.5Figure 4.4**A**). In addition, I stained the cells with the Live/Dead stain, combined with a cell mask stain in order delineate the boundaries of each cell, and hence enumerate the number of Mtb infected cells that may be committed to cell death and might therefore release bacteria into the extracellular milieu in the following one hour (**Figure 4.4 Mtb egress from macrophages without**

**causing host cell lysis** **A** MDM were infected with H37Rv mCherry for 4 hours at MOI 1. Cultures were washed three times with PBS to remove all extracellular bacteria (Time 0). Fresh media was added for 60min. At both time points, uninfected and infected cell cultures were fixed with 4% PFA. Nuclei were counterstained for DAPI and counted in each condition at each time point **B** MDM were infected with Mtb for 4h. Prior to washing, cells were incubated with Live/Dead stain for necrotic cells for 20min at room temperature. Cells were gently washed to remove the stain and fixed in 4%PFA. Cells were permeabilized and counterstained with DAPI + Cell Mask. White arrow heads = live infected MDM, Red arrowheads= dead/ dying infected MDM. **C** Dead/ dying (red) and live cells (white) were enumerated using high content microscopy.

Figure 4.5Figure 4.4**B**). I found < 0.5% of infected cells were dying at or after the initial four hours infection (**Figure 4.4 Mtb egress from macrophages without causing host cell lysis** **A** MDM were infected with H37Rv mCherry for 4 hours at MOI 1. Cultures were washed three times with PBS to remove all extracellular bacteria (Time 0). Fresh media was added for 60min. At both time points, uninfected and infected cell cultures were fixed with 4% PFA. Nuclei were counterstained for DAPI and counted in each condition at each time point **B** MDM were infected with Mtb for 4h. Prior to washing, cells were incubated with Live/Dead stain for necrotic cells for 20min at room temperature. Cells were gently washed to remove the stain and fixed in 4%PFA. Cells were permeabilized and counterstained with DAPI + Cell Mask. White arrow heads = live infected MDM, Red arrowheads= dead/ dying infected MDM. **C** Dead/ dying (red) and live

cells (white) were enumerated using high content microscopy.

Figure 4.5Figure 4.4**C**)

In this analysis also, there was no significant difference between the very small proportions of dying cells in infected and uninfected MDM cultures. These data are consistent with my hypothesis that extracellular Mtb did not arise from host cell lysis.

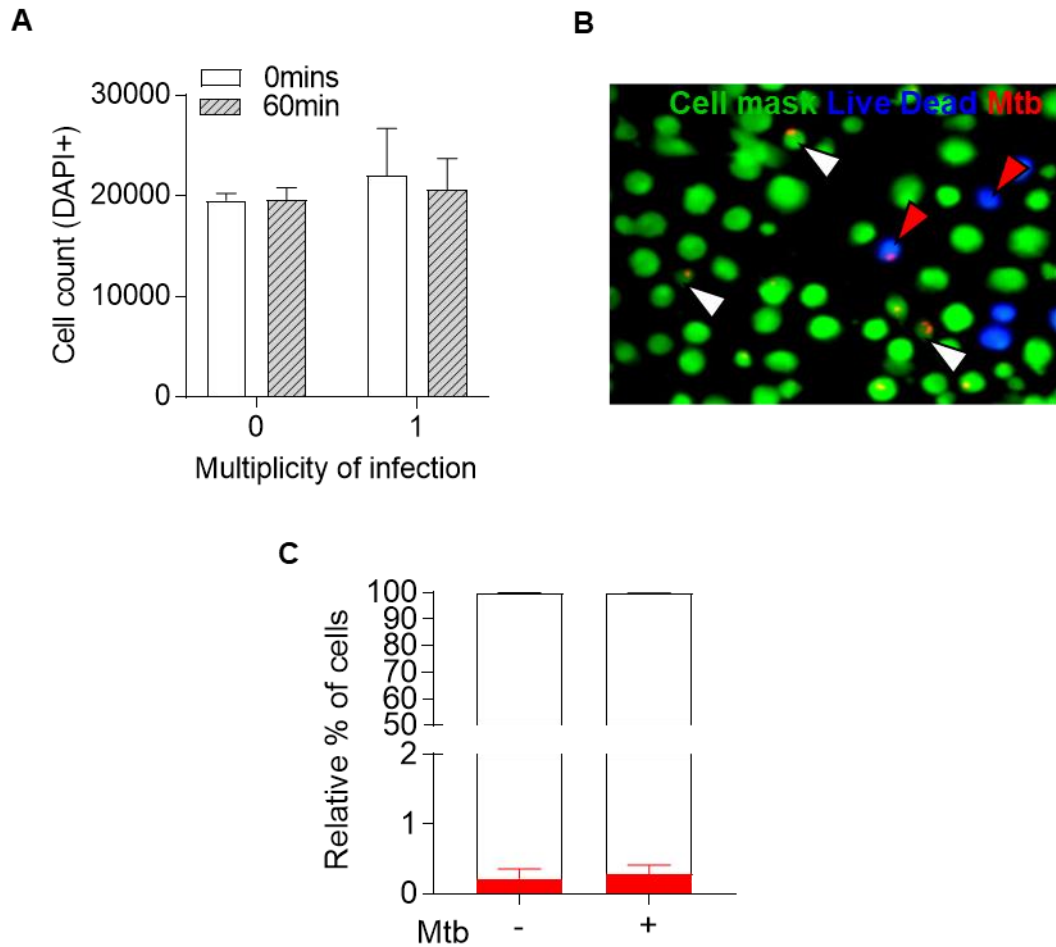


Figure 4.10 **Mtb egress from macrophages without causing host cell lysis** **A** MDM were infected with H37Rv mCherry for 4 hours at MOI 1. Cultures were washed three times with PBS to remove all extracellular bacteria (Time 0). Fresh media was added for 60min. At both time points, uninfected and infected cell cultures were fixed with 4% PFA. Nuclei were counterstained for DAPI and counted in each condition at each time point **B** MDM were infected with Mtb for 4h. Prior to washing, cells were incubated with Live/Dead stain for necrotic cells for 20min at room temperature. Cells were gently washed to remove the stain and fixed in 4%PFA. Cells were permeabilized and counterstained with DAPI + Cell Mask. White arrow heads = live infected MDM, Red arrowheads= dead/ dying infected MDM. **C** Dead/ dying (red) and live cells (white) were enumerated using high content microscopy.

### 4.3.3 Rapid extracellular accumulation not residual adherent bacteria

After establishing an intracellular infection for four hours, cells are washed extensively to remove extracellular bacteria. Nevertheless, some residual extracellular bacteria may remain adherent to the surface of macrophages and therefore counted as 'intracellular'. I hypothesized that over 60mins, these bacteria might detach from macrophages into the extracellular milieu, giving the appearance that they had moved actively between the two compartments.

A common approach to discriminate between intracellular and cell surface bacteria is to differentially immunostain extracellular bacteria with antibodies that cannot cross the cell membrane. However, I was unable to find suitable antibody reagents with sufficient sensitivity or and specificity to use this method (**Figure**

**4.5 Extracellular bacteria at 60mins do not arise from adherent Mtb A** H37Rv mCherry were incubated with anti-PPD primary antibody overnight (or not), washed and counterstained with FITC secondary antibody and analysed by flow cytometry. **B** MDM were infected with Mtb for 4h at 37°C. Extracellular bacteria were removed by extensive washing three times with PBS, and media replaced for 60mins. Cells were incubated on ice (4°C) or at 37°C. At each time point the supernatant was removed and bacteria fixed in 4% PFA. Intracellular bacteria were harvested by washing and lysing the cells. Bacteria were enumerated by flow cytometric analysis. Mean  $\pm$  SEM 3 experiments **C** Example flow cytometry plots of 1 representative experiment

Figure 4.6 **Non-lytic egress is morphologically distinct from cellular necrosis** **A** MDM were infected with Mtb for 4 hours at MOI 5. Extracellular bacteria were removed by extensive washing three times with PBS, and media replaced for 48 hours. Macrophages were subsequently washed

again and media replaced. Macrophages in 1 field of view were imaged at 2 minute intervals for 1 hour. Panels show successive images of (i and ii) non lytic egress where infected macrophages release bacteria but remain intact thereafter (iii) an infected macrophage bursting open following cellular necrosis and releasing bacteria (iv) macrophages harbouring bacteria with no loss of bacteria

#### Figure 4.5A)

Instead, I addressed this question by a different approach. I reasoned that non lytic bacterial egress is likely to represent an active biological process requiring physiological temperatures. In contrast molecular interactions that may mediate bacterial adhesion to the cell surface are generally reduced at lower temperatures. MDM were infected for four hours and washed to remove extracellular bacteria. They were then incubated at 37°C or kept on ice for one hour before enumerating intracellular and extracellular bacteria. I only found extracellular bacteria in MDM cultures incubated at 37°C in keeping with the hypothesis that egress was attenuated in the cold (**Figure 4.5 Extracellular bacteria at 60mins do not arise from adherent Mtb** **A** H37Rv mCherry were incubated with anti-PPD primary antibody overnight (or not), washed and counterstained with FITC secondary antibody and analysed by flow cytometry. **B** MDM were infected with Mtb for 4h at 37°C. Extracellular bacteria were removed by extensive washing three times with PBS, and media replaced for 60mins. Cells were incubated on ice (4°C) or at 37°C. At each time point the supernatant was removed and bacteria fixed in 4% PFA. Intracellular bacteria were harvested by washing and lysing the cells. Bacteria were enumerated by flow cytometric analysis. Mean  $\pm$  SEM 3 experiments **C** Example flow cytometry plots of 1 representative experiment

Figure 4.6 **Non-lytic egress is morphologically distinct from cellular necrosis** **A** MDM were infected with Mtb for 4 hours at MOI 5. Extracellular bacteria were removed by extensive washing three times with PBS, and media replaced for 48 hours. Macrophages were subsequently washed again and media replaced. Macrophages in 1 field of view were imaged at 2 minute intervals for 1 hour. Panels show successive images of (i and ii) non lytic egress where infected macrophages release bacteria but remain intact thereafter (iii) an infected macrophage bursting open following cellular necrosis and releasing bacteria (iv) macrophages harbouring bacteria with no loss of bacteria

Figure 4.5**B and C**), and that the data did not represent a detachment of residual adherent bacteria from surface of macrophages.

Another explanation of this data could be that some macrophages harbouring bacteria may be undergoing necrosis with cell lysis, releasing bacteria into the extracellular milieu. This process may also be abrogated on ice, and therefore the lack of extracellular bacteria after 1 hour is simply a result of less cellular necrosis. I think this is unlikely since few cells are committed to cell death as identified by the live dead stain at 4 hours (**Figure 4.4 Mtb egress from macrophages without causing host cell lysis** **A** MDM were infected with H37Rv mCherry for 4 hours at MOI 1. Cultures were washed three times with PBS to remove all extracellular bacteria (Time 0). Fresh media was added for 60min. At both time points, uninfected and infected cell cultures were fixed with 4% PFA. Nuclei were counterstained for DAPI and counted in each condition at each time point **B** MDM were infected with Mtb for 4h. Prior to washing, cells were incubated with Live/Dead stain for necrotic cells for 20min at room temperature. Cells were gently washed to remove the stain and fixed in 4%PFA. Cells were permeabilized and counterstained with DAPI + Cell Mask. White arrow heads = live infected MDM, Red arrowheads= dead/ dying infected MDM. **C** Dead/ dying (red) and live cells (white) were enumerated using high content microscopy.

Figure 4.5Figure 4.4). In addition, I would not expect necrosis to take place over a short time frame like 1 hour, particularly at low multiplicity of infection.

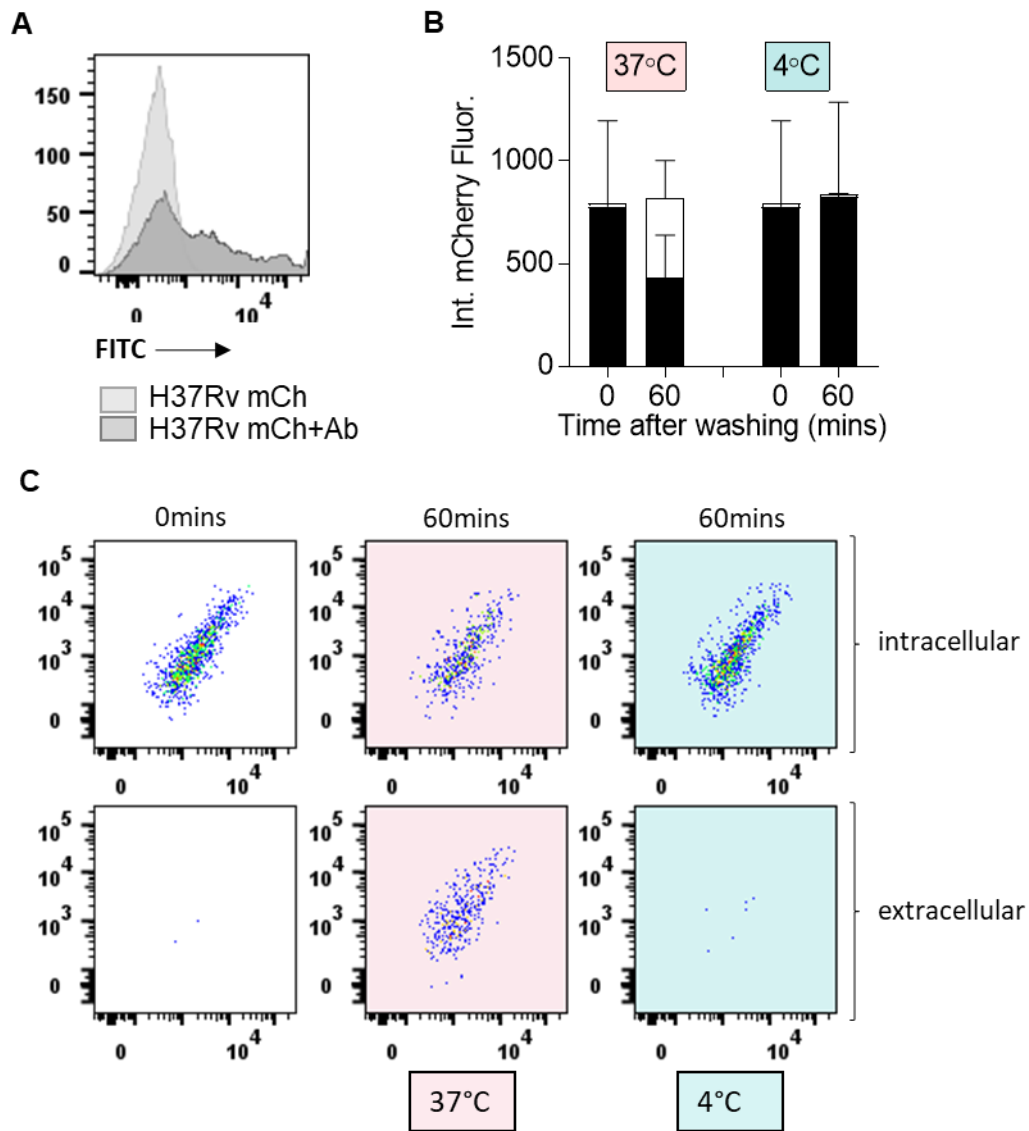


Figure 4.13 **Extracellular bacteria at 60mins do not arise from adherent Mtb A** H37Rv mCherry were incubated with anti-PPD primary antibody overnight (or not), washed and counterstained with FITC secondary antibody and analysed by flow cytometry. **B** MDM were infected with Mtb for 4h at 37°C. Extracellular bacteria were removed by extensive washing three times with PBS, and media replaced for 60mins. Cells were incubated on ice (4°C) or at 37°C. At each time point the supernatant was removed and bacteria fixed in 4% PFA. Intracellular bacteria were harvested by washing and lysing the cells. Bacteria were enumerated by flow cytometric analysis. Mean  $\pm$  SEM 3 experiments **C** Example flow cytometry plots of 1 representative experiment

#### 4.3.4 Visualisation of non-lytic Mtb egress

Taken together my findings provided strong evidence of rapid non-lytic egress of Mtb from MDM. Therefore, I sought to visualize this by live cell imaging. In collaboration with Max Gutierrez (Francis Crick Institute), I infected MDM at high multiplicity (MOI 5), in order to increase the frequency of infected cells. I then imaged a single field of view at two minute intervals for 30 minutes, capturing red fluorescent and phase images at each time point (**Figure 4.6 Non-lytic egress is morphologically distinct from cellular necrosis** A MDM were infected with Mtb for 4 hours at MOI 5. Extracellular bacteria were removed by extensive washing three times with PBS, and media replaced for 48 hours. Macrophages were subsequently washed again and media replaced. Macrophages in 1 field of view were imaged at 2 minute intervals for 1 hour. Panels show successive images of (i and ii) non lytic egress where infected macrophages release bacteria but remain intact thereafter (iii) an infected macrophage bursting open following cellular necrosis and releasing bacteria (iv) macrophages harbouring bacteria with no loss of bacteria

Figure 4.7 **Mtb released by non-lytic egress are viable** MDM were infected with H37Rv mCherry for 4 hours at MOI 1. Cultures were washed three times with PBS to remove all extracellular bacteria. Fresh media was added for 60min. Extracellular bacteria in the supernatant were collected and intracellular bacteria were harvested by washing and lysing cells. Bacteria in each compartment were enumerated for CFU/ml by plating on 7H10 agar in triplicate. Colonies were counted at 3 weeks. Mean + SEM of 3 experiments

Figure 4.6)

In some MDM the red fluorescent bacterial signal was preserved within the host cell throughout the imaging time course. I inferred that these represented

internalized bacteria retained within the intracellular compartment (**Figure 4.6**  
**Non-lytic egress is morphologically distinct from cellular necrosis** A MDM  
were infected with Mtb for 4 hours at MOI 5. Extracellular bacteria were removed  
by extensive washing three times with PBS, and media replaced for 48 hours.  
Macrophages were subsequently washed again and media replaced.  
Macrophages in 1 field of view were imaged at 2 minute intervals for 1 hour.  
Panels show successive images of (i and ii) non lytic egress where infected  
macrophages release bacteria but remain intact thereafter (iii) an infected  
macrophage bursting open following cellular necrosis and releasing bacteria (iv)  
macrophages harbouring bacteria with no loss of bacteria

Figure 4.7 **Mtb released by non-lytic egress are viable** MDM were infected with H37Rv  
mCherry for 4 hours at MOI 1. Cultures were washed three times with PBS to remove all  
extracellular bacteria. Fresh media was added for 60min. Extracellular bacteria in the supernatant  
were collected and intracellular bacteria were harvested by washing and lysing cells. Bacteria in  
each compartment were enumerated for CFU/ml by plating on 7H10 agar in triplicate. Colonies  
were counted at 3 weeks. Mean + SEM of 3 experiments

Figure 4.6, **panel iv**). In another example, the loss of red fluorescence was  
associated with enlargement and then deformation of the host cell (**Figure 4.6**  
**Non-lytic egress is morphologically distinct from cellular necrosis** A MDM  
were infected with Mtb for 4 hours at MOI 5. Extracellular bacteria were removed  
by extensive washing three times with PBS, and media replaced for 48 hours.  
Macrophages were subsequently washed again and media replaced.  
Macrophages in 1 field of view were imaged at 2 minute intervals for 1 hour.  
Panels show successive images of (i and ii) non lytic egress where infected  
macrophages release bacteria but remain intact thereafter (iii) an infected  
macrophage bursting open following cellular necrosis and releasing bacteria (iv)

macrophages harbouring bacteria with no loss of bacteria

Figure 4.7 **Mtb released by non-lytic egress are viable** MDM were infected with H37Rv mCherry for 4 hours at MOI 1. Cultures were washed three times with PBS to remove all extracellular bacteria. Fresh media was added for 60min. Extracellular bacteria in the supernatant were collected and intracellular bacteria were harvested by washing and lysing cells. Bacteria in each compartment were enumerated for CFU/ml by plating on 7H10 agar in triplicate. Colonies were counted at 3 weeks. Mean + SEM of 3 experiments

Figure 4.6, **panel iii**). I inferred that this represented a cell lysis event, which released the bacterial into the cell culture supernatants. In the same field of view, I observed two MDM, in which there was a loss of red fluorescence signal in the absence of any morphological changes consistent with cell lysis (**Figure 4.6 Non-lytic egress is morphologically distinct from cellular necrosis** A MDM were infected with Mtb for 4 hours at MOI 5. Extracellular bacteria were removed by extensive washing three times with PBS, and media replaced for 48 hours. Macrophages were subsequently washed again and media replaced. Macrophages in 1 field of view were imaged at 2 minute intervals for 1 hour. Panels show successive images of (i and ii) non lytic egress where infected macrophages release bacteria but remain intact thereafter (iii) an infected macrophage bursting open following cellular necrosis and releasing bacteria (iv) macrophages harbouring bacteria with no loss of bacteria

Figure 4.7 **Mtb released by non-lytic egress are viable** MDM were infected with H37Rv mCherry for 4 hours at MOI 1. Cultures were washed three times with PBS to remove all extracellular bacteria. Fresh media was added for 60min. Extracellular bacteria in the supernatant were collected and intracellular bacteria were harvested by washing and lysing cells. Bacteria in each compartment were enumerated for CFU/ml by plating on 7H10 agar in triplicate. Colonies were counted at 3 weeks. Mean + SEM of 3 experiments

Figure 4.6, **panel i and ii**). These host cells remained intact for the remainder of

the imaging.

This experiment was conducted only once, and therefore needs repeating with better quality images before it is taken as conclusive evidence for visualisation of non-lytic egress. Ideally I would want to see the bacteria visible inside the cell, then crossing the plasma membrane and subsequently visible outside the cell, with the cell remaining intact.

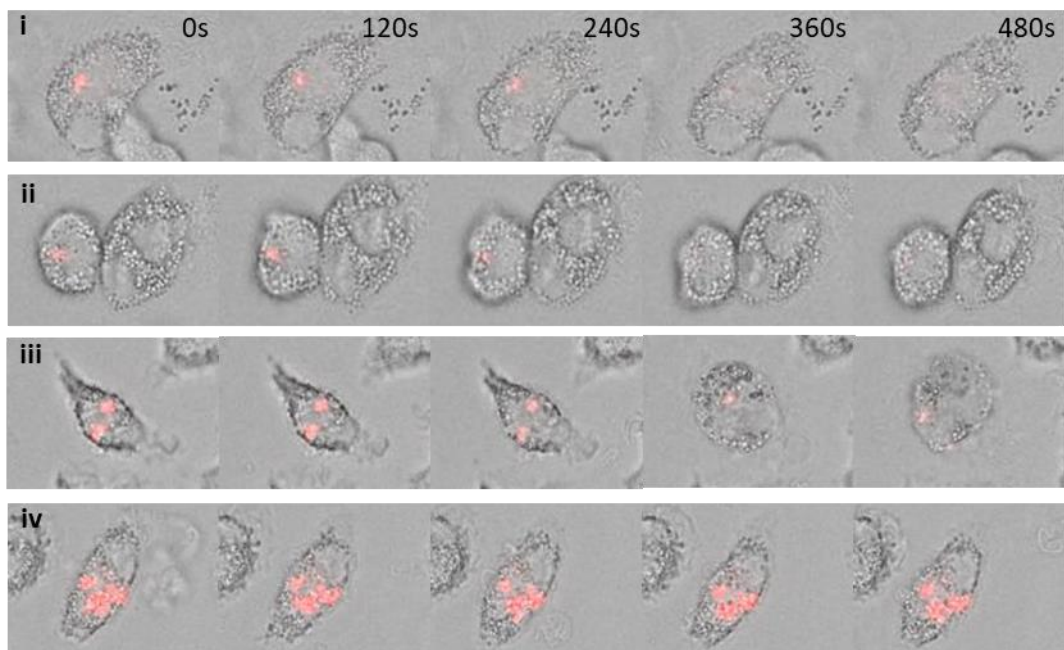


Figure 4.16 **Non-lytic egress is morphologically distinct from cellular necrosis** A MDM were infected with Mtb for 4 hours at MOI 5. Extracellular bacteria were removed by extensive washing three times with PBS, and media replaced for 48 hours. Macrophages were subsequently washed again and media replaced. Macrophages in 1 field of view were imaged at 2 minute intervals for 1 hour. Panels show successive images of (i and ii) non lytic egress where infected macrophages release bacteria but remain intact thereafter (iii) an infected macrophage bursting open following cellular necrosis and releasing bacteria (iv) macrophages harbouring bacteria with no loss of bacteria



#### 4.3.5 Bacteria remain viable after non lytic egress

My model for bacterial growth inside and outside the cell, is based on the premise that there is non-lytic egress of viable bacteria that are able to replicate. Although bacterial fluorescence is lost as mCherry expressing Mtb dies in the presence of isoniazid (Error! Reference source not found.**B**) the time it takes to lose fluorescence was not known. Therefore, some non-viable bacteria may retain fluorescence when they are expelled from the macrophage. I sought to test the hypothesis that the bacteria emerging from cells by non-lytic egress were viable.

After infecting MDM for 4 hours, I quantitated the bacterial load in each compartment by CFU/ml rather than by flow cytometry. Colony counting of viable bacteria replicated the flow cytometry results. There was no growth of extracellular bacteria after washing, but viable bacteria did appear in the extracellular space after one hour and were associated with a concomitant reduction in viable intracellular bacteria (**Figure 4.7 Mtb released by non-lytic egress are viable** MDM were infected with H37Rv mCherry for 4 hours at MOI 1. Cultures were washed three times with PBS to remove all extracellular bacteria. Fresh media was added for 60min. Extracellular bacteria in the supernatant were collected and intracellular bacteria were harvested by washing and lysing cells. Bacteria in each compartment were enumerated for CFU/ml by plating on 7H10 agar in triplicate. Colonies were counted at 3 weeks. Mean + SEM of 3 experiments

Figure 4.8 **Incorporating non-lytic egress into the mathematical model.** **A** MDM were infected with H37Rv mCherry for 4 hours at MOI 1. Cultures were washed three times with PBS to remove all extracellular bacteria. Fresh media was added for 60min. Extracellular bacteria in the

supernatant were collected and intracellular bacteria were harvested by washing and lysing cells. Bacteria were fixed in 4% PFA and analysed by flow cytometry. Calculated non-lytic egress rate as (per bug per hour) of 14 experiments. **B** Mathematical model incorporating non-lytic egress at the experimentally determined rate predicts (lines, intracellular = orange, extracellular= purple) the observed data (squares). Rate of Mtb uptake by macrophages and intracellular replication rates have been determined in silico.

Figure 4.7 **Mtb released by non-lytic egress are viable** MDM were infected with H37Rv mCherry for 4 hours at MOI 1. Cultures were washed three times with PBS to remove all extracellular bacteria. Fresh media was added for 60min. Extracellular bacteria in the supernatant were collected and intracellular bacteria were harvested by washing and lysing cells. Bacteria in each compartment were enumerated for CFU/ml by plating on 7H10 agar in triplicate. Colonies were counted at 3 weeks. Mean + SEM of 3 experiments

)

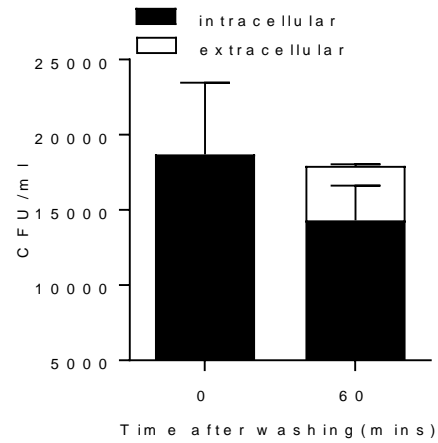


Figure 4.19 **Mtb released by non-lytic egress are viable** MDM were infected with H37Rv mCherry for 4 hours at MOI 1. Cultures were washed three times with PBS to remove all extracellular bacteria. Fresh media was added for 60min. Extracellular bacteria in the supernatant were collected and intracellular bacteria were harvested by washing and lysing cells. Bacteria in each compartment were enumerated for CFU/ml by plating on 7H10 agar in triplicate. Colonies were counted at 3 weeks. Mean + SEM of 3 experiments

#### 4.3.6 Incorporating non-lytic egress into the mathematical model

In Chapter 3, I described how a mathematical model to evaluate the processes that lead to intracellular and extracellular bacillary accumulation had predicted that cellular necrosis and extracellular replication alone cannot explain the amount of extracellular bacteria. Rather, it is non-lytic egress that makes a crucial contribution to extracellular bacterial burden.

However, when we used an optimization algorithm to derive the rate of non-lytic egress, the rate of Mtb uptake by macrophages and the intracellular replication rate, we found that several parameter sets provided an equivalently good fit to the observed data. Moreover, the rate of uptake and the non-lytic egress rates were strongly correlated. We had to measure at least one of these parameters experimentally in order to derive the others.

With the data from my experiments I was now able to experimentally determine the rate of non-lytic egress, defined by the increase in extracellular fluorescence over one hour as a proportion of the initial intracellular fluorescence. We take the integrated fluorescence of the extracellular bacteria at 1 hour ( $E(t)$ ) and subtract the integrated fluorescence of bacteria remaining in the post wash supernatant ( $E(0)$ ) and compare this to the intracellular bacillary load 4 hours after infection ( $I(0)$ ). Non-lytic egress is assumed to occur at a constant per-bacteria rate, resulting in exponential decay of intracellular fluorescence and an equivalent increase in extracellular fluorescence.

$$\eta = -\frac{1}{t} \ln \left( 1 - \frac{E(t) - E(0)}{I(0)} \right) \quad \text{Equation 4}$$

The measured egress rate is  $0.404 \text{ h}^{-1}$  (**Figure 4.8 Incorporating non-lytic egress into the mathematical model.** **A** MDM were infected with H37Rv mCherry for 4 hours at MOI 1. Cultures were washed three times with PBS to remove all extracellular bacteria. Fresh media was added for 60min. Extracellular bacteria in the supernatant were collected and intracellular bacteria were harvested by washing and lysing cells. Bacteria were fixed in 4% PFA and analysed by flow cytometry. Calculated non-lytic egress rate as (per bug per hour) of 14 experiments. **B** Mathematical model incorporating non-lytic egress at the experimentally determined rate predicts (lines, intracellular = orange, extracellular= purple) the observed data (squares). Rate of Mtb uptake by macrophages and intracellular replication rates have been determined in silico.

**Figure 4.9 Estimating the rate of uptake of Mtb in silico** The cell death rate, extracellular growth rate and non-lytic egress rate have all been determined experimentally and are fixed into the model. We take a set of randomly selected parameter values for the unknown parameters (intracellular replication and uptake rate) and run the Nelder Mead algorithm. The initial parameter values are optimized until the algorithm converges to the lowest SSE. This process is repeated 50,000 times. Histogram shows the rate of uptake by macrophages ( $\beta$ ) that gives within 1% of the minimum SSE (i.e. provides a good fit to the data).

**Figure 4.8A).** We then incorporated this rate into the model.

As described in Chapter 3, we used the Nelder Mead optimization algorithm to find the values of the remaining unknown parameters of our model (i.e. the rate of intracellular replication and uptake by macrophages). The cell death rate, extracellular replication rate and non-lytic egress rate are known from our experimental data.

We took a set of randomly selected parameter values and ran the algorithm. The initial parameter values are optimized until the algorithm converges to the lowest

SSE. This process is repeated 50,000 times. We then identified the single set of parameter values for the intracellular replication rate and rate of uptake by macrophages that gives the minimum SSE. Using the egress rate estimated from experimental data, in combination with our other experimentally determined and in silico derived parameters provides a model fit equivalently as good as when the egress rate was allowed to be estimated freely (**Figure 4.8 Incorporating non-lytic egress into the mathematical model. A** MDM were infected with H37Rv mCherry for 4 hours at MOI 1. Cultures were washed three times with PBS to remove all extracellular bacteria. Fresh media was added for 60min. Extracellular bacteria in the supernatant were collected and intracellular bacteria were harvested by washing and lysing cells. Bacteria were fixed in 4% PFA and analysed by flow cytometry. Calculated non-lytic egress rate as (per bug per hour) of 14 experiments. **B** Mathematical model incorporating non-lytic egress at the experimentally determined rate predicts (lines, intracellular = orange, extracellular= purple) the observed data (squares). Rate of Mtb uptake by macrophages and intracellular replication rates have been determined in silico.

Figure 4.9 **Estimating the rate of uptake of Mtb in silico** The cell death rate, extracellular growth rate and non-lytic egress rate have all been determined experimentally and are fixed into the model. We take a set of randomly selected parameter values for the unknown parameters (intracellular replication and uptake rate) and run the Nelder Mead algorithm. The initial parameter values are optimized until the algorithm converges to the lowest SSE. This process is repeated 50,000 times. Histogram shows the rate of uptake by macrophages ( $\beta$ ) that gives within 1% of the minimum SSE (i.e. provides a good fit to the data).

Figure 4.8**B**)

The model had predicted the presence of an alternative process (non-lytic egress) by which Mtb accumulate extracellularly. Here, I validated the model

findings by showing that this process occurs experimentally and the rate at which we find non-lytic egress to occur is able to describe our observed data. This built confidence in both our modelling and experimental strategies.

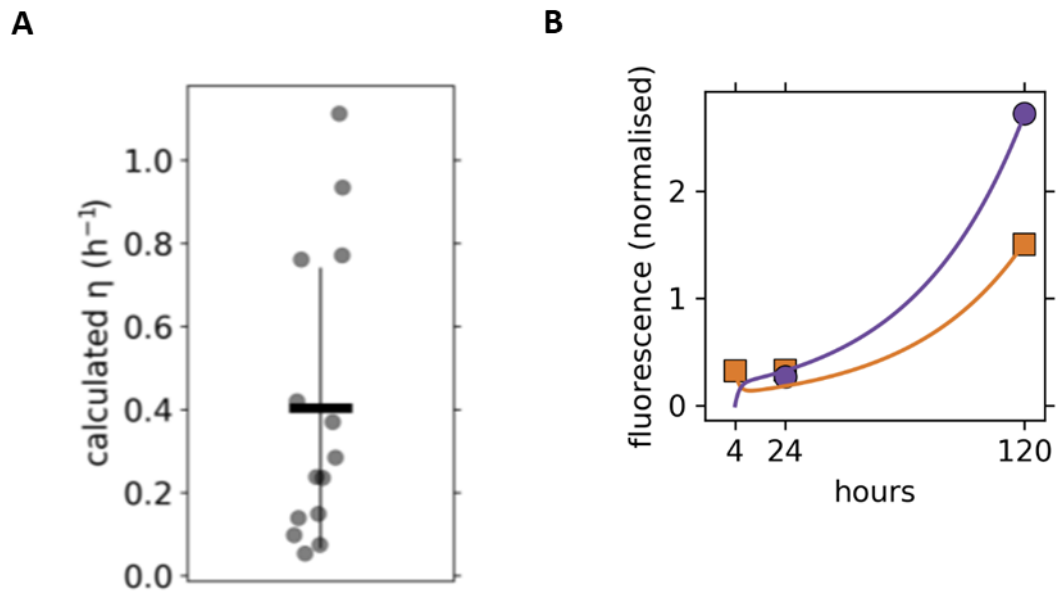


Figure 4.22 **Incorporating non-lytic egress into the mathematical model.** **A** MDM were infected with H37Rv mCherry for 4 hours at MOI 1. Cultures were washed three times with PBS to remove all extracellular bacteria. Fresh media was added for 60min. Extracellular bacteria in the supernatant were collected and intracellular bacteria were harvested by washing and lysing cells. Bacteria were fixed in 4% PFA and analysed by flow cytometry. Calculated non-lytic egress rate as (per bug per hour) of 14 experiments. **B** Mathematical model incorporating non-lytic egress at the experimentally determined rate predicts (lines, intracellular = orange, extracellular= purple) the observed data (squares). Rate of Mtb uptake by macrophages and intracellular replication rates have been determined in silico.

In Chapter 3 I showed that the rates of non-lytic egress and bacterial uptake are strongly correlated, and I needed to find the rate of one of these parameters *in vitro* before the other could be determined.

Having fixed the non-lytic egress rate at  $0.404 \text{ h}^{-1}$ , I set out to determine the rate of Mtb uptake. The Nelder Mead algorithm (run above) had given us 50,000 parameter values with their associated SSE. We identified the parameter set with the lowest SSE. This gave us the model's determination of the best fit for  $\beta$  (the rate of Mtb uptake by macrophages) as  $0.226 \text{ h}^{-1}$ . A histogram demonstrating the value of  $\beta$  which gives within 1% of the lowest SSE is shown in **Figure 4.9**

**Estimating the rate of uptake of Mtb in silico** The cell death rate, extracellular growth rate and non-lytic egress rate have all been determined experimentally and are fixed into the model. We take a set of randomly selected parameter values for the unknown parameters (intracellular replication and uptake rate) and run the Nelder Mead algorithm. The initial parameter values are optimized until the algorithm converges to the lowest SSE. This process is repeated 50,000 times. Histogram shows the rate of uptake by macrophages ( $\beta$ ) that gives within 1% of the minimum SSE (i.e. provides a good fit to the data).

**Figure 4.10 Estimating the intracellular growth rate of Mtb in silico** The cell death rate, extracellular growth rate and non-lytic egress rate have all been determined experimentally and are fixed into the model. We take a set of randomly selected parameter values for the unknown parameters (intracellular replication and uptake rate) and run the Nelder Mead algorithm. The initial parameter values are optimized until the algorithm converges to the lowest SSE.

This process is repeated 50,000 times. Histogram shows the intracellular replication rate ( $r_i$ ) that gives within 1% of the minimum SSE (i.e. provides a good fit to the data). Figure 4.9. The range of values is very narrow (0.225 - 0.227  $\text{h}^{-1}$ ), further building confidence in the parameterization of the model. Interestingly, I noted that the rate of uptake of macrophages is slower than the rate of non-lytic egress.

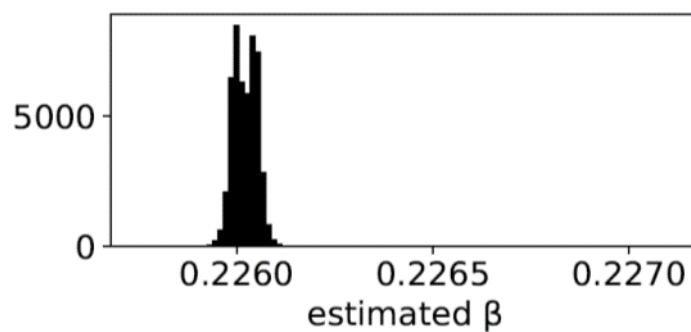


Figure 4.25 **Estimating the rate of uptake of Mtb in silico** The cell death rate, extracellular growth rate and non-lytic egress rate have all been determined experimentally and are fixed into the model. We take a set of randomly selected parameter values for the unknown parameters (intracellular replication and uptake rate) and run the Nelder Mead algorithm. The initial parameter values are optimized until the algorithm converges to the lowest SSE. This process is repeated 50,000 times. Histogram shows the rate of uptake by macrophages ( $\beta$ ) that gives within 1% of the minimum SSE (i.e. provides a good fit to the data).

#### 4.3.7 Equivalent intracellular and extracellular rate of growth

I hypothesized that growth of Mtb is restricted within the macrophage, and escaping the host cell into the extracellular milieu (by non-lytic egress or cellular necrosis) is beneficial to Mtb because it facilitates replication. In order to test this hypothesis I used the mathematical model to predict the intracellular replication rate of Mtb ( $r_{il}$ ).

The Nelder Mead algorithm (run above) had given us 50,000 parameter values with their associated SSE. We identified the parameter set with the lowest SSE. This gave us the model's determination of the best fit for  $r_{il}$  as  $0.023 \text{ h}^{-1}$ , representing a doubling time 31 hours. A histogram demonstrating the values of  $r_{il}$  which gives within 1% of the lowest SSE is shown in **Figure 4.10 Estimating the intracellular growth rate of Mtb in silico**. The cell death rate, extracellular growth rate and non-lytic egress rate have all been determined experimentally and are fixed into the model. We take a set of randomly selected parameter values for the unknown parameters (intracellular replication and uptake rate) and run the Nelder Mead algorithm. The initial parameter values are optimized until the algorithm converges to the lowest SSE. This process is repeated 50,000 times. Histogram shows the intracellular replication rate ( $r_i$ ) that gives within 1% of the minimum SSE (i.e. provides a good fit to the data).

Figure 5.1 **Non-lytic egress is not dependent on MOI.** **A** MDM were infected with H37Rv mCherry for 4 hours at MOI 1, 5 or 10. Cultures were washed three times with PBS to remove all extracellular bacteria. Fresh media was added for 60min. Extracellular bacteria in the supernatant were collected and intracellular bacteria were harvested by washing and lysing cells. Bacteria were fixed in 4% PFA and analysed by flow cytometry Mean  $\pm$  SEM 4 experiments. **B** MDM were infected with H37Rv mCherry for 4 hours at MOI 0, 1, 5 or 10. Cultures were washed three times with PBS to remove all extracellular bacteria. Fresh media was added for 180min. Cells were fixed in 4% PFA. Nuclei were counterstained for DAPI and counted using Hermes microscope. Data analysed by Metamorph software.

Figure 4.10. In contrast to my hypothesis, these data suggested that Mtb replication was not significantly different inside and outside the cell.

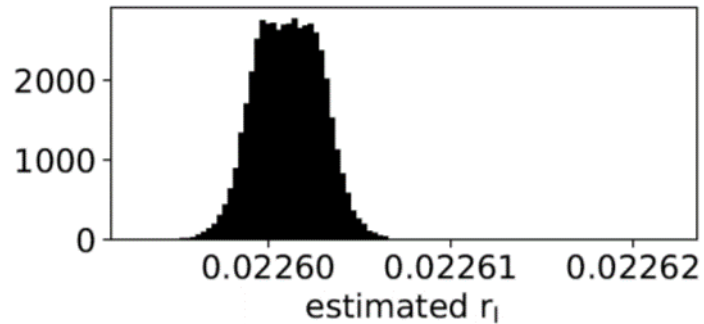


Figure 4.28 **Estimating the intracellular growth rate of Mtb in silico** The cell death rate, extracellular growth rate and non-lytic egress rate have all been determined experimentally and are fixed into the model. We take a set of randomly selected parameter values for the unknown parameters (intracellular replication and uptake rate) and run the Nelder Mead algorithm. The initial parameter values are optimized until the algorithm converges to the lowest SSE. This process is repeated 50,000 times. Histogram shows the intracellular replication rate ( $r_i$ ) that gives within 1% of the minimum SSE (i.e. provides a good fit to the data).

#### 4.4 Discussion

---

Here I demonstrate the non-lytic escape of Mtb from human macrophages experimentally in our model of early host-pathogen interactions (prior to the development of an adaptive immune response).

Cellular escape is intimately linked with the ability of microorganisms to infect neighbouring cells and be transmitted to new hosts (Hybiske and Stephens, 2008). Because of the strong evolutionary pressure to disseminate, several other organisms have evolved diverse strategies to exit their intracellular habitat, including Mm and Mtb from amoeba (Friedrich et al., 2012; Hagedorn et al., 2009; Hybiske and Stephens, 2008). Mtb has never been shown to display this behaviour from human macrophages, but the evidence presented herein, support the notion Mtb also utilizes lytic and non-lytic strategies to facilitate its own survival. In this regard, my finding that Mtb is viable following non-lytic egress is crucial, since these bacteria are able to spread infection to new cells, and replicate within the extracellular space.

My findings rely upon both the adequate removal of extracellular bacteria prior to measuring bacterial loads when assessing for egress, and the accuracy of my measurements of cell death to ensure infected cell lysis was not contributing to extracellular bacillary accumulation. The former is achieved by extensive washing of the macrophage culture, widely accepted as an effective method of removing adherent and non-adherent bacilli (Lee et al., 2013; Lerner et al., 2017). Some groups employ aminoglycoside antibiotics to kill extracellular bacteria (Blischak et al., 2015). I show both by flow cytometric analysis of the post wash supernatant, and the lack of egress demonstrated by Mtb at 4°C, that extensive

washing is adequate to remove extracellular bacteria in this experimental system. Cellular necrosis leading to release of bacteria is unlikely given the short time course over which I conduct my experiments. My data showing that the cell numbers do not change over this period of time, and that less than 1% of infected cells are dying and capable of releasing bacteria, confidently allow me to conclude that Mtb escapes from MDM by non-lytic egress rather than a cytolysis dependent process.

The live cell imaging is highly suggestive of non-lytic egress. Several different morphological characteristics of cells infected with Mtb can be visualized in the same field of view, including the loss of mCherry fluorescence from two cells which remained intact thereafter. The loss of Mtb fluorescence from the macrophages is unlikely to represent bacterial killing because we know that the total fluorescence in the intracellular and extracellular compartments stays constant over this time frame. Unfortunately, due to technical limitations, only 1 field of view could be imaged at one time, and each frame taken 2 minutes apart. Therefore the chances of catching bacterial egress where we see the bacteria exit the cell and appear in the supernatant thereafter (as demonstrated with *C.neoformans* (Johnston and May, 2010)) were extremely low.

Since Mtb is able to survive outside of its host cell, and this confers some survival advantages (transmission and spread of infection), it would be useful to understand the niche in which it prefers to replicate, which has never been directly addressed in the literature. Since the ultimate aim in the treatment of TB disease is to achieve sterilization of bacteria, knowledge of Mtb's preferred growth environment, as well as the specific pathways of pathogen exit would allow

targeting of therapies to achieve optimal bacterial clearance.

The results of our mathematical model suggest that Mtb has an intracellular doubling time of 31 hours, equivalent to its extracellular doubling time of 31.7. I had initially hypothesized that live macrophages would be somewhat restrictive to Mtb growth, given the various lines of evidence that suggest this might be the case (Clay et al., 2007; Fabri et al., 2011; Lerner et al., 2017; Mahamed et al., 2017). In the important study by Mahamed et al where Mtb was tracked in single macrophages over time, live macrophages were found to be growth restrictive (doubling time >100 hours) compared to the extracellular milieu (doubling time 32 hours). The conflict between our data and this study may be explained by the fact that their intracellular growth rate of Mtb was underestimated because they did not account for non-lytic egress, thus not capturing bacteria that had grown within the cell and subsequently escaped.

My findings are more aligned with data from several other papers where macrophages have been shown to facilitate Mtb growth. One such example is mouse alveolar macrophages in vivo, where Huang et al were able to demonstrate the metabolic fitness of Mtb in these cells (Huang et al., 2018); also in zebrafish larvae, incoming phagocytes recruited to the early granuloma are growth permissive (Cambier et al., 2014).

If the intracellular environment does facilitate growth, what then is the advantage to Mtb of leaving the host cell? In our model, the growth rate outside the cell offers no survival advantage. Mtb does not necessarily even need to be extracellular in order to spread infection as other virulent mycobacteria have been shown to participate in direct cell- cell transfer. However, becoming extracellular is likely to

be a much more efficient way in which to propagate infection (Hybiske and Stephens, 2008; Weddle and Agaisse, 2018). Just as host cell lysis and release of viable Mtb is thought to be crucial to the spread of infection to new cells (Behar et al., 2010), the extracellular non-lytic ejection of Mm from amoeba is directly correlated with spreading infection (Hagedorn et al., 2009).

## 5 MECHANISM OF NON- LYTIC EGRESS OF MTB

### 5.1 Introduction

---

In Chapter 4 I showed that Mtb is able to escape from human macrophages by non-lytic egress.

In this chapter, I sought to understand the mechanism by which Mtb might escape the macrophage. In amoeba, mycobacterial egress is dependent on both the bacterial virulence factor ESAT-6, and the host small GTPase RacH (Hagedorn et al., 2009). Mycobacteria are ejected through an actin dense structure termed the ejectosome, though not propelled by actin tails.

Non-lytic egress of Mtb from human macrophages could be driven by bacterial factors, just as phagosomal egress of Mtb seems to be driven by the ESX-1 secretion system (Houben et al., 2012; Simeone et al., 2012). I tested a range of different bacterial conditions which might affect the rate of non-lytic egress, for example, the multiplicity of infection and the aggregation status of bacteria. I also sought to test the hypothesis that dead bacteria do not egress from macrophages, just as non-lytic expulsion of Cryptococci only occurs with live organisms (Ma et al., 2006). Finally, because both necrotic cell death (Behar et al., 2010; Chen et al., 2006; Hsu et al., 2003) and phagosomal egress of Mtb (Simeone et al., 2012) seem to be associated with virulence, I tested the hypothesis that Mtb non-lytic egress was also associated with virulence, by looking for this behaviour in the avirulent BCG.

In Chapter 4 I showed that non-lytic egress seems to be driven by an active cellular process since it can be blocked on ice. I therefore hypothesized that the

host cell machinery governing the movement of organelles was involved in non-lytic egress, e.g. the actin cytoskeleton or microtubule network.

In Chapter 4 I found that the intracellular and extracellular environments are equally growth permissive to Mtb, at least in our in vitro model. However, within the context of a single tuberculous granuloma, and between different granuloma, macrophages have been shown to display a spectrum of pro- and anti-inflammatory phenotypes (Cadena et al., 2017; Lin et al., 2014; Marakalala et al., 2016). Since Mtb growth within macrophages has been shown to be restricted in certain macrophage populations (Cambier et al., 2017; Huang et al., 2018), in particular after activation with IFN $\gamma$  (Fabri et al., 2011), I sought to test the hypothesis that IFN $\gamma$  priming of macrophages may increase the rate of non-lytic egress, as Mtb tries to escape a more restrictive intracellular environment.

## 5.2 Objectives

---

1. To understand whether Mtb egress is associated with virulence and which bacterial factors might be involved in the non-lytic egress of Mtb
2. To determine which host factors might be involved in non-lytic egress of Mtb- specifically to test the actin cytoskeleton or microtubule network
3. To determine if IFN $\gamma$  mediated modification of the host macrophage phenotype might increase the rate of Mtb egress

## 5.3 Results

---

### 5.3.1 Non-lytic egress is not dependent on the MOI

Necrosis of infected cells is thought to occur at high MOI. I hypothesized that, at low MOI, early on in infection and before Mtb reaches its 'burst threshold' of 10-25 bacteria (Park, 2005; Repasy et al., 2013; Welin et al., 2011), non-lytic egress may be the only strategy by which the bacteria can escape the macrophage and disseminate infection.

I addressed my hypothesis by infecting MDM for four hours at MOI 1, 5 and 10 and washed off any remaining extracellular bacteria. I then quantified intracellular and extracellular bacteria after one hour. I found an increase in extracellular Mtb equivalent to the decrease in intracellular Mtb at all MOIs (**Figure 5.1 Non-lytic egress is not dependent on MOI. A** MDM were infected with H37Rv mCherry for 4 hours at MOI 1, 5 or 10. Cultures were washed three times with PBS to remove all extracellular bacteria. Fresh media was added for 60min. Extracellular bacteria in the supernatant were collected and intracellular bacteria were harvested by washing and lysing cells. Bacteria were fixed in 4% PFA and analysed by flow cytometry Mean  $\pm$  SEM 4 experiments. **B** MDM were infected with H37Rv mCherry for 4 hours at MOI 0, 1, 5 or 10. Cultures were washed three times with PBS to remove all extracellular bacteria. Fresh media was added for 180min. Cells were fixed in 4% PFA. Nuclei were counterstained for DAPI and counted using Hermes microscope. Data analysed by Metamorph software.

Figure 5.2 **Non-lytic egress is not dependent on the aggregation status of Mtb. A and B** One aliquot of Mtb suspension cultured in 7H9 containing Tween was fixed in 4% PFA. Another aliquot of the same Mtb suspension was centrifuged to a pellet and subsequently subjected to disaggregation using glass beads. The pellet was resuspended in 7H9 media fixed in 4% PFA. Both suspensions were analysed by flow cytometry. Histograms showing the distribution of fluorescence and size (FSC) of Mtb before and after disaggregation. **C** MDM were infected with aggregated or disaggregated H37Rv mCherry for 4 hours. Cultures were washed three times with PBS to remove all extracellular bacteria. Fresh media was added for one hour. Extracellular bacteria in the supernatant were collected and intracellular bacteria were harvested by washing and lysing cells. Bacteria were fixed in 4% PFA and analysed by flow cytometry. The rate of non-lytic egress in each condition was calculated. Mean  $\pm$  SEM 3 experiments. **Figure 5.1A).**

Since at higher MOI it might be necrotic cell death rather than non-lytic egress contributing to the accumulation of extracellular bacteria, I sought to test if there was any evidence of cell death. I enumerated adherent cells after four hours infection and 180 mins later. This analysis showed no significant loss of cells at MOI 1 or 5. However, at MOI 10, there was, as expected, a small but non-significant attrition in cell number (**Figure 5.1 Non-lytic egress is not dependent on MOI. A** MDM were infected with H37Rv mCherry for 4 hours at MOI 1, 5 or 10. Cultures were washed three times with PBS to remove all extracellular bacteria. Fresh media was added for 60min. Extracellular bacteria in the supernatant were collected and intracellular bacteria were harvested by washing and lysing cells. Bacteria were fixed in 4% PFA and analysed by flow cytometry

Mean  $\pm$  SEM 4 experiments. **B** MDM were infected with H37Rv mCherry for 4 hours at MOI 0, 1, 5 or 10. Cultures were washed three times with PBS to remove all extracellular bacteria. Fresh media was added for 180min. Cells were fixed in 4% PFA. Nuclei were counterstained for DAPI and counted using Hermes microscope. Data analysed by Metamorph software.

Figure 5.2 **Non-lytic egress is not dependent on the aggregation status of Mtb. A and B** One aliquot of Mtb suspension cultured in 7H9 containing Tween was fixed in 4% PFA. Another aliquot of the same Mtb suspension was centrifuged to a pellet and subsequently subjected to disaggregation using glass beads. The pellet was resuspended in 7H9 media fixed in 4% PFA. Both suspensions were analysed by flow cytometry. Histograms showing the distribution of fluorescence and size (FSC) of Mtb before and after disaggregation. **C** MDM were infected with aggregated or disaggregated H37Rv mCherry for 4 hours. Cultures were washed three times with PBS to remove all extracellular bacteria. Fresh media was added for one hour. Extracellular bacteria in the supernatant were collected and intracellular bacteria were harvested by washing and lysing cells. Bacteria were fixed in 4% PFA and analysed by flow cytometry. The rate of non-lytic egress in each condition was calculated. Mean  $\pm$  SEM 3 experiments. Figure 5.1**B**).

From these data I concluded that Mtb does display non-lytic egress even at higher MOIs. However above a certain threshold (approximately 10 bacteria per cell), there may be a combination of both cell death and non-lytic egress contributing

to extracellular bacterial burden, though further data are required to support this hypothesis.

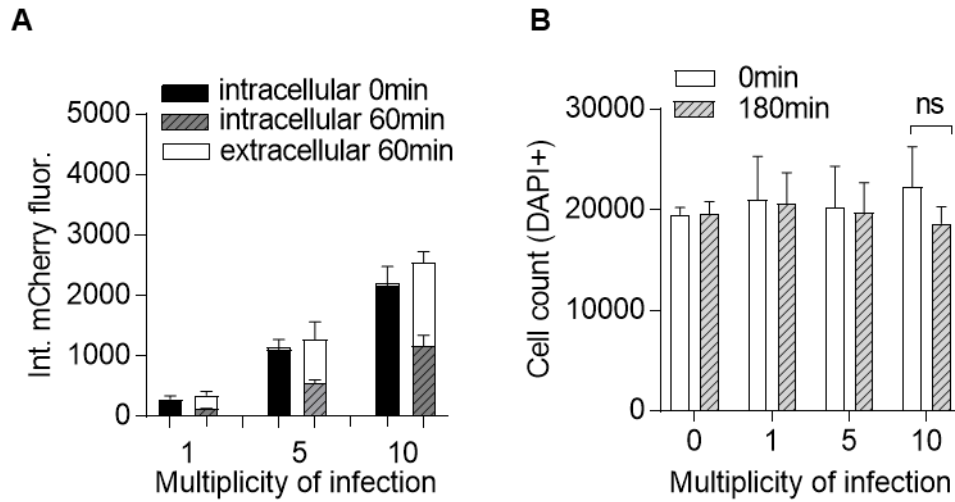


Figure 5.1 **Non-lytic egress is not dependent on MOI.** **A** MDM were infected with H37Rv mCherry for 4 hours at MOI 1, 5 or 10. Cultures were washed three times with PBS to remove all extracellular bacteria. Fresh media was added for 60min. Extracellular bacteria in the supernatant were collected and intracellular bacteria were harvested by washing and lysing cells. Bacteria were fixed in 4% PFA and analysed by flow cytometry Mean  $\pm$  SEM 4 experiments. **B** MDM were infected with H37Rv mCherry for 4 hours at MOI 0, 1, 5 or 10. Cultures were washed three times with PBS to remove all extracellular bacteria. Fresh media was added for 180min. Cells were fixed in 4% PFA. Nuclei were counterstained for DAPI and counted using Hermes microscope. Data analysed by Metamorph software.

### **5.3.2 Non-lytic egress is not dependent on the aggregation status of Mtb**

Mycobacteria display a highly conserved morphotype on solid culture and in liquid media, remaining attached during replication, forming compact colonies containing structures that resemble cords (Howard et al., 2006; Julián et al., 2010). Clumps and cords are not laboratory artefacts; the presence of the clumps and cords of *M. abscessus* (Bernut et al., 2014) and *Mm* (Clay et al., 2008) have been reported in zebrafish, and BCG in mouse splenic granulomas (Ufimtseva, 2015)

However, in most laboratories, infection studies are conducted using homogeneous bacterial suspensions containing isolated bacilli. To obtain non-aggregated cultures, mycobacteria are cultured in media containing detergents, such as Tween, and subsequently subjected to physical disaggregation procedures to obtain a homogeneous suspension of isolated bacilli (Lerner et al., 2017; Takaki et al., 2013).

Because it is likely that macrophages interact with clumps of Mtb and not with single isolated bacteria in the human host, in our group Mtb is cultured in Tween to disperse the largest of clumps but no physical disaggregation is performed prior to infection (Bell et al., 2016; Tomlinson et al., 2014).

In a study by Mahamed et al, human macrophages containing larger clumps of bacteria induced cellular necrosis, whereas smaller clumps and single bacteria did not. Similar to my initial hypothesis regarding non-lytic egress and the MOI, I hypothesized that larger clumps would induce necrosis, while single bacteria my display a higher rate of non-lytic egress, because this may be a more efficient way for them to exit the cell and spread infection (Mahamed et al., 2017).

I first determined that physical disaggregation by glass beads was able to generate a more homogenous suspension of Mtb. Using established protocols (Lerner et al., 2017) I showed by FACS that Mtb could be disaggregated to single bacteria or smaller clumps, as evidence by a reduction in both mCherry fluorescence and size by FSC (**Figure 5.2 Non-lytic egress is not dependent on the aggregation status of Mtb. A and B** One aliquot of Mtb suspension cultured in 7H9 containing Tween was fixed in 4% PFA. Another aliquot of the same Mtb suspension was centrifuged to a pellet and subsequently subjected to disaggregation using glass beads. The pellet was resuspended in 7H9 media fixed in 4% PFA. Both suspensions were analysed by flow cytometry. Histograms showing the distribution of fluorescence and size (FSC) of Mtb before and after disaggregation. **C** MDM were infected with aggregated or disaggregated H37Rv mCherry for 4 hours. Cultures were washed three times with PBS to remove all extracellular bacteria. Fresh media was added for one hour. Extracellular bacteria in the supernatant were collected and intracellular bacteria were harvested by washing and lysing cells. Bacteria were fixed in 4% PFA and analysed by flow cytometry. The rate of non-lytic egress in each condition was calculated. Mean  $\pm$  SEM 3 experiments.

**Figure 5.3 Non-lytic egress is associated with virulence.** MDM were infected with BCG dsRed for four hours. Cultures were washed three times with PBS to remove all extracellular bacteria. Fresh media was added for 60min. Extracellular bacteria in the supernatant were collected and intracellular bacteria were harvested by washing and lysing cells. Bacteria were fixed in 4% PFA and

analysed by flow cytometry Mean  $\pm$  SEM 5 experiments. Figure 5.2A).

I then infected MDM for four hours with both types of bacterial suspension, and washed off any remaining extracellular bacteria. I quantified intracellular and extracellular bacteria after one hour (**Figure 5.2 Non-lytic egress is not dependent on the aggregation status of Mtb. A and B** One aliquot of Mtb suspension cultured in 7H9 containing Tween was fixed in 4% PFA. Another aliquot of the same Mtb suspension was centrifuged to a pellet and subsequently subjected to disaggregation using glass beads. The pellet was resuspended in 7H9 media fixed in 4% PFA. Both suspensions were analysed by flow cytometry. Histograms showing the distribution of fluorescence and size (FSC) of Mtb before and after disaggregation. **C** MDM were infected with aggregated or disaggregated H37Rv mCherry for 4 hours. Cultures were washed three times with PBS to remove all extracellular bacteria. Fresh media was added for one hour. Extracellular bacteria in the supernatant were collected and intracellular bacteria were harvested by washing and lysing cells. Bacteria were fixed in 4% PFA and analysed by flow cytometry. The rate of non-lytic egress in each condition was calculated. Mean  $\pm$  SEM 3 experiments.

Figure 5.3 **Non-lytic egress is associated with virulence.** MDM were infected with BCG dsRed for four hours. Cultures were washed three times with PBS to remove all extracellular bacteria. Fresh media was added for 60min. Extracellular bacteria in the supernatant were collected and intracellular bacteria were harvested by washing and lysing cells. Bacteria were fixed in 4% PFA and analysed by flow cytometry Mean  $\pm$  SEM 5 experiments. Figure 5.2B). As detailed

in Chapter 2, non-lytic egress is calculated using the following equation:

$$\eta = -\frac{1}{t} \ln \left( 1 - \frac{E(t) - E(0)}{I(0)} \right)$$

Essentially this equation uses the amount of extracellular bacteria that appear after 1 hour as a proportion of the initial intracellular bacillary burden to derive rate of non-lytic egress per bug per hour.

Non-lytic egress occurs at similar rates in single and clumped suspensions of Mtb (**Figure 5.2 Non-lytic egress is not dependent on the aggregation status of Mtb. A and B** One aliquot of Mtb suspension cultured in 7H9 containing Tween was fixed in 4% PFA. Another aliquot of the same Mtb suspension was centrifuged to a pellet and subsequently subjected to disaggregation using glass beads. The pellet was resuspended in 7H9 media fixed in 4% PFA. Both suspensions were analysed by flow cytometry. Histograms showing the distribution of fluorescence and size (FSC) of Mtb before and after disaggregation. **C** MDM were infected with aggregated or disaggregated H37Rv mCherry for 4 hours. Cultures were washed three times with PBS to remove all extracellular bacteria. Fresh media was added for one hour. Extracellular bacteria in the supernatant were collected and intracellular bacteria were harvested by washing and lysing cells. Bacteria were fixed in 4% PFA and analysed by flow cytometry. The rate of non-lytic egress in each condition was calculated. Mean  $\pm$  SEM 3 experiments.

**Figure 5.3 Non-lytic egress is associated with virulence.** MDM were infected

with BCG dsRed for four hours. Cultures were washed three times with PBS to remove all extracellular bacteria. Fresh media was added for 60min. Extracellular bacteria in the supernatant were collected and intracellular bacteria were harvested by washing and lysing cells. Bacteria were fixed in 4% PFA and analysed by flow cytometry Mean  $\pm$  SEM 5 experiments. Figure 5.2C). There is however, as expected, less variation in the data using disaggregated suspensions of Mtb.

I concluded that Mtb non-lytic egress was not dependent on whether the bacteria infecting the macrophages were singular or in aggregates.

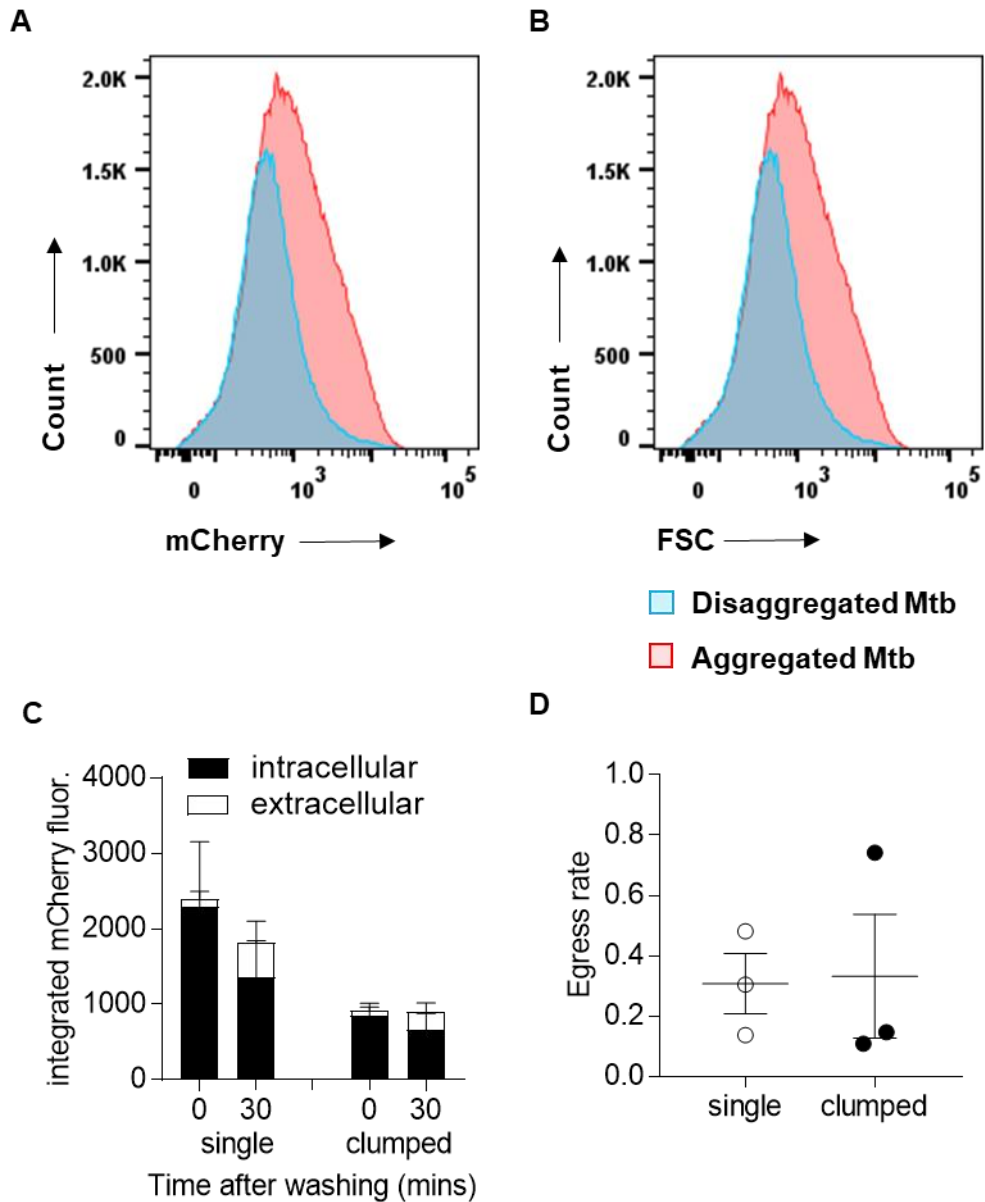


Figure 5.4 **Non-lytic egress is not dependent on the aggregation status of Mtb.** **A and B** One aliquot of Mtb suspension cultured in 7H9 containing Tween was fixed in 4% PFA. Another aliquot of the same Mtb suspension was centrifuged to a pellet and subsequently subjected to disaggregation using glass beads. The pellet was resuspended in 7H9 media fixed in 4% PFA. Both suspensions were analysed by flow cytometry. Histograms showing the distribution of fluorescence and size (FSC) of Mtb before and after disaggregation. **C** MDM were infected with aggregated or disaggregated H37Rv mCherry for 4 hours. Cultures were washed three times with PBS to remove all extracellular bacteria. Fresh media was added for one hour. Extracellular bacteria in the supernatant were collected and intracellular bacteria were harvested by washing and lysing cells. Bacteria were fixed in 4% PFA and analysed by flow cytometry. The rate of non-lytic egress in each condition was calculated. Mean  $\pm$  SEM 3 experiments.

### 5.3.3 Non-lytic egress of Mtb is associated with virulence

In order to test whether a specific behaviour by mycobacteria is associated with virulence, virulent Mtb such as H37Rv is often compared to avirulent M.bovis BCG, or other less virulent mycobacterial strains like M.avium. Mm and Mtb, but not M.avium have been shown to egress from amoeba (Hagedorn et al., 2009). I therefore hypothesized that the non-lytic egress of mycobacteria from human macrophages is also associated with virulence and that the attenuated BCG would not display this behaviour.

The main genetic modification involved in the attenuation of BCG is the deletion of RD1 (Brosch et al., 2002). RD1 encodes two strong immunogenic antigens and virulence factors—ESAT-6 and the culture filtrate protein (CFP-10)—as well as several structural components of the ESX-1 secretion system (Simeone et al., 2009).

I infected MDM with dsRed BCG for 4 hours, and looked for the appearance of extracellular bacteria both 60 mins and 180 mins later. I used these two different timepoints because I reasoned that the kinetics of non-lytic egress may differ between virulent and avirulent strains. While the intracellular burden of mCherry Mtb decreases within 60 minutes, accompanied by the appearance of extracellular bacteria, this is not the case for BCG. The intracellular bacillary load remains constant over time (**Figure 5.3 Non-lytic egress is associated with virulence**). MDM were infected with BCG dsRed for four hours. Cultures were washed three times with PBS to remove all extracellular bacteria. Fresh media was added for 60min. Extracellular bacteria in the supernatant were collected and intracellular bacteria were harvested by washing and lysing cells. Bacteria were

fixed in 4% PFA and analysed by flow cytometry Mean  $\pm$  SEM 5 experiments.

Figure 5.4 **Non-lytic egress occurs with heat killed bacteria.** **A** Bacterial suspension at log phase was heated to 80°C in a dry heat block for 30 minutes. Representative FACS plots of bacterial suspensions pre (Mtb) and post (HKMtb) heat killing. **B** MDM were infected with live or heat killed H37Rv mCherry for four hours. Cultures were washed three times with PBS to remove all extracellular bacteria. Fresh media was added for one hour. Extracellular bacteria in the supernatant were collected and intracellular bacteria were harvested by washing and lysing cells. Bacteria were fixed in 4% PFA and analysed by flow cytometry. **C** The rate of non-lytic egress in each condition was calculated. Mean  $\pm$  SEM 4 experiments. (Figure 5.3).

I concluded that non-lytic egress of Mtb from the host cell may therefore be associated with its virulence.

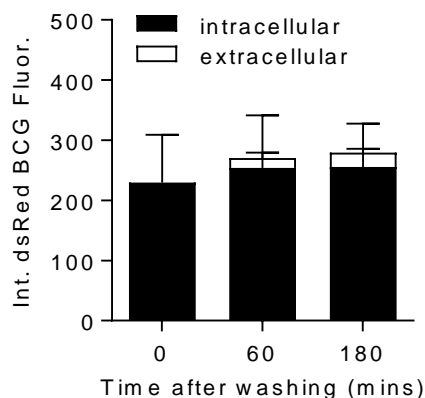


Figure 5.7 **Non-lytic egress is associated with virulence.** MDM were infected with BCG dsRed for four hours. Cultures were washed three times with PBS to remove all extracellular bacteria. Fresh media was added for 60min. Extracellular bacteria in the supernatant were collected and intracellular bacteria were harvested by washing and lysing cells. Bacteria were fixed in 4% PFA and analysed by flow cytometry Mean  $\pm$  SEM 5 experiments.

### 5.3.4 Non-lytic egress occurs with heat killed bacteria

Heat killing of Mtb deactivates the bacteria but heat killed Mtb (HKMtb) is still able to activate TLR2 (Underhill et al., 1999) and other PRRs (Ishikawa et al., 2009), and elicit cytokine responses in macrophages (Underhill et al., 1999). Other Mtb-macrophage interactions require the presence of live bacteria, such as blockade of phagolysosomal fusion (Ramachandra et al., 2001), modulation of antigen presentation (Clemens and Horwitz, 1996; Ramachandra et al., 2001; Steffen Stenger et al., 1998) and phagosomal rupture. The non-lytic expulsion of Cryptococci from macrophages is dependent on the presence of the live pathogen. I therefore sought to test the hypothesis that non-lytic egress of Mtb occurs with live, but not HKMtb.

Heat killing was achieved using established methods (Doig, 2002) by incubating the bacteria in a dry heat block for 30 mins at 80°C. Under these conditions growth on both solid agar and liquid broth was absent after 8 weeks. However, HKMtb retained mCherry fluorescence and therefore bacteria could be quantitated by flow cytometry (**Figure 5.4 Non-lytic egress occurs with heat killed bacteria**). **A** Bacterial suspension at log phase was heated to 80°C in a dry heat block for 30 minutes. Representative FACS plots of bacterial suspensions pre (Mtb) and post (HKMtb) heat killing. **B** MDM were infected with live or heat killed H37Rv mCherry for four hours. Cultures were washed three times with PBS to remove all extracellular bacteria. Fresh media was added for one hour. Extracellular bacteria in the supernatant were collected and intracellular bacteria were harvested by washing and lysing cells. Bacteria were fixed in 4% PFA and analysed by flow cytometry. **C** The rate of non-lytic egress in each condition was

calculated. Mean  $\pm$  SEM 4 experiments.

Figure 5.5 **Blocking non-lytic egress using Cytochalasin D.** **A** MDM were pre-treated with Cytochalasin D (CytoD) for one hour prior to, and during infection with Mtb. After 4 hours, internalized bacteria were measured by washing and lysing the cells and fixing in 4% PFA **B** MDM infected for four hours. Cells were washed and treated with 10 $\mu$ M CytoD or vehicle control (DMSO) for one hour. Cultures were washed again three times with PBS to remove all extracellular bacteria. Fresh media was added for one hour with or without the inhibitor. Extracellular bacteria in the supernatant were collected and intracellular bacteria were harvested by washing and lysing cells. Bacteria were fixed in 4% PFA and analysed by flow cytometry. **C** The rate of non-lytic egress in each condition was calculated. Mean  $\pm$  SEM 4 experiments. **D** MDM infected for four hours. Cells were washed and treated with 10 $\mu$ M CytoD or vehicle control (DMSO) for one hour. Live/ Dead stain was added for 20 mins. Cells were gently washed and fixed in 4% PFA. Cells were counterstained for DAPI+ cell mask and counted using Hermes microscope. Data analysed by Metamorph software to enumerate the number of cells in each condition as a percentage of the number of cells in each well (dead/ dying cells= red, live cells =white).Figure 5.4**A**).

I proceeded to infect macrophages with Mtb or HKMtb for four hours and subsequently looked for the appearance of extracellular bacteria after one hour (**Figure 5.4 Non-lytic egress occurs with heat killed bacteria.** **A** Bacterial suspension at log phase was heated to 80°C in a dry heat block for 30 minutes. Representative FACS plots of bacterial suspensions pre (Mtb) and post (HKMtb)

heat killing. **B** MDM were infected with live or heat killed H37Rv mCherry for four hours. Cultures were washed three times with PBS to remove all extracellular bacteria. Fresh media was added for one hour. Extracellular bacteria in the supernatant were collected and intracellular bacteria were harvested by washing and lysing cells. Bacteria were fixed in 4% PFA and analysed by flow cytometry. **C** The rate of non-lytic egress in each condition was calculated. Mean  $\pm$  SEM 4 experiments.

Figure 5.5 **Blocking non-lytic egress using Cytochalasin D.** **A** MDM were pre-treated with Cytochalasin D (CytoD) for one hour prior to, and during infection with Mtb. After 4 hours, internalized bacteria were measured by washing and lysing the cells and fixing in 4% PFA **B** MDM infected for four hours. Cells were washed and treated with 10 $\mu$ M CytoD or vehicle control (DMSO) for one hour. Cultures were washed again three times with PBS to remove all extracellular bacteria. Fresh media was added for one hour with or without the inhibitor. Extracellular bacteria in the supernatant were collected and intracellular bacteria were harvested by washing and lysing cells. Bacteria were fixed in 4% PFA and analysed by flow cytometry. **C** The rate of non-lytic egress in each condition was calculated. Mean  $\pm$  SEM 4 experiments. **D** MDM infected for four hours. Cells were washed and treated with 10 $\mu$ M CytoD or vehicle control (DMSO) for one hour. Live/ Dead stain was added for 20 mins. Cells were gently washed and fixed in 4% PFA. Cells were counterstained for DAPI+ cell mask and counted using Hermes microscope. Data analysed by Metamorph software to enumerate the number of cells in each condition as a percentage of the number of cells in

each well (dead/ dying cells= red, live cells =white).Figure 5.4**B**). I found no difference in the rate of non-lytic egress (**Figure 5.4 Non-lytic egress occurs with heat killed bacteria**). **A** Bacterial suspension at log phase was heated to 80°C in a dry heat block for 30 minutes. Representative FACS plots of bacterial suspensions pre (Mtb) and post (HKMtb) heat killing. **B** MDM were infected with live or heat killed H37Rv mCherry for four hours. Cultures were washed three times with PBS to remove all extracellular bacteria. Fresh media was added for one hour. Extracellular bacteria in the supernatant were collected and intracellular bacteria were harvested by washing and lysing cells. Bacteria were fixed in 4% PFA and analysed by flow cytometry. **C** The rate of non-lytic egress in each condition was calculated. Mean  $\pm$  SEM 4 experiments.

Figure 5.5 **Blocking non-lytic egress using Cytochalasin D**. **A** MDM were pre-treated with Cytochalasin D (CytoD) for one hour prior to, and during infection with Mtb. After 4 hours, internalized bacteria were measured by washing and lysing the cells and fixing in 4% PFA **B** MDM infected for four hours. Cells were washed and treated with 10 $\mu$ M CytoD or vehicle control (DMSO) for one hour. Cultures were washed again three times with PBS to remove all extracellular bacteria. Fresh media was added for one hour with or without the inhibitor. Extracellular bacteria in the supernatant were collected and intracellular bacteria were harvested by washing and lysing cells. Bacteria were fixed in 4% PFA and analysed by flow cytometry. **C** The rate of non-lytic egress in each condition was calculated. Mean  $\pm$  SEM 4 experiments. **D** MDM infected for four hours. Cells were washed and treated with 10 $\mu$ M CytoD or vehicle control (DMSO) for one

hour. Live/ Dead stain was added for 20 mins. Cells were gently washed and fixed in 4% PFA. Cells were counterstained for DAPI+ cell mask and counted using Hermes microscope. Data analysed by Metamorph software to enumerate the number of cells in each condition as a percentage of the number of cells in each well (dead/ dying cells= red, live cells =white).Figure 5.4**C**). Contrary to my hypothesis, I concluded that this process in macrophages is not dependent on whether the bacteria are alive or dead. This is different to the literature on cryptococcal egress from macrophages, which does not occur with dead fungus (Johnston and May, 2010). Live cell imaging is crucial to definitively show the non-lytic egress of HK Mtb from macrophages.

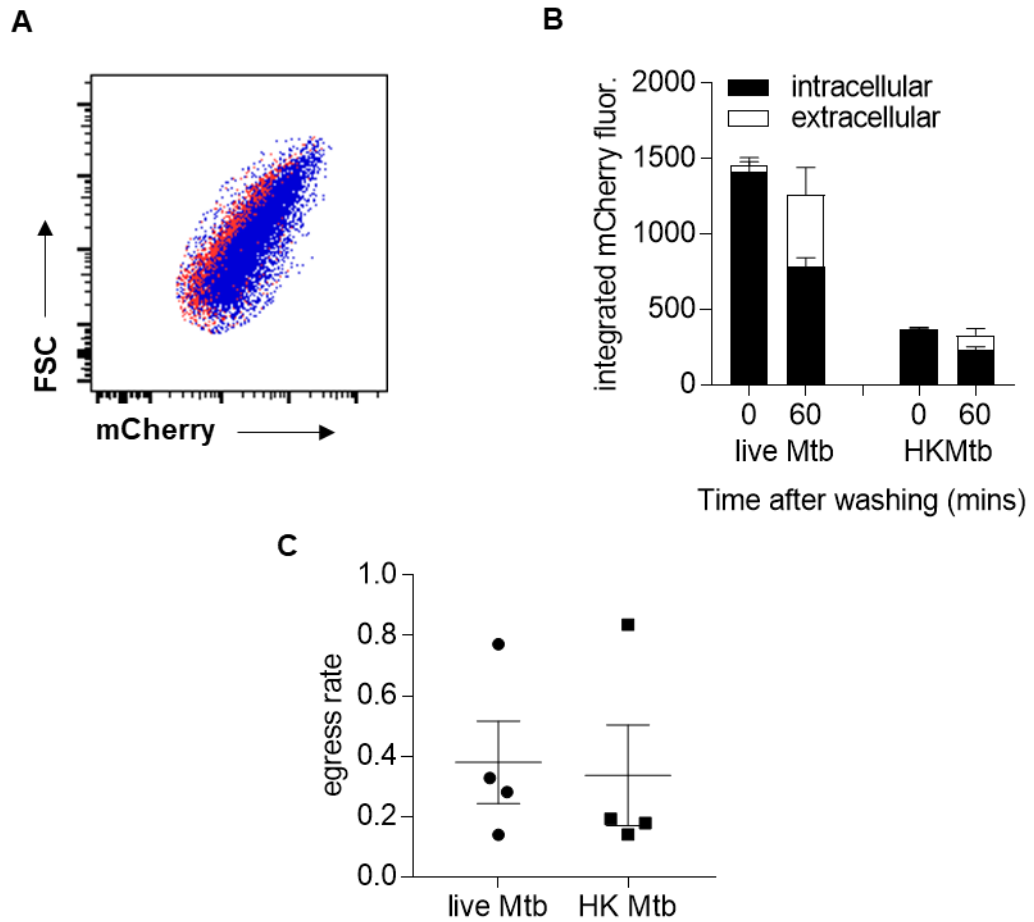


Figure 5.10 **Non-lytic egress occurs with heat killed bacteria.** **A** Bacterial suspension at log phase was heated to 80°C in a dry heat block for 30 minutes. Representative FACS plots of bacterial suspensions pre (Mtb) and post (HKMtb) heat killing. **B** MDM were infected with live or heat killed H37Rv mCherry for four hours. Cultures were washed three times with PBS to remove all extracellular bacteria. Fresh media was added for one hour. Extracellular bacteria in the supernatant were collected and intracellular bacteria were harvested by washing and lysing cells. Bacteria were fixed in 4% PFA and analysed by flow cytometry. **C** The rate of non-lytic egress in each condition was calculated. Mean  $\pm$  SEM 4 experiments.

### 5.3.5 Non-lytic egress is not governed by the actin cytoskeleton

The actin cytoskeleton in eukaryotic cells plays an important role in cell morphology as well as in more dynamic processes, including phagocytosis and cell motility, during which regulated assembly and disassembly of actin filaments may drive cellular movement (Lodish et al., 2000).

*Listeria*, *Shigella* and *Chlamydia* can egress and spread between host cells via propulsive forces due to actin polymerization, which generates protrusions at the plasma membrane (Hybiske and Stephens, 2007; Monack and Theriot, 2001). In mouse BMDM, Mm induces actin polymerization prior to non-lytic egress (Stamm et al., 2003). In cryptococcal infection of macrophages, however, actin polymerization may serve to enhance non-lytic expulsion, as 'actin flashes' try to cage in the fungal pathogen (Johnston and May, 2010).

Cytochalasin D is a cell permeable fungal toxin that binds to the barbed end of actin filaments inhibiting both the association and dissociation of subunits, resulting in the disruption of actin filaments and inhibition of actin polymerization (Lodish et al., 2000). I hypothesized that non-lytic egress of Mtb is driven by the actin cytoskeleton, and could be blocked the addition of Cytochalasin D.

I first determined the effective dose of Cytochalasin D required to block actin polymerization. The actin cytoskeleton participates in phagocytosis, and uptake of Mtb should therefore be inhibited in the presence of Cytochalasin D. Cells were pre-treated for one hour with the inhibitor, then infected with Mtb for four hours. I found that 10 $\mu$ M was the minimum effective dose required to disrupt the actin cytoskeleton (**Figure 5.5 Blocking non-lytic egress using Cytochalasin D. A**

MDM were pre-treated with Cytochalasin D (CytoD) for one hour prior to, and during infection with Mtb. After 4 hours, internalized bacteria were measured by washing and lysing the cells and fixing in 4% PFA **B** MDM infected for four hours. Cells were washed and treated with 10 $\mu$ M CytoD or vehicle control (DMSO) for one hour. Cultures were washed again three times with PBS to remove all extracellular bacteria. Fresh media was added for one hour with or without the inhibitor. Extracellular bacteria in the supernatant were collected and intracellular bacteria were harvested by washing and lysing cells. Bacteria were fixed in 4% PFA and analysed by flow cytometry. **C** The rate of non-lytic egress in each condition was calculated. Mean  $\pm$  SEM 4 experiments. **D** MDM infected for four hours. Cells were washed and treated with 10 $\mu$ M CytoD or vehicle control (DMSO) for one hour. Live/ Dead stain was added for 20 mins. Cells were gently washed and fixed in 4% PFA. Cells were counterstained for DAPI+ cell mask and counted using Hermes microscope. Data analysed by Metamorph software to enumerate the number of cells in each condition as a percentage of the number of cells in each well (dead/ dying cells= red, live cells =white).

Figure 5.5**A**).

Next, I tested the hypothesis that 10 $\mu$ M Cytochalasin D could block non-lytic egress. I infected MDM for four hours with Mtb to establish an intracellular infection. All extracellular bacteria were then washed away, and the inhibitor added for one hour to disrupt the actin filaments. During this time there may have been some egress of bacteria. Therefore after one hour, extracellular bacteria were washed again. I looked for the presence of non-lytic egress of Mtb over the

following 60 minutes. I found an increase in extracellular Mtb equivalent to the decrease in intracellular Mtb (**Figure 5.5 Blocking non-lytic egress using Cytochalasin D**). **A** MDM were pre-treated with Cytochalasin D (CytoD) for one hour prior to, and during infection with Mtb. After 4 hours, internalized bacteria were measured by washing and lysing the cells and fixing in 4% PFA. **B** MDM infected for four hours. Cells were washed and treated with 10 $\mu$ M CytoD or vehicle control (DMSO) for one hour. Cultures were washed again three times with PBS to remove all extracellular bacteria. Fresh media was added for one hour with or without the inhibitor. Extracellular bacteria in the supernatant were collected and intracellular bacteria were harvested by washing and lysing cells. Bacteria were fixed in 4% PFA and analysed by flow cytometry. **C** The rate of non-lytic egress in each condition was calculated. Mean  $\pm$  SEM 4 experiments. **D** MDM infected for four hours. Cells were washed and treated with 10 $\mu$ M CytoD or vehicle control (DMSO) for one hour. Live/ Dead stain was added for 20 mins. Cells were gently washed and fixed in 4% PFA. Cells were counterstained for DAPI+ cell mask and counted using Hermes microscope. Data analysed by Metamorph software to enumerate the number of cells in each condition as a percentage of the number of cells in each well (dead/ dying cells= red, live cells =white).

Figure 5.5**B and C**).

Since Cytochalasin D may be toxic to cells (though usually at higher concentrations), I tested the hypothesis that infected host cells were dying in the presence of cytochalasin D, and contributing to the appearance of extracellular

bacteria over one hour. I infected MDM for four hours with Mtb to establish an intracellular infection. All extracellular bacteria were then washed away, and the inhibitor added for one hour. I then stained the cells with a Live/Dead stain combined with a cell mask in order delineate the boundaries of each cell, and hence enumerate the number of Mtb infected cells that may be committed to cell death in the subsequent one hour. There was no difference in the relative number of Mtb infected cells undergoing necrosis in the absence or presence of the inhibitor (**Figure 5.5 Blocking non-lytic egress using Cytochalasin D. A** MDM were pre-treated with Cytochalasin D (CytoD) for one hour prior to, and during infection with Mtb. After 4 hours, internalized bacteria were measured by washing and lysing the cells and fixing in 4% PFA **B** MDM infected for four hours. Cells were washed and treated with 10 $\mu$ M CytoD or vehicle control (DMSO) for one hour. Cultures were washed again three times with PBS to remove all extracellular bacteria. Fresh media was added for one hour with or without the inhibitor. Extracellular bacteria in the supernatant were collected and intracellular bacteria were harvested by washing and lysing cells. Bacteria were fixed in 4% PFA and analysed by flow cytometry. **C** The rate of non-lytic egress in each condition was calculated. Mean  $\pm$  SEM 4 experiments. **D** MDM infected for four hours. Cells were washed and treated with 10 $\mu$ M CytoD or vehicle control (DMSO) for one hour. Live/ Dead stain was added for 20 mins. Cells were gently washed and fixed in 4% PFA. Cells were counterstained for DAPI+ cell mask and counted using Hermes microscope. Data analysed by Metamorph software to enumerate the number of cells in each condition as a percentage of the number of cells in each well (dead/ dying cells= red, live cells =white).

Figure 5.5D).

I concluded that the bacteria that appeared in the extracellular milieu over one hour in the presence of Cytochalasin D did not appear as a result of inhibitor induced cell death, and that inhibition of actin polymerization by Cytochalasin D did not block nor enhance non-lytic egress of Mtb. I also inferred from this data that non-lytic egress and phagocytosis are driven by two independent processes.

One caveat to the interpretation of this data is that a 10 $\mu$ M of cytochalasin D to block phagocytosis is high, and may indicate that the inhibitor was no longer fully active during the experiments. I would want to repeat these experiments with a new vial of cytochalasin D to ensure the data are replicable.

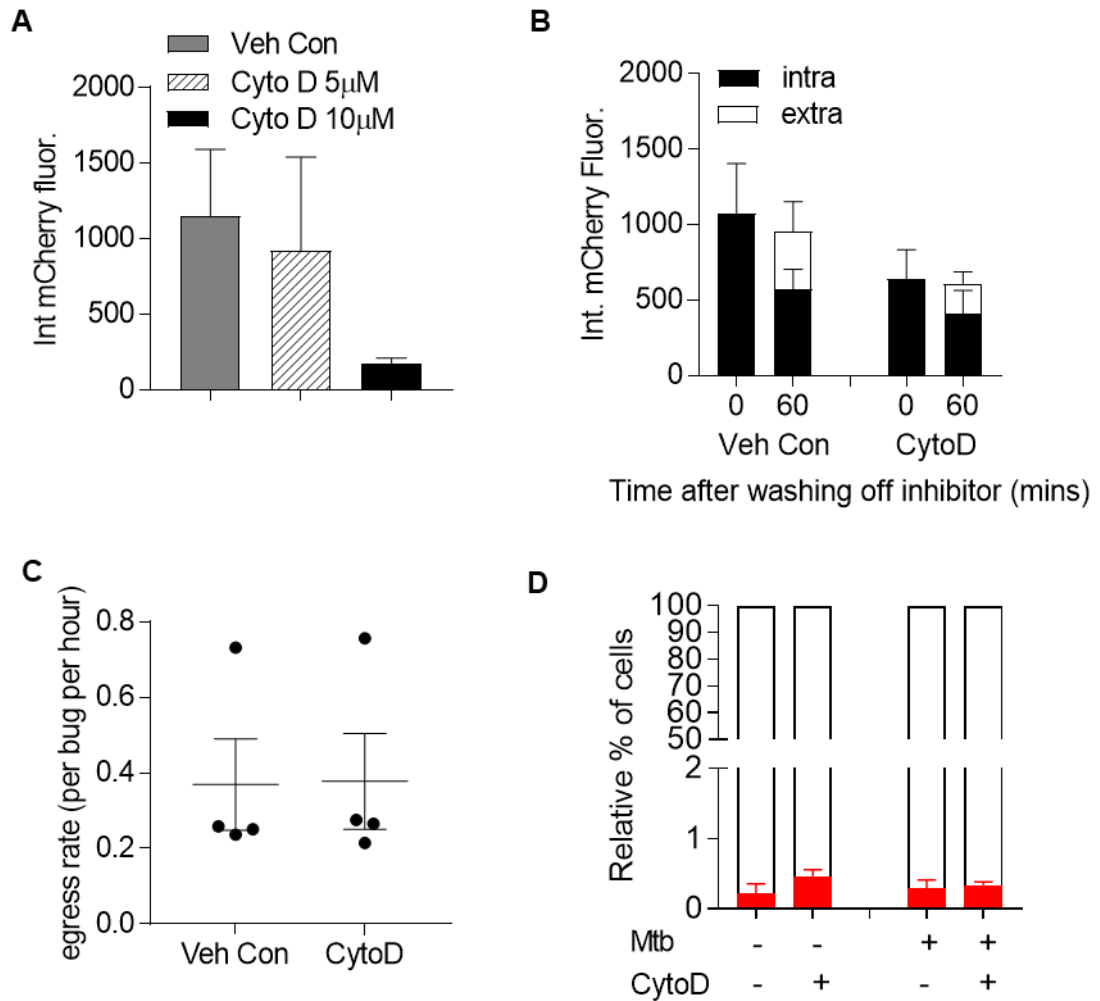


Figure 5.13 **Blocking non-lytic egress using Cytochalasin D.** **A** MDM were pre-treated with Cytochalasin D (CytoD) for one hour prior to, and during infection with Mtb. After 4 hours, internalized bacteria were measured by washing and lysing the cells and fixing in 4% PFA **B** MDM infected for four hours. Cells were washed and treated with 10µM CytoD or vehicle control (DMSO) for one hour. Cultures were washed again three times with PBS to remove all extracellular bacteria. Fresh media was added for one hour with or without the inhibitor. Extracellular bacteria in the supernatant were collected and intracellular bacteria were harvested by washing and lysing cells. Bacteria were fixed in 4% PFA and analysed by flow cytometry. **C** The rate of non-lytic egress in each condition was calculated. Mean  $\pm$  SEM 4 experiments. **D** MDM infected for four hours. Cells were washed and treated with 10µM CytoD or vehicle control (DMSO) for one hour. Live/ Dead stain was added for 20 mins. Cells were gently washed and fixed in 4% PFA. Cells were counterstained for DAPI+ cell mask and counted using Hermes microscope. Data analysed by Metamorph software to enumerate the number of cells in each condition as a percentage of the number of cells in each well (dead/ dying cells= red, live cells =white).

### 5.3.6 Non-lytic egress is not governed by the microtubule network

Another major component of the cell cytoskeleton that governs organelle trafficking and vesicular transport are microtubules (MTs). MTs are composed of  $\alpha$ - and  $\beta$ -tubulin heterodimers that associate to form hollow cylindrical structures. They are highly dynamic, and are constantly lengthening and shortening throughout all phases of the cell cycle (Nogales, 2000).

$\alpha$ -tubulin microtubules can be blocked using the agent nocodazole. Nocodazole causes microtubule depolymerization by binding to free tubulin dimers and preventing them from incorporating into MTs (Hoebeke et al., 1976).

I hypothesized that non-lytic egress of Mtb is driven by the microtubule cytoskeleton, and could be blocked the addition of nocodazole. I first showed that  $\alpha$ -tubulin microtubules were indeed disrupted by nocodazole by imaging cells treated with the inhibitor by confocal microscopy. Where cells had not been exposed to nocodazole, or treated with low concentration (10 $\mu$ M), I was able to visualize tubular/ spindle like structures distributed throughout the cytoplasm of the cell, representative of the MT network. However at 30 $\mu$ M nocodazole, while the nuclei looked intact, the cytoplasmic staining was much dimmer and diffuse and I was not clearly able to visualize the MTs. At 50  $\mu$ M, there was little staining for  $\alpha$ -tubulin, but some nuclei appeared degraded suggestive of cellular death (**Figure 5.6 Effect of Nocodazole on  $\alpha$ -tubulin**. MDM were grown on coverslips and treated with Nocodazole (Nocod) at various concentrations for 1 hour. Cells were washed, permeabilized using Triton X and blocked with 3% NGS. Cells were stained for rat monoclonal alpha tubulin antibody and anti-rat secondary antibody (red). Coverslips were mounted using VectaShield with DAPI and imaged by

confocal microscopy.

Figure 5.7 **Blocking non-lytic egress using Nocodazole.** **A** MDM were infected for four hours. Cells were washed and treated with 30 $\mu$ M Nocod or vehicle control (DMSO) for one hour. Cultures were washed again three times with PBS to remove all extracellular bacteria. Fresh media was added for one hour with or without the inhibitor. Extracellular bacteria in the supernatant were collected and intracellular bacteria were harvested by washing and lysing cells. Bacteria were fixed in 4% PFA and analysed by flow cytometry. **B** The rate of non-lytic egress in each condition was calculated. Mean  $\pm$  SEM 3 experiments. **C** MDM infected for four hours. Cells were washed and treated with 30 $\mu$ M Nocod or vehicle control (DMSO) for one hour. Live/ Dead stain was added for 20 mins. Cells were gently washed and fixed in 4% PFA. Cells were counterstained for DAPI + cell mask and counted using Hermes microscope. Data analysed by Metamorph software to enumerate the number of cells in each condition as a percentage of the number of cells in each well (dead/ dying cells= red, live cells =white).Figure 5.6). I concluded that 30 $\mu$ M was the effective concentration to block  $\alpha$ -tubulin microtubules, without apparent cell toxicity.

Next, I tested whether 30 $\mu$ M nocodazole could block non-lytic egress. I infected MDM for four hours with Mtb to establish an intracellular infection. All extracellular bacteria were then washed away, and the inhibitor added for one hour to disrupt the  $\alpha$ -tubulin microtubules. Therefore after one hour, extracellular bacteria were washed again. I looked for the presence of non-lytic egress of Mtb over the following one hour. I found an increase in extracellular Mtb equivalent to the

decrease in intracellular Mtb, such that the rate of non-lytic egress was not different in the presence or absence of the inhibitor (**Figure 5.7 Blocking non-lytic egress using Nocodazole**). **A** MDM were infected for four hours. Cells were washed and treated with 30 $\mu$ M Nocod or vehicle control (DMSO) for one hour. Cultures were washed again three times with PBS to remove all extracellular bacteria. Fresh media was added for one hour with or without the inhibitor. Extracellular bacteria in the supernatant were collected and intracellular bacteria were harvested by washing and lysing cells. Bacteria were fixed in 4% PFA and analysed by flow cytometry. **B** The rate of non-lytic egress in each condition was calculated. Mean  $\pm$  SEM 3 experiments. **C** MDM infected for four hours. Cells were washed and treated with 30 $\mu$ M Nocod or vehicle control (DMSO) for one hour. Live/ Dead stain was added for 20 mins. Cells were gently washed and fixed in 4% PFA. Cells were counterstained for DAPI + cell mask and counted using Hermes microscope. Data analysed by Metamorph software to enumerate the number of cells in each condition as a percentage of the number of cells in each well (dead/ dying cells= red, live cells =white).

Figure 5.8 **GM-CSF differentiated MDM display the same phenotype as M-CSF MDM** **A** GM-CSF MDM were infected with H37Rv mCherry for 4 hours at MOI 1. Cultures were washed three times with PBS to remove all extracellular bacteria. Fresh media was added for the times specified. At the relevant time point extracellular bacteria in the supernatant were collected. Intracellular bacteria were harvested by washing and lysing cells. Bacteria were fixed in 4% PFA and analysed by flow cytometry. Bacteria quantified by integrated mCherry fluorescence at each time point in each compartment. Mean  $\pm$  SEM 3 separate

experiments **B** MDM were infected with H37Rv mCherry for 4 hours at MOI 1. Cultures were washed three times with PBS to remove all extracellular bacteria. Fresh media was added for 60min. Extracellular bacteria in the supernatant were collected and intracellular bacteria were harvested by washing and lysing cells. Bacteria were fixed in 4% PFA and analysed by flow cytometry. Mean  $\pm$  SEM 2 experiments. (Figure 5.7 **A and B**).

Since nocodazole may be toxic to cells, I tested the hypothesis that infected host cells were dying in the presence of the inhibitor, contributing to the appearance of extracellular bacteria over one hour. I infected MDM for four hours with Mtb to establish an intracellular infection. All extracellular bacteria were then washed away, and the inhibitor added for one hour to disrupt the  $\alpha$ -tubulin microtubules. I then stained the cells with a Live/Dead stain combined with a cell mask in order to delineate the boundaries of each cell, and hence enumerate the number of Mtb infected cells that may be committed to cell death in the subsequent one hour. There was no difference in the relative number of Mtb infected cells undergoing necrosis in the absence or presence of the inhibitor (**Figure 5.7 Blocking non-lytic egress using Nocodazole**). **A** MDM were infected for four hours. Cells were washed and treated with 30 $\mu$ M Nocod or vehicle control (DMSO) for one hour. Cultures were washed again three times with PBS to remove all extracellular bacteria. Fresh media was added for one hour with or without the inhibitor. Extracellular bacteria in the supernatant were collected and intracellular bacteria were harvested by washing and lysing cells. Bacteria were fixed in 4% PFA and analysed by flow cytometry. **B** The rate of non-lytic egress in each condition was calculated. Mean  $\pm$  SEM 3 experiments. **C** MDM infected for four hours. Cells were washed and treated with 30 $\mu$ M Nocod or vehicle control (DMSO) for one

hour. Live/ Dead stain was added for 20 mins. Cells were gently washed and fixed in 4% PFA. Cells were counterstained for DAPI + cell mask and counted using Hermes microscope. Data analysed by Metamorph software to enumerate the number of cells in each condition as a percentage of the number of cells in each well (dead/ dying cells= red, live cells =white).

Figure 5.8 **GM-CSF differentiated MDM display the same phenotype as M-CSF MDM** **A** GM-CSF MDM were infected with H37Rv mCherry for 4 hours at MOI 1. Cultures were washed three times with PBS to remove all extracellular bacteria. Fresh media was added for the times specified. At the relevant time point extracellular bacteria in the supernatant were collected. Intracellular bacteria were harvested by washing and lysing cells. Bacteria were fixed in 4% PFA and analysed by flow cytometry. Bacteria quantified by integrated mCherry fluorescence at each time point in each compartment. Mean  $\pm$  SEM 3 separate experiments **B** MDM were infected with H37Rv mCherry for 4 hours at MOI 1. Cultures were washed three times with PBS to remove all extracellular bacteria. Fresh media was added for 60min. Extracellular bacteria in the supernatant were collected and intracellular bacteria were harvested by washing and lysing cells. Bacteria were fixed in 4% PFA and analysed by flow cytometry. Mean  $\pm$  SEM 2 experiments. Figure 5.7C).

I concluded that the bacteria that appeared in the extracellular milieu over one hour in the presence of nocodazole did not appear as a result of inhibitor induced cell death, and that non-lytic egress was not dependent on an intact microtubule network.



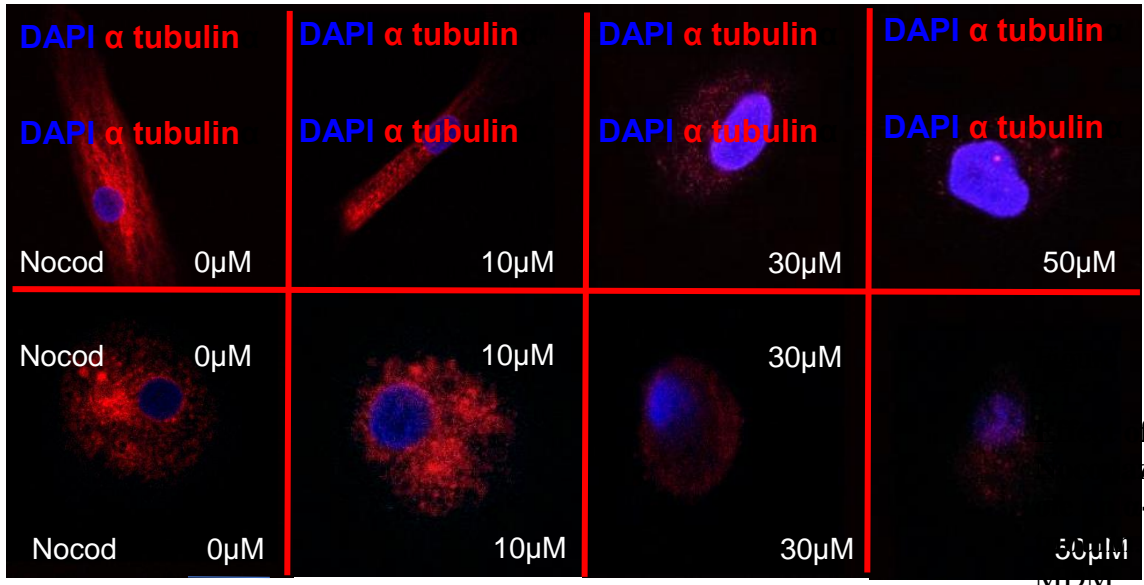


Figure 5.16 **Effect of Nocodazole on  $\alpha$ -tubulin.** MDM were grown on coverslips and treated with Nocodazole (Nocod) at various concentrations for 1 hour. Cells were washed and permeabilized using Triton X and blocked with 3% NGS. Cells were stained for rat monoclonal alpha tubulin antibody and anti-rat secondary antibody (red). Coverslips were mounted using VectaShield with DAPI and imaged by confocal microscopy.

MDM were grown on coverslips and treated with Nocodazole (Nocod) at various concentrations for 1 hour. Cells were washed, permeabilized using Triton X and blocked with 3% NGS. Cells were stained for rat monoclonal alpha tubulin antibody and anti-rat secondary antibody (red). Coverslips were mounted using VectaShield with DAPI and imaged by confocal microscopy.

Nocodazole (Nocod) at various concentrations for 1 hour. Cells were washed, permeabilized using Triton X and blocked with 3% NGS. Cells were stained for rat monoclonal alpha tubulin antibody and anti-rat secondary antibody (red). Coverslips were mounted using VectaShield with DAPI and imaged by confocal microscopy.

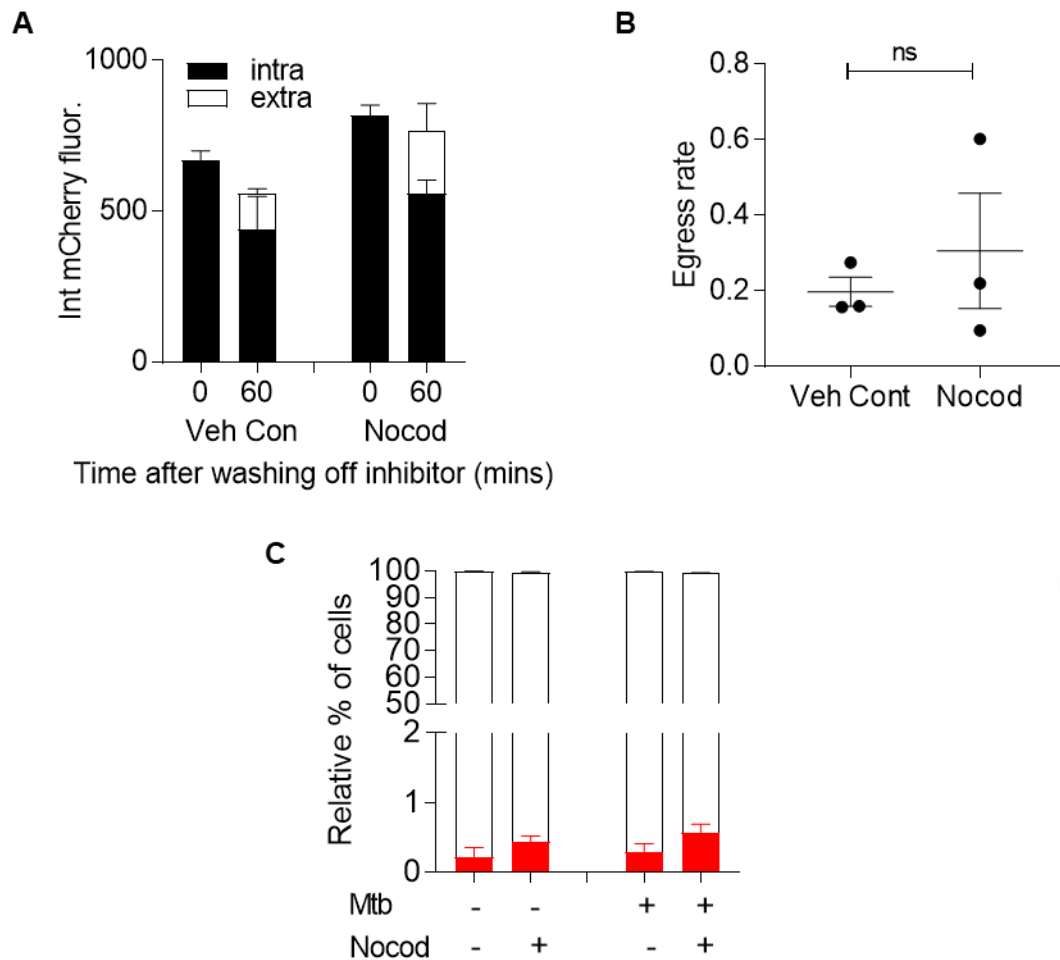


Figure 5.19 **Blocking non-lytic egress using Nocodazole.** **A** MDM were infected for four hours. Cells were washed and treated with 30 $\mu$ M Nocod or vehicle control (DMSO) for one hour. Cultures were washed again three times with PBS to remove all extracellular bacteria. Fresh media was added for one hour with or without the inhibitor. Extracellular bacteria in the supernatant were collected and intracellular bacteria were harvested by washing and lysing cells. Bacteria were fixed in 4% PFA and analysed by flow cytometry. **B** The rate of non-lytic egress in each condition was calculated. Mean  $\pm$  SEM 3 experiments. **C** MDM infected for four hours. Cells were washed and treated with 30 $\mu$ M Nocod or vehicle control (DMSO) for one hour. Live/ Dead stain was added for 20 mins. Cells were gently washed and fixed in 4% PFA. Cells were counterstained for DAPI + cell mask and counted using Hermes microscope. Data analysed by Metamorph software to enumerate the number of cells in each condition as a percentage of the number of cells in each well (dead/ dying cells= red, live cells =white).

Figure 5.20 **GM-CSF differentiated MDM display the same phenotype as M-CSF MDM** **A** GM-CSF MDM were infected with H37Rv mCherry for 4 hours at MOI 1. Cultures were washed three times with PBS to remove all extracellular bacteria. Fresh media was added for the times specified. At the relevant time point extracellular bacteria in the supernatant were collected. Intracellular bacteria were harvested by washing and lysing cells. Bacteria were fixed in 4% PFA and analysed by flow cytometry. Bacteria quantified by integrated mCherry fluorescence at each time point in each compartment. Mean  $\pm$  SEM 3 separate experiments **B** MDM were infected with H37Rv mCherry for 4 hours at MOI 1. Cultures were washed three times with PBS to remove all extracellular bacteria. Fresh media was added for 60min. Extracellular bacteria in the supernatant were collected and intracellular bacteria were harvested by washing and lysing cells. Bacteria were fixed in 4% PFA and analysed by flow cytometry. Mean  $\pm$  SEM 2 experiments. **C** MDM infected for four hours. Cells were washed and treated with 30 $\mu$ M Nocod

### 5.3.7 Non-Lytic Egress of Mtb occurs in alternatively differentiated MDMs

M-CSF and GM-CSF are two commonly used growth factors used in the differentiation of MDM in vitro. However, GM-CSF differentiated macrophages are thought more closely align with alveolar macrophages, I sought to show that the interaction between M-CSF MDM and Mtb (leading to accumulation of extracellular Mtb) was also true in an alternative model of macrophage differentiation.

I first confirmed that extracellular bacteria accumulate following 120 hours co-culture with MDM in GM-CSF differentiated macrophages, as they do with M-CSF MDM. I infected GM-CSF MDM for four hours, washed off any remaining extracellular bacteria, and measured the intracellular and extracellular bacillary loads at 24 and 120 hours (**Figure 5.8 GM-CSF differentiated MDM display the same phenotype as M-CSF MDM**) **A** GM-CSF MDM were infected with H37Rv mCherry for 4 hours at MOI 1. Cultures were washed three times with PBS to remove all extracellular bacteria. Fresh media was added for the times specified. At the relevant time point extracellular bacteria in the supernatant were collected. Intracellular bacteria were harvested by washing and lysing cells. Bacteria were fixed in 4% PFA and analysed by flow cytometry. Bacteria quantified by integrated mCherry fluorescence at each time point in each compartment. Mean  $\pm$  SEM 3 separate experiments **B** MDM were infected with H37Rv mCherry for 4 hours at MOI 1. Cultures were washed three times with PBS to remove all extracellular bacteria. Fresh media was added for 60min. Extracellular bacteria in the supernatant were collected and intracellular bacteria were harvested by washing and lysing cells. Bacteria were fixed in 4% PFA and analysed by flow cytometry.

Mean  $\pm$  SEM 2 experiments.

**Figure 5.9 Rate of non-lytic egress is not affected by IFN $\gamma$  priming of MDM.**

**A** MDM were primed (or not) with IFN $\gamma$  for 24 hours. MDM were then infected for four hours. Cultures were washed three times with PBS to remove all extracellular bacteria. Fresh media was added for 60min. Extracellular bacteria in the supernatant were collected and intracellular bacteria were harvested by washing and lysing cells. Bacteria were fixed in 4% PFA and analysed by flow cytometry. The rate of non-lytic egress in each condition was calculated. Mean  $\pm$  SEM 3 experiments. **B** MDM were primed (or not) with IFN $\gamma$  for 24 hours. MDM were then infected for four hours. Live/ Dead stain was added for 20 mins. Cells were gently washed and fixed in 4% PFA. Nuclei and cells were counterstained for DAPI and counted using Hermes microscope. Data analysed by Metamorph software to enumerate the number of cells in each condition as a percentage of the number of cells in each well (dead/ dying cells= red, live cells =white).Figure 5.8A). My initial observations (Chapter 3) demonstrating extracellular bacillary accumulation that exceeds the intracellular bacillary load could be repeated in this model of macrophage differentiation. Therefore, I next sought to test the hypothesis that non-lytic egress of Mtb also occurred in GM-CSF MDM, and was not just an artefact of M-CSF differentiated MDM.

To look for non-lytic egress I infected MDM for four hours to establish an intracellular infection, and washed off any remaining extracellular bacteria. I then quantified intracellular and extracellular bacteria after one hour. I found an increase in extracellular Mtb equivalent to the decrease in intracellular Mtb,

though these experiments were only carried out twice (**Figure 5.8 GM-CSF differentiated MDM display the same phenotype as M-CSF MDM** **A** GM-CSF MDM were infected with H37Rv mCherry for 4 hours at MOI 1. Cultures were washed three times with PBS to remove all extracellular bacteria. Fresh media was added for the times specified. At the relevant time point extracellular bacteria in the supernatant were collected. Intracellular bacteria were harvested by washing and lysing cells. Bacteria were fixed in 4% PFA and analysed by flow cytometry. Bacteria quantified by integrated mCherry fluorescence at each time point in each compartment. Mean  $\pm$  SEM 3 separate experiments **B** MDM were infected with H37Rv mCherry for 4 hours at MOI 1. Cultures were washed three times with PBS to remove all extracellular bacteria. Fresh media was added for 60min. Extracellular bacteria in the supernatant were collected and intracellular bacteria were harvested by washing and lysing cells. Bacteria were fixed in 4% PFA and analysed by flow cytometry. Mean  $\pm$  SEM 2 experiments.

**Figure 5.9 Rate of non-lytic egress is not affected by IFN $\gamma$  priming of MDM.**

**A** MDM were primed (or not) with IFN $\gamma$  for 24 hours. MDM were then infected for four hours. Cultures were washed three times with PBS to remove all extracellular bacteria. Fresh media was added for 60min. Extracellular bacteria in the supernatant were collected and intracellular bacteria were harvested by washing and lysing cells. Bacteria were fixed in 4% PFA and analysed by flow cytometry. The rate of non-lytic egress in each condition was calculated. Mean  $\pm$  SEM 3 experiments. **B** MDM were primed (or not) with IFN $\gamma$  for 24 hours. MDM were then infected for four hours. Live/ Dead stain was added for 20 mins. Cells were

gently washed and fixed in 4% PFA. Nuclei and cells were counterstained for DAPI and counted using Hermes microscope. Data analysed by Metamorph software to enumerate the number of cells in each condition as a percentage of the number of cells in each well (dead/ dying cells= red, live cells =white).Figure 5.8B).

I concluded that non-lytic egress was not limited to M-CSF derived MDM, but occurred in the GM-CSF model of macrophage differentiation as well.

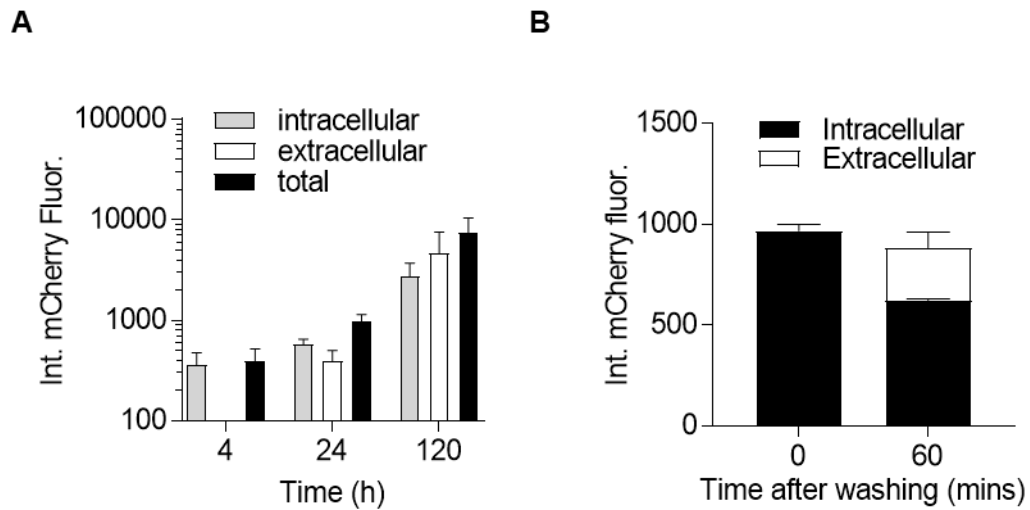


**Figure 5.22 GM-CSF differentiated MDM display the same phenotype as M-CSF MDM** **A** GM-CSF MDM were infected with H37Rv mCherry for 4 hours at MOI 1. Cultures were washed three times with PBS to remove all extracellular bacteria. Fresh media was added for the times specified. At the relevant time point extracellular bacteria in the supernatant were collected. Intracellular bacteria were harvested by washing and lysing cells. Bacteria were fixed in 4% PFA and analysed by flow cytometry. Bacteria quantified by integrated mCherry fluorescence at each time point in each compartment. Mean  $\pm$  SEM 3 separate experiments **B** MDM were infected with H37Rv mCherry for 4 hours at MOI 1. Cultures were washed three times with PBS to remove all extracellular bacteria. Fresh media was added for 60min. Extracellular bacteria in the supernatant were collected and intracellular bacteria were harvested by washing and lysing cells. Bacteria were fixed in 4% PFA and analysed by flow cytometry. Mean  $\pm$  SEM 2 experiments.

### 5.3.8 IFN $\gamma$ does not affect the rate of non-lytic egress

IFN $\gamma$  is crucial to mycobacterial control, and those with defective IFN $\gamma$  responses rapidly succumb to TB infection (Casanova and Abel, 2002). IFN $\gamma$  results in macrophage activation, the induction of autophagy pathways for killing (Gutierrez et al., 2004), and in concert with Vitamin D the production of antimicrobial peptides (Fabri et al., 2011; Rook et al., 1986).

If IFN $\gamma$  treatment of macrophages does create a more restrictive environment, then it might be beneficial for Mtb to escape into the extracellular environment to facilitate replication. I therefore hypothesized that the rate of Mtb non-lytic egress would increase following MDM activation by IFN $\gamma$ .

In order to address this hypothesis I primed MDM for 24 hours with IFN $\gamma$ , and subsequently infected the cells for 4 hours. I looked for the presence of extracellular bacteria one hour later. There was no difference in the rate of non-lytic egress of Mtb in IFN $\gamma$  treated versus untreated MDM, disproving my hypothesis (**Figure 5.9 Rate of non-lytic egress is not affected by IFN $\gamma$  priming of MDM. A** MDM were primed (or not) with IFN $\gamma$  for 24 hours. MDM were then infected for four hours. Cultures were washed three times with PBS to remove all extracellular bacteria. Fresh media was added for 60min. Extracellular bacteria in the supernatant were collected and intracellular bacteria were harvested by washing and lysing cells. Bacteria were fixed in 4% PFA and analysed by flow cytometry. The rate of non-lytic egress in each condition was calculated. Mean  $\pm$  SEM 3 experiments. **B** MDM were primed (or not) with IFN $\gamma$  for 24 hours. MDM were then infected for four hours. Live/ Dead stain was added for 20 mins. Cells were gently washed and fixed in 4% PFA. Nuclei and cells were

counterstained for DAPI and counted using Hermes microscope. Data analysed by Metamorph software to enumerate the number of cells in each condition as a percentage of the number of cells in each well (dead/ dying cells= red, live cells =white).

Figure 6.1 **A model of non-lytic egress contributing to disease pathogenesis.** Mtb escapes from growth permissive macrophages primarily to facilitate spread of bacteria without alerting the host to infection (unlike cellular necrosis that would initiate an inflammatory cascade). Mtb escapes from restrictive macrophages in order to access a growth permissive extracellular environment, and transmit infections to new hosts. (Figure 5.9A). IFN $\gamma$  treatment did not induce significantly more MDM death that might contribute to the accumulation of extracellular bacteria (**Figure 5.9 Rate of non-lytic egress is not affected by IFN $\gamma$  priming of MDM.** **A** MDM were primed (or not) with IFN $\gamma$  for 24 hours. MDM were then infected for four hours. Cultures were washed three times with PBS to remove all extracellular bacteria. Fresh media was added for 60min. Extracellular bacteria in the supernatant were collected and intracellular bacteria were harvested by washing and lysing cells. Bacteria were fixed in 4% PFA and analysed by flow cytometry. The rate of non-lytic egress in each condition was calculated. Mean  $\pm$  SEM 3 experiments. **B** MDM were primed (or not) with IFN $\gamma$  for 24 hours. MDM were then infected for four hours. Live/ Dead stain was added for 20 mins. Cells were gently washed and fixed in 4% PFA. Nuclei and cells were counterstained for DAPI and counted using Hermes microscope. Data analysed by Metamorph software to enumerate the number of cells in each condition as a percentage of the number of cells in each well (dead/

dying cells= red, live cells =white).

Figure 6.1 **A model of non-lytic egress contributing to disease pathogenesis.** Mtb escapes from growth permissive macrophages primarily to facilitate spread of bacteria without alerting the host to infection (unlike cellular necrosis that would initiate an inflammatory cascade). Mtb escapes from restrictive macrophages in order to access a growth permissive extracellular environment, and transmit infections to new hosts. Figure 5.9B).

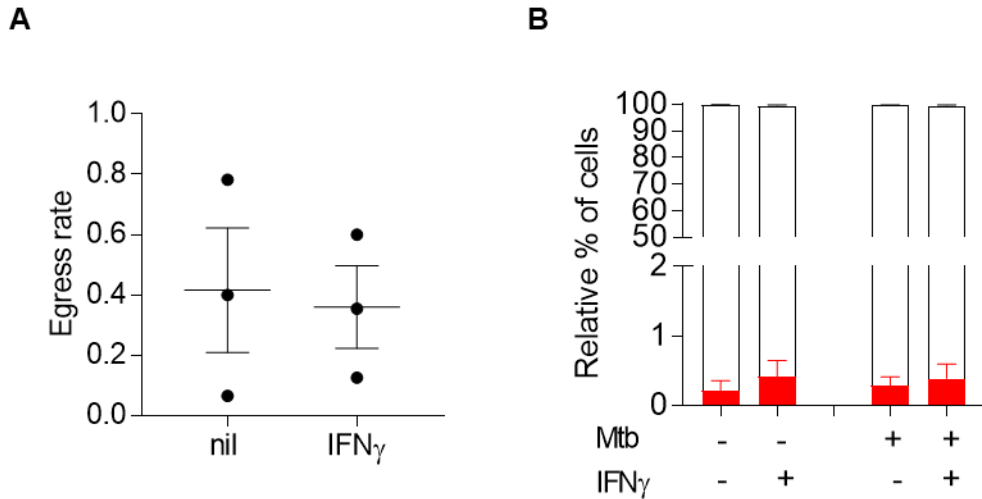


Figure 5.25 **Rate of non-lytic egress is not affected by IFN $\gamma$  priming of MDM.** **A** MDM were primed (or not) with IFN $\gamma$  for 24 hours. MDM were then infected for four hours. Cultures were washed three times with PBS to remove all extracellular bacteria. Fresh media was added for 60min. Extracellular bacteria in the supernatant were collected and intracellular bacteria were harvested by washing and lysing cells. Bacteria were fixed in 4% PFA and analysed by flow cytometry. The rate of non-lytic egress in each condition was calculated. Mean  $\pm$  SEM 3 experiments. **B** MDM were primed (or not) with IFN $\gamma$  for 24 hours. MDM were then infected for four hours. Live/ Dead stain was added for 20 mins. Cells were gently washed and fixed in 4% PFA. Nuclei and cells were counterstained for DAPI and counted using Hermes microscope. Data analysed by Metamorph software to enumerate the number of cells in each condition as a percentage of the number of cells in each well (dead/ dying cells= red, live cells =white).

## 5.4 Discussion

---

In this Chapter I have attempted to define some of the conditions under which non-lytic egress of Mtb occurs. My data suggest that non-lytic egress is associated with virulence since the attenuated BCG does not display the same behaviour. This may well implicate genes within the RD1 region directing non-lytic egress. Not all of the functions of genes in RD1 are known, but the ESX-1 secretion system, is crucial to phagosomal egress of Mtb (Simeone et al., 2012), and its effector protein ESAT-6 has been implicated in Mm escape from amoeba (Hagedorn et al., 2009). In amoeba, non-lytic egress is directly preceded by and dependent on phagosomal escape of mycobacteria into the cytoplasm. Interestingly, *M. avium*, which also lacks the RD1 locus, fails to leave phagosomes and does not egress from amoeba (Hagedorn et al., 2009). It is tempting to consider then whether ESAT-6/ ESX-1 driven phagosomal rupture may be a prerequisite for non-lytic egress of Mtb from human macrophages.

However, the data showing that non-lytic egress of Mtb is not dependent on bacterial viability, since HKMtb displays the same phenotype adds some complexity to the hypothesis presented above. Heat killing of Mtb at 80°C should denature Mtb proteins. It is possible that ESAT-6 or other proteins encoded by the RD1 locus are still viable candidates driving non-lytic egress because they are heat stable. Indeed, the mCherry fluorophore is not denatured by heat as the bacteria remain fluorescent. Not all of the proteins of Mtb have been identified (Cole et al., 1998; Mao et al., 2013), nor their thermostable properties known. An alternative explanation is that non-lytic egress is driven by lipid factors of Mtb, since lipids should remain intact after heat killing. This hypothesis would imply

that a lipid present in Mtb, but not BCG, is implicated in non-lytic egress. A recent comparative lipidomics analysis identified more than 1,000 molecular differences between Mtb and BCG including the previously unknown lipid produced in high abundance, 1-tuberculosinyladenosine (1-TbAd) (Layre et al., 2014). The function of this lipid is unclear, but the protein involved in its synthesis has been found to have a role in the blockade of phagolysosomal fusion (Layre et al., 2014; Pethe et al., 2004).

It would be interesting to use an ESAT-6 Mtb mutant (or BCG complemented with ESAT-6) to specifically address the question of whether non-lytic egress of Mtb is driven by this virulence factor as I hypothesize this to be the most likely protein candidate. Another experimental approach to investigate whether lipid factors are involved in non-lytic egress would be to see if BCG is able to egress in the presence of soluble Mtb lipids within the infecting media.

My data suggest that host factors are also involved in the non-lytic egress of Mtb, as this appears to be an active cellular process that can be blocked on ice (Chapter 4). However, I found that neither blockade of the actin cytoskeleton by cytochalasin D, nor the microtubule network by nocodazole was able to block Mtb egress. There are several reasons why this is possible.

When Hagedorn et al demonstrated Mm and Mtb egress from amoeba, they described an 'ejectosome' dense in F-actin (and myosin/ coronin) from which the bacteria protruded through the plasma membrane (Hagedorn et al., 2009). However, the propulsive mechanism by which they were ejected was not determined, and the bacteria were not accompanied by actin tails (Hagedorn et al., 2009). Further, Mm has been shown to move freely in the cytoplasm propelled

by actin tails but actin tails have never been associated with Mtb (Stamm et al., 2003). Further, although other organisms have been shown to hijack the actin machinery to protrude out of cells (Stevens et al., 2006), this may well not be the case for Mtb from human macrophages. Or, it is possible that chemical inhibition of the actin cytoskeleton by another drug might be more efficacious in blocking non-lytic egress- just as the non-lytic exit of rotavirus can be blocked with jasplakinolide (another inhibitor of the cytoskeleton), but not cytochalasin D or latrunculin (Trejo-Cerro et al., 2017). The authors propose this is because cytochalasin D as well as latrunculin A have been reported to disassemble actin stress fibers. Jasplakinolide disaggregates actin filaments, but it does not disassemble stress fibres (Rotsch and Radmacher, 2000) which could be necessary for rotavirus egress.

Blockade of  $\alpha$  tubulin microtubules also did not abrogate non-lytic egress. To the best of my knowledge the microtubule network has not been implicated in the non-lytic egress of other organisms, and therefore my data are not surprising. However, it is possible that nocodazole was not effective at blocking the MTs, as although I demonstrated disruption of the  $\alpha$ -tubulin fibres by confocal microscopy, activation of cells has been shown to increase acetylated  $\alpha$  -tubulin (Hanania et al., 2012), thereby stabilising the MT network (Piperno et al., 1987). To address this hypothesis I would have liked to look for the increased levels of acetylated  $\alpha$ -tubulin by immunofluorescence or immunoblotting.

Finally, we found that different models of macrophage differentiation (GM-CSF) and activation (IFN $\gamma$ ) did not alter the rate of non-lytic egress. With regards to the former, these data build confidence, since non-lytic egress does not simply seem

to be an artefact of our M-CSF model of macrophage differentiation. With regards to the latter, I was trying to test the hypothesis that IFN $\gamma$  treated macrophages would take on a more restrictive phenotype and therefore enhance non-lytic egress of Mtb. In fact, these experiments should ideally have been done in the presence of 25-hydroxyvitamin D3, because IFN $\gamma$  exerts antimicrobial effects via a Vitamin D dependent pathway (Fabri et al., 2011). It may also be the case that macrophage activation into a 'restrictive' phenotype requires the presence of other cytokines as well as cell- cell interactions (Petruccioli et al., 2012)

## **6 GENERAL DISCUSSION**

### **6.1 Overall Conclusion**

---

In this thesis, I have developed a novel quantitative high-throughput assay to measure the dynamics of Mtb intra- and extracellularly in human macrophage cultures, and combine these experimental measurements with mathematical modelling to estimate the fluxes between the two compartments. Unexpectedly, I have found that intra- and extra-cellular bacteria exist in a dynamic equilibrium, with rapid entry and egress of Mtb, and that egress from macrophages at a low multiplicity of infection likely occurs as a result of a non-lytic process.

### **6.2 Implications**

---

This is the first report of non-lytic egress of Mtb from human macrophages which may contribute to disease pathogenesis by allowing Mtb access to the extracellular space. The extracellular environment (1) provides an alternative niche for growth (2) allows spread of Mtb to neighbouring cells (3) facilitates transmission to new hosts. Importantly non-lytic egress does not cause cellular destruction and is therefore less likely to initiate an inflammatory cascade, which would otherwise lead to recruitment and priming of immune cells for the clearance of infection.

The development of host directed therapies is an emerging area of research to supplement antibacterial agents in the treatment of TB disease. Small molecules and biological agents that enhance macrophage antimicrobial activities, induce autophagy, and alleviate excessive inflammation have been shown to be promising candidates (Kolloli and Subbian, 2017). My data are important because

they suggest there is a rapid flux of Mtb between the intracellular and extracellular compartments, so the development of host directed strategies for immune control of Mtb infection, as well as antibacterial agents should target both compartments to achieve maximum protection. Furthermore, dissecting the molecular mechanism that underpins non-lytic egress will allow researchers to find potential new therapeutic targets to contain bacteria within macrophages, and potentially slow the spread of infection. If this were done in combination with host directed therapies to improve macrophage killing of Mtb, greater sterilization of infection might be achieved.

Finally, my data suggests that future *in vitro* models of Mtb infection that investigate host-pathogen interactions need to look at both the intracellular and extracellular bacterial load in order to make a faithful assessment of the total bacterial burden. This is true also for more recently developed bioengineered 3-dimensional models of Mtb granulomas (Tezera et al., 2017).

### **6.3 Limitations**

---

We use mathematical modelling to conceptualize the biological system that drives macrophage-Mtb interactions. Mathematical models are typically incomplete and tend to simplify some details of the system; nevertheless they are important tools that complement other tools used in biological investigations. Experiments provide parameter values, functions and interactions that are essential for constructing the model. A model, in turn, can suggest new experiments or help explain unexpected results. Reciprocal illumination between the two disciplines has allowed us to advance our understanding more quickly and would have been possible with experimentation alone. That said, our model

has significant limitations because one particular assumption that we make is unlikely to be correct, namely, that all bacteria infecting macrophages are distributed equally. More likely, some macrophages take up more bacteria than others. This is likely to also affect the death rate, because heavily infected macrophages are more likely to die by necrosis and release bacteria into the extracellular space. It is feasible that the observed extracellular bacillary burden in my experimental data could be explained by Mtb heavily infecting some macrophages, triggering cellular necrosis and further replication of bacteria which are then released and grow extracellularly. I do not think this is likely, since the overall degree of necrotic cell death in my system is low; between 24 and 120 hours where I saw the greatest accumulation of extracellular bacteria, there is almost no attrition in cell number at all. However, we need to test this hypothesis by additional parameterization, and whether this would impact the outcome of the model remains to be determined.

Questions also still remain as to whether the observed extracellular bacterial accumulation is due to dissociation of adherent bacteria. I have presented evidence that strongly suggests this is not the case, but the optimal experimental approach would be to find an antibody to Mtb with high specificity that does not stain any bacteria on the surface of cells once the macrophages have been washed.

The other major limitation of this thesis is that we were unable to demonstrate the non-lytic egress definitely by time lapse imaging. Since heat killed Mtb also displays this behaviour, I think the best experimental approach moving forward would be to try and visualize egress in a biosafety level 2 environment with less

restrictions. Frames need to be taken as close together as possible to actually see Mtb exiting the cell.

#### **6.4 A Model of Non Lytic Egress in Disease Pathogenesis**

---

As has been previously discussed, macrophages are extremely plastic cells and their function is influenced by their microenvironment as well as cellular ontogeny. In the context of TB infection, evidence from macaque and human confirms the presence of both anti- and pro- inflammatory macrophage phenotypes in granuloma (Mattila et al., 2013). Consistent with these observations, data from the literature, and the data presented within this thesis, I propose a model where non-lytic egress occurs from different phenotypes of macrophages, is beneficial for Mtb and makes a significant contribution to disease pathogenesis.

In growth permissive macrophages, I hypothesize that Mtb is able to persist and replicate by subverting the innate antimicrobial defences of the cell. Exit from these cells may not be beneficial to Mtb in terms of fostering faster growth, but becoming extracellular may facilitate the spread of infection to neighbouring cells. Early in infection, at low multiplicity of infection, I propose that Mtb escapes preferentially by non-lytic egress, without triggering widespread inflammation associated with cell lysis that may alert the host to the presence of the organism.

More restrictive macrophages also exist, particularly when they are in an activated state from the presence of cytokines such as IFN $\gamma$  and TNF $\alpha$ , and following the interaction with several other cell types. Since different clinical strains differ in their virulence, macrophages may also become more restrictive upon infection with a less virulent strain. These macrophages, with a more pro-inflammatory phenotype, have been shown to be located in the centre of the

necrotic granuloma (Mattila et al., 2013). Here, I hypothesize that non-lytic egress serves as a mechanism by which Mtb is able to escape intracellular restriction, along with cellular necrosis, in order to gain access to the caseum, a growth permissive extracellular environment. Moreover, it is from this environment from which many extracellular bacilli are expectorated in order to transmit infections to new hosts (Eum et al., 2010), the ultimate goal of any infectious pathogen.

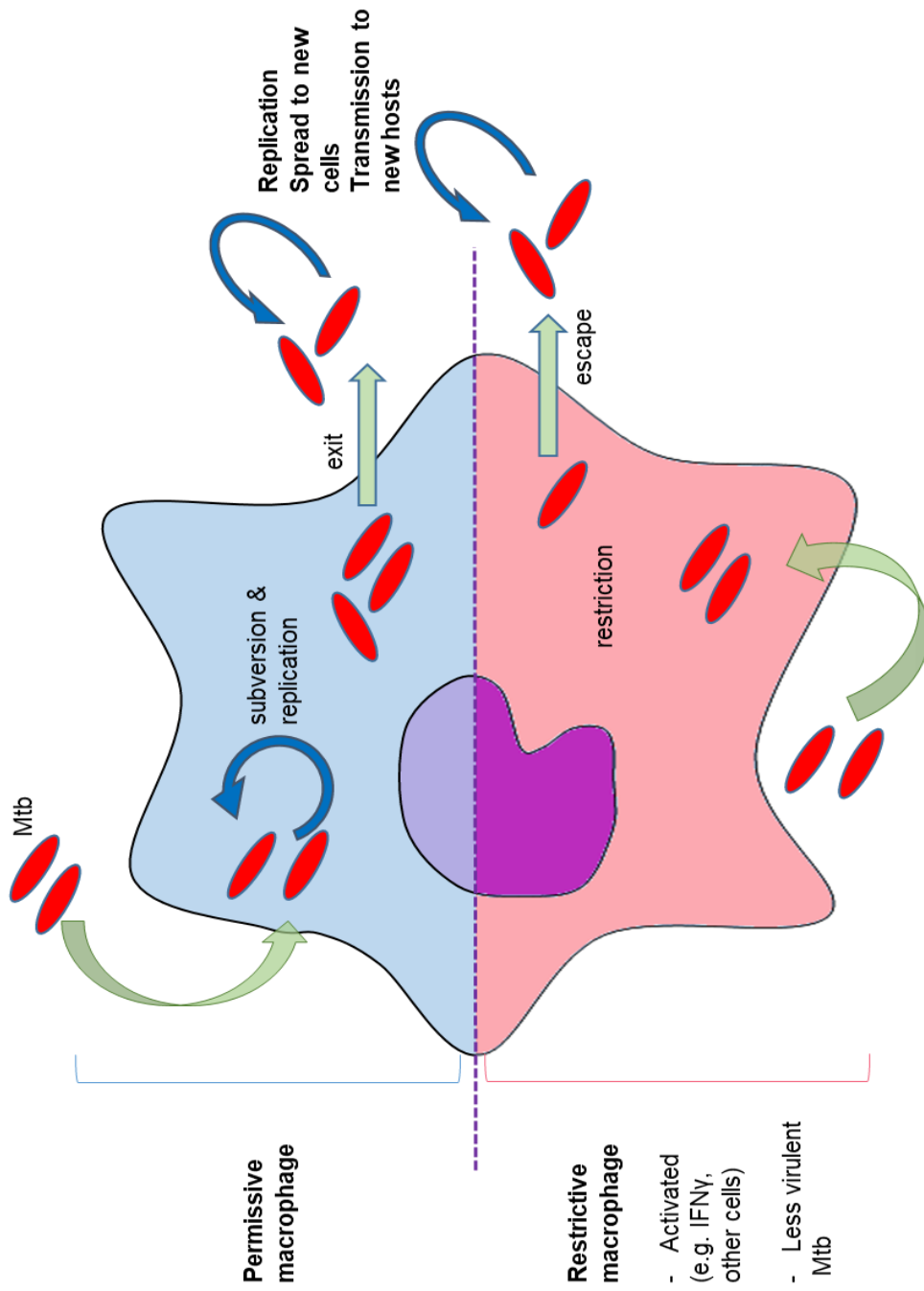


Figure 6.1 **A model of non-lytic egress contributing to disease pathogenesis.** Mtb escapes from growth permissive macrophages primarily to facilitate spread of bacteria without alerting the host to infection (unlike cellular necrosis that would initiate an inflammatory cascade). Mtb escapes from restrictive macrophages in order to access a growth permissive extracellular environment, and transmit infections to new hosts.

Figure 6.2 **Figure 6.3 A model of non-lytic egress contributing to disease pathogenesis.** Mtb escapes from growth permissive macrophages primarily to facilitate spread of bacteria without alerting the host to infection (unlike cellular necrosis that would initiate an inflammatory cascade). Mtb escapes from restrictive macrophages in order to access a growth permissive extracellular environment, and transmit infections to new hosts.

## 7 FUTURE WORK

The research priorities to take this work further need to focus on addressing some of the overall limitations of this thesis presented in Chapter 5. I have already presented some experimental methods that may address the questions raised, and provide more conclusive evidence for the presence of non-lytic egress of Mtb from human macrophages.

The data presented within this thesis also pave the way for investigating the molecular mechanism of non-lytic egress. My data suggest that this process is largely governed by the host cell rather than bacterial factors, since egress can be abrogated on ice, but still occurs with heat killed bacteria. In order to prove this hypothesis, a research priority is to achieve effective blockade of the two major networks that govern movement of organelles within the cell- the actin cytoskeleton and microtubules. One strategy is to use alternative chemical inhibitors. For example, jasplakinolide (an actin inhibitor) is effective at blocking the exit of rotavirus from macrophages when cytochalasin D failed to do so (Trejo-Cerro et al., 2017). To extend the observation that egress can be blocked on ice and is therefore likely to be an active process, it would be interesting to see if we are able to trigger non-lytic egress after the cells have warmed up to physiological temperatures again.

Given the short time frame over which non-lytic occurs (I see extracellular bacteria appearing within 30-60minutes after an intracellular infection is established), one possible pathway for exit of Mtb is via recycling endosomes. The endosomal recycling system represents a dynamic conduit for sorting and re-exporting internalized elements mainly of the plasma membrane. The early

endosome is characterized by the presence of EEA and Rab5 (Granger et al., 2014). From here cargo is sorted. Recycling back to the plasma membrane occurs via the 'fast' pathway (1-2 mins) or the 'slow' pathway (10-12 minutes) (Hao and Maxfield, 2000). Recycling endosomes of the latter acquire Rab11 (Granger et al., 2014). Since Mtb is known to be delivered to the early endosome (Clemens and Horwitz, 1996), it is plausible that it may exit via slow recycling endosomes. This hypothesis could be investigated experimentally, looking for co-localization of Rab11 with mCherry Mtb by immunofluorescence. Visualizing Mtb within Rab11+ endosomes by electron microscopy would be an alternative experimental strategy.

As discussed in Chapter 4, bacterial factors (not affected by heat killing) may still be involved in orchestrating non-lytic egress. A variety of different mycobacterial mutants can be used to investigate this hypothesis. Ideally these would need to be transfected with a fluorophore in order to utilize the high throughput assay described in Chapter 3 that I developed to investigate macrophage-Mtb interactions.

To investigate whether non-lytic egress may be an inherent feature of macrophage biology, I would like to determine if fluorescent beads also display this behaviour. If the beads were to egress, the data would suggest that macrophages have the ability rapidly expel any organism or particulate matter they ingest. Indeed, the fact that *C. neoformans* and other organisms also egress from macrophages suggests it may well be an evolutionarily conserved mechanism. However, if fluorescent beads do not egress from macrophages, this would suggest that the behaviour is specific to a select few organisms and

perhaps confers a survival advantage. Understanding the mechanism of non-lytic egress could lead to significant insights into TB disease pathogenesis.

Several layers of complexity could be added to the *in vitro* model presented in this thesis. Importantly, my data do not account for the important interaction of macrophages and T cells during Mtb infection. In order to incorporate this process, autologous T cells could be isolated using magnetic bead separation techniques and added to infected MDM. It would then be possible to use the same experimental methods to measure cellular death rates, non-lytic egress and even the rate of extracellular growth. This type of co-culture model may provide a more faithful representation of a TB granuloma.

In order to address the question of how macrophage heterogeneity might influence the non-lytic egress of Mtb, MDM in my *in vitro* model should be differentiated under different experimental conditions and then assessed for non-lytic egress. The experimental conditions I consider relevant are macrophages skewed to a highly pro-inflammatory phenotype by the stimulation of LPS, a restrictive phenotype (potentially achieved following stimulation by IFN $\gamma$  in the presence of Vitamin D and GM-CSF), a highly anti-inflammatory phenotype by the addition of IL-10/IL-4, and a more biologically relevant model where monocytes are differentiated in condition media from macrophages (with or without T cells) infected with Mtb. These investigations would help address the hypotheses presented in my proposed model of non-lytic egress from macrophages (**section 6.4**), and provide insight on the role of this process in contributing to disease pathogenesis.

## 8 REFERENCES

- Aguilo, J.I., Alonso, H., Uranga, S., Marinova, D., Arbués, A., de Martino, A., Anel, A., Monzon, M., Badiola, J., Pardo, J., Brosch, R., Martin, C., 2013. ESX-1-induced apoptosis is involved in cell-to-cell spread of *Mycobacterium tuberculosis*. *Cell. Microbiol.* 15, 1994–2005.
- Akira, S., Uematsu, S., Takeuchi, O., 2006. Pathogen recognition and innate immunity. *Cell* 124, 783–801.
- Alonso, S., Pethe, K., Russell, D.G., Purdy, G.E., 2007. Lysosomal killing of *Mycobacterium* mediated by ubiquitin-derived peptides is enhanced by autophagy. *Proc. Natl. Acad. Sci.* 104, 6031–6036
- Alvarez-Jiménez, V.D., Leyva-Paredes, K., García-Martínez, M., Vázquez-Flores, L., García-Paredes, V.G., Campillo-Navarro, M., Romo-Cruz, I., Rosales-García, V.H., Castañeda-Casimiro, J., González-Pozos, S., Hernández, J.M., Wong-Baeza, C., García-Pérez, B.E., Ortiz-Navarrete, V., Estrada-Parra, S., Serafín-López, J., Wong-Baeza, I., Chacón-Salinas, R., Estrada-García, I., 2018. Extracellular Vesicles Released from *Mycobacterium tuberculosis*-Infected Neutrophils Promote Macrophage Autophagy and Decrease Intracellular Mycobacterial Survival. *Front. Immunol.* 9, 272.
- Alvarez, M., Casadevall, A., 2006. Phagosome extrusion and host-cell survival after *Cryptococcus neoformans* phagocytosis by macrophages. *Curr. Biol.* CB 16, 2161–2165.
- Arango Duque, G., Descoteaux, A., 2014. Macrophage Cytokines: Involvement in Immunity and Infectious Diseases. *Front. Immunol.* 5.
- Armstrong, J.A., Hart, P.D., 1975. Phagosome-lysosome interactions in cultured macrophages infected with virulent tubercle bacilli. Reversal of the usual nonfusion pattern and observations on bacterial survival. *J. Exp. Med.* 142, 1–16.
- Bach, H., Papavinasasundaram, K.G., Wong, D., Hmama, Z., Av-Gay, Y., 2008. *Mycobacterium tuberculosis* virulence is mediated by PtpA dephosphorylation of human vacuolar protein sorting 33B. *Cell Host Microbe* 3, 316–322.
- Bals, R., Wang, X., Zasloff, M., Wilson, J.M., 1998. The peptide antibiotic LL-37/hCAP-18 is expressed in epithelia of the human lung where it has broad antimicrobial activity at the airway surface. *Proc. Natl. Acad. Sci. U. S. A.* 95, 9541–9546.
- Banchereau, J., Steinman, R.M., 1998. Dendritic cells and the control of immunity. *Nature* 392, 245–252.

- Barber, G.N., 2001. Host defense, viruses and apoptosis. *Cell Death Differ.* 8, 113–126.
- Behar, S.M., Divangahi, M., Remold, H.G., 2010. Evasion of innate immunity by *Mycobacterium tuberculosis*: is death an exit strategy? *Nat. Rev. Microbiol.*
- Behar, S.M., Martin, C.J., Booty, M.G., Nishimura, T., Zhao, X., Gan, H.-X., Divangahi, M., Remold, H.G., 2011. Apoptosis is an innate defense function of macrophages against *Mycobacterium tuberculosis*. *Mucosal Immunol.* 4, 279–287.
- Behr, M.A., Edelstein, P.H., Ramakrishnan, L., 2019. Is *Mycobacterium tuberculosis* infection life long? *BMJ* I5770.
- Behr, M.A., Edelstein, P.H., Ramakrishnan, L., 2018. Revisiting the timetable of tuberculosis. *BMJ* 362, k2738.
- Bergsbaken, T., Fink, S.L., Cookson, B.T., 2009. Pyroptosis: host cell death and inflammation. *Nat. Rev. Microbiol.* 7, 99–109.
- Bermudez, L.E., Goodman, J., 1996. *Mycobacterium tuberculosis* invades and replicates within type II alveolar cells. *Infect. Immun.* 64, 1400–1406.
- Biragyn, A., Ruffini, P.A., Leifer, C.A., Klyushnenkova, E., Shakhov, A., Chertov, O., Shirakawa, A.K., Farber, J.M., Segal, D.M., Oppenheim, J.J., Kwak, L.W., 2002. Toll-like receptor 4-dependent activation of dendritic cells by beta-defensin 2. *Science* 298, 1025–1029.
- Blischak, J.D., Tailleux, L., Mitrano, A., Barreiro, L.B., Gilad, Y., 2015. Mycobacterial infection induces a specific human innate immune response. *Sci. Rep.* 5.
- Bojarczuk, A., Miller, K.A., Hotham, R., Lewis, A., Ogryzko, N.V., Kamuyango, A.A., Frost, H., Gibson, R.H., Stillman, E., May, R.C., Renshaw, S.A., Johnston, S.A., 2016. *Cryptococcus neoformans* Intracellular Proliferation and Capsule Size Determines Early Macrophage Control of Infection. *Sci. Rep.* 6, 21489.
- Bonilla, D.L., Bhattacharya, A., Sha, Y., Xu, Y., Xiang, Q., Kan, A., Jagannath, C., Komatsu, M., Eissa, N.T., 2013. Autophagy regulates phagocytosis by modulating the expression of scavenger receptors. *Immunity* 39, 537–547.
- Boxx, G.M., Cheng, G., 2016. The Roles of Type I Interferon in Bacterial Infection. *Cell Host Microbe* 19, 760–769.
- Brennan, P., 2003. Structure, function, and biogenesis of the cell wall of *Mycobacterium tuberculosis*. *Tuberculosis* 83, 91–97.

Brodland, G.W., 2015. How computational models can help unlock biological systems. *Semin. Cell Dev. Biol.*, Coding and non-coding RNAs & Mammalian development 47-48, 62–73.

Brosch, R., Gordon, S.V., Marmiesse, M., Brodin, P., Buchrieser, C., Eiglmeier, K., Garnier, T., Gutierrez, C., Hewinson, G., Kremer, K., Parsons, L.M., Pym, A.S., Samper, S., van Soolingen, D., Cole, S.T., 2002. A new evolutionary scenario for the *Mycobacterium tuberculosis* complex. *Proc. Natl. Acad. Sci. U. S. A.* 99, 3684–3689.

Butler, R.E., Brodin, P., Jang, J., Jang, M.-S., Robertson, B.D., Gicquel, B., Stewart, G.R., 2012. The balance of apoptotic and necrotic cell death in *Mycobacterium tuberculosis* infected macrophages is not dependent on bacterial virulence. *PLoS One* 7, e47573.

Byrd, T.F., Green, G.M., Fowlston, S.E., Lyons, C.R., 1998. Differential growth characteristics and streptomycin susceptibility of virulent and avirulent *Mycobacterium tuberculosis* strains in a novel fibroblast-mycobacterium microcolony assay. *Infect. Immun.* 66, 5132–5139.

Cadena, A.M., Flynn, J.L., Fortune, S.M., 2016. The Importance of First Impressions: Early Events in *Mycobacterium tuberculosis* Infection Influence Outcome. *mBio* 7, e00342–16.

Cadena, A.M., Fortune, S.M., Flynn, J.L., 2017. Heterogeneity in tuberculosis. *Nat. Rev. Immunol.* 17, 691–702.

Cambier, C.J., O’Leary, S.M., O’Sullivan, M.P., Keane, J., Ramakrishnan, L., 2017. Phenolic Glycolipid Facilitates Mycobacterial Escape from Microbicidal Tissue-Resident Macrophages. *Immunity* 47, 552–565.e4.

Cambier, C.J., Takaki, K.K., Larson, R.P., Hernandez, R.E., Tobin, D.M., Urdahl, K.B., Cosma, C.L., Ramakrishnan, L., 2014. Mycobacteria manipulate macrophage recruitment through coordinated use of membrane lipids. *Nature* 505, 218–222.

Canetti, 1955. *The tubercle bacillus in the pulmonary lesion of man; histobacteriology and its bearing on the therapy of pulmonary tuberculosis.* Springer, New York.

Capuano, S.V., Croix, D.A., Pawar, S., Zinovik, A., Myers, A., Lin, P.L., Bissel, S., Fuhrman, C., Klein, E., Flynn, J.L., 2003. Experimental *Mycobacterium tuberculosis* Infection of *Cynomolgus* Macaques Closely Resembles the Various Manifestations of Human *M. tuberculosis* Infection. *Infect. Immun.* 71, 5831–5844.

Cardenal-Muñoz, E., Arafah, S., López-Jiménez, A.T., Kicka, S., Falaise, A., Bach, F., Schaad, O., King, J.S., Hagedorn, M., Soldati, T., 2017. *Mycobacterium marinum* antagonistically induces an autophagic response while repressing the autophagic flux in a TORC1- and ESX-1-dependent manner. *PLoS Pathog.* 13, e1006344.

Cardona, P., Cardona, P.-J., 2019. Regulatory T Cells in *Mycobacterium tuberculosis* Infection. *Front. Immunol.* 10.

Caron, E., Hall, A., 1998. Identification of two distinct mechanisms of phagocytosis controlled by different Rho GTPases. *Science* 282, 1717–1721.

Carroll, P., Schreuder, L.J., Muwanguzi-Karugaba, J., Wiles, S., Robertson, B.D., Ripoll, J., Ward, T.H., Bancroft, G.J., Schaible, U.E., Parish, T., 2010. Sensitive Detection of Gene Expression in *Mycobacteria* under Replicating and Non-Replicating Conditions Using Optimized Far-Red Reporters. *PLOS ONE* 5, e9823.

Caruso, A.M., Serbina, N., Klein, E., Triebold, K., Bloom, B.R., Flynn, J.L., 1999. Mice deficient in CD4 T cells have only transiently diminished levels of IFN- $\gamma$ , yet succumb to tuberculosis. *J. Immunol. Baltim. Md 1950* 162, 5407–5416.

Casanova, J.-L., Abel, L., 2002. Genetic dissection of immunity to mycobacteria: the human model. *Annu. Rev. Immunol.* 20, 581–620.

Castillo E, Dekonenko A, Arko-Mensah J, Mandell M, Dupont N, Jiang S, Delgado-Vargas M, Timmins G, Bhattacharya D, Yang H, Hutt J, Lyons C, Dobos M, and Deretic V. Autophagy protects against active tuberculosis by suppressing bacterial burden and inflammation. *Proc Natl Acad Sci U S A.* 2012 Nov 13; 109(46): E3168–E3176.

Chen, C.Y., Huang, D., Wang, R.C., Shen, L., Zeng, G., Yao, S., Shen, Y., Halliday, L., Fortman, J., McAllister, M., Estep, J., Hunt, R., Vasconcelos, D., Du, G., Porcelli, S.A., Larsen, M.H., Jacobs, W.R., Haynes, B.F., Letvin, N.L., Chen, Z.W., 2009. A critical role for CD8 T cells in a nonhuman primate model of tuberculosis. *PLoS Pathog.* 5, e1000392.

Chen, M., Divangahi, M., Gan, H., Shin, D.S.J., Hong, S., Lee, D.M., Serhan, C.N., Behar, S.M., Remold, H.G., 2008. Lipid mediators in innate immunity against tuberculosis: opposing roles of PGE2 and LXA4 in the induction of macrophage death. *J. Exp. Med.* 205, 2791–2801.

Chen, M., Gan, H., Remold, H.G., 2006. A Mechanism of Virulence: Virulent *Mycobacterium tuberculosis* Strain H37Rv, but Not Attenuated H37Ra, Causes Significant Mitochondrial Inner Membrane Disruption in Macrophages Leading to Necrosis. *J. Immunol.* 176, 3707–3716.

Clay, H., Davis, J.M., Beery, D., Huttenlocher, A., Lyons, S.E., Ramakrishnan, L., 2007. Dichotomous Role of the Macrophage in Early *Mycobacterium marinum* Infection of the Zebrafish. *Cell Host Microbe* 2, 29–39.

Clay, H., Volkman, H.E., Ramakrishnan, L., 2008. TNF signaling mediates resistance to mycobacteria by inhibiting bacterial growth and macrophage death but not tuberculous granuloma formation. *Immunity* 29, 283–294.

Clemens, D.L., Horwitz, M.A., 1996. The *Mycobacterium tuberculosis* phagosome interacts with early endosomes and is accessible to exogenously administered transferrin. *J. Exp. Med.* 184, 1349–1355.

Clem, R.J., Miller, L.K., 1993. Apoptosis reduces both the in vitro replication and the in vivo infectivity of a baculovirus. *J. Virol.* 67, 3730–3738.

Cohen, S.B., Gern, B.H., Delahaye, J.L., Adams, K.N., Plumlee, C.R., Winkler, J.K., Sherman, D.R., Gerner, M.Y., Urdahl, K.B., 2018. Alveolar Macrophages Provide an Early *Mycobacterium tuberculosis* Niche and Initiate Dissemination. *Cell Host Microbe* 24, 439–446.e4.

Cole, S.T., Brosch, R., Parkhill, J., Garnier, T., Churcher, C., Harris, D., Gordon, S.V., Eiglmeier, K., Gas, S., Barry Iii, C.E., Tekaiia, F., Badcock, K., Basham, D., Brown, D., Chillingworth, T., Connor, R., Davies, R., Devlin, K., Feltwell, T., Gentles, S., Hamlin, N., Holroyd, S., Hornsby, T., Jagels, K., Krogh, A., McLean, J., Moule, S., Murphy, L., Oliver, K., Osborne, J., Quail, M.A., Rajandream, M.-A., Rogers, J., Rutter, S., Seeger, K., Skelton, J., Squares, R., Squares, S., Sulston, J.E., Taylor, K., Whitehead, S., Barrell, B.G., 1998. Deciphering the biology of *Mycobacterium tuberculosis* from the complete genome sequence. *Nature* 393, 537–544.

Collins, A.C., Cai, H., Li, T., Franco, L.H., Li, X.-D., Nair, V.R., Scharn, C.R., Stamm, C.E., Levine, B., Chen, Z.J., Shiloh, M.U., 2015. Cyclic GMP-AMP Synthase Is an Innate Immune DNA Sensor for *Mycobacterium tuberculosis*. *Cell Host Microbe* 17, 820–828.

Cooper, A.M., 2009. Cell-mediated immune responses in tuberculosis. *Annu. Rev. Immunol.* 27, 393–422.

Cooper, A.M., Dalton, D.K., Stewart, T.A., Griffin, J.P., Russell, D.G., Orme, I.M., 1993. Disseminated tuberculosis in interferon gamma gene-disrupted mice. *J. Exp. Med.* 178, 2243–2247.

- Cooper, A.M., Magram, J., Ferrante, J., Orme, I.M., 1997. Interleukin 12 (IL-12) Is Crucial to the Development of Protective Immunity in Mice Intravenously Infected with *Mycobacterium tuberculosis*. *J. Exp. Med.* 186, 39–45.
- Cronan, M.R., Beerman, R.W., Rosenberg, A.F., Saelens, J.W., Johnson, M.G., Oehlers, S.H., Sisk, D.M., Jurcic Smith, K.L., Medvitz, N.A., Miller, S.E., Trinh, L.A., Fraser, S.E., Madden, J.F., Turner, J., Stout, J.E., Lee, S., Tobin, D.M., 2016. Macrophage Epithelial Reprogramming Underlies *Mycobacterial* Granuloma Formation and Promotes Infection. *Immunity* 45, 861–876.
- Crowle, A.J., Ross, E.J., 1989. Inhibition by retinoic acid of multiplication of virulent tubercle bacilli in cultured human macrophages. *Infect. Immun.* 57, 840–844.
- Dannenberg, A., Lurie, M., 2006. Pathogenesis of Human Pulmonary Tuberculosis: Insights from the Rabbit Model. ASM press.
- Davies, L.C., Jenkins, S.J., Allen, J.E., Taylor, P.R., 2013. Tissue-resident macrophages. *Nat. Immunol.* 14, 986–995.
- Davis, J.M., Ramakrishnan, L., 2009. The role of the granuloma in expansion and dissemination of early tuberculous infection. *Cell* 136, 37–49.
- Davis, M.M., Boniface, J.J., Reich, Z., Lyons, D., Hampl, J., Arden, B., Chien, Y., 1998. LIGAND RECOGNITION BY  $\alpha\beta$  T CELL RECEPTORS. *Annu. Rev. Immunol.* 16, 523–544. <https://doi.org/10.1146/annurev.immunol.16.1.523>
- Dengjel, J., Schoor, O., Fischer, R., Reich, M., Kraus, M., Müller, M., Kreyborg, K., Altenberend, F., Brandenburg, J., Kalbacher, H., Brock, R., Driessen, C., Rammensee, H.-G., Stevanovic, S., 2005. Autophagy promotes MHC class II presentation of peptides from intracellular source proteins. *Proc. Natl. Acad. Sci. U. S. A.* 102, 7922–7927.
- Denis, M., 1991. Interferon-gamma-treated murine macrophages inhibit growth of tubercle bacilli via the generation of reactive nitrogen intermediates. *Cell. Immunol.* 132, 150–157.
- Desvignes, L., Ernst, J.D., 2009. IFN $\gamma$ -responsive nonhematopoietic cells regulate the immune response to *Mycobacterium tuberculosis*. *Immunity* 31, 974–985.
- Diedrich, C.R., O’Hern, J., Wilkinson, R.J., 2016. HIV-1 and the *Mycobacterium tuberculosis* granuloma: A systematic review and meta-analysis. *Tuberculosis* 98, 62–76.

Divangahi, M., Chen, M., Gan, H., Desjardins, D., Hickman, T.T., Lee, D.M., Fortune, S., Behar, S.M., Remold, H.G., 2009. Mycobacterium tuberculosis evades macrophage defenses by inhibiting plasma membrane repair. *Nat. Immunol.* 10, 899–906.

Doig, C., 2002. The efficacy of the heat killing of Mycobacterium tuberculosis. *J. Clin. Pathol.* 55, 778–779.

Dong, C., Davis, R.J., Flavell, R.A., 2002. MAP K INASES IN THE I MMUNE R ESPONSE. *Annu. Rev. Immunol.* 20, 55–72.

Dorman, S.E., Picard, C., Lammas, D., Heyne, K., van Dissel, J.T., Baretto, R., Rosenzweig, S.D., Newport, M., Levin, M., Roesler, J., Kumararatne, D., Casanova, J.-L., Holland, S.M., 2004. Clinical features of dominant and recessive interferon gamma receptor 1 deficiencies. *Lancet Lond. Engl.* 364, 2113–2121.

Douvas, G.S., Looker, D.L., Vatter, A.E., Crowle, A.J., 1985. Gamma interferon activates human macrophages to become tumoricidal and leishmanicidal but enhances replication of macrophage-associated mycobacteria. *Infect. Immun.* 50, 1–8.

Downing, J.F., Pasula, R., Wright, J.R., Twigg, H.L., Martin, W.J., 1995. Surfactant protein a promotes attachment of Mycobacterium tuberculosis to alveolar macrophages during infection with human immunodeficiency virus. *Proc. Natl. Acad. Sci.* 92, 4848–4852

Doz, E., Rose, S., Court, N., Front, S., Vasseur, V., Charron, S., Gilleron, M., Puzo, G., Fremaux, I., Delneste, Y., Erard, F., Ryffel, B., Martin, O.R., Quesniaux, V.F.J., 2009. Mycobacterial Phosphatidylinositol Mannosides Negatively Regulate Host Toll-like Receptor 4, MyD88-dependent Proinflammatory Cytokines, and TRIF-dependent Co-stimulatory Molecule Expression. *J. Biol. Chem.* 284, 23187–23196.

Dubnau, E., Chan, J., Raynaud, C., Mohan, V.P., Lanéelle, M.A., Yu, K., Quémar, A., Smith, I., Daffé, M., 2000. Oxygenated mycolic acids are necessary for virulence of Mycobacterium tuberculosis in mice. *Mol. Microbiol.* 36, 630–637.

Elkington, P.T., 2013. Tuberculosis: Time For A New Perspective? *J. Infect.* 66, 299–302.

Ernst, J.D., 2012. The immunological life cycle of tuberculosis. *Nat. Rev. Immunol.* 12, 581–591.

Ernst, J.D., 1998. Macrophage receptors for Mycobacterium tuberculosis. *Infect. Immun.* 66, 1277–1281.

Eum, S.-Y., Kong, J.-H., Hong, M.-S., Lee, Y.-J., Kim, J.-H., Hwang, S.-H., Cho, S.-N., Via, L.E., Barry, C.E., 2010. Neutrophils are the predominant infected phagocytic cells in the airways of patients with active pulmonary TB. *Chest* 137, 122–128.

Fabri, M., Stenger, S., Shin, D.-M., Yuk, J.-M., Liu, P.T., Realegeno, S., Lee, H.-M., Krutzik, S.R., Schenk, M., Sieling, P.A., Teles, R., Montoya, D., Iyer, S.S., Bruns, H., Lewinsohn, D.M., Hollis, B.W., Hewison, M., Adams, J.S., Steinmeyer, A., Zügel, U., Cheng, G., Jo, E.-K., Bloom, B.R., Modlin, R.L., 2011. Vitamin D is required for IFN-gamma-mediated antimicrobial activity of human macrophages. *Sci. Transl. Med.* 3, 104ra102.

Fang, F.C., 2004. Antimicrobial reactive oxygen and nitrogen species: concepts and controversies. *Nat. Rev. Microbiol.* 2, 820–832.

Fiorentino, D.F., Zlotnik, A., Mosmann, T.R., Howard, M., O'Garra, A., 1991. IL-10 inhibits cytokine production by activated macrophages. *J. Immunol. Baltim. Md* 1950 147, 3815–3822.

Fischer, H.P., 2008. Mathematical modeling of complex biological systems: from parts lists to understanding systems behavior. *Alcohol Res. Health J. Natl. Inst. Alcohol Abuse Alcohol.* 31, 49–59.

Flynn, J.L., 1993. An essential role for interferon gamma in resistance to *Mycobacterium tuberculosis* infection. *J. Exp. Med.* 178, 2249–2254.

Flynn, J.L., Chan, J., Lin, P.L., 2011. Macrophages and control of granulomatous inflammation in tuberculosis. *Mucosal Immunol.* 4, 271–278.

Flynn, J.L., Goldstein, M.M., Chan, J., Triebold, K.J., Pfeffer, K., Lowenstein, C.J., Schreiber, R., Mak, T.W., Bloom, B.R., 1995. Tumor necrosis factor-alpha is required in the protective immune response against *Mycobacterium tuberculosis* in mice. *Immunity* 2, 561–572.

Friedrich, N., Hagedorn, M., Soldati-Favre, D., Soldati, T., 2012. Prison break: pathogens' strategies to egress from host cells. *Microbiol. Mol. Biol. Rev. MMBR* 76, 707–720.

Gan, H., Lee, J., Ren, F., Chen, M., Kornfeld, H., Remold, H.G., 2008. *Mycobacterium tuberculosis* blocks crosslinking of annexin-1 and apoptotic envelope formation on infected macrophages to maintain virulence. *Nat. Immunol.* 9, 1189–1197.

Ganz, T., 2003. Defensins: antimicrobial peptides of innate immunity. *Nat. Rev. Immunol.* 3, 710–720.

Geldmacher, C., Ngwenyama, N., Schuetz, A., Petrovas, C., Reither, K., Heeregrave, E.J., Casazza, J.P., Ambrozak, D.R., Louder, M., Ampofo, W., Pollakis, G., Hill, B., Sanga, E., Saathoff, E., Maboko, L., Roederer, M., Paxton, W.A., Hoelscher, M., Koup, R.A., 2010. Preferential infection and depletion of Mycobacterium tuberculosis-specific CD4 T cells after HIV-1 infection. *J. Exp. Med.* 207, 2869–2881.

Gercken, J., Pryjma, J., Ernst, M., Flad, H.D., 1994. Defective antigen presentation by Mycobacterium tuberculosis-infected monocytes. *Infect. Immun.* 62, 3472–3478.

Germic, N., Frangez, Z., Yousefi, S., Simon, H.-U., 2019. Regulation of the innate immune system by autophagy: monocytes, macrophages, dendritic cells and antigen presentation. *Cell Death Differ.* 26, 715–727.

Gerstenmaier, L., Pilla, R., Herrmann, L., Herrmann, H., Prado, M., Villafano, G.J., Kolonko, M., Reimer, R., Soldati, T., King, J.S., Hagedorn, M., 2015. The autophagic machinery ensures nonlytic transmission of mycobacteria. *Proc. Natl. Acad. Sci.* 112, E687–E692.

Giacometti, A., Cirioni, O., Barchiesi, F., Caselli, F., Scalise, G., 1999. In-vitro activity of polycationic peptides against *Cryptosporidium parvum*, *Pneumocystis carinii* and yeast clinical isolates. *J. Antimicrob. Chemother.* 44, 403–406. <https://doi.org/10.1093/jac/44.3.403>

Gideon, H.P., Phuah, J., Myers, A.J., Bryson, B.D., Rodgers, M.A., Coleman, M.T., Maiello, P., Rutledge, T., Marino, S., Fortune, S.M., Kirschner, D.E., Lin, P.L., Flynn, J.L., 2015. Variability in tuberculosis granuloma T cell responses exists, but a balance of pro- and anti-inflammatory cytokines is associated with sterilization. *PLoS Pathog.* 11, e1004603.

Gilbert, A.S., Seoane, P.I., Sephton-Clark, P., Bojarczuk, A., Hotham, R., Giurisato, E., Sarhan, A.R., Hillen, A., Velde, G.V., Gray, N.S., Alessi, D.R., Cunningham, D.L., Tournier, C., Johnston, S.A., May, R.C., 2017. Vomocytosis of live pathogens from macrophages is regulated by the atypical MAP kinase ERK5. *Sci. Adv.* 3, e1700898.

Glickman, M.S., Cox, J.S., Jacobs, W.R., 2000. A Novel Mycolic Acid Cyclopropane Synthetase Is Required for Cording, Persistence, and Virulence of Mycobacterium tuberculosis. *Mol. Cell* 5, 717–727.

Gordon, S., Plüddemann, A., 2017. Tissue macrophages: heterogeneity and functions. *BMC Biol.* 15, 53.

- Gordon, S., Plüddemann, A., Martinez Estrada, F., 2014. Macrophage heterogeneity in tissues: phenotypic diversity and functions. *Immunol. Rev.* 262, 36–55.
- Granger, E., McNee, G., Allan, V., Woodman, P., 2014. The role of the cytoskeleton and molecular motors in endosomal dynamics. *Semin. Cell Dev. Biol.* 31, 20–29.
- Gresham, H.D., McGarr, J.A., Shackelford, P.G., Brown, E.J., 1988. Studies on the molecular mechanisms of human Fc receptor-mediated phagocytosis. Amplification of ingestion is dependent on the generation of reactive oxygen metabolites and is deficient in polymorphonuclear leukocytes from patients with chronic granulomatous disease. *J. Clin. Invest.* 82, 1192–1201.
- Griffith, J.W., Sokol, C.L., Luster, A.D., 2014. Chemokines and Chemokine Receptors: Positioning Cells for Host Defense and Immunity. *Annu. Rev. Immunol.* 32, 659–702.
- Grosset, J., 2003. Mycobacterium tuberculosis in the Extracellular Compartment: an Underestimated Adversary. *Antimicrob. Agents Chemother.* 47, 833–836.
- Guo, H., Callaway, J.B., Ting, J.P.-Y., 2015. Inflammasomes: mechanism of action, role in disease, and therapeutics. *Nat. Med.* 21, 677–687.
- Gutierrez, M.G., 2013. Functional role(s) of phagosomal Rab GTPases. *Small GTPases* 4, 148–158.
- Gutierrez, M.G., Master, S.S., Singh, S.B., Taylor, G.A., Colombo, M.I., Deretic, V., 2004. Autophagy is a defense mechanism inhibiting BCG and Mycobacterium tuberculosis survival in infected macrophages. *Cell* 119, 753–766.
- Hagedorn, M., Rohde, K.H., Russell, D.G., Soldati, T., 2009. Infection by tubercular mycobacteria is spread by nonlytic ejection from their amoeba hosts. *Science* 323, 1729–1733.
- Haldar, M., Murphy, K.M., 2014. Origin, Development, and Homeostasis of Tissue-resident Macrophages. *Immunol. Rev.* 262, 25–35.
- Hanania, R., Song Sun, H., Xu, K., PustylNIK, S., Jeganathan, S., Harrison, R.E., 2012. Classically Activated Macrophages Use Stable Microtubules for Matrix Metalloproteinase-9 (MMP-9) Secretion. *J. Biol. Chem.* 287, 8468–8483.
- Hao, M., Maxfield, F.R., 2000. Characterization of Rapid Membrane Internalization and Recycling. *J. Biol. Chem.* 275, 15279–15286.

Harding, C.V., Boom, W.H., 2010. Regulation of antigen presentation by *Mycobacterium tuberculosis*: a role for Toll-like receptors. *Nat. Rev. Microbiol.* 8, 296–307.

Harriff, M.J., Cansler, M.E., Toren, K.G., Canfield, E.T., Kwak, S., Gold, M.C., Lewinsohn, D.M., 2014. Human Lung Epithelial Cells Contain *Mycobacterium tuberculosis* in a Late Endosomal Vacuole and Are Efficiently Recognized by CD8+ T Cells. *PLOS ONE* 9, e97515.

Helming, L., Gordon, S., 2007. The molecular basis of macrophage fusion. *Immunobiology* 212, 785–793.

Hinchey, J., Lee, S., Jeon, B.Y., Basaraba, R.J., Venkataswamy, M.M., Chen, B., Chan, J., Braunstein, M., Orme, I.M., Derrick, S.C., Morris, S.L., Jacobs, W.R., Porcelli, S.A., 2007. Enhanced priming of adaptive immunity by a proapoptotic mutant of *Mycobacterium tuberculosis*. *J. Clin. Invest.* 117, 2279–2288.

Hmama, Z., Gabathuler, R., Jefferies, W.A., de Jong, G., Reiner, N.E., 1998. Attenuation of HLA-DR expression by mononuclear phagocytes infected with *Mycobacterium tuberculosis* is related to intracellular sequestration of immature class II heterodimers. *J. Immunol. Baltim. Md* 1950 161, 4882–4893.

Hmama, Z., Peña-Díaz, S., Joseph, S., Av-Gay, Y., 2015. Immuno-evasion and immunosuppression of the macrophage by *Mycobacterium tuberculosis*. *Immunol. Rev.* 264, 220–232.

Hoebeke, J., Van Nijen, G., De Brabander, M., 1976. Interaction of oncodazole (R 17934), a new anti-tumoral drug, with rat brain tubulin. *Biochem. Biophys. Res. Commun.* 69, 319–324.

Hoff, D.R., Ryan, G.J., Driver, E.R., Ssemakulu, C.C., De Groote, M.A., Basaraba, R.J., Lenaerts, A.J., 2011. Location of intra- and extracellular *M. tuberculosis* populations in lungs of mice and guinea pigs during disease progression and after drug treatment. *PLoS One* 6, e17550.

Hoffmann, C., Leis, A., Niederweis, M., Plitzko, J.M., Engelhardt, H., 2008. Disclosure of the mycobacterial outer membrane: cryo-electron tomography and vitreous sections reveal the lipid bilayer structure. *Proc. Natl. Acad. Sci. U. S. A.* 105, 3963–3967.

Höner zu Bentrup, K., Russell, D.G., 2001. Mycobacterial persistence: adaptation to a changing environment. *Trends Microbiol.* 9, 597–605.

Hoover, D.M., Rajashankar, K.R., Blumenthal, R., Puri, A., Oppenheim, J.J., Chertov, O., Lubkowski, J., 2000. The Structure of Human  $\beta$ -Defensin-2 Shows Evidence of Higher Order Oligomerization. *J. Biol. Chem.* 275, 32911–32918.

Houben, D., Demangel, C., Ingen, J. van, Perez, J., Baldeón, L., Abdallah, A.M., Caleechurn, L., Bottai, D., Zon, M. van, Punder, K. de, Laan, T. van der, Kant, A., Vries, R.B., Willemsen, P., Bitter, W., Soolingen, D. van, Brosch, R., Wel, N. van der, Peters, P.J., 2012. ESX-1-mediated translocation to the cytosol controls virulence of mycobacteria. *Cell. Microbiol.* 14, 1287–1298.

Hsu, T., Hingley-Wilson, S.M., Chen, B., Chen, M., Dai, A.Z., Morin, P.M., Marks, C.B., Padiyar, J., Goulding, C., Gingery, M., Eisenberg, D., Russell, R.G., Derrick, S.C., Collins, F.M., Morris, S.L., King, C.H., Jacobs, W.R., 2003. The primary mechanism of attenuation of bacillus Calmette-Guerin is a loss of secreted lytic function required for invasion of lung interstitial tissue. *Proc. Natl. Acad. Sci. U. S. A.* 100, 12420–12425.

Huang, L., Nazarova, E.V., Tan, S., Liu, Y., Russell, D.G., 2018. Growth of Mycobacterium tuberculosis in vivo segregates with host macrophage metabolism and ontogeny. *J. Exp. Med.* jem.20172020.

Hybiske, K., Stephens, R.S., 2008. Exit strategies of intracellular pathogens. *Nat. Rev. Microbiol.* 6, 99–110.

Hybiske, K., Stephens, R.S., 2007. Mechanisms of host cell exit by the intracellular bacterium Chlamydia. *Proc. Natl. Acad. Sci. U. S. A.* 104, 11430–11435.

Imlay, J.A., Linn, S., 1988. DNA damage and oxygen radical toxicity. *Science* 240, 1302–1309.

Ingalls, B.P., 2013. *Mathematical modeling in systems biology: an introduction.* MIT Press, Cambridge, Massachusetts.

Ishikawa, E., Ishikawa, T., Morita, Y.S., Toyonaga, K., Yamada, H., Takeuchi, O., Kinoshita, T., Akira, S., Yoshikai, Y., Yamasaki, S., 2009. Direct recognition of the mycobacterial glycolipid, trehalose dimycolate, by C-type lectin Mincle. *J. Exp. Med.* 206, 2879–2888.

Itoh, N., Yonehara, S., Ishii, A., Yonehara, M., Mizushima, S., Sameshima, M., Hase, A., Seto, Y., Nagata, S., 1991. The polypeptide encoded by the cDNA for human cell surface antigen Fas can mediate apoptosis. *Cell* 66, 233–243.

Jamwal, S.V., Mehrotra, P., Singh, A., Siddiqui, Z., Basu, A., Rao, K.V.S., 2016. Mycobacterial escape from macrophage phagosomes to the cytoplasm represents an alternate adaptation mechanism. *Sci. Rep.* 6, 23089.

Jayachandran, R., Sundaramurthy, V., Combaluzier, B., Mueller, P., Korf, H., Huygen, K., Miyazaki, T., Albrecht, I., Massner, J., Pieters, J., 2007. Survival of mycobacteria in macrophages is mediated by coronin 1-dependent activation of calcineurin. *Cell* 130, 37–50.

Jeon, C.Y., Murray, M.B., 2008. Diabetes Mellitus Increases the Risk of Active Tuberculosis: A Systematic Review of 13 Observational Studies. *PLoS Med.* 5, e152.

Jick, S.S., Lieberman, E.S., Rahman, M.U., Choi, H.K., 2006. Glucocorticoid use, other associated factors, and the risk of tuberculosis. *Arthritis Rheum.* 55, 19–26.

Johnston, S.A., May, R.C., 2010. The human fungal pathogen *Cryptococcus neoformans* escapes macrophages by a phagosome emptying mechanism that is inhibited by Arp2/3 complex-mediated actin polymerisation. *PLoS Pathog.* 6, e1001041.

Johnston, S.A., Voelz, K., May, R.C., 2016. *Cryptococcus neoformans* Thermotolerance to Avian Body Temperature Is Sufficient For Extracellular Growth But Not Intracellular Survival In Macrophages. *Sci. Rep.* 6.

Kamath, A.B., Woodworth, J., Xiong, X., Taylor, C., Weng, Y., Behar, S.M., 2004. Cytolytic CD8<sup>+</sup> T Cells Recognizing CFP10 Are Recruited to the Lung after *Mycobacterium tuberculosis* Infection. *J. Exp. Med.* 200, 1479–1489.

Kang, P.B., Azad, A.K., Torrelles, J.B., Kaufman, T.M., Beharka, A., Tibesar, E., DesJardin, L.E., Schlesinger, L.S., 2005. The human macrophage mannose receptor directs *Mycobacterium tuberculosis* lipoarabinomannan-mediated phagosome biogenesis. *J. Exp. Med.* 202, 987–999.

Kaplan, G., Post, F.A., Moreira, A.L., Wainwright, H., Kreiswirth, B.N., Tanverdi, M., Mathema, B., Ramaswamy, S.V., Walther, G., Steyn, L.M., Barry, C.E., Bekker, L.-G., 2003. *Mycobacterium tuberculosis* growth at the cavity surface: a microenvironment with failed immunity. *Infect. Immun.* 71, 7099–7108.

Kathania, M., Raje, C.I., Raje, M., Dutta, R.K., Majumdar, S., 2011. Bfl-1/A1 acts as a negative regulator of autophagy in mycobacteria infected macrophages. *Int. J. Biochem. Cell Biol.* 43, 573–585.

Keane, J., Balcewicz-Sablinska, M.K., Remold, H.G., Chupp, G.L., Meek, B.B., Fenton, M.J., Kornfeld, H., 1997. Infection by *Mycobacterium tuberculosis* promotes human alveolar macrophage apoptosis. *Infect. Immun.* 65, 298–304.

Kerr, J.F., Wyllie, A.H., Currie, A.R., 1972. Apoptosis: a basic biological phenomenon with wide-ranging implications in tissue kinetics. *Br. J. Cancer* 26, 239–257.

Kim, K.H., An, D.R., Song, J., Yoon, J.Y., Kim, H.S., Yoon, H.J., Im, H.N., Kim, J., Kim, D.J., Lee, S.J., Kim, K.-H., Lee, H.-M., Kim, H.-J., Jo, E.-K., Lee, J.Y., Suh, S.W., 2012. Mycobacterium tuberculosis Eis protein initiates suppression of host immune responses by acetylation of DUSP16/MKP-7. Proc. Natl. Acad. Sci. 109, 7729–7734.

Klug-Micu, G.M., Stenger, S., Sommer, A., Liu, P.T., Krutzik, S.R., Modlin, R.L., Fabri, M., 2013. CD40 ligand and interferon- $\gamma$  induce an antimicrobial response against Mycobacterium tuberculosis in human monocytes. Immunology 139, 121–128.

Knutson, K.L., Hmama, Z., Herrera-Velitz, P., Rochford, R., Reiner, N.E., 1998. Lipoarabinomannan of *Mycobacterium tuberculosis* Promotes Protein Tyrosine Dephosphorylation and Inhibition of Mitogen-activated Protein Kinase in Human Mononuclear Phagocytes: ROLE OF THE Src HOMOLOGY 2 CONTAINING TYROSINE PHOSPHATASE 1. J. Biol. Chem. 273, 645–652.

Kolloli, A., Subbian, S., 2017. Host-Directed Therapeutic Strategies for Tuberculosis. Front. Med. 4, 171.

Kumar, D., Nath, L., Kamal, M.A., Varshney, A., Jain, A., Singh, S., Rao, K.V.S., 2010. Genome-wide analysis of the host intracellular network that regulates survival of Mycobacterium tuberculosis. Cell 140, 731–743.

Lamb, C.A., Yoshimori, T., Tooze, S.A., 2013. The autophagosome: origins unknown, biogenesis complex. Nat. Rev. Mol. Cell Biol. 14, 759–774.

Lawrence, T., Natoli, G., 2011. Transcriptional regulation of macrophage polarization: enabling diversity with identity. Nat. Rev. Immunol. 11, 750–761.

Layre, E., Lee, H.J., Young, D.C., Jezek Martinot, A., Buter, J., Minnaard, A.J., Annand, J.W., Fortune, S.M., Snider, B.B., Matsunaga, I., Rubin, E.J., Alber, T., Moody, D.B., 2014. Molecular profiling of Mycobacterium tuberculosis identifies tuberculosinyl nucleoside products of the virulence-associated enzyme Rv3378c. Proc. Natl. Acad. Sci. 111, 2978–2983.

Lazarevic, V., Flynn, J., 2002. CD8<sup>+</sup> T Cells in Tuberculosis. Am. J. Respir. Crit. Care Med. 166, 1116–1121.

Lee, W., VanderVen, B.C., Fahey, R.J., Russell, D.G., 2013. Intracellular *Mycobacterium tuberculosis* Exploits Host-derived Fatty Acids to Limit Metabolic Stress. J. Biol. Chem. 288, 6788–6800.

Lenaerts, A., Barry, C.E., Dartois, V., 2015. Heterogeneity in tuberculosis pathology, microenvironments and therapeutic responses. Immunol. Rev. 264, 288–307.

Lerner, T.R., Borel, S., Greenwood, D.J., Repnik, U., Russell, M.R.G., Herbst, S., Jones, M.L., Collinson, L.M., Griffiths, G., Gutierrez, M.G., 2017. *Mycobacterium tuberculosis* replicates within necrotic human macrophages. *J. Cell Biol.* 216, 583–594.

Lerner, T.R., Borel, S., Gutierrez, M.G., 2015. The innate immune response in human tuberculosis. *Cell. Microbiol.* 17, 1277–1285.

Lin, P.L., Ford, C.B., Coleman, M.T., Myers, A.J., Gawande, R., Ioerger, T., Sacchettini, J., Fortune, S.M., Flynn, J.L., 2014. Sterilization of granulomas is common in active and latent tuberculosis despite within-host variability in bacterial killing. *Nat. Med.* 20, 75–79.

Lin, P.L., Pawar, S., Myers, A., Pegu, A., Fuhrman, C., Reinhart, T.A., Capuano, S.V., Klein, E., Flynn, J.L., 2006. Early Events in *Mycobacterium tuberculosis* Infection in *Cynomolgus* Macaques. *Infect. Immun.* 74, 3790–3803.

Lin, P.L., Rodgers, M., Smith, L., 'kneitah, Bigbee, M., Myers, A., Bigbee, C., Chiose, I., Capuano, S.V., Fuhrman, C., Klein, E., Flynn, J.L., 2009. Quantitative Comparison of Active and Latent Tuberculosis in the *Cynomolgus* Macaque Model. *Infect. Immun.* 77, 4631–4642.

Lin, P.L., Rutledge, T., Green, A.M., Bigbee, M., Fuhrman, C., Klein, E., Flynn, J.L., 2012. CD4 T cell depletion exacerbates acute *Mycobacterium tuberculosis* while reactivation of latent infection is dependent on severity of tissue depletion in *cynomolgus* macaques. *AIDS Res. Hum. Retroviruses* 28, 1693–1702.

Liu, P.T., Stenger, S., Li, H., Wenzel, L., Tan, B.H., Krutzik, S.R., Ochoa, M.T., Schaub, J., Wu, K., Meinken, C., Kamen, D.L., Wagner, M., Bals, R., Steinmeyer, A., Zügel, U., Gallo, R.L., Eisenberg, D., Hewison, M., Hollis, B.W., Adams, J.S., Bloom, B.R., Modlin, R.L., 2006. Toll-Like Receptor Triggering of a Vitamin D-Mediated Human Antimicrobial Response. *Science* 311, 1770–1773.

Liu, P.T., Stenger, S., Tang, D.H., Modlin, R.L., 2007. Cutting edge: vitamin D-mediated human antimicrobial activity against *Mycobacterium tuberculosis* is dependent on the induction of cathelicidin. *J. Immunol. Baltim. Md* 1950 179, 2060–2063.

Liu, Y., Tan, S., Huang, L., Abramovitch, R.B., Rohde, K.H., Zimmerman, M.D., Chen, C., Dartois, V., VanderVen, B.C., Russell, D.G., 2016. Immune activation of the host cell induces drug tolerance in *Mycobacterium tuberculosis* both in vitro and in vivo. *J. Exp. Med.* 213, 809–825.

Lodish, H., Berk, A., Zipursky, S.L., Matsudaira, P., Baltimore, D., Darnell, J., 2000. *The Dynamics of Actin Assembly*. *Mol. Cell Biol.* 4th Ed.

Lugo-Villarino, G., Troegeler, A., Balboa, L., Lastrucci, C., Duval, C., Mercier, I., Bénard, A., Capilla, F., Al Saati, T., Poincloux, R., Kondova, I., Verreck, F.A.W., Cougoule, C., Maridonneau-Parini, I., Sasiain, M. del C., Neyrolles, O., 2018. The C-Type Lectin Receptor DC-SIGN Has an Anti-Inflammatory Role in Human M(IL-4) Macrophages in Response to Mycobacterium tuberculosis. *Front. Immunol.* 9.

MacMicking, J.D., North, R.J., LaCourse, R., Mudgett, J.S., Shah, S.K., Nathan, C.F., 1997. Identification of nitric oxide synthase as a protective locus against tuberculosis. *Proc. Natl. Acad. Sci.* 94, 5243–5248.

MacMicking, J.D., Taylor, G.A., McKinney, J.D., 2003. Immune control of tuberculosis by IFN-gamma-inducible LRG-47. *Science* 302, 654–659.

Mahamed, D., Boulle, M., Ganga, Y., Mc Arthur, C., Skroch, S., Oom, L., Catinas, O., Pillay, K., Naicker, M., Rampersad, S., Mathonsi, C., Hunter, J., Wong, E.B., Suleman, M., Sreejit, G., Pym, A.S., Lustig, G., Sigal, A., 2017. Intracellular growth of Mycobacterium tuberculosis after macrophage cell death leads to serial killing of host cells. *eLife* 6.

Ma, H., Croudace, J.E., Lammas, D.A., May, R.C., 2006. Expulsion of live pathogenic yeast by macrophages. *Curr. Biol. CB* 16, 2156–2160.

Majlessi, L., Brosch, R., 2015. Mycobacterium tuberculosis Meets the Cytosol: The Role of cGAS in Anti-mycobacterial Immunity. *Cell Host Microbe* 17, 733–735.

Malik, Z.A., Denning, G.M., Kusner, D.J., 2000. Inhibition of Ca(2+) signaling by Mycobacterium tuberculosis is associated with reduced phagosome-lysosome fusion and increased survival within human macrophages. *J. Exp. Med.* 191, 287–302.

Manca, C., Tsenova, L., Bergtold, A., Freeman, S., Tovey, M., Musser, J.M., Barry, C.E., Freedman, V.H., Kaplan, G., 2001. Virulence of a Mycobacterium tuberculosis clinical isolate in mice is determined by failure to induce Th1 type immunity and is associated with induction of IFN-alpha /beta. *Proc. Natl. Acad. Sci. U. S. A.* 98, 5752–5757.

Manca, C., Tsenova, L., Freeman, S., Barczak, A.K., Tovey, M., Murray, P.J., Barry, C., Kaplan, G., 2005. Hypervirulent M. tuberculosis W/Beijing strains upregulate type I IFNs and increase expression of negative regulators of the Jak-Stat pathway. *J. Interferon Cytokine Res. Off. J. Int. Soc. Interferon Cytokine Res.* 25, 694–701.

Man, S.M., Karki, R., Kanneganti, T.-D., 2017. Molecular mechanisms and functions of pyroptosis, inflammatory caspases and inflammasomes in infectious diseases. *Immunol. Rev.* 277, 61–75.

Manzanillo, P.S., Shiloh, M.U., Portnoy, D.A., Cox, J.S., 2012. Mycobacterium Tuberculosis Activates the DNA-Dependent Cytosolic Surveillance Pathway within Macrophages. *Cell Host Microbe* 11, 469–480.

Mao, C., Shukla, M., Larrouy-Maumus, G., Dix, F.L., Kelley, L.A., Sternberg, M.J., Sobral, B.W., de Carvalho, L.P.S., 2013. Functional assignment of Mycobacterium tuberculosis proteome revealed by genome-scale fold-recognition. *Tuberc. Edinb. Scotl.* 93, 40–46.

Marakalala, M.J., Martinez, F.O., Plüddemann, A., Gordon, S., 2018. Macrophage Heterogeneity in the Immunopathogenesis of Tuberculosis. *Front. Microbiol.* 9.

Marakalala, M.J., Raju, R.M., Sharma, K., Zhang, Y.J., Eugenin, E.A., Prideaux, B., Daudelin, I.B., Chen, P.-Y., Booty, M.G., Kim, J.H., Eum, S.Y., Via, L.E., Behar, S.M., Barry, C.E., Mann, M., Dartois, V., Rubin, E.J., 2016. Inflammatory signaling in human tuberculosis granulomas is spatially organized. *Nat. Med.* 22, 531–538.

Marino, S., Cilfone, N.A., Mattila, J.T., Linderman, J.J., Flynn, J.L., Kirschner, D.E., 2015. Macrophage Polarization Drives Granuloma Outcome during Mycobacterium tuberculosis Infection. *Infect. Immun.* 83, 324–338.

Martin, C.J., Booty, M.G., Rosebrock, T.R., Nunes-Alves, C., Desjardins, D.M., Keren, I., Fortune, S.M., Remold, H.G., Behar, S.M., 2012. Efferocytosis is an innate antibacterial mechanism. *Cell Host Microbe* 12, 289–300.

Martineau, A.R., Wilkinson, K.A., Newton, S.M., Floto, R.A., Norman, A.W., Skolimowska, K., Davidson, R.N., Sørensen, O.E., Kampmann, B., Griffiths, C.J., Wilkinson, R.J., 2007. IFN-gamma- and TNF-independent vitamin D-inducible human suppression of mycobacteria: the role of cathelicidin LL-37. *J. Immunol. Baltim. Md* 1950 178, 7190–7198.

Martinez, F.O., Gordon, S., 2014. The M1 and M2 paradigm of macrophage activation: time for reassessment. *F1000Prime Rep.* 6.

Mattila, J.T., Ojo, O.O., Kepka-Lenhart, D., Marino, S., Kim, J.H., Eum, S.Y., Via, L.E., Barry, C.E., Klein, E., Kirschner, D.E., Morris, S.M., Lin, P.L., Flynn, J.L., 2013. Microenvironments in tuberculous granulomas are delineated by distinct populations of macrophage subsets and expression of nitric oxide synthase and arginase isoforms. *J. Immunol. Baltim. Md* 1950 191, 773–784.

Mayer-Barber, K.D., Andrade, B.B., Barber, D.L., Hieny, S., Feng, C.G., Caspar, P., Oland, S., Gordon, S., Sher, A., 2011. Innate and adaptive interferons suppress IL-1 $\alpha$  and IL-1 $\beta$  production by distinct pulmonary myeloid subsets during Mycobacterium tuberculosis infection. *Immunity* 35, 1023–1034.

Mayer-Barber, K.D., Andrade, B.B., Oland, S.D., Amaral, E.P., Barber, D.L., Gonzales, J., Derrick, S.C., Shi, R., Kumar, N.P., Wei, W., Yuan, X., Zhang, G., Cai, Y., Babu, S., Catalfamo, M., Salazar, A.M., Via, L.E., Barry, C.E., Sher, A., 2014. Host-directed therapy of tuberculosis based on interleukin-1 and type I interferon crosstalk. *Nature* 511, 99–103.

McDonough, K.A., Kress, Y., 1995. Cytotoxicity for lung epithelial cells is a virulence-associated phenotype of *Mycobacterium tuberculosis*. *Infect. Immun.* 63, 4802–4811.

McDonough, K.A., Kress, Y., Bloom, B.R., 1993. Pathogenesis of tuberculosis: interaction of *Mycobacterium tuberculosis* with macrophages. *Infect. Immun.* 61, 2763–2773.

Medzhitov, R., Janeway, C., 2000. Innate immunity. *N. Engl. J. Med.* 343, 338–344.

Mogues, T., Goodrich, M.E., Ryan, L., LaCourse, R., North, R.J., 2001. The Relative Importance of T Cell Subsets in Immunity and Immunopathology of Airborne *Mycobacterium tuberculosis* Infection in Mice. *J. Exp. Med.* 193, 271–280.

Möller, M., de Wit, E., Hoal, E.G., 2010. Past, present and future directions in human genetic susceptibility to tuberculosis. *FEMS Immunol. Med. Microbiol.* 58, 3–26.

Möller, M., Kinnear, C.J., Orlova, M., Kroon, E.E., van Helden, P.D., Schurr, E., Hoal, E.G., 2018. Genetic Resistance to *Mycobacterium tuberculosis* Infection and Disease. *Front. Immunol.* 9, 2219.

Molloy, A., Laochumroonvorapong, P., Kaplan, G., 1994. Apoptosis, but not necrosis, of infected monocytes is coupled with killing of intracellular bacillus Calmette-Guérin. *J. Exp. Med.* 180, 1499–1509.

Monack, D.M., Theriot, J.A., 2001. Actin-based motility is sufficient for bacterial membrane protrusion formation and host cell uptake. *Cell. Microbiol.* 3, 633–647.

Mosser, D.M., Edwards, J.P., 2008. Exploring the full spectrum of macrophage activation. *Nat. Rev. Immunol.* 8, 958–969.

Murray, P.J., 2017. Macrophage Polarization. *Annu. Rev. Physiol.* 79, 541–566.

Nagata, S., Tanaka, M., 2017. Programmed cell death and the immune system. *Nat. Rev. Immunol.* 17, 333–340.

Nathan, C., 2002. Inducible Nitric Oxide Synthase in the Tuberculous Human Lung. *Am. J. Respir. Crit. Care Med.* 166, 130–131.

Nathan, C.F., Hibbs, J.B., 1991. Role of nitric oxide synthesis in macrophage antimicrobial activity. *Curr. Opin. Immunol.* 3, 65–70.

Nathan, C., Shiloh, M.U., 2000. Reactive oxygen and nitrogen intermediates in the relationship between mammalian hosts and microbial pathogens. *Proc. Natl. Acad. Sci. U. S. A.* 97, 8841–8848.

Neiman-Zenevich, J., Stuart, S., Abdel-Nour, M., Girardin, S.E., Mogridge, J., 2017. *Listeria monocytogenes* and *Shigella flexneri* Activate the NLRP1B Inflammasome. *Infect. Immun.* 85.

Nicholson, S., Bonecini-Almeida, M. da G., Lapa e Silva, J.R., Nathan, C., Xie, Q.W., Mumford, R., Weidner, J.R., Calaycay, J., Geng, J., Boechat, N., Linhares, C., Rom, W., Ho, J.L., 1996. Inducible nitric oxide synthase in pulmonary alveolar macrophages from patients with tuberculosis. *J. Exp. Med.* 183, 2293–2302.

Nicola, A.M., Robertson, E.J., Albuquerque, P., Derengowski, L. da S., Casadevall, A., 2011. Nonlytic Exocytosis of *Cryptococcus neoformans* from Macrophages Occurs In Vivo and Is Influenced by Phagosomal pH. *mBio* 2, e00167–11.

Niyonsaba, F., Ogawa, H., Nagaoka, I., 2004. Human beta-defensin-2 functions as a chemotactic agent for tumour necrosis factor-alpha-treated human neutrophils. *Immunology* 111, 273–281.

Nogales, E., 2000. Structural Insights into Microtubule Function. *Annu. Rev. Biochem.* 69, 277–302.

Nogueira, C.V., Lindsten, T., Jamieson, A.M., Case, C.L., Shin, S., Thompson, C.B., Roy, C.R., 2009. Rapid Pathogen-Induced Apoptosis: A Mechanism Used by Dendritic Cells to Limit Intracellular Replication of *Legionella pneumophila*. *PLoS Pathog.* 5, e1000478.

Noss, E.H., Pai, R.K., Sellati, T.J., Radolf, J.D., Belisle, J., Golenbock, D.T., Boom, W.H., Harding, C.V., 2001. Toll-like receptor 2-dependent inhibition of macrophage class II MHC expression and antigen processing by 19-kDa lipoprotein of *Mycobacterium tuberculosis*. *J. Immunol. Baltim. Md* 1950 167, 910–918.

Novikov, A., Cardone, M., Thompson, R., Shenderov, K., Kirschman, K.D., Mayer-Barber, K.D., Myers, T.G., Rabin, R.L., Trinchieri, G., Sher, A., Feng, C.G., 2011. Triggers Host Type I IFN Signaling To Regulate IL-1 $\beta$  Production in Human Macrophages. *J. Immunol.* 187, 2540–2547.

Nusbaum, R.J., Calderon, V.E., Huante, M.B., Sutjita, P., Vijayakumar, S., Lancaster, K.L., Hunter, R.L., Actor, J.K., Cirillo, J.D., Aronson, J., Gelman, B.B.,

Lisinicchia, J.G., Valbuena, G., Endsley, J.J., 2016. Pulmonary Tuberculosis in Humanized Mice Infected with HIV-1. *Sci. Rep.* 6, 21522.

Oddo, M., Renno, T., Attinger, A., Bakker, T., MacDonald, H.R., Meylan, P.R., 1998. Fas ligand-induced apoptosis of infected human macrophages reduces the viability of intracellular *Mycobacterium tuberculosis*. *J. Immunol. Baltim. Md 1950* 160, 5448–5454.

O’Leary, S., O’Sullivan, M.P., Keane, J., 2011. IL-10 blocks phagosome maturation in mycobacterium tuberculosis-infected human macrophages. *Am. J. Respir. Cell Mol. Biol.* 45, 172–180.

Pai, M., Behr, M.A., Dowdy, D., Dheda, K., Divangahi, M., Boehme, C.C., Ginsberg, A., Swaminathan, S., Spigelman, M., Getahun, H., Menzies, D., Raviglione, M., 2016. Tuberculosis. *Nat. Rev. Dis. Primer* 2, 16076.

Paludan, C., Schmid, D., Landthaler, M., Vockerodt, M., Kube, D., Tuschl, T., Münz, C., 2005. Endogenous MHC class II processing of a viral nuclear antigen after autophagy. *Science* 307, 593–596.

Park, J.S., 2005. Virulent clinical isolates of *Mycobacterium tuberculosis* grow rapidly and induce cellular necrosis but minimal apoptosis in murine macrophages. *J. Leukoc. Biol.* 79, 80–86.

Pathak, S.K., Basu, S., Basu, K.K., Banerjee, A., Pathak, S., Bhattacharyya, A., Kaisho, T., Kundu, M., Basu, J., 2007. Direct extracellular interaction between the early secreted antigen ESAT-6 of *Mycobacterium tuberculosis* and TLR2 inhibits TLR signaling in macrophages. *Nat. Immunol.* 8, 610–618.

Patterson, S.D., Spahr, C.S., Daugas, E., Susin, S.A., Irinopoulou, T., Koehler, C., Kroemer, G., 2000. Mass spectrometric identification of proteins released from mitochondria undergoing permeability transition. *Cell Death Differ.* 7, 137–144.

Pethe, K., Swenson, D.L., Alonso, S., Anderson, J., Wang, C., Russell, D.G., 2004. Isolation of *Mycobacterium tuberculosis* mutants defective in the arrest of phagosome maturation. *Proc. Natl. Acad. Sci.* 101, 13642–13647.

Petruccioli, E., Romagnoli, A., Corazzari, M., Coccia, E.M., Butera, O., Delogu, G., Piacentini, M., Girardi, E., Fimia, G.M., Goletti, D., 2012. Specific T cells restore the autophagic flux inhibited by *Mycobacterium tuberculosis* in human primary macrophages. *J. Infect. Dis.* 205, 1425–1435.

Pfyffer, G., Palicova, F., 2011. *Mycobacterium: General Characteristics, Laboratory Detection, and Staining Procedures.*, in: *Manual of Clinical Microbiology*. ASM press, pp. 472–502.

Pieters, J., 2008. Mycobacterium tuberculosis and the Macrophage: Maintaining a Balance. *Cell Host Microbe* 3, 399–407

Piperno, G., LeDizet, M., Chang, X.J., 1987. Microtubules containing acetylated alpha-tubulin in mammalian cells in culture. *J. Cell Biol.* 104, 289–302.

Ponpuak, M., Davis, A.S., Roberts, E.A., Delgado, M.A., Dinkins, C., Zhao, Z., Virgin, H.W., Kyei, G.B., Johansen, T., Vergne, I., Deretic, V., 2010. Delivery of cytosolic components by autophagic adaptor protein p62 endows autophagosomes with unique antimicrobial properties. *Immunity* 32, 329–341.

Queval, C.J., Brosch, R., Simeone, R., 2017. The Macrophage: A Disputed Fortress in the Battle against Mycobacterium tuberculosis. *Front. Microbiol.* 8.

Raffetseder, J., Pienaar, E., Blomgran, R., Eklund, D., Brodin, V.P., Andersson, H., Welin, A., Lerm, M., 2014. Replication Rates of Mycobacterium tuberculosis in Human Macrophages Do Not Correlate with Mycobacterial Antibiotic Susceptibility. *PLOS ONE* 9, e112426.

Ramachandra, L., Noss, E., Boom, W.H., Harding, C.V., 2001. Processing of Mycobacterium tuberculosis Antigen 85B Involves Intraphagosomal Formation of Peptide–Major Histocompatibility Complex II Complexes and Is Inhibited by Live Bacilli that Decrease Phagosome Maturation. *J. Exp. Med.* 194, 1421–1432.

Ramakrishnan, L., 2012. Revisiting the role of the granuloma in tuberculosis. *Nat. Rev. Immunol.* 12, 352–366.

Rao, V., Fujiwara, N., Porcelli, S.A., Glickman, M.S., 2005. Mycobacterium tuberculosis controls host innate immune activation through cyclopropane modification of a glycolipid effector molecule. *J. Exp. Med.* 201, 535–543.

Reiley, W.W., Calayag, M.D., Wittmer, S.T., Huntington, J.L., Pearl, J.E., Fountain, J.J., Martino, C.A., Roberts, A.D., Cooper, A.M., Winslow, G.M., Woodland, D.L., 2008. ESAT-6-specific CD4 T cell responses to aerosol Mycobacterium tuberculosis infection are initiated in the mediastinal lymph nodes. *Proc. Natl. Acad. Sci. U. S. A.* 105, 10961–10966.

Repasy, T., Lee, J., Marino, S., Martinez, N., Kirschner, D.E., Hendricks, G., Baker, S., Wilson, A.A., Kotton, D.N., Kornfeld, H., 2013. Intracellular Bacillary Burden Reflects a Burst Size for Mycobacterium tuberculosis In Vivo. *PLOS Pathog.* 9, e1003190.

Riendeau, C.J., Kornfeld, H., 2003. THP-1 Cell Apoptosis in Response to Mycobacterial Infection. *Infect. Immun.* 71, 254–259.

- Rink, J., Ghigo, E., Kalaidzidis, Y., Zerial, M., 2005. Rab conversion as a mechanism of progression from early to late endosomes. *Cell* 122, 735–749.
- Roberts, E.A., Chua, J., Kyei, G.B., Deretic, V., 2006. Higher order Rab programming in phagolysosome biogenesis. *J. Cell Biol.* 174, 923–929.
- Robinson, C.M., Nau, G.J., 2008. Interleukin-12 and Interleukin-27 Regulate Macrophage Control of *Mycobacterium tuberculosis*. *J. Infect. Dis.* 198, 359–366.
- Roca, F.J., Ramakrishnan, L., 2013. TNF dually mediates resistance and susceptibility to mycobacteria via mitochondrial reactive oxygen species. *Cell* 153, 521–534.
- Rohde, K.H., Veiga, D.F.T., Caldwell, S., Balázsi, G., Russell, D.G., 2012. Linking the Transcriptional Profiles and the Physiological States of *Mycobacterium tuberculosis* during an Extended Intracellular Infection. *PLoS Pathog.* 8, e1002769.
- Romagnoli, A., Etna, M.P., Giacomini, E., Pardini, M., Remoli, M.E., Corazzari, M., Falasca, L., Goletti, D., Gafa, V., Simeone, R., Delogu, G., Piacentini, M., Brosch, R., Fimia, G.M., Coccia, E.M., 2012. ESX-1 dependent impairment of autophagic flux by *Mycobacterium tuberculosis* in human dendritic cells. *Autophagy* 8, 1357–1370.
- Rook, G.A., Steele, J., Fraher, L., Barker, S., Karmali, R., O’Riordan, J., Stanford, J., 1986. Vitamin D3, gamma interferon, and control of proliferation of *Mycobacterium tuberculosis* by human monocytes. *Immunology* 57, 159–163.
- Rostam, H.M., Reynolds, P.M., Alexander, M.R., Gadegaard, N., Ghaemmaghami, A.M., 2017. Image based Machine Learning for identification of macrophage subsets. *Sci. Rep.* 7, 3521.
- Rotsch, C., Radmacher, M., 2000. Drug-induced changes of cytoskeletal structure and mechanics in fibroblasts: an atomic force microscopy study. *Biophys. J.* 78, 520–535.
- Russell, D.G., Barry, C.E., Flynn, J.L., 2010a. Tuberculosis: What We Don’t Know Can, and Does, Hurt Us. *Science* 328, 852–856.
- Russell, D.G., Cardona, P.-J., Kim, M.-J., Allain, S., Altare, F., 2009. Foamy macrophages and the progression of the human tuberculosis granuloma. *Nat. Immunol.* 10, 943–948.
- Russell, D.G., VanderVen, B.C., Lee, W., Abramovitch, R.B., Kim, M., Homolka, S., Niemann, S., Rohde, K.H., 2010b. *Mycobacterium tuberculosis* wears what it eats. *Cell Host Microbe* 8, 68–76.

Sahoo, M., Ceballos-Olvera, I., del Barrio, L., Re, F., 2011. Role of the Inflammasome, IL-1  $\beta$ , and IL-18 in Bacterial Infections. *Sci. World J.* 11, 2037–2050.

Saini, N.K., Baena, A., Ng, T.W., Venkataswamy, M.M., Kennedy, S.C., Kunnath-Velayudhan, S., Carreño, L.J., Xu, J., Chan, J., Larsen, M.H., Jacobs, W.R., Porcelli, S.A., 2016. Suppression of autophagy and antigen presentation by *Mycobacterium tuberculosis* PE\_PGRS47. *Nat. Microbiol.* 1, 16133.

Sakai, S., Mayer-Barber, K.D., Barber, D.L., 2014. Defining features of protective CD4 T cell responses to *Mycobacterium tuberculosis*. *Curr. Opin. Immunol.* 29, 137–142.

Saunders, B.M., Frank, A.A., Orme, I.M., Cooper, A.M., 2002. CD4 is required for the development of a protective granulomatous response to pulmonary tuberculosis. *Cell. Immunol.* 216, 65–72.

Scanga, C.A., Mohan, V.P., Yu, K., Joseph, H., Tanaka, K., Chan, J., Flynn, J.L., 2000. Depletion of Cd4 + T Cells Causes Reactivation of Murine Persistent Tuberculosis despite Continued Expression of Interferon  $\gamma$  and Nitric Oxide Synthase 2. *J. Exp. Med.* 192, 347–358.

Schaechter, M., Bozeman, F.M., Smadel, J.E., 1957. Study on the growth of rickettsiae. *Virology* 3, 160–172.

Schäfer, G., Jacobs, M., Wilkinson, R.J., Brown, G.D., 2009. Non-opsonic recognition of *Mycobacterium tuberculosis* by phagocytes. *J. Innate Immun.* 1, 231–243.

Schlesinger, L.S., Bellinger-Kawahara, C.G., Payne, N.R., Horwitz, M.A., 1990. Phagocytosis of *Mycobacterium tuberculosis* is mediated by human monocyte complement receptors and complement component C3. *J. Immunol. Baltim. Md* 1950 144, 2771–2780.

Schlesinger, L.S., Hull, S.R., Kaufman, T.M., 1994. Binding of the terminal mannosyl units of lipoarabinomannan from a virulent strain of *Mycobacterium tuberculosis* to human macrophages. *J. Immunol. Baltim. Md* 1950 152, 4070–4079.

Schmid, D., Pypaert, M., Münz, C., 2007. Antigen-loading compartments for major histocompatibility complex class II molecules continuously receive input from autophagosomes. *Immunity* 26, 79–92.

Schnettger, L., Rodgers, A., Repnik, U., Lai, R.P., Pei, G., Verdoes, M., Wilkinson, R.J., Young, D.B., Gutierrez, M.G., 2017. A Rab20-Dependent Membrane Trafficking Pathway Controls *M. tuberculosis* Replication by

Regulating Phagosome Spaciousness and Integrity. *Cell Host Microbe* 21, 619–628.e5.

Seto, S., Tsujimura, K., Koide, Y., 2012. Coronin-1a inhibits autophagosome formation around *Mycobacterium tuberculosis*-containing phagosomes and assists mycobacterial survival in macrophages. *Cell. Microbiol.* 14, 710–727.

Shin, D.-M., Jeon, B.-Y., Lee, H.-M., Jin, H.S., Yuk, J.-M., Song, C.-H., Lee, S.-H., Lee, Z.-W., Cho, S.-N., Kim, J.-M., Friedman, R.L., Jo, E.-K., 2010a. *Mycobacterium tuberculosis* Eis Regulates Autophagy, Inflammation, and Cell Death through Redox-dependent Signaling. *PLoS Pathog.* 6.

Shin, D.-M., Yuk, J.-M., Lee, H.-M., Lee, S.-H., Son, J.W., Harding, C.V., Kim, J.-M., Modlin, R.L., Jo, E.-K., 2010b. Mycobacterial lipoprotein activates autophagy via TLR2/1/CD14 and a functional vitamin D receptor signalling: Mycobacterial lipoprotein induces autophagy. *Cell. Microbiol.* 12, 1648–1665.

Shin, S.Y., Kang, S.W., Lee, D.G., Eom, S.H., Song, W.K., Kim, J.I., 2000. CRAMP analogues having potent antibiotic activity against bacterial, fungal, and tumor cells without hemolytic activity. *Biochem. Biophys. Res. Commun.* 275, 904–909.

Shui, W., Petzold, C.J., Redding, A., Liu, J., Pitcher, A., Sheu, L., Hsieh, T.-Y., Keasling, J.D., Bertozzi, C.R., 2011. Organelle membrane proteomics reveals differential influence of mycobacterial lipoglycans on macrophage phagosome maturation and autophagosome accumulation. *J. Proteome Res.* 10, 339–348.

Simeone, R., Bobard, A., Lippmann, J., Bitter, W., Majlessi, L., Brosch, R., Enninga, J., 2012. Phagosomal Rupture by *Mycobacterium tuberculosis* Results in Toxicity and Host Cell Death. *PLoS Pathog.* 8, e1002507.

Simeone, R., Bottai, D., Brosch, R., 2009. ESX/type VII secretion systems and their role in host-pathogen interaction. *Curr. Opin. Microbiol.* 12, 4–10.

Simeone, R., Sayes, F., Song, O., Gröschel, M.I., Brodin, P., Brosch, R., Majlessi, L., 2015. Cytosolic access of *Mycobacterium tuberculosis*: critical impact of phagosomal acidification control and demonstration of occurrence in vivo. *PLoS Pathog.* 11, e1004650.

Smith, L.M., May, R.C., 2013. Mechanisms of microbial escape from phagocyte killing. *Biochem. Soc. Trans.* 41, 475–490.

Sonawane, A., Santos, J.C., Mishra, B.B., Jena, P., Progida, C., Sorensen, O.E., Gallo, R., Appelberg, R., Griffiths, G., 2011. Cathelicidin is involved in the intracellular killing of mycobacteria in macrophages: The role of cathelicidin in mycobacteria killing. *Cell. Microbiol.* 13, 1601–1617.

- Srinivasan, L., Ahlbrand, S., Briken, V., 2014. Interaction of Mycobacterium tuberculosis with Host Cell Death Pathways. Cold Spring Harb. Perspect. Med. 4, a022459–a022459.
- Stamm, L.M., Morisaki, J.H., Gao, L.-Y., Jeng, R.L., McDonald, K.L., Roth, R., Takeshita, S., Heuser, J., Welch, M.D., Brown, E.J., 2003. *Mycobacterium marinum* Escapes from Phagosomes and Is Propelled by Actin-based Motility. J. Exp. Med. 198, 1361–1368.
- Stanley, S.A., Johndrow, J.E., Manzanillo, P., Cox, J.S., 2007. The Type I IFN response to infection with Mycobacterium tuberculosis requires ESX-1-mediated secretion and contributes to pathogenesis. J. Immunol. Baltim. Md 1950 178, 3143–3152.
- Stenger, S., Hanson, D.A., Teitelbaum, R., Dewan, P., Niazi, K.R., Froelich, C.J., Ganz, T., Thoma-Uszynski, S., Melián, A., Bogdan, C., Porcelli, S.A., Bloom, B.R., Krensky, A.M., Modlin, R.L., 1998. An antimicrobial activity of cytolytic T cells mediated by granulysin. Science 282, 121–125.
- Stenger, S., Mazzaccaro, R.J., Uyemura, K., Cho, S., Barnes, P.F., Rosat, J.P., Sette, A., Brenner, M.B., Porcelli, S.A., Bloom, B.R., Modlin, R.L., 1997. Differential effects of cytolytic T cell subsets on intracellular infection. Science 276, 1684–1687.
- Stenger, S., Niazi, K.R., Modlin, R.L., 1998. Down-Regulation of CD1 on Antigen-Presenting Cells by Infection with Mycobacterium tuberculosis. J. Immunol. 161, 3582–3588.
- Stevens, J.M., Galyov, E.E., Stevens, M.P., 2006. Actin-dependent movement of bacterial pathogens. Nat. Rev. Microbiol. 4, 91–101.
- Stout, R.D., Jiang, C., Matta, B., Tietzel, I., Watkins, S.K., Suttles, J., 2005. Macrophages sequentially change their functional phenotype in response to changes in microenvironmental influences. J. Immunol. Baltim. Md 1950 175, 342–349.
- Stout, R.D., Suttles, J., 2004. Functional plasticity of macrophages: reversible adaptation to changing microenvironments. J. Leukoc. Biol. 76, 509–513.
- Sun, L., Wu, J., Du, F., Chen, X., Chen, Z.J., 2013. Cyclic GMP-AMP synthase is a cytosolic DNA sensor that activates the type I interferon pathway. Science 339, 786–791.
- Szondy, Z., Sarang, Z., Kiss, B., Garabuczi, É., Köröskényi, K., 2017. Anti-inflammatory Mechanisms Triggered by Apoptotic Cells during Their Clearance. Front. Immunol. 8.

Takeuchi, O., Akira, S., 2010. Pattern Recognition Receptors and Inflammation. *Cell* 140, 805–820.

Teles, R.M.B., Graeber, T.G., Krutzik, S.R., Montoya, D., Schenk, M., Lee, D.J., Komisopoulou, E., Kelly-Scumpia, K., Chun, R., Iyer, S.S., Sarno, E.N., Rea, T.H., Hewison, M., Adams, J.S., Popper, S.J., Relman, D.A., Stenger, S., Bloom, B.R., Cheng, G., Modlin, R.L., 2013. Type I interferon suppresses type II interferon-triggered human anti-mycobacterial responses. *Science* 339, 1448–1453.

Tezera, L.B., Bielecka, M.K., Chancellor, A., Reichmann, M.T., Shammari, B.A., Brace, P., Batty, A., Tocheva, A., Jogai, S., Marshall, B.G., Tebruegge, M., Jayasinghe, S.N., Mansour, S., Elkington, P.T., 2017. Dissection of the host-pathogen interaction in human tuberculosis using a bioengineered 3-dimensional model. *eLife* 6.

Thoma-Uszynski, S., Stenger, S., Takeuchi, O., Ochoa, M.T., Engele, M., Sieling, P.A., Barnes, P.F., Rollinghoff, M., Bolcskei, P.L., Wagner, M., Akira, S., Norgard, M.V., Belisle, J.T., Godowski, P.J., Bloom, B.R., Modlin, R.L., 2001. Induction of direct antimicrobial activity through mammalian toll-like receptors. *Science* 291, 1544–1547.

Ting, J.P.-Y., Willingham, S.B., Bergstralh, D.T., 2008. NLRs at the intersection of cell death and immunity. *Nat. Rev. Immunol.* 8, 372–379.

Tobin, D.M., Roca, F.J., Oh, S.F., McFarland, R., Vickery, T.W., Ray, J.P., Ko, D.C., Zou, Y., Bang, N.D., Chau, T.T.H., Vary, J.C., Hawn, T.R., Dunstan, S.J., Farrar, J.J., Thwaites, G.E., King, M.-C., Serhan, C.N., Ramakrishnan, L., 2012. Host genotype-specific therapies can optimize the inflammatory response to mycobacterial infections. *Cell* 148, 434–446.

Trejo-Cerro, Ó., Eichwald, C., Schraner, E.M., Silva-Ayala, D., López, S., Arias, C.F., 2017. Actin-Dependent Nonlytic Rotavirus Exit and Infectious Virus Morphogenetic Pathway in Nonpolarized Cells. *J. Virol.* 92.

Tucker, S.C., Casadevall, A., 2002. Replication of *Cryptococcus neoformans* in macrophages is accompanied by phagosomal permeabilization and accumulation of vesicles containing polysaccharide in the cytoplasm. *Proc. Natl. Acad. Sci.* 99, 3165–3170.

Tufariello, J.M., Chan, J., Flynn, J.L., 2003. Latent tuberculosis: mechanisms of host and bacillus that contribute to persistent infection. *Lancet Infect. Dis.* 3, 578–590.

Ulrichs, T., Lefmann, M., Reich, M., Morawietz, L., Roth, A., Brinkmann, V., Kosmiadi, G.A., Seiler, P., Aichele, P., Hahn, H., Krenn, V., Göbel, U.B.,

Kaufmann, S.H., 2005. Modified immunohistological staining allows detection of Ziehl–Neelsen-negative Mycobacterium tuberculosis organisms and their precise localization in human tissue. *J. Pathol.* 205, 633–640.

Underhill, D.M., Ozinsky, A., Smith, K.D., Aderem, A., 1999. Toll-like receptor-2 mediates mycobacteria-induced proinflammatory signaling in macrophages. *Proc. Natl. Acad. Sci.* 96, 14459–14463.

van der Vaart, M., Korbee, C.J., Lamers, G.E.M., Tengeler, A.C., Hosseini, R., Haks, M.C., Ottenhoff, T.H.M., Spaank, H.P., Meijer, A.H., 2014. The DNA damage-regulated autophagy modulator DRAM1 links mycobacterial recognition via TLR-MYD88 to autophagic defense [corrected]. *Cell Host Microbe* 15, 753–767.

van der Wel, N., Hava, D., Houben, D., Fluitsma, D., van Zon, M., Pierson, J., Brenner, M., Peters, P.J., 2007. *M. tuberculosis* and *M. leprae* translocate from the phagolysosome to the cytosol in myeloid cells. *Cell* 129, 1287–1298.

van Zyl-Smit, R.N., Binder, A., Meldau, R., Mishra, H., Semple, P.L., Theron, G., Peter, J., Whitelaw, A., Sharma, S.K., Warren, R., Bateman, E.D., Dheda, K., 2011. Comparison of Quantitative Techniques including Xpert MTB/RIF to Evaluate Mycobacterial Burden. *PLoS ONE* 6, e28815.

Velmurugan, K., Chen, B., Miller, J.L., Azogue, S., Gurses, S., Hsu, T., Glickman, M., Jacobs, W.R., Porcelli, S.A., Briken, V., 2007. Mycobacterium tuberculosis *nuoG* is a virulence gene that inhibits apoptosis of infected host cells. *PLoS Pathog.* 3, e110.

Via, L.E., Deretic, D., Ulmer, R.J., Hibler, N.S., Huber, L.A., Deretic, V., 1997. Arrest of mycobacterial phagosome maturation is caused by a block in vesicle fusion between stages controlled by rab5 and rab7. *J. Biol. Chem.* 272, 13326–13331.

Via, L.E., Schimel, D., Weiner, D.M., Dartois, V., Dayao, E., Cai, Y., Yoon, Y.-S., Dreher, M.R., Kastenmayer, R.J., Laymon, C.M., Carny, J.E., Flynn, J.L., Herscovitch, P., Barry, C.E., 2012. Infection Dynamics and Response to Chemotherapy in a Rabbit Model of Tuberculosis using [18F]2-Fluoro-Deoxy-d-Glucose Positron Emission Tomography and Computed Tomography. *Antimicrob. Agents Chemother.* 56, 4391–4402.

Vogt, G., Nathan, C., 2011. In vitro differentiation of human macrophages with enhanced antimycobacterial activity. *J. Clin. Invest.* 121, 3889–3901.

Volkman, H.E., Clay, H., Beery, D., Chang, J.C.W., Sherman, D.R., Ramakrishnan, L., 2004. Tuberculous granuloma formation is enhanced by a mycobacterium virulence determinant. *PLoS Biol.* 2, e367.

Warwick-Davies, J., Dhillon, J., O'Brien, L., Andrew, P.W., Lowrie, D.B., 1994. Apparent killing of *Mycobacterium tuberculosis* by cytokine-activated human monocytes can be an artefact of a cytotoxic effect on the monocytes. *Clin. Exp. Immunol.* 96, 214–217.

Wassermann, R., Gulen, M.F., Sala, C., Perin, S.G., Lou, Y., Rybniker, J., Schmid-Burgk, J.L., Schmidt, T., Hornung, V., Cole, S.T., Ablasser, A., 2015. *Mycobacterium tuberculosis* Differentially Activates cGAS- and Inflammasome-Dependent Intracellular Immune Responses through ESX-1. *Cell Host Microbe* 17, 799–810.

Watson, R.O., Manzanillo, P.S., Cox, J.S., 2012. Extracellular *M. tuberculosis* DNA targets bacteria for autophagy by activating the host DNA-sensing pathway. *Cell* 150, 803–815.

Weddle, E., Agaisse, H., 2018. Principles of intracellular bacterial pathogen spread from cell to cell. *PLOS Pathog.* 14, e1007380.

Welin, A., Eklund, D., Stendahl, O., Lerm, M., 2011. Human Macrophages Infected with a High Burden of ESAT-6-Expressing *M. tuberculosis* Undergo Caspase-1- and Cathepsin B-Independent Necrosis. *PLOS ONE* 6, e20302.

Wolf, A.J., Desvignes, L., Linas, B., Banaiee, N., Tamura, T., Takatsu, K., Ernst, J.D., 2008. Initiation of the adaptive immune response to *Mycobacterium tuberculosis* depends on antigen production in the local lymph node, not the lungs. *J. Exp. Med.* 205, 105–115.

Wolf, A.J., Linas, B., Trevejo-Nuñez, G.J., Kincaid, E., Tamura, T., Takatsu, K., Ernst, J.D., 2007. *Mycobacterium tuberculosis* infects dendritic cells with high frequency and impairs their function in vivo. *J. Immunol. Baltim. Md* 1950 179, 2509–2519.

Wong, D., Bach, H., Sun, J., Hmama, Z., Av-Gay, Y., 2011. *Mycobacterium tuberculosis* protein tyrosine phosphatase (PtpA) excludes host vacuolar-H<sup>+</sup>-ATPase to inhibit phagosome acidification. *Proc. Natl. Acad. Sci. U. S. A.* 108, 19371–19376.

World Health Organization, 2017. Global Tuberculosis Report.

World Health Organization, 2011. Global tuberculosis control: WHO report 2011. Geneva : World Health Organization, Geneva.

Xu, S., Cooper, A., Sturgill-Koszycki, S., van Heyningen, T., Chatterjee, D., Orme, I., Allen, P., Russell, D.G., 1994. Intracellular trafficking in *Mycobacterium tuberculosis* and *Mycobacterium avium*-infected macrophages. *J. Immunol. Baltim. Md* 1950 153, 2568–2578.

- Yates, R.M., Hermetter, A., Russell, D.G., 2005. The kinetics of phagosome maturation as a function of phagosome/lysosome fusion and acquisition of hydrolytic activity. *Traffic Cph. Den.* 6, 413–420.
- Yona, S., Kim, K.-W., Wolf, Y., Mildner, A., Varol, D., Breker, M., Strauss-Ayali, D., Viukov, S., Guilliams, M., Misharin, A., Hume, D.A., Perlman, H., Malissen, B., Zelzer, E., Jung, S., 2013. Fate mapping reveals origins and dynamics of monocytes and tissue macrophages under homeostasis. *Immunity* 38, 79–91.
- Yuk, J.-M., Shin, D.-M., Lee, H.-M., Yang, C.-S., Jin, H.S., Kim, K.-K., Lee, Z.-W., Lee, S.-H., Kim, J.-M., Jo, E.-K., 2009. Vitamin D3 induces autophagy in human monocytes/macrophages via cathelicidin. *Cell Host Microbe* 6, 231–243.
- Zanetti, M., 2004. Cathelicidins, multifunctional peptides of the innate immunity. *J. Leukoc. Biol.* 75, 39–48.
- Zasloff, M., 2002. Antimicrobial peptides of multicellular organisms. *Nature* 415, 389–395.
- Zhang, Z., Fan, W., Yang, G., Xu, Z., Wang, J., Cheng, Q., Yu, M., 2017. Risk of tuberculosis in patients treated with TNF- $\alpha$  antagonists: a systematic review and meta-analysis of randomised controlled trials. *BMJ Open* 7, e012567.
- Zimmerli, S., Edwards, S., Ernst, J.D., 1996. Selective receptor blockade during phagocytosis does not alter the survival and growth of *Mycobacterium tuberculosis* in human macrophages. *Am. J. Respir. Cell Mol. Biol.* 15, 760–770.